PB84-239409

REPORT NO.
UCB/EERC-84/05
JUNE 1984

EARTHQUAKE ENGINEERING RESEARCH CENTER

U.S. - JAPAN COOPERATIVE EARTHQUAKE RESEARCH PROGRAM: EARTHQUAKE SIMULATION TESTS AND ASSOCIATED STUDIES OF A 1/5th-SCALE MODEL OF A 7-STORY REINFORCED CONCRETE TEST STRUCTURE

by

V. V. BERTERO
A. E. AKTAN
F. A. CHARNEY
R. SAUSE

Report to Sponsor:
National Science Foundation

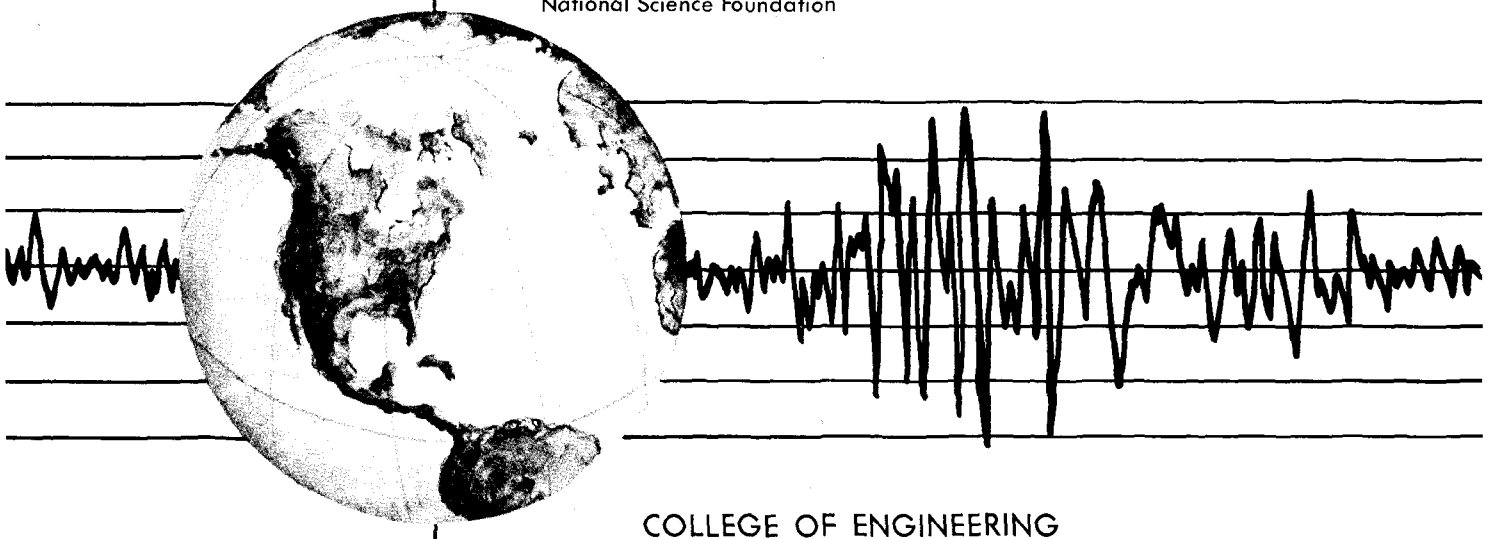

COLLEGE OF ENGINEERING

UNIVERSITY OF CALIFORNIA · Berkeley, California

For sale by the National Technical Information Service, U.S. Department of Commerce, Springfield, Virginia 22161.

See back of report for up to date listing of EERC reports.

DISCLAIMER

50272-101

REPORT DOCUMENTATION PAGE	1. REPORT NO. NSF/CEE-84020	2.	3. Recipient's Accession No. PB84 239409
4. Title and Subtitle: Earthquake Simulation Tests and Associated Studies of a 1/5th-Scale Model of a 7-Story Reinforced Concrete Frame-Wall Test Structure			5. Report Date: June 1984 6.
7. Author(s): V. V. Bertero, A. E. Aktan, F. A. Charney and R. Sause			8. Performing Organization Rept. No. UCB/EERC-84/05
9. Performing Organization Name and Address: Earthquake Engineering Research Center, University of California, Berkeley, 1301 South 46th Street, Richmond, Calif. 94804			10. Project/Task/Work Unit No. 11. Contract(C) or Grant(G) No. (C) (G) CEE-80-09478
12. Sponsoring Organization Name and Address: National Science Foundation, 1800 G. Street, N.W., Washington, D.C. 20550			13. Type of Report & Period Covered 14.

15. Supplementary Notes

16. Abstract (Limit: 200 words)

This report summarizes research conducted at Berkeley as part of the R/C (seven-story frame-wall) Building Structure Phase of the U.S.-Japan Cooperative Earthquake Research Program. Besides describing the studies conducted at Berkeley on a 1/5th-scale model of the test building, the report has the following main objectives: (a) to evaluate the results of these studies and discuss the degree of correlation between the experimental responses of the full-scale model tested in Japan and the 1/5th-scale model tested in Berkeley, and between analytically predicted and experimental responses; (b) to assess the states of art and practice of seismic resistant design and construction of reinforced concrete frame-wall structures in light of this evaluation; and (c) to formulate recommendations for improvement in the states of the practice and art.

The following aspects of the study are considered in the report: soundness of the preliminary design; the determination of the largest scale model of the full-scale structure that could be accommodated on the shaking table at Berkeley; the design of the 1/5th-scale model, the selection and fabrication of the model materials, the construction of the model and instrumentation. Problems encountered in achieving similitude with the full-scale model are noted.

17. Document Analysis a. Descriptors

b. Identifiers/Open-Ended Terms

c. COSATI Field/Group

18. Availability Statement: Release Unlimited	19. Security Class (This Report)	21. No. of Pages: 199
	20. Security Class (This Page)	22. Price

(See ANSI-Z39.18) See Instructions on Reverse

OPTIONAL FORM 272 (4-77) (Formerly NTIS-35) Department of Commerce

U.S.-JAPAN COOPERATIVE EARTHQUAKE RESEARCH PROGRAM

EARTHQUAKE SIMULATION TESTS AND ASSOCIATED STUDIES OF A 1/5th-SCALE MODEL OF A 7-STORY R/C FRAME-WALL TEST STRUCTURE

by

V. V. Bertero

Professor of Civil Engineering
University of California, Berkeley

Ahmet E. Aktan

Associate Research Engineer
Earthquake Engineering Research Center
University of California, Berkeley

Finley A. Charney

Research Assistant
Department of Civil Engineering
University of California, Berkeley

Richard Sause

Research Specialist
University of California, Berkeley

Report to Sponsor:
National Science Foundation

Report No. UCB/EERC-84/05
Earthquake Engineering Research Center
College of Engineering
University of California
Berkeley, California

June 1984

ABSTRACT

This report summarizes the research conducted at Berkeley as part of the Reinforced Concrete Building Structure (a seven-story frame-wall structure) Phase of the U.S.-Japan Cooperative Earthquake Research Program. Besides describing the studies conducted at Berkeley on the 1/5th-scale model of the test building, the report has the following main objectives: (a) to evaluate the results of these studies and discuss the degree of correlation between the experimental response of the full-scale model tested in Japan and the 1/5th-scale model tested in Berkeley, and between the anlytically predicted and experimental responses; (b) to assess the states of art and practice of seismic resistant design and construction of reinforced concrete frame-wall structures in light of this evaluation; and (c) to formulate recommendations for improvement in the states of the practice and art.

The report is divided into seven parts. The analytical studies conducted to review the soundness of the preliminary design and to produce the analytical information required to determine the largest scale model of the full-scale structure that could be accommodated on the shaking table at Berkeley are discussed first. The design of the 1/5th-scale model, the selection and problems encountered in the fabrication of the model materials, as well as in the determination of the mechanical characteristics of these materials, and in the construction of the model and instrumentation are discussed next. Problems encountered in achieving similitude with the full-scale model are noted. In the fourth part the results of the experiments designed to determine the initial mechanical characteristics (static and dynamic) of the 1/5th-scale model are presented and compared to analytically predicted values and to experimental values from tests of the full-scale model.

The fifth, sixth, and seventh parts of the report are devoted to: A discussion of the experiments conducted on the 1/5th-scale model at the Berkeley earthquake simulator facility, and the illustration of maximum responses; A comparison of experimental results with those obtained for the full-scale model tests and those predicted analytically; An analysis of the implications of the above results on the states of the practice and art of seismic resistant design and

construction of reinforced concrete frame-wall structures and an analysis of the results as they relate to the reliability of the experimental technique of testing reduced-scale models on earthquake simulator facilities.

In the last part of the report, after summarizing the studies conducted, the main conclusions of these studies are presented, and recommendations for improvement in the states of the art and practice of seismic resistant design of R/C frame-wall structures are formulated.

ACKNOWLEDGMENTS

The research reported here was supported by the National Science Foundation Grant Number CEE 80-09478. Any opinions, discussions, findings, conclusions, and recommendations are those of the authors. The authors acknowledge the financial support provided by N.S.F. and the continuing encouragement of the program managers, Drs. S. C. Liu and J. B. Scalzi.

Many thanks are expressed to all the members of the Technical Coordinating Committee of the U.S.-Japan Cooperative Research Program Utilizing Large-Scale Testing Facilities for the many stimulating conversations during the meetings held to discuss this research. The efforts of Dr. M. Watabe of the Building Research Institute of Tsukuba, Japan, and Professor R. Hanson in coordinating the research program are greatly appreciated.

The close cooperation of Professor J. K. Wight of the University of Michigan and of the Japanese researchers of the Building Research Institute at Tsukuba in supplying information regarding the full-scale test building is greatly appreciated.

The authors would like to express their appreciation to Dr. G. W. Corley, Director of the Engineering Development Division, Construction Technology Laboratories, Portland Cement Association, for supplying some of the reinforcing bars used in the model, and to Professor H. Krawinkler of Stanford University for his loan of the wire-knurling device.

The authors are indebted to Professors H. G. Harris of Drexel University and R. Clough and M. Polivka of the University of California at Berkeley for their invaluable advice during the course of this research.

The many and valuable contributions of T. Nagashima, visiting scholar from Takenaka Komuten Co., Ltd., Japan; A. A. Chowdhurry and S. Moazzami, graduate students; D. Clyde, Development Engineer; C. Llopiz, Assistant Specialist; and of other support personnel are gratefully acknowledged. J. Sanders edited the report and R. Steele prepared the illustrations.

Table of Contents

LIST OF TABLES

LIST OF FIGURES

I. INTRODUCTION

1.1 Introductory Remarks

The research reported here was conducted at the University of California, Berkeley, as part of the Reinforced Concrete Building Structure Phase of the U.S.-Japan Cooperative Research Program [1]. The U.C. Berkeley research program originally had the following main objectives:

(1) To review and improve, if necessary, the design of the reinforced concrete full-scale test building.

(2) To determine the reliability of available linear and nonlinear structural analysis computer programs used to predict the seismic performance of buildings.

(3) To determine the reliability of experimental analysis based on tests conducted on the earthquake simulator facility of the University of California, which accommodated a 1/5th-scale model of the test building.

(4) To determine the reliability of mathematical models based on experiments conducted on reduced-scale models of the basic subassemblages of a building using controlled loading facilities available at Berkeley, and to predict seismic response based on such mathematical models.

(5) To evaluate the results as they pertained to the seismic resistant design and construction of reinforced concrete frame-wall buildings.

In the course of the program at U.C. Berkeley the following basic questions, as yet unanswered by the engineering profession, were considered:

(1) How does a well-designed, multi-story reinforced concrete frame-wall structural system—with precisely controlled and documented design, construction, and force and deformation history—respond to earthquakes of different intensity and damage potential, ranging from minor to major? What would be the stiffness, strength, energy dissipation, frequency, and damping characteristics of such a

structure, and how would these characteristics change during successive earthquakes? What would be the failure and collapse characteristics of the structure? What would be the effect of different types of nonstructural elements on the response of such a structure?

(2) Are destructive tests of full-scale structures necessary to answer the questions in (1) above? To what extent do dynamic tests of true replica or distorted models of medium- or small-scale simulate the limit state responses of reinforced concrete structures to earthquakes?

(3) What are the force, deformation, and energy dissipation demands from subassemblages of a well-designed reinforced concrete frame-wall structure during limit states of response to earthquakes? How reliable are predictions of seismic response of complete structures based on data from static tests of components? Are the loading histories commonly applied during component and subassemblage testing realistic, or are they exaggerated? Are the components and subassemblages being over-tested?

(4) What is the state-of-the-art in analytically predicting the seismic response of reinforced concrete frame-wall structures at all limit states? How might the state-of-the-art of such analyses best be advanced? Can analytical models and procedures for frame-wall structures be improved based solely on the results of static tests of reduced-scale components or subassemblages of structures? Or will it be necessary to perform dynamic tests on small- or medium-scale distorted or true replica models of structural systems?

(5) Will researchers from different institutions agree as to the basic conclusions to be drawn from studies coordinated by the Joint Technical Coordinating Committee [1]? What answers will these researchers pose to the questions in (1) to (4) above? Is it possible to establish international standards for experimental and analytical research on the earthquake engineering of reinforced concrete?

Neither the research program at U.C. Berkeley nor the cooperative research program [1] was expected to provide definitive answers to all these questions, partly due to limitations imposed by investigating just one model of many possible variations when multi-story reinforced concrete frame-wall structural systems are constructed, and partly due to limitations of the pseudo-dynamic testing to which the full-scale model was subjected [2]. The results obtained from tests of the full-scale and reduced-scale models of the building structure are not wholly adequate to answer the questions in (1), since both models were tested along only one horizontal response direction and the full-scale model was idealized as a single-degree-of-freedom system in establishing its displacement program [3]. Furthermore, the models were completely fixed at the foundation level to the test floor. The relation of experimental and analytical responses to the actual response of the modeled structure (with a deformable soil-foundation system and excited simultaneously by all components of real base motion) should therefore be carefully evaluated in answering the questions posed in (1) above.

1.2 Objectives and Scope of Report

The main objectives of this report are:

(1) To summarize briefly the studies conducted at Berkeley.

(2) To evaluate results and discuss the degree of correlation between the experimental responses of the full- and 1/5th-scale models and between experimentally and analytically predicted response.

(3) To assess the implications of the results obtained regarding the state-of-the-art, and particularly the state-of-the-practice, of the seismic resistant design and construction of reinforced concrete frame-wall structures as reflected in present seismic codes.

(4) To formulate recommendations for the improvement of U.S. seismic codes and for research needs to advance the state-of-the-art in the analysis and design of

reinforced concrete frame-wall structures.

This report is divided into seven parts. After a brief description of the studies conducted at Berkeley, the results of analytical studies conducted prior to the experimental program are summarized in the first part. In the second part, the design, construction, and instrumentation of the 1/5th-scale model are described and the degree of success in simulating the full-scale model is evaluated. This evaluation paves the way for discussing the state-of-the-art and the state-of-the-practice of the design and fabrication of reduced-scale models of reinforced concrete frame-wall structures. In the third part, the results of a preliminary series of tests conducted on the 1/5th-scale model to determine its mechanical characteristics in the serviceability range of behavior are presented. These experimental results are compared with those for the full-scale model and those predicted analytically. The overall response obtained in the experiments conducted at the earthquake simulator facility on the 1/5th-scale model is discussed in the fourth part. The various resistance mechanisms that contributed to the total shear and overturning moment strengths are discussed and quantified. In the fifth part, results of tests conducted at the earthquake simulator facility are compared with similar results obtained in experiments conducted on the full-scale model and with analytically predicted responses in order to evaluate the degree of correlation between these results. In the sixth part, the results obtained in the above studies are assessed with respect to the state-of-the-art and particularly the state-of-the-practice of the design of reinforced concrete frame-wall structures. Finally, after the results of the studies described here and conclusions drawn from those studies have been summarized, improvements in U.S. seismic code provisions for the design of reinforced concrete frame-wall structures are suggested, as is research needed to improve present analytical techniques (computer programs) for predicting seismic response.

II SUMMARY OF ANALYTICAL STUDIES

2.1 Introductory Remarks

The studies conducted at U.C. Berkeley related to the Reinforced Concrete Building Structure Phase of the U.S.-Japan Cooperative Research Program [1] can be grouped into four main phases.

First Phase: Analytical studies:

(1) To review the preliminary design of the reinforced concrete test building in order to determine if this design satisfied the present state-of-the-practice as reflected by the seismic provisions of the 1979 *Uniform Building Code* [4], hereafter the UBC.

(2) (a) To conduct analyses required to determine the largest scale model of the full-scale structure which might be tested in accordance with the capacity of the available earthquake simulator facility at Berkeley; (b) To estimate the critical ground motions and the sequence of intensity of these ground motions according to the desired range of behavior or limit states to be studied during testing of the reduced-scale model; and (c) To design the instrumentation for the model.

(3) To determine the reliability of analytical predictions of the seismic response of the test building through the use of available linear and nonlinear structural analysis computer programs by comparing the analytical results with those to be obtained in the experiments.

All these analytical studies are described in this section of the paper.

Second Phase: Based on the results obtained in the first phase, it was determined that the maximum size model that could be tested on the Berkeley earthquake simulator was a 1/5th-scale model of the full-scale model, shown in Fig. 1. This second phase of the study therefore concentrated on:

(1) The design of the 1/5th-scale model.

(2) The selection, design, and fabrication of the model material; the determination of actual mechanical characteristics; and the degree of correlation with the characteristics of the material used in the full-scale model.

(3) The analytical prediction of the seismic response of the model.

(4) The design of instrumentation for the model.

(5) The construction and instrumentation of the model.

(6) The static and dynamic tests required to determine the mechanical characteristics of the model. Comparison of these mechanical characteristics with those obtained in similar tests conducted on the full-scale model and with those predicted analytically.

(7) The tests on the earthquake simulator.

Third Phase: This phase was devoted to correlation studies of the results obtained from the earthquake simulator tests of the 1/5th-scale model with those obtained from the pseudo-dynamic tests of the full-scale model [3] and with those predicted analytically, both prior [5] and subsequent to testing the 1/5th-scale model.

Fourth Phase: The results of the above studies were assessed with regard to the present state-of-the-art and particularly the state-of-the-practice of the seismic resistant design of reinforced concrete frame-wall structures. This required thorough comparison of the response expected according to present UBC [4] seismic design provisions and ATC 3-06 [6] recommendations with the responses obtained experimentally.

2.2 Analytical Studies

2.2.1 Review of Full-Scale Model Design. Detailed analysis of the preliminary design of the full-scale building shown in Fig. 1 was discussed in Ref. 5. The design did not strictly satisfy the 1979 UBC requirements for structures classified as UBC Type 3 (a dual-bracing system consisting of a shear wall interacting with a ductile moment-resisting space frame) because:

Columns. The columns could not be classified as ductile moment-resisting space frame columns according to the UBC because the detailing of the reinforcement at their critical regions did not satisfy the UBC requirements for concrete confinement. Furthermore, a comparison of the envelope of the axial-flexural (N-M) diagram as controlled by shear strength with the envelope corresponding to the axial-flexural strength showed [5] that the design of the columns did not satisfy the UBC requirement for shear strength when $(P_e/A_g) \leqslant 0.12f_c'$, because for a range of axial force just below the value given, the shear resistance provided by the ties alone was insufficient. As pointed out in [5], however, because the shear and axial forces to which the columns would be subjected were relatively low, and because the response of the shear wall would control overall behavior, this lack of code-required confinement and shear resistance was not regarded as a major problem. The columns could be considered ductile.

Beam-Column Joints and Anchorages. The detailing of the anchorage of the beam main reinforcement in the joint with the exterior columns did not satisfy the UBC code requirement. Also, the confinement of the core of the beam-column joints was not adequate. But again, because the shear stress introduced at the exterior column joint by the main beam reinforcement was relatively low ($4.35\sqrt{f_c'(\text{psi})}$ [$11.42\sqrt{f_c'(kPa)}$]), this violation of the UBC was considered inconsequential [5].

Shear Wall. The detailing of the shear wall, except for the ties of the edge members, satisfied the minimum reinforcement requirements of the 1979 UBC code for the design of walls for seismic zones 3 and 4.

In summary, while the detailing of the preliminary design did not strictly satisfy the 1979 UBC requirements for Type 3 structures (for which a horizontal force factor $K = 0.8$ could be used), due to the low shear stresses in all elements and the relatively low axial forces in the columns and walls, sufficiently ductile behavior of the frame could be expected so that the frame could be considered a ductile moment-resisting space frame. The detailing of the structure satisfied the 1979 UBC seismic require-

ments for reinforced concrete buildings designed for a horizontal force factor of K = 1.0.

During earthquake shaking, the response of an existing structure will depend on how it was constructed, and the forces which develop will be the same no matter how the designer or analyst classifies the structure, i.e., Type 1 or 3 with K = 1.0 or K = 0.8, respectively.

UBC Lateral Load Analysis. Based on an estimated weight, W, for the total reactive mass, M, of the test building (Fig. 1) of 2501 kips (11.13 MN) and assuming that the structure, because of its detailing, would be classified as Type 1 (i.e., K = 1.0), and considering a fundamental period, T = 0.47 sec. (estimated according to the UBC empirical expression $T = 0.05\ h_n/\sqrt{D}$ *) the total base shear, V, for which the building had to be designed according to the 1979 UBC was 242 kips (1.08 MN).

The structure in Fig. 1 was analyzed [5] under a combination of the 1979 UBC factored lateral load (242 × 1.4 = 339 kips (1.50 MN)) and factored gravity (dead and live) loads, assuming that: all members remained uncracked; there was no out-of-plane interaction between frames; the floor slabs acted as diaphragms rigid in their own plane; and the bases of the columns and shear wall were totally fixed. The main results from *the linear elastic analyses* are as follows:

1. Frame B (see Fig. 1(a)) carried 95% of the total base shear.
2. None of the columns developed axial tension force, and the demanded axial-flexural strengths of the columns were significantly less than the supplied strengths.
3. Almost all of the negative moments at the ends of the girders of frame B exceeded the strength specified by the UBC (i.e., the design flexural strength $M_d = 0.9\ M_n$) despite the fact that in calculating this strength the contribution of the

* h_n is the height in feet of the building; D is the dimension of the structure, in feet, in a direction parallel to the ground motion.

slab steel for a total effective width of 60 in. (1.52 m) was included. If the redistribution of moment allowed by the UBC were neglected, the structure in Fig. 1 would be overstressed according to the UBC. On the other hand, if the moment redistribution allowed by UBC Section 2608(e) were incorporated (which according to the detailing of the girders was estimated to be 18.4%) the girders would not be overstressed and the design could be considered acceptable.

4. The demanded shear wall forces (axial, shear, and flexural moments) determined from this linear elastic analysis were well below the strengths supplied to the shear wall. The UBC requires, however, that the wall alone resist the entire lateral force for either $K = 0.8$ or $K = 1.0$. (In the former case, this is clearly stated in Table 23-I of the UBC; in the latter case, where the moment-resisting space frame does not conform to the requirements for a ductile frame, the shear wall should resist 100% of the design lateral force [see EXCEPTION in Section 2312(j)C of UBC [4]].)

5. If the shear wall alone must resist all of the required shear force (i.e., 100% of the UBC seismic design lateral force), the design would not satisfy all the UBC strength design requirements. The shear strength was estimated to be 0.85 × 296 kips = 252 kips (1.12 MN) (considering the contribution of panel steel only) if the shear resistance offered by the concrete were neglected, as suggested by Paulay [7], or 0.85 × 168 + 252 kips = 395 kips (1.76 MN) to 0.85 × 278 kips + 252 kips = 488 kips (2.17 MN), where 168 kips (0.75 MN) and 278 kips (1.24 MN) represent the contribution of concrete shear resistance based on 2.0 $\sqrt{f_c'(psi)}$ (5.25 $\sqrt{f_c'(kPa)}$) or 3.3 $\sqrt{f_c'(psi)}$ (8.66 $\sqrt{f_c'(kPa)}$), respectively.** (As

** While Section 2611(k)5 of the 1982 edition of the UBC permits the use of up to $V_c = 2\sqrt{f_c'(psi)}\,hd$ [5.25 $\sqrt{f_c'(kPa)}\,hd$] for a wall subjected to compression, Section 2611(k)6 requires that for earthquake loads on buildings in seismic zones 3 and 4, V_c shall be the lesser of $V_c = 3.3\sqrt{f_c'(psi)}\,hd$ (8.66 $\sqrt{f_c'(kPa)}\,hd$) or $V_c = [0.6\sqrt{f_c'(psi)} + \frac{1.25l_w}{\frac{M_u}{V_u} - \frac{l_w}{2}}]\,hd$, (where $0.6\sqrt{f_c'(psi)} = 1.57\sqrt{f_c'(kPa)}$). For the wall in Fig. 1, the second equation controls and $V_c < 2.0\sqrt{f_c'(psi)}\,hd$ [5.25 $\sqrt{f_c'(kPa)}\,hd$]. The question then is why the UBC permits the use of $V_c = 2\sqrt{f_c'(psi)}\,hd$ [5.25

explained in [5], although contrary to the UBC requirements, 3.3 $\sqrt{f_c'(psi)}$ [8.66 $\sqrt{f_c'(kPa)}$] is a better estimate of the concrete contribution to the shear resistance of the wall in Fig. 1, according to the detailing of the structure and the forces acting on it.) Because the shear strength demand for the case where K = 1.0 is 2.0 E = 2.0 × 242 = 484 kips (2.15 MN), it is obvious that only if we can tolerate $V_c = 3.3\sqrt{f_c'(psi)}\,hd$* (8.66 $\sqrt{f_c'(kPa)}\,hd$), which the UBC does not permit, will the supplied shear strength be acceptable.

For the case where K = 0.8, the supplied shear strength is acceptable even if $V_c = 2.0\sqrt{f_c'(psi)}\,hd$ (5.25 $\sqrt{f_c'(kPa)}\,hd$), because the demanded shear strength would be V_u = 0.8 × (2 × 242) = 387 kips (1.72 MN), i.e. less than 395 kips (1.76 MN).

The axial-flexural strength demanded from the shear wall (203000 K-in. (22.9 MN-m) and 162000 K-in. (18.4 MN-m) for the cases K = 1.0 and K = 0.8, respectively) was far from being satisfied by the supplied design strength. The total estimated axial-flexural design strength (under an axial load of 740 kips [3.29 MN] due to gravity) without considering the increase in supplied strength due to strain hardening of the reinforcement and other factors discussed later, was 0.9 × 150000 K-in. = 135000 K-in. (15.3MN-m). Thus, the demanded flexural strength is 50% or 20% higher than the supplied strength for the cases K = 1.0 and 0.8, respectively.

Although where K = 0.8 the demanded flexural strength of 162000 K-in. (18.4 MN-m) is only 20% higher than the supplied design strength, the UBC (Section 2627(c)) requires for a lateral force-resisting system classified as Type 3 (i.e., K = 0.8), that the concrete shear walls be provided special vertical boundary ele-

$\sqrt{f_c'(kPa)\,hd}$]?

* h = overall thickness of member, inches;
d = distance from extreme compression fiber to center of force of all reinforcement in tension, but need not be less than 0.80 l_w where l_w is the horizontal length of the wall in inches.

ments at the edges, and that these elements be designed to carry all vertical stresses resulting from the wall loads in addition to tributary dead and live loads and those from horizontal seismic forces. The main reinforcement and detailing of the wall edge members were such that they supplied a design flexural strength to the wall of 98100 K-in. (11.1 MN-m), i.e., only 60% of the demanded strength. The amount of reinforcing steel supplied to the edge elements of the wall was only 1.22% of the area of the edge member, which is very low. Thus, the flexural cracking resistance of the wall was very close to its flexural yielding capacity. An additional result of this low amount of reinforcement, however, was that the deformability of the wall would be large, and although it did not satisfy the UBC code for a $K = 0.8$ structural system, its potential seismic behavior was considered good [5].

For walls of structural systems categorized as $K = 1.0$, no special vertical boundary elements are required. There should, however, be a complete vertical load-carrying space frame. Thus, for the building shown in Fig. 1 to be considered in the $K = 1.0$ category, the vertical boundary members of the main wall must be considered as frame columns.

6. If the design is for $K = 0.8$, the UBC requires that the ductile moment-resisting space frame shall resist not less than 25% of the total required lateral force. In investigating this requirement, the following questions arose.

   (a) For the structural system shown in Fig. 1, which components should be considered to comprise the system that should be considered the ductile moment-resisting frame?

   (i) the complete three-dimensional space frame after removing the panel of the main wall as if it were merely an infill panel? or

   (ii) frames A + C alone? or

(iii) frames A + C + the two free-standing columns of frame B?

Although not clearly stated by the UBC, the authors believe that if there had been girders at each floor of the wall, the more rational answer would be (i). Although there were no girders in the bay of the wall, answer (i) is still believed to be best.

(b) How should the capacity of the ductile moment-resisting space frame be estimated in order to verify whether it resists at least 25% of the required lateral force? Should it be based on a limit analysis or on a linear elastic analysis? Although no answer is given by the UBC provisions, because the UBC design procedure is based on linear elastic analysis, it is believed that the intention of the UBC provisions is to estimate capacity using linear elastic analysis.

(c) On what model of the structural frame-wall system should the analysis of the capacity of the ductile moment-resisting space frame be based? On a complete new model based on the space frame alone or on the model of the frame-wall system? Again, the code neither specifies nor gives any guidelines regarding the analytical model to be adopted in the capacity analysis of the frame. Results [5] indicate that if the linear elastic analysis is conducted using the frame-wall model because of the high flexural stresses developed at the ends of the beams that frame into the wall in frame B (Fig. 1(a)), the frame will be overstressed before it can resist 25% of the total lateral load. On the other hand, linear analysis of a model of the space frame alone and subjected to the code-specified pattern of lateral load showed that it can resist a total shear of 250 kips (1.11 MN), considerably larger than 25% of 339 kips = 85 kips.* A limit analysis of the preliminary design [5] showed that: (1) the lateral resistance capacity of the space frame model alone, based on the flexural design strength computed according to the UBC, is 375 kips (1.67 MN), which is considerably higher than the 25% of the

* The base shear strength of the frame alone, computed according to the code for the frame subjected to a specified lateral load pattern, was 250 kips (1.11 MN). This was in fact adequate to meet the code base shear demand for the complete structure assuming this to be a ductile moment-resisting space frame structure (Type 4, $K = 0.67$).

UBC total required lateral force = 0.25 × (339) = 85 kips (0.38 MN); and (2) the capacity of the whole frame wall-structure based on a limit analysis using for the plastic moments the UBC design strengths of the sections was 607 kips (2.70 MN) and 664 kips (2.80 MN) when a more realistic nominal element strength (including strain hardening of reinforcement) was used. These limit analyses assumed that the deformability of the critical regions of the frame elements and wall was sufficiently large to allow a collapse mechanism to form.

7. The stiffness of the designed structure satisfied the UBC requirements. The resulting lateral displacements under the unfactored loads (V = 242 kips (1.08 MN)) and based on uncracked member stiffnesses was estimated to result in a maximum interstory drift smaller than 0.001, which is considerably less than the UBC maximum acceptable drift of 0.005. Even if the effect of the cracked sections on lateral stiffness were considered, the lateral stiffness of the designed structure would comply with the UBC requirements.

Summarizing, the designed structure did not satisfy the strength requirements for a UBC Type 3 (K = 0.8) lateral force-resisting system despite the fact that the static lateral force capacity was estimated to be 607 kips, i.e. 607/339 = 1.79 times that required by the UBC. Also, the designed structure did not satisfy the requirements of the UBC for a structural system corresponding to K = 1.0, especially in view of the low flexural strength of the wall. Despite this noncompliance with the UBC seismic regulations, the authors believed that the actual seismic behavior would be satisfactory because of the low shear and axial stresses that would be present in the regions of critical flexural demand. The minimum demanded or *expected* seismic behavior according to UBC design demands for a K = 0.8 and K = 1.0 structure is illustrated in Fig. 2. The capacity of the designed structure obtained through a limit analysis is also indicated.

2.2.2 Predicted Dynamic Characteristics of Designed Structure. The following

mechanical characteristics were predicted.

Flexibility Matrix. Using elastic properties of the members based on a cracked, transformed cross section moment of inertia, I, the seven(lateral)-degree-of-freedom flexibility matrix for the total structure of Fig. 1 in the direction of the main shear wall is given in Table 1(a). A cracked, transformed cross section, I_{cr}, was used rather than an uncracked, I_{gross}, cross section to investigate the dynamic characteristics of the structure just before an extreme ground shaking, which was assumed to occur after the structure had been subjected to service loads (gravity and lateral due to wind and minor or even moderate earthquakes) which would have induced cracking. If the extreme shaking were assumed to occur immediately after the removal of the formwork, the dynamic characteristics of the structure could have been more closely estimated using a flexibility matrix based on uncracked I. This uncracked flexibility matrix is given in Table 1(b). Comparison of the two flexibility matrices given in Tables 1(a) and 1(b) shows that, as expected, they are quite different, the larger cracked flexibility coefficients being more than three times those of the uncracked ones. This was expected because the uncracked I of the wall and of the columns was about seven times the cracked I and for the girders the uncracked I was more than three times the cracked I. Comparison with the experimental flexibility matrix, Table 1(c), obtained from tests conducted by Japanese researchers [3] on the full-scale model shows that the initial flexibility characteristics of the structure were closer to but somewhat smaller (10%) than those obtained using uncracked I. The analytical cracked flexibility matrix can be considered an upper bound on the flexibility of the structure after being subjected to service loads. To study the significance of the main wall stiffness on the inelastic behavior of the whole structure, a new flexibility matrix of the structure, assuming that the wall has developed a mechanical hinge at its base, was evaluated and is shown in Table 1(d). This should be compared with the matrix in Table 1(a).

Mode Shapes and Frequencies of Vibration. Based on the flexibility matrix given in

Tables 1(a) and 1(b), the vibrational characteristics of the structure were determined using the SAP-80 computer program [8]. The values obtained for the first three mode shapes (cracked I) and periods (cracked and uncracked I) are shown in Fig. 3(a). Figure 3(b) gives similar results obtained experimentally on the full-scale model in Japan [3]. The periods based on the uncracked I were closer to those measured in the full-scale model of the structure before any test was conducted (0.474 sec. vs. 0.43 sec.). Only after tests conducted up to yielding of the model does the fundamental period become closer to the value of T based on cracked I (0.850 sec. vs. 0.55 sec. before yielding to 1.16 sec. after yielding).

2.2.3 Predicted Behavior of Structure under Monotonically Increased Lateral Loads. The test building was analyzed under a monotonically increased lateral load using a modified version of the computer program ULARC [9]. The main results [5] are illustrated in Fig. 4(a) as lateral force-displacement relations. There are two curves, one representing the response of the structure to an inverted triangular distribution of lateral force, as assumed by the UBC, and the other based on a rectangular distribution. The P-Δ effect was also studied and the resulting curve for the case of gravity load plus uniform distributed (rectangular) lateral force is shown in Fig. 4(b). From the results presented in Fig. 4, it can be seen that:

1. The P-Δ effects were relatively small—about 5% at the largest displacement.
2. The lateral shear resistance of the structure under a uniform distribution of lateral force is about 30% higher than that under an inverted triangular distribution, 819 kips vs. 664 kips (3.64 MN vs. 2.95 MN).
3. For a uniform distribution of lateral load, the shear wall yields in flexure under a total lateral load of about 471 kips (2.10 MN). After the shear wall has yielded, the lateral stiffness of the structure decreases by about 60%, which clearly indicates the importance of the main wall in controlling lateral response. This is also clearly shown by the flexibility matrices of Tables 1(a) and 1(d).

The maximum shear induced in the wall under uniform lateral load was less than the 488 kips/0.85 = 574 kips (2.55 MN) estimated as nominal shear resistance of the wall using UBC procedures.

From comparison of the responses shown in Figs. 2 and 4, the lateral overstrength of the structure with respect to the demanded (or expected) UBC strength becomes clear (the supplied quasi-static strength under a triangular lateral force distribution is 664 kips (2.95 MN) versus the UBC demanded strength of 272 kips (1.21 MN), i.e. 2.4 times larger). If the distribution of lateral force were actually uniform, then the supplied quasi-static strength of 819 kips (3.64 MN) would be 3 times larger than the UBC demanded strength.

The small difference between the predicted collapse load of 607 kips (2.70 MN) of Fig. 2 and the 664 kips (2.95 MN) of Fig. 4 was due to different deformation hardening characteristics. In comparing the stiffness of the expected UBC response of Fig. 2 and that of the estimated response of Fig. 4, it is also clear that the supplied initial stiffness of the designed structure was considerably higher than that required by the UBC.

2.2.4 Seismic Response of Structure. The nonlinear response of the full-scale model of Fig. 1 to two ground motions (the Miyagi Oki (MO) earthquake record shown in Fig. 5 and the first 4 seconds of the Derived Pacoima Dam (DPD) earthquake record shown in Fig. 6) was analyzed by Charney and Bertero [5] using the nonlinear dynamic analysis computer program DRAIN 2D [10]. The goals of these analyses were:

(1) To evaluate the nonlinear behavior of the structure when subjected to intense ground motion and, in this way, to be able to judge the soundness of the designed structure and determine the type of ground motion which would be critical for such a structure so that a rational experimental program could be formulated for the 1/5th-scale model shaking table tests.

(2) To gather data on the expected magnitude of response (forces, displacements, rotations, and accelerations) so that instrumentation for the 1/5th-scale model could be designed and installed.

The Japanese researchers conducted similar nonlinear analyses under the MO earthquake record using a computer program developed by Chavez [11].

The modeling of the structure for such analyses was as follows. A detailed discussion of the modeling is given in Refs. 5 and 12.

Global Modeling. In modeling the structure, an analytical model such as that shown in Fig. 7 would commonly be used. This model can be considered pseudo-three-dimensional since only in-plane interaction is considered.

Local Modeling. The individual beam, column, and wall elements of the structure shown in Fig. 1 or of its model (Fig. 7) were modeled as one- and two-component models. For the columns of the structure, a two-component beam-column element was used. Figure 8 illustrates the associated yield surface used for the two-component model. The girders and the shear wall were modeled by a single-component model with stiffness degradation. Figure 9 illustrates the one-component model, the modified Takeda hysteretic model, and the yield surface used. In the analyses conducted at Berkeley under the two earthquake ground motions, it was assumed that the structure had already been subjected to maximum wind loads and minor earthquakes. For that reason, the modeling of the elements was based on cracked, transformed section mechanical characteristics. On the other hand, the results obtained by the Japanese researchers were based on uncracked cross-section characteristics.

Summary of Main Results. Only the envelopes of base shear vs roof displacement, illustrated in Fig. 10, are presented here. While Chavez [11] predicted that under the 0.36g MO earthquake record the structure would develop a maximum shear of 661 kips (2.94 MN) at a lateral roof displacement of 8.1 inches (206 mm), analyses conducted by Charney and Bertero [5] indicated a maximum base shear of 767 kips (3.41 MN) at

a roof displacement of 5.7 inches (145 mm). While the *maximum base shear* predicted by Charney and Bertero [5] using nonlinear dynamic analysis was 16% greater than that predicted by Chavez, it was between the two base shears (664 and 819 kips (2.95 and 3.64 MN, respectively)) predicted under static load (Fig. 4). The response of the model used by Charney and Bertero to the 0.40g DPD earthquake record (Fig. 6) showed that the model developed a maximum base shear of 868 kips (3.86 MN) when the roof displaced laterally about 8.0 inches (203 mm) [5].

From the results obtained in these nonlinear analyses, it was concluded that the strength supplied to the designed structure could reach 868 kips (3.86 MN), 3.19 times the strength required by the UBC (1.4E for $K = 0.8$) (Figs. 2 and 10). The results also indicated that if the MO record were used during the simulated earthquake tests, the model could be subjected to ground motions simulating not only 0.36g MO, but also 0.40g MO, and perhaps even an 0.45g MO earthquake record.

Furthermore, the results showed clearly that the main shear wall controlled the behavior of the whole structure, resisting almost 90% of the total shear in the elastic range. At maximum shear force in the structure under the MO record, the main shear wall resisted 71% of the total base shear. Similar results were obtained under the DPD record.

2.3 Concluding Remarks Regarding Analytical Studies

2.3.1 Soundness of Full-Scale Model Design. Strictly speaking, the design did not satisfy UBC requirements for either a $K = 0.8$ or a $K = 1.0$ structural system. However, because of the way that the members were proportioned and detailed, very small shear and axial stresses were expected to develop during a major earthquake. Therefore, desirable behavior of the structure with adequate deformability was expected.

The results from all analyses indicated that the response of the structure would be controlled by the behavior of the shear wall, which in the linear elastic range would

resist almost 90% of the total lateral force. Once the wall had yielded, which was expected to occur under a total shear varying from 400 to 500 kips (1.78 to 2.23 MN), there could be a considerable drop in stiffness of the whole structural system (decreasing by about 60%), and the frame would begin to resist a larger percentage of shear. At yielding of the whole structure, expected to occur under a total base shear varying from 664 to 868 kips (2.95 to 3.87 MN), the shear wall would resist about 70% of the total base shear.

The results of all analyses conducted also indicated that the strength supplied to the structure (664 to 868 kips (2.95 to 3.87 MN)) should be between 2.4 to 3.2 times the strength demanded by the UBC (272 kips (1.21 MN)). The stiffness of the resulting designed structure was significantly larger than the UBC required lateral stiffness. The P-Δ effect was negligible.

2.3.2 Critical Ground Motion. The nonlinear dynamic analyses conducted under the MO and DPD records indicated that since the MO record induced a large number of cycles of significant yielding with near full reversal of deformation, it would be desirable to test the model under this ground motion rather than under the DPD record. For the MO record, the structure was assessed to be capable of resisting this type of ground motion normalized to a peak acceleration of 0.40g, and perhaps even 0.45g. It was also recommended that other ground motion records which would induce more yielding cycles with full or nearly full reversal of deformation be investigated for possible use in testing.

2.3.3 Largest-Scale Model that Could be Tested to Collapse on Earthquake Simulator. Analysis indicated that the weight of the structure to be tested (Fig. 1) was 2501 kips (11.13 MN) and that it would be necessary to simulate ground motions such as the MO record with a peak acceleration of 0.40g and even 0.45g to induce failure of the structure. Based on these analyses, and considering the limitations on capacity of the earthquake simulator facility at U.C. Berkeley, the largest model of the test building

that could be accommodated was a 1/5th-scale model [13].

III DESIGN AND CONSTRUCTION OF 1/5th-SCALE MODEL

3.1 Introductory Remarks

A main objective of the U.S.-Japan research program and of the studies conducted at Berkeley was to evaluate the reliability of experimental techniques for predicting the seismic response at all limit states of reinforced concrete frame-wall structures, such as the test building in Fig. 1, by utilizing a medium-scaled replica of the full-scale model. Every effort was therefore made to design and fabricate a true replica on the largest feasible scale. The scale chosen for the model test specimen was dictated by the limitations of the U.C. Berkeley shaking table [14,15]. The maximum weight that can be accommodated by the table is about 120 kips (0.53 MN) if the table is to induce accelerations of the order of 0.40g. Based on this limitation and the desire to study the seismic response of the building to failure, with particular emphasis on the detailed study of failure mechanisms, a 1/5th-scale model of the test building in Fig. 1 was selected. A summary of problems encountered in the design and fabrication of this 1/5th-scale model is presented below. These problems have been discussed in detail in Refs. 13, 16, 17, and 18. The overall design of the model is summarized first, then the mechanical characteristics of the constituent materials of the 1/5th-scale model are presented and compared with those of the full-scale model. After a brief description of the 1/5th-scale model fabrication and instrumentation, problems encountered in the simulation of the reactive mass and gravity forces and the simulation of boundary and loading conditions are briefly discussed.

3.2 Design of 1/5th-Scale Model

As discussed in detail in Ref. 13, the model was designed to comply with the similitude requirements for a direct reduced-scale model of the full-scale model shown in Fig. 1. Of the three types of direct models suggested in Ref. 19 ((1) a true replica model; (2) a model which uses materials with the same properties as materials in the

full-scale model but with additional nonstructural mass; and (3) an identical model in which gravity forces are neglected), the most suitable model was determined to be type (2), i.e., a model which satisfies similitude with regard to geometric and loading parameters and also complies with all material requirements, except for mass density. To satisfy the similitude requirement governing mass density, the reinforced concrete mass was augmented by lead ballast attached to the roof and floor slabs so as to avoid any significant effect on the structural stiffnesses and strengths of the bare model.

3.2.1 Geometric Similitude. This similitude requirement was satisfied by designing and fabricating the model as a 1/5th-scale true replica of the full-scale model within a tolerance of 0.06 in. (1.5 mm) in the finished dimensions. There were two exceptions to this. First, the design of the 1/5th-scale model foundation differed from that of the full-scale model to enable proper attachment of the 1/5th-scale model to the shaking table. Although the foundation had a different shape, design, and detailing than the full-scale model, its stiffness was sufficiently large (as was that of the full-scale model) that it was considered to be a rigid foundation. Although the 1/5th-scale model foundation mass did not satisfy the similitude requirements, this did not matter because this mass is not part of the structure's reactive mass.

The second exception was in the geometric similitude of the free-standing, first-story columns. As illustrated in Fig. 11, force transducers were inserted near the mid-height of these columns. Since the distribution of internal forces among the structural components (columns and main shear wall) at the base of the structure was considered to be a very important response characteristic, the internal forces (shear and axial forces and moments) were measured at each of the first-story columns directly by using specially designed force transducers with nearly the same axial and flexural stiffness as the reinforced concrete of the region of the columns that they replaced. A detailed description of the design, fabrication, calibration, installation, and use of these transducers is given in Ref. 18.

The reinforcing bars of the full-scale model were reproduced on a one-to-one basis in the reduced-scale model. Figure 11 illustrates typical reinforcement detailing of frames A, B, and C of the model. The three types of reinforcement used in the model and their effective cross sectional areas were evaluated to satisfy similitude within 10% [17]. Also, the concrete aggregate used in the full-scale model was scaled by using microconcrete in the 1/5th-scale model.

3.2.2 Model Materials and Mechanical Characteristics. The most difficult step in attaining a true replica model, with the same strain response history as the full-scale model when subjected to similar seismic effects, was in satisfying requirements for the mechanical characteristics of the constituent materials. Because a main objective of the research program was to evaluate the reliability of experimental analyses of reduced-scale models in predicting the behavior of full-scale models at all limit states up to collapse, the individual stress-strain relations as well as bond characteristics of the reduced-scale model microconcrete and reinforcing steel had to be close to those of the materials used in the fabrication of the full-scale model throughout the expected range of strain up to and including those which would occur during the collapse limit state responses of the structure.

Due to difficulties involved in fabricating model materials with identical stress-strain relations up to failure, the elements of the structure which would control structural behavior were first identified as were the critical regions of those elements where inelastic behavior would concentrate. If the critical regions of the controlling structural members which will behave inelastically are identified, then only at these regions will it be necessary that the complete stress-strain relation of the original materials be identical. In regions that remain elastic, only the material mechanical characteristics necessary to reproduce elastic behavior need be reproduced. This identification philosophy was followed in the selection and fabrication of the model materials.

Linear and nonlinear analyses of the structure were used to identify the critical

regions of the structure and to assess the material response characteristics which particularly influenced the post-yield response of critical regions [5]. From evaluation of the results obtained in these analyses, it was concluded that characteristics of the main flexural reinforcement of the wall edge members within the first story and of the beams within their end regions constituted the critical material responses that would control the post-yield response of the complete structure. The stress-strain characteristics of concrete, particularly under plane stress conditions, were expected to control the serviceability and initial damageability responses of the structure up to flexural cracking of the wall which was close to first yielding of the wall reinforcement.

Reinforcing Steel. Three sizes of reinforcement, D10 (9.5 mm), D19 (19.1 mm), and D22 (22.2 mm), were used in the design and construction of the full-scale model above the foundation level [20]. The areas of these bars are given in Table 2 and their main mechanical characteristics are given in Table 3 and illustrated in Figs. 12-14 [17]. Reinforcing bars geometrically similar in the 1/5th-scale to those in the full scale were not commercially available. The required diameter of such bars would have been 2, 3.8, and 4.4 in mm. In a search of most of the research institutions at which investigations of reduced-scale models of reinforced concrete structures are conducted, it was discovered that the Portland Cement Association (PCA) has used deformed bars designated as PCA/D2 and PCA/D2.5, which could be considered to satisfy the geometric similitude requirements for the D19 and D22 bars used in the full-scale model. The mechanical characteristics of these two available bars were therefore investigated to ascertain whether they would satisfy the similitude requirements. Furthermore, it was decided that to simulate the D10 bars, it would be necessary to deform plain wire in the laboratory at Berkeley. The areas of the model reinforcing bars determined by various techniques are given in Table 4.

The stress-strain responses of reinforcing steel were considered to be characterized by: the modulus of elasticity, yield stress, length of the yield plateau, initial strain

hardening modulus, maximum tensile strength, and ultimate strain. Hysteretic stress-strain response characteristics were also considered important in assessing material response similitude [17].

Comparison of the stress-strain relationships of two of the three original (virgin) available model reinforcements (Fig. 15) with those for the full-scale materials (Figs. 13, 14), and the values given in Table 3 clearly indicate that they were quite different. To tailor the stress-strain relationship of the model reinforcing bars to that of the steel bars used in the full-scale specimens, the 1/5th-scale model reinforcement was subjected to extensive trials by heat-treatment processes [17]. After determining the correct heat treatment process for each bar type, all model reinforcement was subjected to such treatment. The final stress-strain characteristics are illustrated in Figs. 12-14 and summarized in Table 5.

In the case of the reinforcement used in the wall panel, slabs, and for transverse reinforcement in the beams and columns, heat treatment was followed by cold-working in order to straighten the material. Since this material consisted of 0.08 in. (2 mm) diameter wire, which was knurled in the laboratory, it tended to be coiled and twisted and had to be straightened after heat treatment. This induced further changes in its stress-strain response [17].

The main characteristics of the 1/5th-scale and full-scale model reinforcement are compared in Tables 6 and 7. Although the model reinforcement characteristics were determined statistically from an adequate number of tests, the characteristics of the full-scale reinforcement were determined as the mean of only three tests conducted for each type of bar. While good correlation exists for the modulus of elasticity, yield force, and maximum tensile strength and strain, large differences in the length of the yield plateau (ϵ_{STH} - ϵ_y) and initial strain hardening moduli are observed. In accordance with the identification philosophy adopted, additional effort was made in the selection of reinforcement bars to be used in the edge members of the 1/5th-scale

model shear wall. These bars were carefully selected from available heat-treated bars so that better correlation with the reinforcement used in the full-scale model could be achieved for all important response parameters.

Concrete. Data available from the construction of the full-scale model in Japan are summarized in Tables 8 and 9, and a typical stress-strain relationship is shown in Fig. 16.

Several trial mixes were designed and tested to obtain a microconcrete mix which could be considered satisfactory. Exact similitude between the stress-strain responses of the model microconcrete and the concrete in the full-scale model was an exceptionally difficult problem.

First, the stress-strain response parameters of concrete, particularly under biaxial stress—as in the panel of the structural wall—and triaxial stress—as in the confined cores of the wall edge columns—were the critical parameters. Unfortunately, neither general constitutive relations nor failure criteria have been reliably established for concrete under such multi-axial stress states. In fact, the state-of-the-art in the experimental determination of concrete stress-strain response characteristics under multi-axial stress states for this material does not allow for reliable general constitutive relations and failure criteria. Consequently, only established experimental procedures were used to determine correlation between the responses of full-scale and microconcrete. These consisted of tests of cylinder specimens (6-in. by 12-in. for the full-scale concrete and 3-in. by 6-in. for the microconcrete; 1 in. = 25.4 mm) under compression and splitting, and modulus of rupture beam specimens tested under flexure. Tests to determine the shrinkage and bond characteristics of the microconcrete were also conducted.

Secondly, as has been reported in the literature, microconcrete is usually less stiff and the compressive strain capacity and tensile strength are larger than those of concrete with the same compressive strength [21].

The microconcrete mix design finally selected for the 1/5th-scale model is given in Table 10. The main mechanical characteristics of the microconcrete are given in Table 11. The uniaxial stress-strain responses of the full-scale and microconcrete cylinder specimens taken during casting of the first stories of the full- and 1/5th-scale models are compared in Fig. 16. The microconcrete was selected based on the correlation between the 28-day response of trial mixes and the 145-day response of the full-scale concrete. It was projected at the time that the microconcrete was 28 days old that its response would approach that of the full-scale concrete by aging. The more than 58% increase in its strength by aging, however, was not anticipated, and the microconcrete at 216 days was 38% stronger than the full-scale concrete.

The average tensile strength of the microconcrete at the age of testing of the 1/5th-scale model (747 psi (5.15 MPa)) was approximately twice that of the full-scale concrete. Its Poisson's ratio was measured during cylinder tests to be between 0.13 and 0.33, depending upon stress level. Its shrinkage coefficient, determined from standard tests, was 0.0011 at 40 days [17]. An average maximum bond stress of $13\sqrt{f_c'(psi)}$ ($34.1\ \sqrt{f_c'(kPa)}$) between column reinforcement and microconcrete occurred during pull-out tests [17]. The tensile strength, Poisson's ratio, shrinkage coefficient, and bond stress capacity of concrete were response parameters that were not simulated. Furthermore, although the shear modulus of rigidity, thermal coefficient of expansion, and the influence of strain rate, strain gradient, and multi-axial stress fields and histories on the constitutive relations and failure criteria were important characteristics of the concrete in the full-scale model which inevitably affected the limit state responses of the structure, these characteristics were not explicitly simulated by the microconcrete used in the 1/5th-scale model.

The anchorage lengths of all reinforcing bars were directly scaled down from those specified for the full-scale model, and because of the better bond characteristics of the smaller diameter bars, the anchorage of the 1/5th-scale model reinforcing bar was

significantly better than that of the full-scale model reinforcement.

From comparison of the data available from the concrete used in the fabrication of the full-scale model and the microconcrete used in the 1/5th-scale model, it was concluded [17] that although it was possible to achieve good similitude for the modulus of elasticity E_c and the Poisson's ratio ν_c at stress levels corresponding to serviceability limit states (and therefore good correlation could be expected in the so-called linear elastic range of concrete), the tensile strength and bond characteristics of the concrete in the full-scale model could not be simulated by the 1/5th-scale model microconcrete, for which shrinkage was also substantially larger. The reliability of the microconcrete in simulating the cracking limit state of the full-scale material is therefore questionable.

3.3 Model Fabrication

The 1/5th-scale model, constructed by a private contractor in Berkeley specializing in the construction of models, was constructed over a period of about six months in the earthquake simulator laboratory. After heat treatment and straightening, all reinforcing bars were carefully selected and classified before providing them to the contractor in 12-foot lengths. The concrete materials were batched after determining the moisture content of the aggregate and then stored in airtight containers and provided to the contractor. In Ref. 22, the construction of the model is discussed in detail. Only those aspects that may depart from the ordinary construction of full-scale structures and those that could significantly affect the mechanical behavior of the model are summarized below.

Because the reinforcement in the full-scale model was spliced by a special gas-welding process which could not be duplicated, vertical splicing of reinforcement was avoided wherever possible. The vertical reinforcement of the main shear wall and of its edge members was spliced only once at the middle of the third story. The reinforcement of all free-standing columns was cut and welded to plates located near the mid-height of the first story to leave the required space for the internal force transducers

(Fig. 11), and this reinforcement was then spliced only once at the middle of the fifth story.

After the foundation and the bottom halves of all first-story free-standing columns had been cast, the model was cast story-by-story, the construction joint being located just above the floor slab in each story. The microconcrete was mixed in two 3 cu. ft. mixers and was transported by buckets and placed in the formwork. During the eight times that concrete was cast, the slump varied between 7-1/2 to 9-1/2 in. (191 mm to 241 mm), fluctuating due to differences in humidity and temperature.

No problems were encountered in the placement of the concrete, except for the first-story peripheral end walls, which were only 1-3/16 in. (30 mm) thick and had two curtains of reinforcement. The microconcrete was compacted by vibrators mounted externally against the formwork and wet-cured by retaining all the formwork at all the levels through the end of construction, and for another 28 days for the uppermost floors.

A very large number of control specimens (cylinders and beams) were cast as each story of the model was cast. After 14 days these specimens were put on the corresponding floor of the model in order to subject them to the curing conditions of the concrete in the model.

After the forms were stripped, a check of the errors as far as overall plan and elevation dimensions indicated that these were within $\pm 1/8$ in. (3 mm). A check of the member dimensions indicated that a maximum variation from the specified dimensions of $\pm 1/8$ in. (3 mm) existed in some beams and columns, except at some beam-column joints where it was noticed that deviations on the order of $\pm 1/4$ in. (6 mm) had occurred. Whenever possible the excess of microconcrete was chiseled out and/or ground out and cement paste was used to patch regions where insufficient microconcrete had been cast.

After the model had been fabricated, the uniformity of the microconcrete mechanical characteristics through the model was investigated using the rebound or impact hammer test devised by Schmidt [23]. The rebound numbers were consistent with the desired strengths and quite uniform throughout the model.

3.4 Instrumentation.

Besides the Internal Force Transducers (IFT) [18] at mid-height of the first story columns, the model was instrumented to record overall response and local behavior of the critical regions of the most severely strained members. Internal and external gages to measure average strain along the main reinforcing bars and at the surface of the microconcrete were placed at the critical regions of structural members (Figure 17). Rotations in the critical regions of the main shear wall and the first-story columns and regions of the girders expected to undergo large inelastic behavior were measured by special arrangements of DCDT's (Direct Current Linear Voltage Differential Transformers).*

Displacement transducers (L.P.'s*, i.e. linear potentiometers and DCDT's) were located at each floor of the model and connected to a steel reference frame placed outside the shaking table to record the overall lateral response of the model (Fig. 17). At least two accelerometers were also located at each floor to measure total lateral acceleration. Two accelerometers were placed at the top of the free-standing columns of frame B to measure vertical acceleration. Vertical displacement of the roof and lateral displacement in the direction perpendicular to the direction of ground motion were measured by DCDT's connected to the three-dimensional steel truss located around the model as illustrated in Fig. 18. In total, 124 channels of instrumentation were used to record the input motions and the global and local behavior of the model. Eleven of these channels were used to record the responses of the shaking table.

* The LP's were 30-in. position/displacement transducers manufactured by CELESCO, Inc. of Canoga Park, California, and the DCDT's were 0.2, 1.2, and 6-in. Direct Current Linear Voltage Differential Transformers manufactured by Hewlett Packard in Palo Alto, California, abbreviated as DCDT.

3.5 Simulation of Reactive Mass and Gravity Forces

In order to attain gravity stresses in the 1/5th-scale model similar to those within the full-scale model, and to simulate the reactive mass of the full-scale model, the mass of the 1/5th-scale model was augmented by lead ballast such that the total reactive mass was related to that of the full-scale structure by the inverse of the square of the scale factor ($1/S_f^2$) [19]. Lead bricks or ingots were distributed and prestressed on the floor slabs [24], so that the gravity stress distribution within the model would be similar to the distribution evaluated for the full-scale structure. Steel and rubber pads were used under the bricks to avoid altering the axial or flexural stiffnesses of the diaphragm system while still enabling the lead to be excited by the same acceleration as the diaphragm. Figure 19 illustrates the arrangement and attachment of the lead ingots to the model floor slab and an overall view of the model loaded with ballast.

3.6 Simulation of Boundary and Loading Conditions

The foundations of both the 1/5th-scale and full-scale models were designed to simulate fixed-base conditions. The loading conditions, however, differed significantly. The full-scale structure, tested pseudo-statically, was loaded at each floor by a horizontal actuator, except at the roof where there were two horizontal actuators that restrained the roof diaphragm against torsional rotation. The actuators applied an inverted triangular distribution of force to the structure at all times, and the roof displacement was controlled in order to apply a displacement history which was obtained through an on-line computer-controlled (active) loading scheme, termed the pseudo-dynamic method [25].

After the foundation of the 1/5th-scale model had been prestressed to the very rigid platform (table) of the earthquake simulator, the model was tested by shaking it through horizontal motions introduced by the action of the table. In addition to horizontal motion, however, the table exhibited some small vertical and rotational motions, which resulted in different base conditions for the full- and 1/5th-scale

models. Due to differences in the methods used to test the two structures, the strain rates developed in the 1/5th-scale model were significantly higher than those developed in the full-scale structure, which was under almost sustained load due to the relatively slow pseudo-dynamic loading process used.

The time scale factor for the model is equal to the square root of the linear dimension scale factor ($S_l^{1/2}$) [19]. Thus, even if the full-scale model had been tested on a shaking table, it would have been subjected to a ground motion $\sqrt{S_l} = \sqrt{5} = 2.24$ times slower than that used to test the 1/5th-scale model and the frequency of response of the 1/5th-scale model would be 2.24 times higher than that of the full-scale model, resulting in a corresponding increase in the rate of strain of the reduced-scale model material with respect to that of the full-scale model.

Furthermore, the excitation histories applied to the full- and 1/5th-scale models were not of similar duration. Due to the time required to apply displacements, and the error accumulation problems in the pseudo-dynamic test scheme, the full-scale structure was tested for short durations of the ground motion. The 1/5th-scale model was tested under complete durations of ground motion records, as will be described subsequently. Consequently, although the response histories of the two structures are related they do not correlate well, making the evaluation of correlation studies of experimental results for the reduced- and full-scale models difficult.

3.7 Simulation of Initial Conditions for Each Experiment

It was considered impractical to attempt complete similitude of initial conditions, here defined as the state of forces and distortions and the mechanical characteristics of the structure prior to testing. During fabrication of the 1/5th-scale model the gravity stresses were significantly smaller than those that developed during construction of the full-scale model. For the gravity stresses to be equal at all times, it would have been necessary to load each floor of the 1/5th-scale model with auxiliary mass (lead ballast) as soon as it was constructed, or at least as soon as the formwork of the floor was

removed. The forces and distortions in the 1/5th-scale model, prior to the addition of auxiliary mass, were measured and determined to be strongly influenced by the shrinkage as well as thermal expansion characteristics of the microconcrete. The internal forces at the base of the structure due to either shrinkage and differential shrinkage, or daily cycles of temperature, were of the same order as the gravity forces [18, 24]. Since the volumetric change characteristics of the microconcrete were evaluated to differ significantly from those of the concrete in the full-scale model, the initial states of force and distortion in the 1/5th- and full-scale models were expected to differ. Fortunately, the initial flexibility characteristics, fundamental frequency, and damping characteristics of the two models were reasonably close after the mass of the 1/5th-scale model had been augmented by the lead ballast.

IV INITIAL MECHANICAL CHARACTERISTICS OF 1/5th-SCALE MODEL

4.1 Introductory Remarks

After the bare model had been fabricated and cured it was subjected to a series of static and dynamic tests to determine its initial flexibility or stiffness, frequency, and damping characteristics [24]. These tests were repeated after the lead ballast had been added so that similitude requirements for the gravity stress level as well as translational reactive mass were satisfied. The objectives of these tests were to assess the reliability of: (1) experimental analysis of reinforced concrete frame-wall structures based on medium-scale, true or distorted (gravity forces neglected) models; and (2) analytical response prediction through commonly applied analytical modeling schemes. For both these cases, the initial, uncracked serviceability limit state of the structure, and the narrow-crack serviceability limit state, for which elasticity is generally assumed, were used. Another objective was to establish the initial static and dynamic characteristics and force distribution of the model structure before the earthquake simulator tests were begun.

4.2 Results of Studies

The results of the dynamic tests are summarized in Table 12. The structure's fundamental frequency, before and after the addition of the auxiliary mass (lead ballast), was obtained by ambient vibration, dynamic analyzer, forced-vibration, and free-vibration techniques [24]. Except for the ambient vibration tests, an equivalent viscous damping coefficient was also estimated during the experiments.

As expected, the fundamental frequency differed somewhat depending on the technique used in its determination. In tests conducted on the model before the addition of the auxiliary mass (lead ballast), the maximum variation was 15 percent. This maximum variation was only 5 percent when the model was loaded with lead. The variations arose from differences in stress level induced by the test procedures and were

not as pronounced after the ballast load had been applied. The damping coefficient of the structure appears to have decreased after the model was loaded by the lead ingots, but not as much as might have been expected since for elastic structures this coefficient is inversely proportional to the square root of mass and stiffness. When loaded by the lead ingots, not only did the mass increase, but also the stiffness because existing microcracks in the wall and columns closed, leading to a stiffer concrete.

The pure analytical results shown in Table 12 indicate that the linear elastic analytical model—based on uncracked transformed section stiffnesses, rigid joint zones, a secant modulus of elasticity of concrete at 15 percent of ultimate strength (the average stress level assessed to be induced during these service level dynamic tests), and a Poisson's ratio of 0.20—overestimated the stiffness of the structure significantly, leading to a frequency of 12.45 Hz for the structure prior to loading with ballast. This is 43 percent higher than the frequency obtained from the free-vibration test.

The pure analytical result after the ballast had been applied, 5.09 Hz, is only 7 percent higher than the experimental frequency obtained from the free-vibration test. The semi-analytical results given in Table 12 were obtained by using measured flexibility characteristics and a theoretical lumped-mass representation of the structure. These results agree closely with the experimental results, indicating that the errors in the analytically computed frequencies are due to the idealized modeling of stiffness, not the idealized modeling of mass.

The frequency and damping coefficients of the full-scale model (after increasing the measured frequency by multiplying it by $\sqrt{S_l} = \sqrt{5}$ so that it could be compared with that of the 1/5th-scale model) were 5.20 Hz and 2.1%, respectively. The frequencies of the full-scale and 1/5th-scale models from the free-vibration technique differed, therefore, only by 9%, indicating that the initial dynamic characteristics of the models were reasonably similar before the earthquake simulator tests were begun.

The axial force distribution measured at the base of the 1/5th-scale model, after

the auxiliary mass had been added, is compared to the distribution calculated based on the tributary areas of the vertical members in Fig. 20. The analytical and experimental forces differ considerably, exceeding 40% in the case of the main wall. These differences are due to differences in the shrinkage of vertical members, which was not incorporated in the analytical procedures. Since the rate and amount of shrinkage increases with the ratio of the exposed surface area to the volume of a member, it is obvious that significant differential shrinkage occurred between the walls and the columns. Furthermore, both shrinkage and differential shrinkage expected from the 1/5th-scale model were substantially higher than the corresponding value for the full-scale structure [17], indicating a distortion in the initial stress state of the reduced-scale model. Upon cracking and release of the stresses associated with shrinkage, however, this distortion would have been expected to decrease and disappear at ultimate limit states.

The flexibility characteristics of the model prior to and after the ballast had been applied are illustrated in Fig. 21. The lateral stiffness of the structure increased significantly when the ballast load was added. Since the lead ballast gave rise to an increase in gravity load of more than 400 percent, the compressive axial force in the columns and particularly in the walls also increased significantly. At the base of the main wall, the axial force increased from approximately zero compression (due to differential shrinkage) to approximately 10% of its balanced axial force on the axial-flexural curve. This increase in axial compression caused an increase in the stiffness of the columns and particularly of the wall because the microcracking that would have developed due to shrinkage was closed. This resulted in an increase in the average lateral stiffness of the structure of approximately 40% [24]. The observed effect of axial stress on lateral stiffness is not usually incorporated in the analysis of structures. The cross-sectional analyses conducted for the wall, using the measured stress-strain relations for concrete, did not indicate any appreciable increase in the effective flexural

rigidity of the cross section due to the increase in axial compression from zero to 10 percent of the balanced axial force. Comparison and analysis of the experimental displacement profiles from the model before and after the ballast had been applied indicate that although both the flexural and shear stiffnesses increased due to increased axial stress, the larger increase was in the shear stiffness. This is in accord with results obtained previously which indicated that the shear rigidity of concrete may be substantially affected by an increase in compressive stress [26].

The lateral flexibility characteristics of the 1/5th-scale model approached those of the full-scale structure (Fig. 21), and the analytical flexibility characteristics were reasonably close to measured values, after similitude in the gravity stress level was satisfied. The effect of axial stress level on lateral stiffness also explains the discrepancy in the analytical and measured frequencies of the model before loading the ballast (Table 12). This discrepancy was substantially smaller after the ballast had been added.

V EARTHQUAKE SIMULATOR RESPONSES OF 1/5th-SCALE MODEL

5.1 Earthquake Simulator Test Program

After the 1/5th-scale model had been placed on the shaking table and loaded with the necessary auxiliary mass (lead ballast) and its initial mechanical characteristics had been determined by the series of tests described in the previous section, the foundation of the model was subjected to a series of simulated ground motions, described in the excitation program summarized in Table 13. Also included in Table 13 are the measured frequency and damping characteristics of the model during the course of the general test program. The earthquake simulator tests were classified into three series. The first series was intended to be diagnostic, i.e., low amplitude tests, conducted to check the operation of the earthquake simulator, data acquisition system, and instrumentation and to generate the initial uncracked serviceability limit state responses. Due to a breakdown of the simulator, however, the model was subjected to transverse excitation, which induced some cracking, during the final earthquake shaking test (#33) of the first series.

The second series of tests, which consisted of base motions of increasing intensity, was designed to induce successive stages of damageability and collapse limit state responses, resulting in a complete flexural failure at the base of the main wall and extensive yielding throughout all frame elements.

Before the third series, the model was repaired and retrofit by strengthening and stiffening the bottom 6.5 inches of the wall. The model was then subjected to a series of particularly intense base motions to study the effectiveness of the repair as well as the collapse limit state response characteristics.

As indicated in Table 13, the model was subjected to a total of sixty-two tests. Some were harmonic motion or free-vibration tests conducted to determine changes in the frequency and damping characteristics of the model and to assess the effect of pos-

sible table-structure interaction on the reproduction of ground motion.

5.1.1 Shaking Table Input Motions. The main tests were conducted using as input to the shaking table the displacement time histories corresponding to two acceleration records designated as Miyagi-Oki (MO) and Taft (T). These records (normalized to a peak acceleration of 1.0g and with adjusted time scales, i.e., compressed by $\sqrt{5}$) are modified versions of recorded ground motions (Fig. 22). The modifications were introduced by Japanese researchers to make them suitable for the pseudo-dynamic testing of the full-scale structure. The modified records were used as source inputs by the institutions participating in the joint cooperative research program.

The displacement time histories obtained by integration of these modified acceleration records were used as input to the U.C. Berkeley earthquake simulator after scaling the time by a factor of $1/\sqrt{5}$.

The Fourier amplitude spectra of these two records, shown in Fig. 23, indicate that the Taft input had a broader frequency content (wider frequency range) with damage potential, while the Miyagi-Oki input was considerably less intense over the complete range of frequency. However, the Miyagi-Oki record appears to possess damage potential concentrated at certain frequencies in the range 1.5-3.0 Hz.

5.1.2 Measured or Output Base Accelerations. The base accelerations measured on the platform (table) of the earthquake simulator differed from the input signals, changes arising during the simulation, but mainly from simulator-model interaction. In order to relate the motions measured at the base of the model, the intensity coefficient suggested by Arias [27]* was utilized. For selected tests, the peak measured table acceleration and the corresponding intensity coefficient are shown in columns 1 and 3 of Table 14. A scale factor for the input signal was calculated such that the scaled input

---

* Intensity coefficient, $I = \frac{\pi}{2g} \int_0^t a^2(t)dt$, where a is the acceleration at time t and g is the acceleration of gravity.

signal would have the same intensity coefficient as the measured table acceleration. The peak acceleration of this scaled input signal is given for these tests in Table 14, column 2.

Comparison of the peak acceleration of the measured signal and that of the scaled input signal for different tests indicates that the peak acceleration of the scaled input signal is consistently less. The discrepancy between the peak accelerations listed in columns 1 and 2 of Table 14 may be considered a measure of the lack of fidelity of the earthquake simulator. During test #46, using the Miyagi-Oki record, the discrepancy was as large as 22%, i.e., in this test if the input motion could have been exactly reproduced by the simulator at the base of the structure with the same peak acceleration as the motion actually measured, the damage potential of this hypothetical base motion would have been substantially greater. As a result, the peak acceleration of the scaled input signal (Table 14, column 2) should be compared with the peak acceleration of the input signals used in the analytical and experimental studies conducted at the various institutions participating in the cooperative research program.

5.2 Global Responses: Floor Displacements and Forces

5.2.1 Lateral Forces and Displacement Responses. After analyses of the data and results obtained in all the tests described in Table 13, some tests were selected to represent the successive limit state response characteristics of the structure and are presented herein. These were Tests #7 and #9 from Series 1, Tests #45, #46, #48, and #50 from Series 2, and Test #62 from Series 3, as shown in Table 13.

Tests #7 and #9 were considered to represent the serviceability limit state responses of the structure while Tests #45, #46, #48, and #50 from Series 2 were considered to represent the successive damageability and collapse limit state responses. Test #62 was selected to represent the collapse limit state responses of the structure after the base of the wall had been repaired and retrofit. These tests will be designated as MO 5.0, MO 9.7, MO 14.7, MO 24.7, MO 28.3, T 40.3, and T 46.3, respectively, by

the source motion and the measured peak base acceleration in percent of g.

Envelopes. Envelopes of base shear and base overturning moment, obtained by plotting the maximum base shears and overturning moments during these tests against the maximum interstory drift induced in the structure, are presented in Fig. 24.

Comparison of the base shear-interstory drift curve of Fig. 24 with the similar curves of Figs. 2 and 10 shows that the overstrength of the model was very large not only with respect to the UBC demanded strength (Fig. 2) but also with respect to the predicted strength (Fig. 10).

The 1979 UBC (for $K = 1.0$) and ATC 3-06 lateral force requirements (E load) for seismic design of the full-scale model, assuming it to be located in the zone of highest seismic risk, were 9.67 and 10.61 percent of the weight, W, of the superstructure, respectively. The base overturning demands were 6.61% WH and 7.25% WH (where H is the height of the superstructure), from the 1979 UBC and ATC 3-06 prescribed lateral forces, respectively. The strengths of the structure in shear and overturning moment during the T40.3 test were, therefore, more than 5 times the corresponding demands from the lateral force requirements of the above design documents. Even if the seismic forces of the UBC were multiplied by the given load factors (1.4 for flexural and 2.0 for shear design) the actual measured available strength is still considerably higher than the UBC demanded design strength.

The maximum global response quantities and the time at which these occurred are tabulated in Table 15, together with the effective fundamental frequency of the structure, derived from the overturning moment response through a Fourier transformation procedure [28]. These frequency values can be compared with the values of the fundamental frequency of the model obtained from free-vibration tests, which are included in Tables 12 and 13, indicating that the initial frequency of 4.75 Hz (Table 12) was reduced to 3.67 Hz at the end of the first series of tests (Table 13) to 2.33 Hz at the end of the second series of tests (Table 13) and to 1.96 Hz before the end of the

excitation program (Table 13). The free vibration frequencies are slightly higher than the effective fundamental frequencies given in Table 15, which indicate a change from 4.2 Hz to 1.5 Hz from the MO 5.0 test to the T 46.3 excitation. The initial global lateral stiffness of the structure may be considered to have been reduced by 40% at the end of the first test series, by 75% at the end of the second test series, and by 80% by the end of the test program, based on changes in its fundamental frequency (which means that the initial fundamental period of 0.21 secs. increased to 0.27 secs., 0.43 secs., and 0.51 secs. at the end of the first, second, and third series of tests).

The maximum base shear and overturning moment vs. the maximum interstory drift envelopes in Fig. 24 indicate substantial changes in the stiffness characteristics after the MO 9.7, MO 24.7, and T 40.3 tests.

5.2.2 Time Histories. Typical time histories of the main response parameters are presented in Figs. 25 through 28.

Relative Displacement Time Histories. The relative displacement histories of the top of the structure during the MO 9.7, MO 24.7, MO 28.3, and T 40.3 tests are presented in Figs. 25(a) - (d). While the MO 9.7 response exhibits contributions of a wide range of frequencies, the MO 24.7 response does not and resembles simple harmonic response. The fundamental frequency of the structure decreased to 2.63 Hz before this test, which is a frequency falling within the predominant frequencies of the base motion, as observed from the Fourier spectra in Fig. 23(a).

Although the base excitations during the consecutive MO 24.7 and MO 28.3 tests were similar in frequency content and only 15 percent different in amplitude, the MO 28.3 response exhibits contributions from more frequency components than the MO 24.7 response. The structure was observed to yield during the MO 28.3 response, and this led to changes in its stiffness which were reflected in its response histories.

The T 40.3 response in Fig. 25(d) also contains many frequency components, reflecting the fact that the Taft record has a relatively broad frequency content.

Frequencies of the Taft record were capable of partially exciting the higher modes of the model.

The maximum accelerations at the top of the structure and maximum interstory drift indices during these tests, as shown in Table 15, were 27.4% of g and 0.17% for MO 9.7, 65.2% of g and 0.69% for MO 24.7, 81.3% of g and 1.08% for MO 28.3, and 88.8% of g and 1.68% for T 40.3. Despite such severe and extensive base excitation, a critical permanent set was not observed even after the T 40.3 motion.

The mechanisms of shear and overturning resistance, and the changes in these mechanisms which cause significant changes in the stiffness characteristics of the structure (limit states) during the MO 9.7, MO 24.7, MO 28.3, and T 40.3 tests, will be discussed subsequently. The effects of these tests on the structure, observed in the envelopes in Fig. 24, are reminiscent of the cracking, yielding, deformation hardening, and ultimate capacity of a reinforced concrete flexural element or of a basic flexural subassemblage.

Shear and Overturning Moment Time Histories. The time histories of base shear and base overturning moment of the model during the MO 9.7, MO 24.7, MO 28.3, and T 40.3 tests are presented in Figs. 26 and 27. The shear and moment responses of the structure were evaluated by measuring the translational accelerations at each floor during tests. Assuming the translational mass of the structure to be lumped at each floor, the translational inertial (seismic) forces at each floor were taken as the product of mass and the measured acceleration at that floor. Since $\approx$ 80% of the mass resulted from the ballast load, concentrated at each floor level of the structure, the lumped mass idealization was considered justified.

The force and moment responses of the structure were evaluated by assuming the translational inertial forces and the moments arising from these forces would be resisted solely by the internal forces and moments in the structure. The contribution of any external damping to structural resistance, the contribution of the rotational inertia of

horizontal structural elements to the seismic moments and the effects of vertical acceleration were neglected.

The displacement, shear, and overturning moment responses in Figs. 25, 26, and 27 indicate that these were in phase during each of the MO 9.7, MO 24.3, MO 28.3, and T 40.3 excitations, i.e., the zero crossings and peaks in displacements, shear and moment responses occur nearly simultaneously. The maxima of the displacement and force responses, shown in Table 15, also occur simultaneously during the MO 9.7 excitation. Although the absolute maximum force and displacement responses during the MO 24.7, MO 28.3, and T 40.3 tests do not occur simultaneously, the displacement at the time of maximum force response is very close to the absolute maximum displacement.

Displacement and force responses of the structure during the MO 9.7 excitation (Figs. 25(a), 26(a), and 27(a)) exhibit contributions from a wide band of frequencies. The input signal apparently contained [28] relatively little energy at frequencies close to the fundamental frequency of the structure, 4.1 Hz, as observed from the Fourier amplitude spectra in Fig. 23(a). The response was therefore dominated not only by the fundamental frequency of the structure, but also by the predominant frequencies of the input motion.

The force responses measured during the T 40.3 excitation indicate some higher mode contributions in a manner similar to the measured displacement responses. The MO 24.7 force responses (which are similar to the MO 24.7 displacement response) indicate a simple harmonic response between 1.6 and 8.8 secs., with 17 cycles of full, large amplitude force and displacement reversals. The peak force and displacement demands during all 17 cycles are close to the maxima listed in Table 15. This excitation is observed to be unusually demanding, particularly given the number of large amplitude reversals. At 7.26 secs, i. e., near the end of the phase of severe response, the main wall reached its maximum flexural resistance, that is, its critical section at the

base of the wall reached a fully plastic state. Therefore, the MO24.7 may be considered a critical damageability excitation for the main shear wall, leading to a substantial change in wall stiffness. In spite of the decrease in the wall stiffness, the overall stiffness of the whole structure did not decrease very much.

The decrease in the slope of the base shear-interstory drift envelope response in Fig. 24 after the MO 24.7 test is approximately 68%. The effective stiffness after the MO 24.7 test was 52% of the stiffness prior to this test, as synthesized from the effective frequencies given in Table 15. The MO 28.3 excitation caused extensive yielding of the structure as a result of which its stiffness decreased in the order of 40% as synthesized from the effective frequencies listed in Table 15.

During the T 40.3 test, the model was excited to its maximum shear and overturning strengths and this is indicated in Table 15 and Fig. 24, the corresponding values being 50.8% W and 33.7% WH. The average interstory drift in the structure was larger than 1.5% during the large amplitude response. As illustrated in Figs. 25(d), 26(d), and 27(d), the model underwent at least 3 cycles of near full force-and-displacement reversals with peak force and distortion demands near the maxima given in Table 15. The maximum acceleration at the top of the structure was approximately 0.9g during this test.

Axial Force Time Histories of Columns and Wall. Typical time histories of axial force induced in the interior columns of the exterior frames and the main wall during the MO 9.7, MO 24.7, MO 28.3 and T 40.3 tests are illustrated in Figs. 28(a) through (h). The planar behavior of frames and walls does not alone explain these responses. The interior column A-2 of frame A would be expected to undergo small changes in axial force during horizontal ground motion in the plane of the frame and these changes would be expected to be symmetric. Such changes in column A-2 were, however, unsymmetric (particularly for the MO 24.7, MO 28.3 and T 40.3 tests) and the axial force variation in tension was as high as 9.8 kips (43.6 kN) for the MO 24.7, 13.1

kips (58.3 kN) for the MO 28.3, and 14.6 kips (64.9 kN) during the T 40.3 motion (Figs. 28(b) - (d)). The time variations of the induced axial force change for the column (Figs. 28(a) - (d)). agree with those obtained for the displacement at the top of the structure (Figs. 25(a) - (d)). It was also observed that the larger the tension induced in the columns, the smaller the corresponding moment and shear resisted by the column.

The main wall axial force time histories were also unsymmetric, but the changes in axial compression were larger. Under the MO 24.7 input, the change in axial compression reached a value of 18 kips (80.1 kN). Under MO 28.3 input, the maximum change in compression was 27 kips (120.2 kN), and under the T 40.3 motion the change became 34 kips (151.3 kN), nearly 1.4 times the expected compressive axial force in the wall due to gravity forces. This variation with time occurred with a frequency twice that observed for the displacement (compare Figs. 28(f) - (h) with Figs. 25(b) - (d)).

The asymmetry in axial force in the columns and wall and the higher frequency of change in the wall are due to the three-dimensional interaction of the wall and the frames due to the rocking of the wall. This effect will be discussed in section 5.2.4.

5.2.3 Displacement and Force Profiles Along Height of Model. The distribution of the seismic forces along the elevation of the structure, the corresponding shears and overturning moments, and the relative displacements at maximum response during the MO 9.7, MO 24.7, MO 28.3, and T 40.3 tests, are presented in Fig. 29. The resultant seismic force is observed to act between $0.64H$ to $0.75H$ from the base of the superstructure at maximum shear and overturning responses during all three tests. The location of the resultant lateral force prescribed by both the ATC 3-06 or 1979 UBC for the seismic design of this structure was $0.71H$.

In general, maximum shear and overturning moment would not be expected to occur at identical times. The force and displacement responses of the model were

influenced predominantly by a single mode, i.e., as if the structure were an approximately linear single-degree-of-freedom oscillator with one effective frequency. In fact, the zero crossings and peaks of displacement, base shear, and base overturning moment responses occur nearly simultaneously, as discussed in the previous section, an indication of predominantly single-mode response. This should not be generalized to the seismic response of multistory reinforced concrete structures and is believed to have been caused in part by the lack of power in the source acceleration records to excite frequencies exceeding 7 Hz, as demonstrated by the Fourier spectra in Fig. 23.

The second-mode frequency of the model was measured to be 18 Hz before the excitation program was begun, and softening of the structure could not have shifted this second-mode frequency under 7 Hz. Note that the fundamental frequency during the MO 24.7 test was 2.7 Hz (Table 15) and the second-mode frequency is expected to remain at least approximately three times this value, i.e., larger than 7 Hz. Consequently, the source accelerograms could not excite the second or higher modes significantly, and as a result the response is predominantly in a single mode.

The analysis of the results obtained pointed out the following observation regarding the force distribution along the wall as opposed to the inertial force distribution along the whole structure. In general, the moment to shear ratio at the base of the wall was substantially less than that as implied by the inertial force distribution along the structure, due to the frame-wall interactions. For example, at the times of maximum shear and moment responses of the structure, during the MO 24.7, MO 28.3 and T 40.3 tests, the moment-to-shear ratios at the base of the structure as caused by inertial forces were $0.66H$, $0.65H$ and $0.65H$, respectively (Fig. 29). The corresponding moment-to-shear ratios at the base of the wall, meanwhile, were $0.55H$, $0.39H$ and $0.26H$, respectively, decreasing substantially with further yielding of the wall at each consecutive test. Therefore, it appears that it will be unconservative to design the wall against shear using an inverted triangular distribution of the lateral forces along its

height.

5.2.4 Hysteretic Behavior. The base overturning moment-top floor relative displacement hysteresis relations of the structure are illustrated in Fig. 30 for certain critical durations of the MO 9.7, MO 24.7, MO 28.3, and T 40.3 responses. During these critical time periods, the maximum shear, moment, and displacement occurred. Although the hysteretic energy dissipation of the structure increased with each successive test, the response appears to be approximately linear and it is not possible to observe a pronounced yielding of the structure, with a structural deformation ductility exceeding 4-6, as envisioned by SEAOC or ATC 3-06. This apparently resulted from the test program to which the model had been subjected and should not in any way be interpreted to represent what will occur should a similar structure (practically in its virgin state) be subjected suddenly to a very severe earthquake such as the T 40.3 motion.

The behavior was approximately linear because the model had been subjected to a series of earthquake ground motions of increasing intensity. After each such test, the stiffness of the structure had deteriorated. Because during subsequent tests the intensity did not increase very much from one test to the next, relatively small yielding (and therefore dissipation of energy by hysteretic behavior) occurred. If the whole set of hysteresis loops from each test were drawn in one graph, it would be possible to detect considerable yielding and dissipation of energy due to inelastic behavior. This is partially illustrated in Fig. 30(f) and is also clearly illustrated by the envelope shown in the positive quadrant in Fig. 24.

There was no clear yielding plateau in the hysteretic behavior of the model as would be expected from an ideal linear elastic-perfectly plastic mathematical (or mechanical) model. It is well known, however, that no practical structure exhibits such behavior. What should be pointed out is that this structure offered an unexpectedly high deformation hardening after the first detected yielding of the wall, which, as has been noted before, controlled the behavior of the whole structure.

Local yielding at the base of the wall may have occurred in the structure as early as the MO 9.7 test and definitely by the MO 14.7 test. As discussed before, the wall reached full yield during the MO 24.7 test. Despite this, a definite yield point for the structure can only be identified when the resistance reached a maximum (Figs. 30(c), (d) and (e)) during the largest displacement excursions of MO 24.7, MO 28.3 and the T 40.3 tests. These responses may be designated as "approximately linear" and can be explained only by the particular test program to which the model was subjected and by the high rate of deformation hardening of the structure.

A correct identification of the resistance mechanisms leading to this observed deformation hardening was considered to be extremely important. The outriggering provided to the wall by the frames oriented within and transverse to the plane of the wall was identified as a major cause of the deformation hardening. The wall tended to rotate with respect to its base as an almost rigid body after a plastic hinge had formed at its base, i.e. after all main reinforcement of the edge member had yielded. The displacements of the wall, assuming it was free to rotate about its base, and based on measured plastic rotations along a 7.5-in. (190-mm) plastic hinge length at its base, are indicated within the displacement profiles in Fig. 29 by dotted lines. The displacements arising from such rigid body rotations of the wall resulted in 20, 46, 55, and 78 percent of the total relative displacements at the top of the structure during maximum displacement response during the MO 9.7, MO 24.7, MO 28.3, and T 40.3 tests, respectively.

The outriggering action of the frames on the wall (illustrated in Figs. 31(a) through (c)) and the deformation hardening of the wall at its base would be expected to have restrained the rigid body rotations of the wall. Indeed, substantial increases in axial compression were recorded at the base of the wall (over 100%), and this is clear evidence of the restraint provided by the outriggering system (Fig. 31) against the wall rigid body rotations. The tendency of the wall to grow axially due to cracking and accumulation of permanent strain in its main flexural reinforcement within the plastic hinge

region at the base (first story) also led to axial compression arising from the restraining of such axial growth by the outriggering frame system. The axial compressive force at the base of the wall was measured to have increased from approximately 12% to 28% of its balanced axial force level (Fig. 31(d)).

The stiffness provided to the wall by the outriggering system was not as significantly affected by flexural yielding of the beams (framing into the wall) as one would expect in a perfectly plastic structure, because as the yielding of these beams increased, the contribution of the attached slab (particularly its reinforcement) also increased. Therefore, the flexural stiffness of the complete diaphragm system contributed significantly to the stiffness of the outriggering system. Furthermore, the increase in the axial compression of the wall due to this outriggering mechanism led to an increase in yielding strength and prevented a complete loss in flexural stiffness of the wall at yielding.

The observed levels of deformation hardening in the global overturning moment–top floor relative displacement hysteresis responses in Fig. 30 were therefore mainly caused by the outriggering system provided by the frames to the wall and the hardening of the outriggering action due to the increased contribution of the slab reinforcement. The outriggering system was particularly beneficial during the collapse limit state responses to the third series of tests, after the complete flexural failure of the wall at its base. The restraint and axial compression provided by the outriggering system were so effective that the shear resistance of the wall remained practically constant even after the wall had failed in flexure, as will be discussed later.

5.3 Resistance Mechanisms of Structure

A quantitative study of the resistance mechanisms of the structure was possible since the column forces at the mid first story were monitored by the force transducers, and the axial forces in the peripheral walls could be estimated from concrete strain readings [28], rendering the first story of the structure statically determinate.

5.3.1 Shear Resistance Mechanisms. The total shear resisting mechanisms at the base were the main wall and ten frame columns. Due to their very small out-of-plane lateral stiffness, the contribution of the peripheral walls to the shear resistance in the loading direction was negligible. The total base shear and wall base shear vs the maximum roof drift envelopes are compared in Fig. 32. The contribution of the wall to the total shear resistance was 80% during the MO 9.7 response, decreasing consistently to 66% during the T 40.3 test and to less than 60% by the T 46.3 test.

The difference between the total base shear and wall shear represents the contribution of the free-standing columns, which increases from 20% to 40% in the course of the excitation program. This implies that the wall lateral stiffness decreased more quickly than the frame lateral stiffness at the first story as a result of horizontal and diagonal cracking and yielding of the wall, which occurred earlier than the cracking and yielding of the beams and columns.

5.3.2 Overturning Moment Resistance Mechanisms. The total base overturning moment of the structure was resisted by the flexure in the wall, flexure in the frame columns, and, particularly, by the moment resistance arising from the axial forces of the columns and peripheral walls. The total base overturning moment and wall base moment vs the maximum roof drift envelopes are presented in Fig. 32. Wall flexure contributed 56% to the total overturning resistance during the MO 9.7 test. The contribution of wall flexure decreased to 22% during the T 46.3 test, indicating a more significant deterioration of the wall flexural stiffness as compared to the lateral stiffness of the frame and, particularly, the axial stiffness of the peripheral elements, which contributed to the overturning resistance by their outriggering action. The bending moments induced in the frame columns contributed less than 7% of the total overturning resistance, indicating that the outriggering system accounted for approximately 35% to 70% of the total overturning resistance, its contribution increasing with the accumulation of damage at the first story of the shear wall.

5.3.3 Local Responses of Wall. The main wall was the most important element of the structural system in terms of lateral stiffness and resistance, contributing more than 80% of the total shear resistance and 56% of overturning resistance at the base during the serviceability limit state responses. The wall was instrumented at the first story such that its local responses could be evaluated. The measured quantities were (see Fig. 17): the concentrated rotation (which may be termed the fixed-end or pull-out rotation) at the base of the wall, along a 1 in. (25 mm) region from the interface with the foundation; the rotation along a 3 in. (76 mm) distance adjacent to the first 1 in. region; and the rotation along a 3.5 in. (89 mm) region adjacent to the 3 in. (76 mm) region (Fig. 17(c)). The total rotation along the 7.5 in. (191 mm) at the base could, therefore, be obtained by summing the measured rotations along the first 1 in. (25 mm), the adjacent 3 in. (76 mm), and subsequent 3.5 in. (89 mm) regions. This represented the total plastic hinge rotation at the base of the wall, as the concentrated cracking, spalling and deterioration of panel concrete during the ultimate level responses were indeed observed to be primarily confined to the immediate 7.5 in. (191 mm) at the base. The displacement profiles of the wall, assuming it to rotate as a rigid body at its base through an angle equal to the total measured plastic hinge rotation, are shown in Fig. 29 and were discussed previously in relation to this figure. The displacements that arose at the roof from the plastic hinge rotation at the base of the wall accounted for approximately 20, 46, 55, and 78 percent of the total displacement during the MO 9.7, MO 24.7, MO 28.3, and T 40.3 tests at peak displacement response.

Other local response quantities which were measured were the distortions of the wall along its two diagonals at the first and second stories (Fig. 17(f)). The lateral displacement of the wall at these stories that arose from average shear distortion was, as discussed in Ref. 28, derived from these measured distortions.

The contributions of deformation mechanisms of the wall to the total lateral displacement measured at the first floor are illustrated in Fig. 33 where the wall shear vs

corresponding first floor displacement (and interstory drift) envelope at the time of maximum base shear is presented. The contributions were due to fixed-end rotation, as measured along the first 1 in. (25 mm) region at the base of the wall adjacent to the foundation; measured shear displacement arising from the average shear distortion of the wall alone; and flexural deformation along the wall of the first story. This last contribution includes flexural deformation along the plastic hinge region (except for the fixed-end rotation) and throughout the remainder of the first story. Since the floor displacements were measured from the exterior edge of the diaphragm, rather than at the wall interface, the diaphragm growth is included with flexural displacement. The diaphragm growth could not be measured during the tests due to limitations imposed by the instrumentation. The crack widths measured along the diaphragm after the T 40.3 test indicated a possible cumulative growth on the order of 0.1 in. (2.5 mm) (approximately 20% of total measured maximum displacement at the first floor level during this test).

Figure 33 indicates that the shear displacement accounted for 26, 45, 43 and 34 percent of the total displacement at MO 14.7, MO 24.7, MO 28.3, and T 40.3 peak shear responses, respectively. The relative contribution of shear displacement increased until the MO 24.7 test, after which it decreased somewhat, while the total shear deformations increased.

The fixed-end rotation at the base accounted for 12, 12, 17, and 33 percent of the total displacement at the first floor at MO 14.7, MO 24.7, MO 28.3, and T 40.3 peak shear responses, respectively. Except for within the "elastic" range, the fixed end rotation's relative contribution consistently increased with the successive inelastic limit state excitations as a result of the accumulation of damage and bond deterioration of the reinforcing bars along their anchorage length in the foundation. The remaining flexural displacement of the wall shown in Fig. 33 (which includes the diaphragm growth) is observed to account for 61, 43, 40, and 32 percent of the total first floor dis-

placement at MO 14.7, MO 24.7, MO 28.3, and T 40.3 peak shear responses, respectively. The flexural deformations contribute relatively less to the total displacement as the fixed-end rotation and its contribution increases with each successive excitation.

The fixed-end rotations increased substantially after 3.14 seconds of T 40.3 response, which is the point represented in Fig. 33. The reinforcement in the wall boundary members began to rupture at the foundation interface at 3.16 secs. of T 40.3 response, leading to significant levels of rigid body rotation at the base of the wall, a phenomenon which may be expressed as rocking. At 3.49 secs. of response, fixed-end rotation accounted for 77% of the total first floor displacement, at a magnitude of approximately 0.01 radians.

The migration of the center of rotation and neutral axis of the wall during excitation was an especially critical phenomenon affecting the distribution of demands from adjoining frame elements. The wall increasingly tended to rotate about its base as a rigid body, as discussed previously, in the course of the excitation program, and the migration of the center of rotation at its base significantly affected deformation demands throughout the structure. Average axial strains, computed from the distortions along the 1 in. (25 mm), 3 in. (76 mm) and 3.5 in. (89 mm) regions, measured successively along the steel of the boundary members, from the interface of the wall at the foundation, during times of maximum first floor displacements for different tests, are presented in Fig. 34. Assuming the strain distribution along the wall foundation interface to be linear (Bernouilli-Navier assumption), the neutral axis location at the base of the wall was also estimated and is indicated in Fig. 34(a-f).

In Figs. 34(a) and (b), the strains at maximum first floor displacement in both directions during the MO 9.7 test are illustrated. The apparent average strain* along the first 1 in. (25 mm) regions exceeded 0.002 ($\approx$ yield strain of steel) at both 3.86

* It should be noted that average strain is actually a fictitious strain because the measured deformation along this 1-in. length includes the relative slippage of the reinforcing bar with respect to the face of the foundation. For this reason, this average strain will hereafter be termed apparent average strain.

secs. and 4.05 secs. while the strains along the second 3 in. (76.2 mm) and third 3.5 in. (88.9 mm) regions were below the resolution of the instruments. The neutral axis remained close to the centroid.

In Figs. 34(c) and (d), the strains that occurred during peak first floor displacement responses of the MO 24.7 test are presented. The apparent average strain along the first 1 in. (25 mm) region of the boundary members exceeded 0.03, and the neutral axis migrated significantly within the wall panel. The Bernouilli-Navier assumption is not expected to apply to the wall cross section and the indicated locations of the neutral axis in Figs. 34(a-f) may therefore be in error.

Figures 34(e) and (f) present the measured average strains during T 40.3 response. At 3.16 seconds, the apparent average strain at the foundation interface was 0.23 in tension and 0.05 in compression faces, and the neutral axis has moved close to the boundary column. The steel in the column under tension began to break during this peak at 3.16 sec. During the subsequent displacement peak in the opposite direction at 3.49 seconds, shown in Fig. 34(f), an apparent tensile strain of 0.37, exceeding even the monotonic strain capacity of steel, was recorded. The neutral axis moved to the center of the boundary column under compression, and the wall rotated about this point as a nearly rigid body.

5.4 Successive Limit States and Distribution and Accumulation of Damage in Model.

From analyses of the results obtained and presented as the shear-interstory drift and overturning moment-interstory drift envelopes in Fig. 24 and the specific values given in Tables 13 and 15 which list the measured and effective frequencies of the structure, the structure clearly underwent significant changes in stiffness and frequency characteristics after the MO 9.7, MO 24.7, MO 28.3, and T 40.3 tests. Since the main wall was identified as the major contributor to the stiffness of the structure, its limit states were expected to strongly influence the structure. Indeed, from analyses of the wall base shear and moment envelopes given in Figs. 24 and 32, it can be seen that

significant changes in the shear and flexural stiffnesses of the wall occurred after the MO 9.7, MO 24.7, MO 28.3, and T 40.3 excitations, and that these changes in the wall stiffness were reflected in the response envelopes of the overall structure.

Although no indication of damage was observed in the wall (which is believed to have resulted from difficulties in inspecting the wall) after the MO 9.7 test, the moment at the base was evaluated to have exceeded its cracking capacity and a fixed-end rotation at the base was measured for the first time during this test (0.18×10^{-3} radians at maximum overturning), indicating that a crack at the interface of the wall and foundation may have occurred.

Although the stiffness of the model continually degraded after the MO 9.7 test, a particularly significant change occurred after the MO 24.7 excitation. A study of the MO 24.7 data indicated that at the end of the phase of severe response [see Fig. 27(b)] the moments evaluated at the first story of the wall exceeded the computed yield moment of the section (all the edge member reinforcing bars yielded). Fixed-end rotations exceeding 0.001 radians were recorded. The total plastic rotation along the lower 7.5 in. (191 mm) region of the wall was 0.003 radians at maximum overturning.

During the MO 24.7 test, all beams in frame B yielded at the wall interface. Many exhibited cracking at the external column interfaces as well, and crack widths of 0.012 in. (0.3 mm) were recorded indicating extensive yielding at both ends of most of these beams. The observed crack patterns of the wall-frame (frame B) and one of the exterior frames (frame A) after the MO 24.7 test are presented in Figs. 35 and 36 and indicate that most of the beams of the exterior frames (A and C) also exhibited yielding close to the column interfaces. Since the tensile strength of the concrete was high (747 psi (5.15 MPa)), and the beams had low reinforcement ratios (0.6% at either face at the support regions), the cracking and yielding moments of the beams were close. Consequently, the number of cracks were few but concentrated and generally wide at the end of this test.

In conclusion, although the first yielding at the base of the wall could have occurred as early as during the MO 9.7 test, wall yielding occurred at the end of the phase of severe response during the MO24.7 test. After the MO 24.7 test, the structure was subjected to the more intense MO 28.3 test (Tables 14 and 15) before the T 40.3 excitation. Figures 24, 32, and 33 show the maximum responses during this MO 28.3 test. Significant structural yielding as envisioned by ATC 3-06 probably occurred during this MO28.3 test and definitely during the T40.3 test.

The T 40.3 test may be considered a test of the maximum lateral resistance capacity of the model. An incipient collapse mechanism, seen in the envelopes in Figs. 24, 32, and 33, formed during this test. During the maximum moment responses to the T 40.3 test at 3.14 and 3.44 seconds (Fig. 27(c)), the main flexural reinforcement of the wall boundary members began to break, and the complete wall cross section was severed from the foundation at the end of the test with the exception of one main reinforcing bar. The wall rocked freely at the base, with the center of rotation shifting close to each boundary member (Fig. 34(f)). A maximum fixed-end rotation of 0.01 radians was measured at 3.49 secs., with almost no rotation along the rest of the plastic hinge region, indicating that the wall was rotating (rocking) about its base almost as a rigid body, without significant flexural distortion along its length.

The crack patterns of the interior wall-frame (frame B) and the exterior frame (frame A) after the T 40.3 test are presented in Figs. 37 and 38. The damage of the wall was confined to the first story. The beams of the wall-frame (frame B) were extensively cracked throughout their length, indicating that yielding had propagated along these members. Beams along the exterior spans of the exterior frame were also extensively and widely cracked close to the column joints.

The transverse beams and the complete diaphragm system were significantly cracked after the test, signifying yielding of the transverse beams at both ends and of the diaphragm along many yield lines. Because the lead ballast covered the top surfaces

of the diaphragms and limited access to the bottom surfaces of the diaphragms, the crack patterns of the diaphragms were inspected only after the final T 46.3 test. The crack pattern at the top of the first floor slab, observed after the T 46.3 test, is presented in Fig. 39. The damage to the diaphragm is an indication of the restraint provided by the frame-diaphragm system around the wall, restraining its uplift due to rocking as well as the accumulation of plastic strain (Fig. 31). Due to this restraint, the total axial compression in the wall reached a value during the test of more than double the axial compression due to the gravity force level and this total axial compression was approximately 28% of the balanced axial force in the N-M diagram (Fig. 31(d)).

The increase in compression over the wall cross section led to an improved shear-friction capacity, and the shear resisted by the wall was progressively higher than in previous tests, up to and including the T 40.3 test, in spite of the observed extent of damage and deterioration of the other shear-resisting mechanisms of the wall (dowel capacity of the boundary members and resistance provided by the panel reinforcement had diminished during the T 40.3 test).

VI COMPARISON OF 1/5th-SCALE MODEL SHAKING TABLE TEST RESULTS WITH THOSE OBTAINED IN FULL-SCALE MODEL TESTS AND THOSE PREDICTED ANALYTICALLY

6.1 Overview of Full-Scale Model Tests and Responses

The full-scale model was subjected to a series of four tests and then repaired and retrofit. Further tests were conducted on the model after its repair, retrofitting, and the installation of nonstructural elements. The information contained in Ref. 3 is the basis of the next two sections in which the responses of the full-scale model are briefly reviewed and the global responses of the full- and 1/5th-scale models are compared.

During the first four tests of the full-scale model, an inverted triangular lateral force distribution whose magnitude varied over time was applied along the structure's height. This distribution facilitated the pseudo-dynamic testing of the structure, thereby converting the structure to a single-degree-of-freedom system. The final testing of the structure to shear failure of the wall after repair and retrofitting was carried out by applying a uniform lateral force distribution along its elevation.

The test program during the initial series of four tests is presented in Table 16. The tests were designated PSD-1 through PSD-4, and were carried out with the input signals given in column 2 of Table 16. The durations of input signal were selected and processed such that the structure would essentially respond in the first mode, as was assumed when the inverted triangular lateral load pattern was established. The first two tests, PSD-1 and PSD-2, were conducted for only 1.3 seconds of base motion. Consequently, these tests resulted in a total of only nine full displacement reversal cycles in which a drift of 0.15% was attained only once.

The third test, PSD-3, was based on 10 seconds of base motion and resulted in five cycles reaching 0.25% drift and four cycles in which 0.75% or greater roof drift was attained. The fundamental frequency of the structure changed from 1.82 Hz at the beginning of this test to 0.86 Hz at its completion, indicating a substantial loss,

approximately 78%, in the average stiffness of the structure. The stiffness at the end of PSD-3 was approximately 14 percent of the stiffness of the virgin structure.

The time history of roof displacement of the full-scale model during the PSD-3 test is given in Fig. 40. During this test, the model exhibited extensive cracking along the first three stories of the wall, and at the ends of all the girders along the main as well as in the transverse directions of response. The concrete of the boundary columns started crushing at the base after the cover of the columns had spalled. The reported damage may be considered to characterize extensive yielding of the structure and the formation of an incipient mechanism.

The PSD-4 test, with a duration of 6.5 sec., induced four more cycles of full displacement reversal, and a roof drift index of 1.56%. Although no new cracks were observed to develop during this test, existing cracks progressed and increased in width. The width of the crack at the base of the wall boundary column was 4 mm (0.16 in.), and the cracks in the wall panel were wider than 1 mm (0.04 in.).

The envelopes of base shear and base overturning moment vs. roof drift index during tests PSD-1 through PSD-4 are presented in Fig. 41 and compared with the shear and overturning moment envelopes for the 1/5th-scale model. Figure 41 also shows the base shear-roof drift envelope during the final testing of the repaired and retrofit structure utilizing the uniform distribution of lateral load.

6.2 Comparison of Full-Scale and 1/5th-Scale Structural Response

6.2.1 Maximum Overturning Moment and Base Shear vs. Corresponding Roof Drift Index Envelopes. Comparison of the envelopes for the full- and 1/5th-scale models in Fig. 41 leads to the following observations:

1. The initial average stiffness characteristics of both the 1/5th- and full-scale models were similar, as observed previously when the initial mechanical characteristics of the 1/5th-scale model were discussed (see Fig. 21). Even to a level of stress near first steel yielding (which corresponded to the MO 9.7 test of the 1/5th-scale model, i.e.

for a base shear of about 18%W) the envelope of responses for the 1/5th- and full-scale models were quite similar. This holds true despite substantially different initial states of stress (residual stress) due to different volumetric changes characteristic of the full-scale concrete and the 1/5th-scale microconcrete. The similarity of the stiffnesses along the service limit states is believed to be a consequence of the effort to maintain similitude and particularly similitude in the value of E for the concrete and the micro-concrete.

2. The maximum base shear attained by the 1/5th-scale model (51%W) is 40% greater than the shear attained by the full-scale model (36.5%W) loaded under the inverted triangular lateral force distribution at the same level of drift. The maximum shear at which the full-scale model failed when tested under a uniformly distributed lateral force was practically the same as the maximum shear under which the 1/5th-scale model failed.

3. The lateral stiffness and therefore the shear attained by the two models remained close until a drift index of approximately 0.25%H, after which the difference in lateral stiffness and therefore the difference in shear resisted by the full- and 1/5th-scale models at the same drift increased progressively to a peak of 40%.

As shown in Fig. 40, during test PSD-3 (Taft 32.7%g) at approximately 4 seconds of response, the full-scale model experienced a monotonic increase in displacement from a total roof drift of (-)0.55% to (+)1.10%. After a few minor cycles another severe displacement from approximately (+)0.80% to (-)1.10% of drift is observed at about 9 seconds. These two severe cycles of deformation produced significant deterioration in the stiffness of the full-scale model. No such large deterioration was observed in the stiffness of the 1/5th-scale model during the MO 14.7, MO 24.7, and MO 28.3 tests which produced similar levels of drift in the 1/5th-scale model as the PSD-3 test induced in the full-scale structure. This is despite the significantly larger number of cycles of severe deformation reversals experienced by the 1/5th-scale model

during the MO 14.7, MO 24.7, and MO 28.3 excitations.

4. The maximum overturning moment envelopes of the two models exhibit similar stiffness and resistance until a roof drift index of 0.40%H occurred,after which the 1/5th-scale model remained stiffer and was increasingly capable of resisting more overturning moment. At 1.4%H roof drift the overturning resistance of the 1/5th-scale model was 34%WH, 33% larger than the corresponding resistance of the full-scale model, 25.6%WH. The maximum overturning moment resisted by the full-scale model tested under a uniformly distributed lateral force was 29%WH.

5. The moment-shear ratio at the base of the full-scale model was constant at 0.72H by virtue of the inverted triangular distribution of force. This ratio continually changed during the response of the 1/5th-scale model, and values between 0.64H and 0.75H were characteristically obtained at peak response (Fig. 29), the lower bound corresponding to maximum shear response while the upper bound corresponded to the maximum moment or top displacement responses.

6.2.2 Hysteretic Behavior. From a comparison of the base overturning moment-top relative displacement hysteresis responses (Figs. 30(f) and 54) and the area bounded by each hysteresis loop the hysteretic energy (accounting for the model scales) dissipated by the 1/5th- and full-scale models was assessed to have differed significantly. Before a roof drift index of 1.4% occurred, the 1/5th-scale model was subjected to over forty full reversals of displacement, each exceeding 0.5% drift index. By the time that an identical 1.4%H roof drift occurred in the full-scale model, however, that model had been subjected to a total of only sixteen full displacement reversals of such intensity. Although the full-scale model dissipated about the same or even perhaps a somewhat greater amount of energy during the first comparable cycle in which both models reached a selected peak roof drift, because of the significantly larger number of severe cycles to which the 1/5th-scale model was subjected, the total energy dissipated by the 1/5th-scale model considerably surpassed that of the full-scale struc-

ture.

6.2.3 Crack Patterns. The crack patterns of the wall-frame of the 1/5th- and full-scale model at 1.4%H roof drift are compared in Fig. 42. The distribution of cracking within the wall panel and edge columns differed significantly. Apart from the existing shrinkage cracks in the second, third, and fourth story wall panels, no further cracking was observed above the first story in the wall of the 1/5th-scale model. In the full-scale model, however, finely distributed diagonal cracking of the wall was observed in the first three stories.

A concentrated crack at the wall-foundation interface of the 1/5th-scale model was the most important characteristic of the induced damage. Although this crack may have begun to form at the MO 9.7 test, it was first observed to extend completely through the edge columns and wall panel during the MO 24.7 test. By the end of the T 40.3 test, the panel steel and all the main reinforcing bars in the boundary members—except one—had ruptured, and the concrete at both faces of this concentrated crack had deteriorated and spalled due to repeated abrasion. As discussed previously, the fixed-end rotation at the base of the wall arising from bond slip contributed significantly to the lateral displacement of the structure.

The wall of the full-scale structure did not exhibit a similar visible concentration of cracking and damage at the foundation interface. Although preliminary information reveals a large concentrated curvature indicating a fixed-end rotation at the base of the full-scale wall, curvatures of similar order continued to be measured (unlike the 1/5th-scale model) to approximately 0.67 of the height of the first story. In the 1/5th-scale wall the curvature measured at the foundation interface attenuated significantly in only 7.5 in. (0.25 of the height of the first story), and the wall rotated almost as a rigid body above this level. The local deformations and crack patterns of the 1/5th-scale and full-scale models, particularly in their walls, therefore differed substantially.

For both of these walls the contribution of average shear distortion to the total

first floor displacement was approximately similar, about 40%, at times of peak displacement response after approximately a 0.5% roof drift index had occurred. It follows that the full-scale wall should have been significantly less stiff in shear than the 1/5th-scale wall, as the maximum shear resisted by the 1/5th-scale model was about 40% higher than that of the full-scale structure.

The finely distributed diagonal cracking all through the first 2-½ stories of the full-scale wall should have caused a substantial reduction in the shear stiffness of this wall in comparison to that of the 1/5th-scale model.

Although it is generally recognized that the total number of cracks and the width of cracks decrease as the model size decreases [29], the following reasons were identified in this study for the differences.

1. *The tensile strength* of the 1/5th-scale model microconcrete was approximately double that of the full-scale model concrete. Since the typical reinforcement percentages of the elements were low, the cracking moment and the yielding moment levels of the beams, columns and wall were nearly equal in the 1/5th-scale model due to the increase in the tensile strength of the microconcrete. As a consequence, cracking and yielding occurred almost simultaneously, leading to the formation of fewer but wider cracks in the 1/5th-scale model as compared to the full-scale model.

2. *Length of the reinforcing bar yield plateau.* The yield plateau of the 1/5th-scale model beam and column flexural reinforcement was longer than that of the full-scale reinforcement. Consequently, relative crack widths were larger in the 1/5th-scale model and the initiation of newer cracks was delayed until strain hardening began in the yielded reinforcing bars within the crack.

3. *Bond.* It is well-known that the spacing of cracks depends on the tensile strength of concrete and on bond strength. The better the bond, the smaller the spacing of the cracks. As discussed in the section on model materials and their mechanical characteristics, test results indicated that the bond between the model reinforcing bars

and the microconcrete was better than expected between the full-scale reinforcing bars and concrete. Thus, if all other parameters affecting cracking had been kept similar, the spacing of cracks in the model should have been smaller than in the full scale. As this is not what occurred, it is clear that other factors must have contributed more to the observed crack patterns. A discussion of these factors follows.

4. *The average strain gradient* within the cross sections and along the members of the 1/5th-scale model was five times larger than in the full-scale model, as a direct consequence of scaled modeling, i.e., maintaining the similitude in strains between a scaled, smaller model and the full scale. It is well recognized that in a material such as concrete the smaller the strain gradient the larger is the probability of increased cracking.

5. *Strain Rate.* The strain rates of the two models differed significantly. While the full-scale model was tested by pseudo-dynamically, leading to almost sustained load due to the slow nature of the loading process (several seconds of excitation were simulated over several hours of testing), the 1/5th-scale model was tested on the earthquake simulator with a model time which was $\sqrt{5}$ times faster than normal. Consequently, while there was adequate time for crack widening and propagation, and the opening of new cracks in the full-scale model, this was not the case in the 1/5th-scale model and sparser cracking resulted.

6.2.4 Causes of Variations in Stiffness and Strength. As a result of differences in the tensile strength of concrete, strain gradient and strain rate between the 1/5th-scale and full-scale models, cracking and damage characteristics differed significantly. Due to the difference in crack pattern, the stiffness characteristics, particularly of the walls, differed.

Shear Stiffness: The shear stiffness of the full-scale wall was considerably lower than that of the 1/5th-scale wall due to the large number of local relative distortions that occurred along each of the finely distributed diagonal cracks.

Flexural and Axial Stiffnesses: The flexural stiffness of the 1/5th-scale model was also greater than that of its counterpart due to fewer flexural cracks, and the superior bond-slip characteristics of reinforcement and deformability of concrete. Although the plastic hinge rotations were more concentrated at the base of the 1/5th-scale wall, the hardening of the moment-rotation relationship at this plastic hinge was expected to exceed the hardening of the more distributed plastic hinge at the base of the full-scale wall due to better bonding characteristics of the 1/5th-scale materials. Recent studies at Berkeley [30] have shown that reduced-scale models whose hysteretic behavior is controlled by bond deterioration can substantially overestimate the energy dissipation capacity of the full-scale model.

The axial and flexural stiffnesses of the frames in the 1/5th-scale model were also expected to be superior to those characteristics of the similar frames in the full-scale structure as a result of fewer cracks, better deformability (Fig. 16), and the bond-slip characteristics of the reinforcing bars in the 1/5th-scale model.

Strength. In addition to differences in stiffness and strength characteristics of the two models arising from the differences in crack pattern and damage mechanisms, two other reasons for the higher strength of the 1/5th-scale model were the following.

1. *Hyper-Strength of Reinforcement.* The slightly higher yield force of the main reinforcement of the edge columns of the wall of the 1/5th-scale model (approximately 8% higher) and, more importantly, the inherently higher hyper-strength of the model reinforcement as compared to full-scale reinforcement were identified as causes of the relatively higher strength of the 1/5th-scale model.

The model reinforcement was deformed by indenting a circular cross-section whereas the full-scale reinforcement was hot rolled with ribs complementing a circular cross-section [17]. Test coupons from the model reinforcement yielded at the weakest, smallest cross-section during tensile testing. Due to the notches on these reinforcing bars, the probability that a cross-section would be smaller and weaker than an adjacent

cross-section was higher for the 1/5th-scale than for the full-scale model reinforcement. Consequently, the test coupons of the 1/5th-scale model yielded at such relatively smaller and/or weaker cross-sections and the chance that yielding would propagate was small, causing the localization of yield to a specific, smaller than average and/or deficient cross-section. On the other hand, the probability that such a cross-section would be located at the critical cross-section of the most critical element of the 1/5th-scale model was low, and the reinforcement at the critical cross-section of such an element would be likely to have a higher yield and ultimate strength than that implied by the coupon test results.

The greater the variability of area and strength in a cross-section along a reinforcing bar, the greater will be the underestimation of the possible strength of the reinforcement at the critical location of the critical member. Consequently, the hyper, or hidden, or statistical strength increase in the 1/5th-scale model was expected to be higher than that of the full-scale model contributing to the observed discrepancy in strengths.

2. *Lateral Force Distribution.* Still another reason for the higher shear and flexural strengths of the 1/5th-scale model was due to changes in its lateral force distributions while subjected to base excitation on the earthquake simulator as opposed to the constant upper triangular lateral force distribution applied to the full-scale structure. The lateral force distribution of the 1/5th-scale model alternated between an upper parabolic and lower parabolic distribution at times of peak moment and shear responses, such that the moment-to-shear ratios generally approached $0.75H$ and $0.65H$ at peak moment and shear responses, respectively. This was a more favorable loading condition for the structure than the inverted triangular distribution as the moment associated with peak shear demand and the shear associated with the peak moment demand were less than in the inverted triangular distribution which had a constant moment-to-shear ratio of $0.72H$.

6.3 Correlation of Analytical and Experimental Results

6.3.1 Analysis of 1/5th-Scale Model Subsequent to Shaking Table Tests. The analytical studies carried out on the prototype prior to dynamic testing did not include many aspects of three-dimensional behavior which were subsequently recognized to contribute greatly to the model stiffness and strength. The principal mechanisms involved in this three-dimensional behavior were the rocking and growth of the shear wall, and the associated restraint provided by the outriggering frames surrounding the wall. The girders, both parallel and orthogonal to the plane of the wall, were very effective in providing this restraint.

In order to quantify some aspects of this three-dimensional behavior, a new series of analytical studies is presently underway at Berkeley, using currently available computer programs for the static and dynamic analysis of linear and nonlinear structures, and limit analyses carried out by hand.

The computer program ANSR-I [31] was used to perform a step-by-step analysis of the 1/5th-scale model subjected to monotonically increasing static lateral load. Emphasis was placed on obtaining realistic force-deformation relations for the girders, both parallel and orthogonal to the plane of the wall. Complete three-dimensional behavior was considered, but the wall was assumed to rock about its centroidal axis rather than about the compression-side boundary element as observed during tests of the 1/5th-scale model. Realistic methods for modeling wall behavior, including neutral axis migration and axial growth, are currently under investigation.

Modeling of Sectional Moment-Curvature Relationships. Given the basic material properties of the reinforcing steel and microconcrete of the model, and assuming constitutive relations for the steel and the confined and unconfined concrete, moment-curvature relations were generated for sections representing critical regions of the beams, columns, and the main wall of the model [32]. For all sections, the Bernouilli-Navier hypothesis, i.e. that plane sections remain plane, was assumed to be valid.

Although this assumption may be accurate for rectangular sections subjected to flexure with low shear, it can produce unrealistic results when the sections are deep or nonrectangular, such as reinforced concrete T-beams with very wide flanges, or when the sections are subjected to relatively high shear. The beams of the 1/5th-scale model were subjected to relatively low shear because they were lightly reinforced. However, since they were monolithically cast with the slab, this gave rise to a significant contribution from the slab (T-beam action). Hence, the assumptions that hold for rectangular sections may not be valid.

The moment-curvature relations based on assumptions that the constitutive relationships for the materials under uniaxial stress would be representative and that plane sections remain plane are presented in Fig. 43 for positive and negative moment for the end sections of girder G3 (Fig. 1). In this figure, six curves are shown, three for positive moment, and three for negative moment. The three curves in each case correspond to three assumptions about the effective width of the slab. The width of the slab that was assumed in each case is indicated in the figure. The largest value of slab width corresponds to the assumption that the complete slab contributed to the T-beam section. Although not apparent in the figure due to the scale used, the initial slopes of these curves vary.

For the positive moment curves, the assumed effective flange width significantly influences the strength of the section due to the fact that at ultimate load the neutral axis is in the slab and so close to the top that all the steel in the slab is stressed in tension. It should be noted, however, that the strength predicted for the section with the widest slab is unconservative (i.e. too high), since the concrete would not crush simultaneously over the complete flange width, but would first crush over the part of the flange adjacent to the beam web. Both the resultant compression force and the moment arm will be smaller than those assumed for the fully effective slab, thereby reducing the ultimate strength of the section. Therefore, when positive moment strength is used to

model the critical regions of these girders, the total slab width cannot be assumed to be effective.

Based on the above considerations, the moment-curvature relation used to model sections located in the critical region of girder G3 as subjected to positive moment was based on initial stiffness and cracking moment for the 11.8 in. (300 mm) flange and yield and ultimate moments and curvatures for the 23.6 in. (600 mm) flange. The resulting trilinear curve is shown in Fig. 44.

It is much more difficult to establish a trilinear analytical curve for negative moment for the end region of girder G3, since curves based on the "plane section remain plane" assumption contain significant errors. When girders such as G3 are subjected to large inelastic deformation, the steel at the top of the beam stem (web) will yield first. Under increasing deformation, the steel in the portion of the slab adjacent to the beam steel will also begin to yield, with the number of slab bars reaching yield increasing as deformations increase. Ultimately, all the bars in the slab may have reached yield, with many, especially those adjacent to the beam web, being strained well into strain hardening. This gradual progression of yielding is not accounted for in the curves shown in Fig. 43 since these curves assume that all steel across the slab will have the same strain and thus will yield simultaneously. The curve corresponding to a flange width of 47.2 in. (1200 mm) exhibits relatively little curvature ductility as a consequence of the assumption that all steel in the 47.2 in. (1200 mm) wide flange will yield at the same time. In reality, the maximum moment (if reached at all) indicated by this curve would occur at a larger curvature than that shown in Fig. 43 as the portion of the slab (flange) in which the steel is yielding will increase gradually with the increase in curvature.

Based on the above observations, it was decided to use an ultimate negative moment as determined from the moment-curvature analysis for the case of full slab width, i.e. 47.2 in. (1200 mm), but to use for ultimate curvature the value correspond-

ing to concrete crushing, i.e. $\Phi = 0.012$. For yield moment and curvature, the computed values for the 23.6 in. (600 mm) slab were used, and for cracking moment and curvature, the computed values for the 11.8 in. (300 mm) slab were used. The resulting trilinear moment-curvature relation used to model the critical regions of the element subjected to negative moment is shown in Fig. 44.

Significant uncertainties were confronted in determining a representative cross-sectional response for the girder-slab system. These uncertainties indicate that more realistic compatibility conditions than those provided by the Bernoulli-Navier hypothesis are urgently needed in cross-sectional analysis. Since the assumed cross-sectional response for girder end regions under negative bending (the slab in tension) affected the overall stiffness and strength characteristics of the structure as well as the sequence of plastic hinging and local response characteristics significantly, investigations of more reliable cross-sectional analytical procedures are in progress.

Modeling of Elements and Critical Regions. All elements of the structure were modeled as one-dimensional, two-component models. Since the lateral loading was increased monotonically until a mechanism state occurred, only monotonic force-deformation primary curves were established. The method used to generate these curves is described below where girder G3 of the 1/5th-scale model is used as an example.

Typically, the two-component model, when loaded in flexure without axial load, can be characterized by the initial and strain hardening stiffnesses of the components, and the positive and negative moment strengths of the plastic hinges. The distribution of flexibility along the length of the element may be incorporated by specifying appropriate element stiffness coefficients. If the element is subjected to constant moment along its length, and/or if the sectional moment-curvature relation displays no strain hardening, the moment-curvature relation may be used directly to supply the required element stiffness and strength. Otherwise, the moment-curvature relationships

cannot be used directly to specify these properties. Since the latter case applied for the girders under consideration, it was necessary to carry out additional analysis (on the element level) before the two-component modeling parameters could be supplied to ANSR-I.

The typical moment-rotation relationships from the two-component model loaded first by gravity load and then by monotonically increasing equal end rotations (similar to those that would typically occur during earthquake loading) are illustrated in Fig. 45. Limit states 1 through 4 indicated in Fig. 45 correspond to: (1) gravity loading; (2) yielding in positive moment at the right end of the beam; (3) yielding in negative moment at the left end of the beam; and (4) additional loading with both ends yielded and in strain-hardening.

Since any real beam must be modeled by a moment-rotation relationship similar to that in Fig. 45, it was decided: (a) to force a more complex model of the real beam to undergo the same loading history as described above for the simple two-component model; (b) to generate the resulting moment-rotation relations; (c) to fit a two-component model curve through the analytical curve; and (d) then to assign the yield strengths and initial and strain hardening stiffnesses to the simpler two-component model.

The basic assumption in this modeling procedure is in the displacement patterns through which the ends of the beams are forced to move. For modeling the principal longitudinal girders it was assumed that the rotations at either end of the beam were equal. While this is not necessarily the case when the structure is elastic, it was found from analysis that rotations at the ends of girders tend to approach the same value as the response of the structure enters the nonlinear range, particularly after the shear wall hinges at its base. Obviously, some errors are introduced, but it must be kept in mind that the basic goal is to determine properties of a highly simplified analytical model (the two-component model). It seems reasonable to determine these properties based on

the behavior of a highly refined analytical model of the same beam, conducting the analytical simulation of an experiment where the analytical beam is subjected to a rotation history similar to that which may occur during a typical earthquake cycle.

A computer program, ELMO (for ELement MOdelling) was developed to discretize the beam into a number of finite elements and to synthesize the moment-rotation relations for both ends of the beam based on trilinear moment-curvature characteristics prescribed for each finite element.

The ELMO model, shown in Fig. 46, was used to generate moment-rotation relations for girder G3 (Fig. 47). For negative moment, these curves display significant hardening. This is a direct result of the large strain hardening stiffness of the moment-curvature relations and accounts for the progressive yielding of the steel in the slab. For positive moment, the hardening is small, as would be expected from the moment-curvature relations. A maximum rotation of 0.012 radians was assumed for this analysis, corresponding to a total maximum roof drift index of about 1.2 percent (i.e. a roof displacement of 2 in. for the 1/5th-scale model, 10 in. for the full-sacle model). This level of drift is of the same order of magnitude as would be expected to occur during a damageability level earthquake. In order to derive stiffness and strength parameters for the ANSR-I analysis, the two-component model was forced to display the same negative moment strength at this rotation of 0.012 radians. Stiffnesses for the model were based on providing areas under the analytical curve approximately equal to the areas under the model curve. However, a large number of two-component element parameters representing nonlinear response may be selected. Despite the refined analytical generation of the nonlinear moment-rotation response, the bilinear idealizations for negative and positive moment directions (i.e. selection of the coordinates of the yield points and the strain-hardening stiffness) are subjective and the choice might affect the global response of the structure. Analytical elements which permit a closer representation of the generated moment-rotation responses than the two-component

model shown in Fig. 47 are necessary for more refined modeling of reinforced concrete beam response.

A similar analysis was carried out for each of the principal and transverse girders of the model. For the columns, which were assumed to remain elastic except at the foundation, and the shear wall, such analyses were not performed. Instead, the strengths were taken directly from the derived axial-flexural interaction diagram, the initial stiffness was taken (somewhat arbitrarily) as 50 percent of the gross section stiffness, and the strain hardening stiffness was taken as 1 percent of the initial stiffness, which was a decision based on the low strain hardening displayed by the reinforcing steel.

Global Modeling Concepts. The model used for the entire structure, shown in Fig. 48, included all the elements of frames A, B, and C, as well as the transverse beams (girders G4), which span frames A and B, and B and C. The four end (peripheral) walls were also included, and were modeled as truss elements in parallel with the exterior beam-columns of the frames. The transverse beams shown in the figure were included to account for the interactions of frames A, B, and C that arose due to the different vertical displacements of the exterior frames A and C and the interior (center) wall-frame B in an idealized manner. To simplify the analysis, a single frame, termed frame A′, was used to represent the total strength and stiffness of frames A and C. The floor system was assumed to be infinitely rigid in plane. The shear wall was assumed to rotate about its centroidal axis. The effect of wall rocking is discussed below in the section on limit analyses. Although small, P-Δ effects were nevertheless considered in the analyses via the fictitious frame shown at the right in Fig. 48.

Force-Displacement Response. Using the modeling procedures described above, the 1/5th-scale model was analyzed for two loading cases, under uniformly distributed and triangularly distributed lateral loads. The first case results in larger shear forces at a

given displacement and the second case results in larger overturning moment. Since the dynamic response of the structure was expected to be predominantly in the first mode, and since any higher mode effects were expected to be less important as the response became increasingly nonlinear, the triangular and uniform lateral loadings were expected to provide lower and upper bounds, respectively, on the actual dynamic responses of this structure.

The resulting force-displacement curves are shown in Figs. 49 and 50 for the triangular and rectangular loadings, respectively. In each of these figures the response of the total structure is shown, together with the load carried by each of the individual frames (frames A′ and B).

As can be seen from Figs. 49 and 50, the percentage of shear taken by frame B is largest when the response is elastic, but once the elements of this frame begin to yield, the contribution is reduced. For triangular loading, frame B initially carries 92 percent of the load, but at a roof drift index of 1.20 percent this reduces to 68 percent. Similarly, for uniform load, frame B starts out with 92 percent, but this value decreases to 72 percent at a roof drift index of 1.20 percent. In either case, whether under uniform or triangular loading, frame A′ has a similar response because after a hinge forms at the wall's base, the structure's lateral displacements are governed by the wall's nearly rigid-body movement. Thus, the response of frame A′ is predominantly controlled by the compatibility condition imposed by the wall rotating at its base after a plastic hinge has formed at the base of the wall, regardless of the distribution of lateral loading.

Comparison of Analytical and Experimental Results. The analytical static response is compared to the dynamic response envelope of the 1/5th-scale model and with the envelope values from the pseudo-dynamic testing of the full-scale model as shown in Fig. 51. The analytical curves (C and D) fall between the envelope values from the two experimental curves (A and B). The analytical curve for the triangular loading is similar in shape but lies above the envelope from the full-scale model (in which the

structure was also loaded with an upper triangular force pattern). Curve D falls well below the envelope of values from the shaking table tests, however. The analytical curve for the uniform loading is well above the envelope values from the full-scale model and at the same time well below the envelope curve from the 1/5th-scale model tests, especially at roof drifts exceeding 0.5 percent.

Although there are several reasons for the differences in the curves shown in Fig. 51, quantitative justification of these differences is difficult, especially for curves A and B, the two experimental curves. These differences and their possible causes have been discussed in previous sections and the comparison made here is for curves A, C, and D.

Many adjustments could have been made in the analytical model in order that analytical results would correlate better with experimental results. From curves C and A, for example, it is apparent that the strain hardening stiffnesses of the wall and beams were underestimated (at drifts greater than about 0.5 precent) and the intermediate stiffness of the wall and perhaps the beams overestimated (at drifts between 0.15 percent and 0.35 percent) when compared to experimental values. If the initial strain hardening and stiffness of the wall was increased, the initial stiffnesses of the girders decreased, and the strain hardening stiffnesses of the girders increased, the shapes of curves A and C would tend to be similar. This type of parameter juggling was not attempted, first because there are many combinations such as those given above which can be used to force the experimental and analytical curves to correlate better, as also discussed in relation to Fig. 47, and, secondly and more importantly, because it was considered more productive to explain the observed differences between analytical and experimental results by closely studying overall experimental behavior and by investigating mechanisms of response, rather than by attempting to improve correlation by parameter juggling.

Although in the shaking table tests during which the roof drift index exceeded

approximately 0.75% it was observed that the shear wall tended to "rock" with the center of rotation alternating between the boundary elements of the wall, this behavior was not included in the analyses. During these tests it was observed that as the wall rocked to the right, the center of rotation moved towards the right side boundary element, and as the wall rocked to the left, the center of rotation switched to the left side boundary element. Also, since the girders (both parallel and orthogonal) to the tension side boundary elements were subjected to larger relative end displacements than were the girders attached to the compression side elements, due to both rocking of the wall and its growth, they developed larger shear forces which were transferred into the shear wall causing the wall to undergo increases of up to 34 kips over the gravity level of 26 kips. Similarly, there was an unsymmetric dynamic response in the interior columns of frames A and C (see Fig. 28) as the differences in force and distortion in the tension and compression sides of the wall were transmitted to the side frames through the flexural rigidity of the diaphragm system including the transverse girders. The increases in axial compression of the wall due to the restraint of the diaphragm system and the outriggering frames increased the flexural and shear capacities of the wall.

Analytical models that can incorporate the effects of axial force on the stiffness of R/C elements, neutral axis migration, axial growth of wall elements, restraint provided by a diaphragm system leading to out-of-plane interactions between walls and frames, and the contribution of R/C slabs to the moment capacity (particularly the hardening characteristics of girders), are being developed. Experimental observations of the test structure's actual response characteristics were essential in understanding the deficient aspects of current analytical modeling procedures.

6.3.2 Limit Analyses. A series of limit analyses of the model were carried out. Unlike the step-by-step analyses discussed in the previous section, limit analyses did not require a nonlinear analysis computer program. Although information regarding the displacements of the structure are not generated during limit analysis, the max-

imum resistance of the structure can be obtained. In case a complete mechanism is attainable, the force distribution in the structure at maximum resistance can also be obtained. Several analyses of different analytical models of a structure may be carried out economically, investigating the effects of different design parameters and analysis assumptions on the collapse state forces. This makes limit analysis a powerful tool in designing for the ultimate limit states.

The procedures followed in the limit analyses were: (1) to construct an analytical model of the structure, (2) to establish the plastic moment capacities of the members, (3) to assume a kinematically admissible collapse mechanism, (4) to evaluate the internal work, the external work (based on an assumed distribution of seismic forces), and the collapse load of the structure from the principle of virtual work, (5) to check that the assumed mechanism, in conjunction with the assumed plastic moment capacities of the members, results in a stable statically admissible field, i.e. to satisfy the statics and the yield conditions everywhere, (6) to check that the deformation capacities of the critical regions of members are adequate to supply the maximum rotation demands in conjunction with the assumed mechanism state.

In this manner, analyses were repeated for: different collapse mechanisms of two or three-dimensional analytical models; different assumptions on member plastic moment capacities; and for several assumed lateral force distributions, as discussed next, and summarized in Table 17.

Analytical Models Considered in the Limit Analyses. Either two, or, simplified (pseudo) three-dimensional analytical models of the structure were considered. In all the analytical models the two side frames A and C were lumped together in a resulting frame A'. This frame A' and the wall-frame B were constrained to have identical lateral displacement at each floor level, as shown in Fig. 48. This corresponded to assuming infinite in-plane stiffness (axial, shear, and flexural) for the diaphragm. In the two-dimensional (planar) analyses, frames A' and B were assumed to have indepen-

dent vertical displacement and rotation characteristics. This corresponded to assuming zero flexural and torsional stiffness of the diaphragm in the transverse (out of plane) direction. In the pseudo-three-dimensional analyses, the transverse girder-slab system was assumed to be effective in relating the vertical displacements of the side frames and the wall-frame. The internal work done by the transverse girder-slab system in resisting relative vertical displacements between the side frames and wall-frame were considered in these analyses. The torsional resistance of the floor system in resisting the relative rotation characteristics of the adjacent frames, however, were not considered.

In both analytical models considered, the joint zones were assumed to be rigid. Plastic hinges were assumed to possibly occur at the faces of joints only.

Mechanisms Considered in Analyses. Although several different types of collapse mechanisms have been analyzed, only the results obtained from the two sidesway mechanisms shown in Fig. 52 will be presented and discussed herein. In the first mechanism, the plastic hinge at the base of the wall was assumed to occur at the centroid of the wall cross section. In the second mechanism, this hinge was assumed to occur at the neutral axis of the wall cross section at the base of the wall. The neutral axis of the cross section was determined by iteration based on the axial force of the wall at the attainment of its maximum resistance. Analyses considering the location of the neutral axis at the centroid of the edge column, as well as at the extreme face of the edge column, were also conducted for the three-dimensional model, in order to investigate the effect of higher wall axial forces on the collapse load.

In checking if the assumed collapse mechanisms were associated with stable static admissible fields, hinging of columns instead of beams were identified in several beam-column joint locations for certain analyses. In such cases, the mechanisms were corrected.

Element Force-Deformation Relationships. All elements were assumed to have rigid-plastic moment-rotation characteristics. The plastic moment capacities of the

elements were obtained based on either specified or measured material properties, considering the effect of axial force on the flexural capacity.

The plastic moment capacity of the wall was determined either at the geometric centroid, or at the neutral axis of the cross section, based on where the plastic hinge was assumed to occur in the mechanism under consideration.

The plastic moment capacity of the girders was determined for various assumed effective flange widths, in each case incorporating the slab steel corresponding to the assumed flange width. In the cases where the full slab width corresponding to each frame was assumed to be contributing to girder plastic capacity, the computed maximum resistance for negative moment (flange in tension) was reduced by 20 percent. The reasoning behind this reduction was discussed in Section 6.3.1 where the step-by-step analyses were presented.

In the three-dimensional analyses, the entire slab width associated with each transverse girder was assumed as effective in contributing to the girders' flexural capacity. The computed maximum negative moment resistances of the transverse girders were reduced by 20 percent, similarly to those of the girders along the main response direction.

Lateral Force Distributions considered in the Analyses. Three different lateral force distributions were considered. They were: an inverted triangular distribution, a uniform distribution and a parabolic distribution equal to the one measured during the T 40.3 test at the time of the maximum moment and shear of the structure, which occurred simultaneously (Fig. 29).

All the parameters considered in the limit analyses were summarized in Table 17. The results of the analyses are discussed next.

Results of Limit Analyses. Results are summarized in Table 18. The computed maximum resistance of the structure is observed to vary between 20.3 kips and 57.4 kips, indicating the significant effect of the various assumptions on the computed

maximum resistance of the structure: (a) Incorporating the ACI-defined slab contribution for positive moment to computation of girder negative moment capacity as opposed to neglecting the slab contribution is observed to increase the resistance approximately 15 percent. (b) Using the measured material properties and the entire slab width as opposed to using the specified material properties and the ACI-defined effective slab width is observed to increase the resistance approximately 80 percent. (c) Considering the pseudo-three-dimensional model as opposed to the two-dimensional model increased the resistance approximately 10 percent. (d) Considering the wall plastic hinge occurring at the neutral axis rather than the centroid increased the resistance approximately 2 percent. The axial compression in the wall was either 26 kips or 35 kips when mechanisms G and H (Table 18) were considered. As indicated in Table 17, the wall plastic hinge is located at the centroid in mechanism G, and at the neutral axis in mechanism H. Under the axial load of 26 kips the wall plastic moment capacity taken at the centroid was 1377 kip-in. In mechanism H the axial compression increased to 35 kips and the wall plastic moment capacity taken at the centroid increased to 1528 kip-in. However, when this moment is expressed at the neutral axis, it decreased to only 907 kip-in. Mechanism H resulted in larger internal work done by the girders and larger negative external work done by the gravity loads due to net upward displacements in the structure as compared to mechanism G. Consequently, in spite of the significant reduction in the wall plastic moment when expressed with respect to the neutral axis, mechanism H resulted in 2 percent larger resistance than mechanism G. Assuming the wall plastic hinge at the centroidal axis (mechanism G) as opposed to at the extreme face of the edge column (mechanism J), lead to only a 1 percent difference in the computed collapse load. (e) Assuming a uniform lateral force distribution as opposed to a triangular one was observed to increase the resistance by more than 20 percent. The measured distribution of the lateral force led to approximately 10 percent larger collapse load than the triangular distribution.

Concluding Remarks. The maximum lateral resistance of the structure during the T 40.3 test was measured as 53.9 kips. The simplified three-dimensional analysis H (Tables 17 and 18), considering measured material properties, incorporating contribution of the entire slab to girder capacities in both main response direction and the transverse direction, plastic hinging of the wall at the neutral axis, and considering the lateral force distribution measured during the T 40.3 test, resulted in a computed maximum resistance of 52.1 kips i.e. only 3 percent less than the measured value. It may be concluded that limit analysis, conducted on a simplified (pseudo) three-dimensional model of the structure, and assuming the total slab to contribute to the plastic moment capacity of the girders, was quite successful in estimating the measured lateral force capacity of the structure.

VII IMPLICATIONS OF RESULTS FOR STATES OF ART AND PRACTICE OF SEISMIC RESISTANT DESIGN AND CONSTRUCTION OF REINFORCED CONCRETE FRAME-WALL STRUCTURES

7.1 General Remarks

One of the main objectives of the U.S.-Japan cooperative research program, of which the studies reported here form a part, is to mitigate the hazards of earthquakes by improving the seismic resistant design and construction of buildings. Therefore, one of the main objectives of the studies conducted at Berkeley has been to assess the implications of the results obtained regarding the state of the art and particularly the state of the practice of seismic resistant design and construction of reinforced concrete frame-wall structures.

Although all results have not yet been assessed, observations made during the experiments and comparison of results of the analytical studies conducted prior to the experiments with the experimental data that have already been processed (some of which have been presented here) permits a series of observations.

While some of the results have categorically confirmed observations from previous investigations, visual observations during the experiments and some of the experimental results have shed new light on the problem of the seismic behavior of frame-wall structures. Although there have been many findings from this research as discussed below, the most important are: (1) the three-dimensional interaction of the wall and frame (due to differences in the deformation characteristics of the wall, particularly its rocking, and the frame which induced the beneficial outriggering action of the space frame on the wall); (2) the significant effects of variations in axial force on the lateral stiffness and strength of the columns and particularly of the wall; (3) the importance of controlling the amount of shear at the critical regions of the main members of a structure by proper layout, proportioning, and detailing; and (4) the tremendous contribution of the floor system (slab) to the ultimate strength of the structure.

Before assessing the implications of the results obtained regarding the states of the art and practice, it should be noted that the overall performance of the models (full-scale and 1/5th-scale) has been excellent. The tests have shown that the frame-wall structural system is capable of surviving safely, i.e. without collapse (pancaking) or dangerous structural damage, the larger horizontal component of a possible extreme ground motion which can be anticipated in the U.S. The experimental studies conducted clearly confirm that if the limitations of reinforced concrete materials are recognized and considered in proportioning and detailing of structural members and their connections, and such a design is adequately constructed, it is possible to achieve reinforced concrete frame-wall structures with excellent seismic performance.

Strictly speaking, the conclusions and observations noted below apply only to the building fabricated and tested under the conditions described above. The results and conclusions might be extrapolated to similar structures with different boundary and initial conditions and reactive mass and subjected to all components of actual earthquake ground motions, but only with extreme care. To reiterate: (1) the test building was tested under one horizontal component of earthquake ground motion; (2) the structure's torsional rigidity was increased significantly by the use of special peripheral walls that also acted as effective outriggers and contributed to the structure's overturning moment capacity, (3) the foundation was rigidly fixed to the shaking table, i.e. no soil-foundation interaction was possible; (4) the reactive mass was only slightly larger (less than 9%) than the mass corresponding to the weight of the bare structure; and (5) the building was subjected to a series of tests with ground motions whose intensities were gradually increased.

7.2 Implications for State of Practice

In assessing the implications of the results it is assumed that the state of the practice is reflected in existing seismic codes. The results of the studies have shown that:

1. Despite the fact that the design and detailing of the frame-wall structure did not satisfy the UBC seismic requirements for buildings of either Type 3 ($K = 0.8$) or Type 1 ($K = 1.0$), the behavior of the two models was excellent.

2. The soundness of the UBC requirements that permit the use of a UBC Type 1 ($K = 1.0$) structural system, which includes walls that lack special confined vertical boundary elements and concrete space frames that do not satisfy the ductility requirements for ductile moment-resisting space frames, should be investigated. Comparative designs and analyses of the test building shown in Fig. 1 using $K = 1.0$ vs $K = 0.8$ show that the design for $K = 1.0$, i.e. Type 1, leads to a final structure which can have the same or somewhat lower strength* than the structure designed for $K = 0.8$, i.e. Type 3, but its capacity to dissipate energy is considerably less because the wall and frame members would be significantly less ductile. Because a Type 1 ($K = 1.0$) structure is easier to detail and construct and is therefore more economical than a Type 3 ($K = 0.8$) structure, it may erroneously appear as a very attractive solution for the designer who may not recognize the importance of energy dissipation capacity in seismic resistant design.

3. Dual structural systems (i.e. frame-wall systems) offers considerable advantages over structural systems composed of only ductile moment-resisting space frames or systems based on walls alone. The addition of the wall to the ductile moment-resisting frame significantly increased the strength and stiffness of the frame. Studies that are at present in progress indicate that while a ductile moment-resisting frame (based on 3 frames identical to frame A) would have satisfied UBC analyses of its behavior under the Taft ground motion used in the tests, normalized to a peak acceleration of 0.40g, indicated that interstory drift

* Despite the fact that the UBC total base shear, V, when $K = 1.0$ is 25% higher than when $K = 0.8$, the requirements that for Type 3 ($K = 0.8$) structure, the space frame be designed to resist 25% of the total V and that not only the wall but its edge members must resist all vertical stress due to the effect of V, results in a wall that is at least as strong as the wall designed for $K = 1.0$, and as the frame in this case is not required to be designed for 25% of the total V, the final structure designed for $K = 0.8$ would be as strong or stronger than that which would have been designed for $K = 1.0$.

indices of the order of 2% would have been induced in the first two stories. Therefore, although the use of the frame alone would have permitted the building to survive the Taft 0.40g horizontal component without collapse, the amount of nonstructural damage due to the larger interstory drift would have been larger (particularly at the first two stories) than expected from the frame-wall models tested.

The addition of just one wall increased the initial lateral stiffness of the frame by a factor of five and the strength by more than 100%. The increase in lateral stiffness significantly decreases the damage to nonstructural components as well as to structural members at all limit states. Under service level earthquake loads, drift of the test structure was less than 0.0015, considerably smaller than the value of 0.0025 specified as a maximum drift index for wind and than the 0.0040 allowed for earthquakes for Type 3 ($K = 0.8$) structures. Even under a severe earthquake ground motion, as in the T 40.3g test, the maximum interstory drift was about 1.7% which is just a little larger than 1.5%, the maximum acceptable value recommended by ATC 3-06.

4. Due to differences in the deformation characteristics of the wall and the moment-resisting space frame (when the structure is loaded or deformed laterally) significant interacting three-dimensional effects are induced. The axial growth and rocking of the wall at its base triggered a beneficial three-dimensional outriggering action of the surrounding space frame.

5. The interacting three-dimensional effects created by the axial growth and rocking of the wall and consequential outriggering action of the space frame should be recognized and considered in the design of frame-wall structures. This three-dimensional interaction induces internal forces and deformation demands in structural members that cannot be visualized considering only planar behavior. From analyses of the three-dimensional behavior illustrated in Fig. 31 and of the results

presented in Fig. 28 it becomes clear that due to the earthquake ground motion horizontal component acting in the plane of the wall: (1) the girders framing perpendicularly to the wall plane can be subjected to significant bending moment (up to ultimate capacity); (2) the interior columns of the exterior frame can be subjected to significant tensile axial forces and bi-axial moments; and (3) the wall can be subjected to significant compressive axial forces. Neglecting these forces in design may lead to poor seismic performance.

6. All structural members of a frame-wall structure, and not merely those required by design to be part of the lateral force-resisting system, as presently permitted by the UBC, should be designed as ductile members. The interacting three-dimensional effects require significant inelastic deformations in the girders framing perpendicularly to the wall plane, and the girders will undergo these deformations without failure (loss of strength) only if they have been designed according to the requirements for a ductile moment-resisting space frame.

7. Interacting three-dimensional effects, observed during experimentation, give rise to serious doubt about the soundness of present UBC provisions that allow structures to be designed and constructed to resist total lateral seismic forces assumed to act nonconcurrently in the direction of each of the main axes of the structure. Whether the related provision of ATC 3-06 which requires that elements be designed considering 30% of the orthogonal effects is adequate should be investigated.

8. The contribution of the reinforced concrete slab to the stiffness and particularly to the ultimate strength of the frame-wall structural system was observed to be significant. At present, building code requirements for reinforced concrete recognize some contribution of concrete slabs cast monolithically with beams only when the beam is subjected to positive moment, i.e. the slab is subjected to compression. The present codes do not mention the contribution of the slab rein-

forcement to the negative moment capacity of the beams. The analytical results presented in Fig. 43 and the observations made during the experiments have clearly shown that the contribution of the reinforced slab to the positive and particularly to the negative moment capacity of the beams is significant. The contribution of the slab increases with increases in plastic deformation of the beams.

This contribution of the reinforced concrete slab should not be neglected because although in very ductile structures it can be of great benefit, as in this case, it can also have adverse effects such as: (1) the ultimate flexural strength of girders may be so large that it may exceed the axial-flexural capacity of the columns, thus forcing plastic regions to form in the columns; (2) the increase in girder flexural capacity attracts additional shear which can lead to a decrease in beam ductility if the beam has not been designed for such an increase; (3) the increase in the flexural capacity of the beams at their ends can bring about an increase in shear in the beam-column joints which can be detrimental to the behavior of the joint if the increased shear has not been considered in the design; and (4) as the additional beam shears are transferred to the columns and walls as axial forces, these additional axial forces can change the resistance and/or ductility of these elements adversely.

The importance of the increase in shear stresses due to increases in the flexural capacities of members (particularly the beams due to slab contributions) is clearly illustrated by comparing the values of the nominal shear stresses for which the members were designed, with those obtained according to the observed maximum shear developed during tests of the 1/5th-scale model. These values are given in Table 19. The increase in shear due to the flexural overstrength supplied to the beams was about 54%.

9. The slab's contribution to the end moment capacity of beams makes estimating the stresses on, and therefore the design of, beam-column joints very difficult.

Present code design methods which consider only the effect of beam reinforcement that passes through or is anchored to the joint core do not seem realistic.

10. It is of utmost importance that the amount of shear that develops within the structure and particularly within the critical regions of the structural components that control the yielding of the structure be controlled. One of the main reasons for the excellent behavior of the structure has been that it was designed for very low nominal shear stresses as shown in Table 19. Despite the fact that the maximum nominal shear developed was considerably higher (due to the flexural overstrength supplied to the members) these maximum values were not large enough to jeopardize the ductility (energy dissipation capacity) of the structure.

11. The larger the ductility and energy dissipation capacity (stable hysteretic behavior) supplied to a structure, the better will be the seismic performance of that structure. Although the wall began to yield when the total shear was about 400 kips* (1780 kN) and had undergone significant flexural yielding when the total base shear was 650 kips (2893 kN), due to the low shear stresses and the proper detailing of the reinforcement the whole structure developed a complete three-dimensional mechanism with fully plastic moments utilizing nearly the full tensile strength of the main reinforcement in most members, resulting in a maximum total shear resistance of about 1350 kips (6008 kN), three and one half times the value at which yielding occurred.

12. For the type of frame-wall used in this test building, the wall did not need to be framed at each story by a floor girder as required by present Japanese philosophy of shear wall design. From data available it is believed that for standard sizes of story wall panels in which the *maximum* shear stress can be kept below $10\sqrt{f_c'(psi)}$ $(26.25\sqrt{f_c'(kPa)})$ there is no need for floor girders framing the wall

* This force value as well as values given below have been determined from results for the 1/5th-scale model but have been converted to corresponding values for the full-scale model.

panels. The floor slab alone offers sufficient restraint to arrest the propagation of diagonal tension cracks to other stories.

13. When the nominal shear stress in the column does not exceed $4\sqrt{f_c'(psi)}$ $(10.50\sqrt{f_c'(kPa)})$ the UBC (and ACI-318) requirement that the nominal shear strength provided by the concrete, V_c, be considered zero when $P_e/A_g < 0.12f_c'(psi)$ $(0.83f_c'(kPa))$ (or when $P_e/A_g \leqslant 0.05f_c'(psi)$) $(\leqslant 0.34f_c(kPa))$ according to ACI 318-83) seems too stringent. As discussed previously, the transverse reinforcement used in the columns of the structure did not satisfy the code requirements for shear resistance in order for the columns to be classified as members of a ductile moment-resisting space frame when the P_e/A_g was below $0.12f_c'$. No indication of initiation of shear failure was, however, observed in the columns. Thus, it appears that this code requirement can be relaxed for cases similar to those of the test building, i.e. where $v_u \leqslant 4\sqrt{f_c'(psi)}$ $(10.50\sqrt{f_c'(kPa)})$ and axial forces are just below the corresponding $P_e/A_g = 0.12f_c'$ $(0.83f_c'(kPa))$. The sharp change in the supplied shear resistance estimated by these codes (the UBC and the ACI) is illustrated in Fig. 53 and does not seem rational. A transition curve such as that indicated in Fig. 53 is suggested.

14. Present UBC (and ACI 318) regulations for estimating the supplied shear strength of the walls appear to be inconsistent and too conservative. According to the 1979 UBC, the *maximum design shear strength* based on the actual measured mechanical characteristics of the wall should have been 450 kips $(4.4\sqrt{f_c'}A_{cw}$ **) (2002 kN), which corresponds to a *nominal shear strength* of 529 kips $(5.2\sqrt{f_c'}A_{cw})$ (2354 kN). The experiments showed that the wall resisted 893 kips $(8.7\sqrt{f_c'}A_{cw})$ (3974 kN) without sign of shear failure in the wall panel, i.e. a

** A_{cw} is the effective shear area of wall, $0.8\,h\,l_w$, where h is the wall panel thickness and l_w is the total length of the wall in the direction of the shear force.

nominal shear strength 69% higher than the UBC computed nominal shear strength of 529 kips. It is clear that the reliability of the UBC (and ACI-318) equations for computing supplied strength needs to be investigated.

15. The UBC specified seismic forces are unrealistically low, i.e. do not represent the forces that could be developed according to the supplied strength following the UBC requirements for proportioning and detailing structural members. It has been shown (Figs. 2, 10, 24, and 33) that the strength supplied to the structure was nearly five times that required by the UBC. Although the materials used were stronger than the minimum specified strength used in the design ($f_c' = 5610$ psi [38600 kPa] vs specified 3850 psi [26500 kPa] and $f_y = 59$ ksi [406 MPa] for columns and wall edge members vs specified 50 ksi [345 MPa]) these differences (which in general practice would not always occur) do not alone justify the observed strength. The main reasons for the observed overstrength are:

(1) UBC specifications requiring that: (a) the wall acting independently shall resist the total lateral force, which results not only in an overturning moment overstrength demand from the wall but also in an unrealistic M/V ratio due to the unrealistic distribution of lateral load; (b) the ductile moment-resisting space frame shall have the capacity to resist not less than 25% of the required lateral force; and (c) the wall edge members shall be designed to carry all the vertical stresses resulting from the wall loads in addition to tributary dead and live loads and from the prescribed horizontal seismic force. It was in fact fortunate that requirements (a) and particularly (c) were not satisfied in the design of the test building. If these requirements had been satisfied, the overturning moment overstrength of the wall would have been so large that the model might have failed in shear with relatively very small amounts of flexural yielding.

(2) The strain hardening of the main reinforcement, which increased the resistance offered by the reinforcement from the yielding strength, 59 ksi (406 MPa),

to practically its tensile strength, 79 ksi (544 MPa), in the case of the wall's edge members.

(3) The significant contribution of the reinforced concrete floor slab, particularly the contribution of its reinforcement to the negative moment capacity of the beams, which is not considered at all in the UBC specifications.

(4) The three-dimensional interaction of the wall and the surrounding space frame which through outriggering action restrained both the growth* in height of the wall and the uplift of the wall during rocking behavior.

Because the strength of the test building was found to be just sufficient to survive the effects of a horizontal component of an extreme earthquake ground motion expected in the U.S., it appears that the seismic forces specified by the UBC (as well as procedures recommended for the estimations of demanded resistance for the components of the structure) should be reviewed to make these expressions more compatible with the strengths that are supplied according to UBC design and detailing requirements.

16. The distribution of the total lateral seismic force over the height of the structure specified by the UBC (i.e. the inverted triangular distribution) appears to be adequate for the estimation of the demands for the axial-flexural design of members (i.e. estimation of maximum overturning moment) but is not conservative for the estimation of story shear strength demands. For shear strength demands it appears more rational to consider a uniform distribution rather than the inverted triangular distribution specified by the code (Fig. 29).

17. The effective fundamental period, T, of the 1/5th-scale model varied between 0.21 to 0.67 secs (see Tables 12 and 15) (which can be translated to the full-scale model as 0.47 to 1.5 secs), depending on the damage introduced by previous

* This growth in height of the wall is due to the accumulation of permanent plastic elongation of the reinforcement at the wall base as well as slippage of this reinforcement along its embedment length in the concrete at the foundation.

excitations and the amplitude of the vibrations at the time that T was measured. These values agree very well with those measured in the full-scale model: 0.43 to 1.47 secs. After the 1/5th-scale model was subjected to shaking that can be considered to represent minor earthquake motion, i.e. at the service limit state, the period when translated to the full-scale model was already between 0.5 and 0.6 secs. Thus, two practical questions arise: First, what is the period that should be considered for the preliminary design of structures? Secondly, how well do these measured values correlate with the values recommended by the UBC?

A unique answer cannot be provided to the first question because the period to be used in preliminary design will depend on the design criteria, i.e. the parameter or limit state that controls the design. For example, if strength controls the design, the designer should analyze both elastic and inelastic response spectra and select from the potential service range of T^* the value that is critical, i.e. the value that results in the largest required seismic resistance coefficient. Where lateral drift controls, the value of T should be that which in the service range of T results in the maximum lateral displacement.

In answer to the second question, it should first be noted that the UBC allows T to be estimated by the formula $0.05h_n/\sqrt{D}$ to facilitate preliminary design. For the test structure, this formula results in $T = 0.47$ secs, very close to the lower value measured in the model. Although in this case the UBC value agrees very well with the measured value, use of this equation generally does not result in reliable values [33]. In comparing the measured value of T with that given by the UBC formula, it should be noted that the measured T represents the value corresponding to just the bare structure. The UBC formula should, on the other hand, give the value of T for the whole building, i.e. considering the interaction of the

* That is, the range between the value of T from the moment that construction is completed, in this case 0.47 secs, to the value that T can have due to the damage (cracking) introduced by the service loads (live, wind, minor earthquake, etc.) to which the building might be subjected before a major earthquake occurs, say $T = 0.6$ sec.

nonstructural components with the structural system. Thus, a finding that the measured value correlates well with the UBC prediction does not indicate that the expression is reliable. The code should provide equations that will yield ranges of values of T rather than an expression for estimating a single value.

7.3 Implications for State of Art

The results of this study were analyzed to assess implications for the states of the art of seismic resistant design and the art of predicting seismic response where experimental techniques are based on reduced-scale models tested on earthquake simulators.

7.3.1 State of Art in Seismic Resistant Design of Frame-Wall Structures. As pointed out in the introduction to this report, a major objective of the studies conducted at the University of California, Berkeley, was to assess the implications of results on the state of the art of seismic resistant *design and construction* of reinforced concrete frame-wall structures. In attempting to do so, it must be recognized that *design* is something more than analysis. There must first be a design for there to be an analysis. Although this is true for the analysis of structural response to any excitation, the dependence of analysis on design is of paramount importance to seismic resistant design since even the earthquake excitations for which a building is designed depend upon the design. It is therefore important to distinguish clearly between the state of the art of predicting the seismic response of designed structures and the state of the art of seismic resistant design.

Seismic Resistant Design. Proper design of seismic resistant structures requires that the intimate interrelationship between the two sides of the design equation, i.e. between demand and supply, be recognized. Preliminary design of a frame-wall structure requires that the designer visualize how the proportioning of the structural components will affect the demands of first the seismic forces that will be developed and then of the internal forces that these seismic forces in combination with existing gravity forces will induce. With respect to this required visualization of the *overall behavior* of frame-wall

structures, the experiments described here clearly indicate that:

1. Present knowledge of the three-dimensional seismic behavior of frame-wall structures is not satisfactory. There is especially a lack of understanding of behavior in the inelastic range. The tendencies of the test wall to grow in height, and particularly to rock about its edge members thereby triggering significant outriggering action from the space frame surrounding the wall, are phenomena that have not been considered properly.

2. Present knowledge of the participation of the floor system in contributing to the lateral stiffness and particularly to the lateral resistance (strength) needs to be improved.

3. Present methods of estimating the actual supplies of stiffness, strength, and energy dissipation capacity (hysteretic behavior) need to be improved as discussed in more detail below. If by proper proportioning and detailing of the critical regions of structural members these regions are provided with sufficiently large ductility, then it is possible to estimate the maximum strength of three-dimensional structures using a limit analysis approach. This relatively simple way of estimating the maximum strength can be used to advantage in the *preliminary design of frame-wall* structural systems.

Predictions of Seismic Response. From the problems encountered in analytically predicting the seismic response of the full-scale and 1/5th-scale models and from a comparison of these predicted values with experimental values, the following are observed:

1. It is well recognized that present mathematical modeling of three-dimensional building-foundation-soil systems is far from realistic [34]. The studies reported here demonstrate that even in the *case of a simple symmetric three-dimensional bare frame-wall structural system* where the design—proportioning and detailing—is well documented and the fabrication of structural materials and construction are

carefully controlled, analytical modeling (particularly modeling of wall and T-beam behavior) is seriously inadequate. Improvement is needed in the analytical modeling of the following:

(a) *Beams*, where the contribution of the floor system to beam stiffness and strength is considered (compare Figs. 7 through 9 with Figs. 43 through 47). Present methods for modeling the hysteretic behavior of girders either as one- or two-component models are adequate only for symmetrically reinforced prismatic elements, subjected to moment only at their ends and only where flexural behavior controls response. Models need to be developed in which the analyst can exercise more control over the behavior of the element, and preprocessing software needs to be developed which may help the analyst formulate the numerical parameters that govern the response of such models. Furthermore, the analytical techniques used to determine average moment-curvature relations for sections, and which assume that plane sections remain plane, cannot predict accurately the strength and ductility of sections when wide reinforced slabs are cast monolithically with the beam stem.

(b) *Walls* which are considered as beam-column elements with a fixed neutral axis at the longitudinal centroidal axis of the cross section. The observed migration of the neutral axis should be considered. Furthermore the effects of axial force on the stiffness and strength of walls are not realistically modeled as discussed in more detail below.

(c) *Column stiffnesses*, which usually neglect the effect of varying axial force. This is unrealistic and is also discussed in more detail below.

2. Present techniques of modeling three-dimensional multistory frame-wall structures as pseudo-three-dimensional models based on the assumption of independent planar behavior of each frame and frame-wall are not realistic. The experiments clearly show the significant three-dimensional interactive effects of the wall

and the frame members framing perpendicular to the plane of the wall. Differences in vertical deformations of the wall and frames induces an outrigger-ing action of the space frame on the wall that significantly influences the stiffness and strength of the whole structure because it leads to the development of changes in axial force in the columns and the wall.

3. The results have categorically shown the important role of axial force in determining the lateral stiffness of reinforced concrete structural elements, columns, and particularly walls. When axial force is increased in compression between zero and the value that corresponds to the balance point in the M-N diagram, the flexural and particularly the shear stiffnesses of nonslender columns and walls increase significantly. When the axial force is tensile, increased tension decreases flexural and shear stiffnesses. These observed effects of axial force on the columns and wall need to be introduced in analytical modeling of columns and walls if realistic analytical predictions, particularly in the inelastic range, are desired. Reliable data regarding how the flexural (EI), shear (GA) and axial (EA) stiffnesses are affected by the intensity and history of variations of the axial force in columns and walls are needed before realistic analytical modeling of the hysteretic behavior of these elements can be formulated.

4. The analytically predicted responses prior to testing the full-scale and 1/5th-scale models did not correlate well with the measured responses. The analytical predictions significantly underestimated the observed dynamic strength at different limit states, particularly at the ultimate state (Fig. 10). Reasons for this underestimation have already been discussed. Only after modifying the mathematical model of the structure according to behavior observed during the tests was it possible to correlate the analytical and measured behavior of the models reasonably well. By including the observed three-dimensional effects due to the rocking movement of the wall and a more realistic contribution of the floor slab to the lateral strength of

the structure as well as the realistic distribution of seismic force over the height of the structure, reasonable estimates of the observed maximum strength of the 1/5th-scale model were obtained (Fig. 51 and Table 18). The results of these correlation studies emphasize the importance of integrated experimental and analytical research if the state of the art of the seismic resistant design of structures is to be improved.

7.3.2 State of Art of Reduced-Scale Models and Earthquake Simulator Facilities. The following conclusions are based on the response of the 1/5th-scale model tested on the shaking table at the Berkeley Earthquake Simulator Laboratory.

Construction of 1/5th-Scale Model. The most difficult step in attaining a true replica of the full-scale model with the same strain response history when subjected to similar seismic effects was in satisfying the similitude requirements for the mechanical characteristics of the constituent materials. The state of the art of design and fabrication of microconcrete was inadequate. Although it was possible to achieve good similitude for the modulus of elasticity and the Poisson's ratio at stress levels corresponding to serviceability limit states, the strain at maximum compressive strength, the tensile strength, bond characteristics, and volumetric changes could not properly be simulated. The ability of the model microconcrete to simulate the cracking limit state of the full-scale model was therefore questionable.

The substantially larger shrinkage of the microconcrete in the 1/5th-scale model and the fact that the gravity (dead load) axial stresses after removal of the formwork were just 1/5 (i.e. $1/S_l$) of those in the full-scale model resulted in an initial state of stress quite different from that in the full-scale model. The effect of this difference was evident from the the lateral flexibility of the two models. This result points out the importance of limiting the shrinkage of microconcrete and of loading reduced-scale models with auxiliary mass to simulate gravity stresses as models are constructed or as soon as possible after the removal of formwork.

Performance of Shaking Table. The fidelity of earthquake ground motions reproduced by the earthquake shaking table to input ground motion was not very good, particularly for larger intensity inputs (Table 14) due to the interaction of the simulator and model. The table was loaded by the maximum weight that it can accommodate when severe ground motion such as the largest motions used in these tests are applied. This lack of fidelity has not affected the correlation studies for the 1/5th-scale model and the full-scale model, as discussed later, and will not significantly affect further analytical studies presently being conducted on the response of the 1/5th-scale model because the measured table motions will be used as input. If, however, the results reported here are evaluated with a view to evaluating the performance of similar buildings subjected to a ground motion such as the T 40.3g, it is important to recognize that the motion to which the 1/5th-scale model was subjected was not the original recorded Taft accelerogram normalized to 40.3%g, but a distorted one, with lesser damage potential, due to a lack of fidelity in the simulation of motion.

Correlation of 1/5th-Scale Model and Full-Scale Model. Because the 1/5th-scale and the full-scale models were subjected to quite different numbers, duration, sequence, and even type of excitation, it is very difficult to correlate the experimental results. (Compare Tables 13 and 16.) Although the ground motion records were initially the same (the Miyagi-Oki, MO, record) the duration of the record, and the manner in which the earthquake excitation was introduced and particularly the rate of application of these excitations was quite different in the two cases. These differences render any attempt to correlate results very difficult. From the preliminary correlation studies conducted the following observations can be drawn.

1. *Static and Dynamic Mechanical Characteristics.* (a) *Initial Lateral Flexibility.* Because the initial states of stress in the two models after construction differed so greatly (particularly the axial stress state) due to differences in the volumetric change characteristics of the concrete used in the full-scale model and the micro-

concrete and the lack of similitude in mass, the lateral flexibility of the 1/5th-scale model was significantly larger. Only after the simulation of mass was accomplished by adding the auxiliary mass did the initial lateral flexibility correlate well.

(b) *Dynamic Characteristics.* Once the necessary auxiliary mass had been added the periods and equivalent viscous damping ratios agreed well. As the damage induced in the two models (at similar levels of imposed lateral deformation) increased, the correlation of values of the periods and damping ratios decreased and after being subjected to a roof drift index of 1.5% the fundamental period of the full-scale model was 25% higher than the value obtained for the 1/5th-scale model when an appropriate conversion factor is used. The damping ratio of the 1/5th-scale model after a roof drift index of 1.5% was about 7.7% while the corresponding ratio for the full-scale model for this same drift was 11.4%.

2. *Overall Lateral Load-Deformation Correlation.* The correlation at the serviceability limit states was good (Fig. 41). After roof drift indices that induced yielding, the 1/5th-scale model exhibited a relatively larger lateral strength (resistance) for similar lateral displacements. The maximum base shear for the 1/5th-scale model ($51\%W$) was 40% greater than that of the full-scale model ($36.5\%W$) when loaded with an inverted triangular distribution of lateral force. This significant difference was due to the methods of testing used, particularly the different distributions of total lateral force along the height of the structure. A somewhat better correlation is obtained when the envelope of overturning moment to roof drift index is compared. When the full-scale structure was loaded under a uniform distribution of lateral load, its maximum strength was practically the same as the scaled maximum strength obtained in tests of the 1/5th-scale model. The roof drift index at which the 1/5th-scale and full-scale models reached their maximum lateral strength correlate very well: 1.4% for the 1/5th-scale model and 1.5% for the full-scale model (Fig. 41) for triangular loading and 1.35% in the case of uni-

form lateral loading.

3. *Hysteretic Behavior.* The full-scale model as well as the 1/5th-scale model exhibited excellent hysteretic behavior. Although the individual hysteresis loops do not match well since the models were subjected to different excitation histories, the shape of these loops (particularly for the most severe excitations) are quite similar. (Compare Figs. 30(f) and 54. Note that in Fig. 54, the hysteretic response of the full-scale model has been converted to 1/5th-scale.) Although both structures show some pinching in their hysteretic behavior, the amount was significantly smaller than that which one would expect from the experimental behavior of isolated shear walls. The main reason for this better behavior appears to be the three-dimensional interaction of space frame and wall, particularly the outriggering action of the surrounding ductile space frame on the wall after flexural yielding and even after the failure of its reinforcement. The energy dissipated by the 1/5th-scale model considerably surpassed that of the full-scale model, again primarily due to the method of testing: dynamic vs pseudo-dynamic (rate of straining) and particularly due to loading history.

4. *Crack Pattern.* The overall crack pattern at the critical regions was similar, but the number and spacing of cracks differed. The total number of cracks was smaller in the 1/5th-scale model. Reasons for this lack of correlation are: (a) the higher tensile strength of the microconcrete; (b) the considerably higher strain rate induced in the 1/5th-scale model; (c) the higher strain gradient along the length of the critical regions of the members and through the critical sections of the members of the 1/5th-scale model. The main cracks of the floor slabs along the edges of the main beams were similar. The cracks in the slabs of the full-scale model were, however, considerably larger in number due to the manner in which force was applied.

5. *Failure Mechanisms.* (Fig. 55) At first sight the failure mechanisms appear to be quite different: while the 1/5th-scale model failed due to buckling and/or due to tensile fracture of the wall main reinforcement after crushing and spalling of the concrete cover of the wall edge members at the base of the wall, the failure of the full-scale model was due to crushing and spalling of the concrete at the wall edge member and particularly crushing in the wall panel which led to a final sliding shear failure of the wall at the first story with buckling and fracture of some of the reinforcement. These differences in failure mechanism are attributable to differences in crack pattern and to the fact that at failure the nominal shear stresses were practically the same in the full-scale and 1/5th-scale models, while actual compressive strength and therefore shear resistance of the microconcrete was significantly higher in the 1/5th-scale model. Furthermore, a close examination of the state of damage in the 1/5th-scale model wall panel after failure revealed that there was some slight crushing and spalling as illustrated in the photo of Fig. 55(a), indicating that it was very close to a shear-compression type of wall panel failure such as that observed in the full-scale model. It can be concluded that the failure mechanism observed in the 1/5th-scale model was very close to the margin separating the observed flexural failure from the shear-compression wall panel failure observed in the full-scale model under a uniform distribution of seismic force.

6. *Concluding Remarks.* Despite significant differences in the methods of testing, time history of the applied excitations, and mechanical characteristics of the concrete materials, the correlation of behavior at the serviceability limit states and of the maximum lateral shear resistance and roof drift index was excellent.

   The results obtained in the tests conducted on the shaking table of the 1/5th-scale model are of great importance especially since these results provide a better idea of the dynamic response of the structure to earthquake ground motion than the

pseudo-dynamic tests as conducted on the full-scale structure. The advantages of testing reduced scale models on earthquake simulators over pseudo-dynamic testing of the full-scale model can be summarized as follows:

1. Reduced scale testing is more economical.

2. The structure is subjected to more realistic simulation of earthquake excitation and responses are therefore more realistic.

It should also be noted that during the experimental research several problems were encountered whose solution could be improved on in future studies. The following are recommendations for such improvement: (a) It would be desirable to increase the scale of the model. This would simplify fabrication of structural materials (concrete and reinforcing steel), construction of the model, and reduce shrinkage of the model concrete. A relatively smaller auxiliary mass would be needed, the effects of strain rate and strain gradient on the cracking pattern would be reduced and therefore their effect on the stiffness and strength of the model would be reduced. Finally, if a larger model could be used, instrumentation would be less difficult. (b) It would be desirable if the fidelity of the shaking table in reproducing ground motion could be improved, and if the table were capable of introducing at least the two independent horizontal components of recorded ground motion. (c) The implementation of control devices that would shut off all input excitation when the shaking table control system breaks down during testing would be desirable. This is related to one of the main disadvantages of using an earthquake simulator in lieu of pseudo-dynamic testing. Once the test has begun it cannot be stopped to observe the sequence of damage. The smaller the scale the shorter the duration of the test and therefore the greater the difficulty of observing the damage sequence. (d) There is a need to increase the present capability of the data acquisition system at the Berkeley facility for studies similar to that reported here.

VIII SUMMARY, CONCLUSIONS, AND RECOMMENDATIONS

8.1 Summary

This report summarized the research conducted at Berkeley as part of the Reinforced Concrete Building Structure (a seven-story frame-wall structure) Phase of the U.S.-Japan Cooperative Research Program. Besides summarizing the studies conducted at Berkeley on the 1/5th-scale model of the test building, the report has the following main objectives: (a) to evaluate the results of these studies and discuss the degree of correlation between the experimental response of the full-scale model tested in Japan and the 1/5th-scale model tested in Berkeley, and between the analytically predicted and experimental responses; (b) to assess the states of art and practice of seismic resistant design and construction of reinforced concrete frame-wall structures in light of this evaluation; and (c) to formulate recommendations for improvement in the states of the practice and art.

The analytical studies conducted to review the soundness of the preliminary design and to produce the analytical information required to determine the largest scale model of the full-scale structure that could be accommodated on the shaking table at Berkeley were discussed first. The design of the 1/5th-scale model, the selection and problems encountered in the fabrication of the model materials, as well as in the determination of the mechanical characteristics of these materials, and in the construction of the model and instrumentation were discussed next. Problems encountered in achieving similitude with the full-scale model were noted. The results of the experiments designed to determine the initial mechanical characteristics (static and dynamic) of the 1/5th-scale model were presented and compared to analytically predicted values and to experimental values from tests of the full-scale model.

The remainder of the report was devoted to: (a) a discussion of the experiments conducted on the 1/5th-scale model at the Berkeley earthquake simulator facility, and the illustration of maximum responses; (b) a comparison of experimental results with

those obtained for the full-scale model tests and those predicted analytically; (c) an analysis of the implications of the above results on the states of the practice and art of seismic resistant design and construction of reinforced concrete frame-wall structures; and (d) an analysis of the results as they relate to the reliability of the experimental technique of testing reduced-scale models on earthquake simulator facilities.

8.2 Conclusions

Specific conclusions regarding problems encountered in the studies conducted have been drawn where such problems were first discussed. Only the most important of conclusions regarding the objectives of the U.S.-Japan Cooperative Research Program are reported below. *These conclusions are, strictly speaking, valid only for the test building considered here and for the type of excitation to which this model was subjected. These conclusions should therefore be extrapolated only after the limitations of the study have been carefully evaluated.* Some of these limitations are: (a) that the test building consisted of just a bare structure (the effects of nonstructural components being therefore not considered) and the reactive mass was less than 9 percent larger than the bare structure's mass; (b) the foundation of the bare structure was very stiff and was prestressed to the rigid shaking table; (c) the structure was subjected to only one horizontal component of ground motion in the direction of the main shear wall plane; and (d) the torsional rigidity of the structure was increased significantly by the use of special peripheral walls which also acted as effective outriggers and contributed to the overturning capacity of the structure.

8.2.1 Design of Test Structure. From a review of the original preliminary design, it can be concluded that:

1. The design of the model was conceptually good. The main members of the beams, columns, and the main wall of the test structure were slender and lightly reinforced. Therefore, these members developed relatively low shear stresses and were capable of undergoing large inelastic deformation and had sufficient ductility

to permit the test structure to be converted into a complete mechanism. As a result, the structure was able to dissipate a large amount of energy through the dynamic motion of this mechanism.

2. The design did not satisfy the 1979 UBC requirements for either a $K = 0.8$ or a $K = 1.0$ structural system. The demanded axial-flexural strengths of the wall were 50% and 20% higher than the supplied strengths for $K = 1.0$ and 0.8, respectively. For $K = 0.8$, the supplied strength to the wall edge members was only 60% of the UBC demanded strength. If the test structure were classified as a $K = 1.0$ structural system, the demanded shear strength from the wall would be higher than the supplied strength computed according to UBC regulations. For $K = 0.8$, and where redistributions of moment are not considered, the flexural strength demanded of the beams of the central frame (i.e. the frame with the wall) exceeded the supplied strength. The column detailing did not satisfy the UBC requirements for confinement and shear resistance.

3. Despite noncompliance with the 1979 UBC requirements, with the exception of some improvement in the detailing of the reinforcement, no significant modification of the original preliminary design was recommended. This decision was taken as a consequence of conclusion 1 above.

4. The lateral strength, based on a limit analysis and considering only planar behavior of the wall and frames, was 607 kips (2701 kN) which was 1.8 times the UBC required strength for $K = 0.8$ structural systems.

8.2.2 Reliability of Predictions of Seismic Behavior from Experiments Conducted on Reduced-Scale Models and Using Earthquake Simulator Facilities. From a comparison of results from tests on the 1/5th-scale model with those from tests on the full-scale model, and from analytical studies, it can be concluded that the shaking table tests of the 1/5th-scale model provided reliable results from which the seismic behavior of the bare building structure could be predicted for the ground excitations used.

8.2.3 Reliability of Predicting Seismic Behavior Using Available Linear and Nonlinear Structural Analysis Computer Programs.

1. Present computer programs for linear dynamic analysis of multistory buildings can be used with sufficient practical accuracy in the serviceability limit state provided that correct assumptions regarding the stiffness of members and damping ratio are made. Reliable experimental data are needed regarding these two parameters.

2. Presently, computer programs for nonlinear dynamic analysis cannot provide good predictions of seismic structural behavior in the range beyond the serviceability limit states.

3. There is an urgent need to improve the mathematical modeling of the nonlinear behavior: of beams, including the effect of the contributions of floor slabs on their stiffness and strength; of columns, including the effect of varying axial force on their stiffness; and of walls, including the effect of varying axial force on their stiffness as well as the effect of changes in location of the neutral axis.

4. Nonlinear dynamic analysis computer programs must be developed which incorporate the observed three-dimensional effects such as the outriggering action of the frames on the walls that resulted from the growth in height of the wall and the uplift due to its rocking response.

8.2.4 Reliability of Maximum Strength Prediction by Limit Analysis. Limit analysis incorporating: (i) measured material properties; (ii) the effects of axial force on moment capacity of R/C columns and wall; (iii) contribution of the entire slab and the steel in the slab to the moment capacity of all girders; (iv) contribution of the transverse girder-slab system to lateral resistance (3-D effect); and (v) the experimentally measured lateral force distribution (at the time of maximum base shear during the T 40.3 test) was successful in predicting the measured maximum lateral resistance of the structure during the T 40.3 test.

8.2.5 States of Practice and Art of Seismic Resistant Design and Construction of Frame-Wall Structures.

1. Significant interacting three-dimensional effects occur due to differences in the lateral and vertical deformation characteristics of the wall and frames. These three-dimensional interactions give rise to significant outriggering action of the frames on the walls. Given that this outriggering action was observed when the structure was loaded in only one lateral direction, the importance of testing with all components of ground motion acting simultaneously is obvious. In fact, many of the conclusions noted here may have to be modified if the stiffness, strength, and energy dissipation demands imposed by the other horizontal (transverse), vertical, and torsional components of ground motion were to occur simultaneously with the demands imposed by the excitations along the test direction.

2. Present UBC seismic design regulations are based on seismic forces that are unrealistically low when compared with the seismic forces that develop in resulting UBC designs (see conclusion 4 below).

3. The UBC lateral seismic force distribution along the height of the structure is not conservative for design against shear.

4. The UBC design procedure results in a design with lateral (shear and overturning) strength significantly higher than the demanded strength.

5. The UBC methods of estimating the axial-flexural and shear strength capacities of beams, columns, and walls for seismic excitations are too conservative. The rationality of present UBC formulae for predicting the supplied shear strength of columns and walls for seismic excitation is highly questionable.

6. Designs should not be based on a single deterministic value for the fundamental periods of structures. The period increases with increases in the degree of damage. Even lateral loads at service level can produce significant changes in the period, so possible bounds should be considered.

8.3 Recommendations for Improvement in States of Art and Practice of Seismic Resistant Design of Reinforced Concrete Frame-Wall Structures

From the problems encountered during the studies described here, further research on the subjects indicated below should be conducted if the understanding of the behavior of reinforced concrete frame-wall structures is to be improved and the experimental and analytical techniques used to predict such behavior refined. As an interim solution, some changes should be introduced to present code regulations.

8.3.1 Research Needs

1. Experimental studies on the mechanical characteristics and physical properties of microconcrete should be carried out so that the simulation of concrete in small-scale models can be improved. Techniques used to test concrete to determine reliable constitutive relations and failure criteria for this material under all possible strain states should be developed and standardized. Special attention should be paid to the effects of specimen size as well as strain rate and gradient.

2. Integrated experimental and analytical studies should be carried out on the contribution of reinforced concrete slabs to the lateral stiffness and strength of structures at all limit states. Studies should focus on the variation of this contribution as the lateral deformation increases from zero to the value at which a structure fails.

3. The growth in height of shear walls with increases in lateral deformation and number of reversals, and the effects of this growth on the three-dimensional behavior of the frame surrounding the wall in a frame-wall structural system should be studied.

4. The effects of varying axial force on the stiffness and strength of columns and walls should be investigated experimentally and analytically.

5. The effects of all components of ground motion acting simultaneously on the

foundation of frame-wall structures should be investigated experimentally and analytically, with particular emphasis on the effects on three-dimensional behavior of these structures.

6. The possible effects of flexible foundations and soil foundation-superstructure interaction on the overall response of frame-wall structures should be evaluated.

8.3.2 Improvement in State of Practice of Seismic Resistant Design and Construction of Frame-Wall Structures

1. Present UBC seismic regulations need to be improved in at least six areas: (a) the level of seismic force should be increased to make it compatible with the actual supplied stiffnesses and strengths that result from present UBC computational procedures for estimating supplies. (b) The UBC analysis and design procedure should be modified to incorporate the many observed mechnisms of strength provided by a properly conceptually designed and constructed structure, which are presently ignored. In this manner, the designer should be guided to conduct a realistic evaluation of both *DEMANDS* and *SUPPLIES* in the design process. (c) The effects of at least the two horizontal components of ground motion that act simultaneously on the foundation of a structure should be considered. (d) The fundamental period of structures should be estimated by formulae that allow for possible bounds on its value. (e) The distribution of lateral seismic force along the height of a wall for its design against shear should be changed to a uniform distribution. (f) Provisions for estimating the supplied shear strength of columns and walls should be reviewed.

2. The UBC should add, either in its earthquake regulations or in a special commentary, a recommendation that emphasizes the need to control the amount of shear that can be developed at the critical regions of the structural components of a R/C frame-wall structural system. The importance of proper selection of the structural layout, the slenderness ratio of the members, and the amount of flexural

reinforcement should be clearly spelled out.

3. The UBC seismic regulations or a special commentary to these regulations should make designers aware of the importance of three-dimensional interacting behavior of walls and surrounding frames, and of the significance of rocking and growth of the wall at the base and the consequential outriggering action that the surrounding frames will exert on walls. These interacting three-dimensional effects should be considered in selecting the proper number and distribution of walls in the plan of the structure. Further, due to the effects of three-dimensional interacting behavior, the UBC should require that all frame elements, even those that are not part of the primary lateral load-resisting system, should be designed with adequate ductility.

4. In the requirements for the design of beams, the UBC should add regulations regarding the contribution of slab reinforcement to the negative bending moment capacity of beams, and the influence that this contribution would have on the design of beam-column joints and columns.

REFERENCES

[1] U.S.-Japan Planning Group, Cooperative Research Program Utilizing Large-Scale Testing Facilities, "Recommendations for a U.S.-Japan Cooperative Research Program Utilizing Large-Scale Testing Facilities," *Report No. UCB/EERC-79/26*, Earthquake Engineering Research Center, University of California, Berkeley (1979).

[2] S. A. Mahin and M. E. Williams, "Computer Controlled Seismic Performance Testing," paper presented at the Second ASCE-EMD Speciality Conference on Dynamic Response of Structures, Atlanta, Georgia (1981).

[3] S. Okamoto *et al.*, "A Progress Report on the Full-Scale Seismic Experiment of a Seven Story Reinforced Concrete Building—Part of the U.S.-Japan Cooperative Program," *Proceedings of the Third Joint Technical Committee U.S.-Japan Cooperative Program*, Building Research Institute, Tsukuba, Japan (1982).

[4] *Uniform Building Code,* 1979 Edition, International Conference of Building Officials, Whittier, California (1979).

[5] F. A. Charney and V. V. Bertero, "An Evaluation of the Design and Analytical Seismic Response of a Seven-Story Reinforced Concrete Frame-Wall Structure," *Report No. UCB/EERC-82/08*, Earthquake Engineering Research Center, University of California, Berkeley (1982).

[6] "Tentative Provisions for the Development of Seismic Regulations for Buildings," *ATC Publication No. ATC 3-06, NBS Publication 510, NSF Publication 78-8*, prepared by the Applied Technology Council (1978).

[7] T. Paulay, "Earthquake Resistant Structural Walls," *Proceedings of a Workshop on Earthquake Resistant Reinforced Concrete Building Construction [ERCBC]*, V. V. Bertero, organizer, Vol. III, pp. 1339-1365, University of California, Berkeley (1977).

[8] E. L. Wilson, "SAP-80: Structural Analysis Programs for CP/M Microcomputer Systems," Structural Analysis Programs, Inc., El Cerrito, California (1980).

[9] A. Sudhakar, *et al.,* "ULARC Documentation," National Information Service for Earthquake Engineering (NISEE), Computer Applications, Earthquake Engineering Research Center, University of California, Berkeley, California (1973).

[10] A. E. Kanaan and G. H. Powell, "DRAIN-2D, A General Purpose Computer Program for Dynamic Analysis of Planar Structures," *Report No. UCB/EERC-73/06*, Earthquake Engineering Research Center, University of California, Berkeley (1973).

[11] J. W. Chávez, "Study of the Seismic Behavior of Two-Dimensional Buildings: A Computer Program for Dynamic Analysis: INDRA," *Bulletin of IISEE,* Tsukuba, Japan, Vol. 18 (1980).

[12] F. A. Charney and V. V. Bertero, "Correlation of Experimental and Analytical Response of a 1/5 Scale Reinforced Concrete Frame-Wall Structure," *Proceedings of the Fourth Joint Technical Coordinating Committee*, U.S.-Japan Joint Cooperative Earthquake Research Program, Tsukuba, Japan (1983).

[13] H. G. Harris, V. V. Bertero, and R. W. Clough, "One-Fifth Scale Model of a Seven-Story Reinforced Concrete Frame-Wall Building Under Earthquake Loading," *Proceedings of the Seminar on Dynamic Modelling of Structures,* Joint I. Struct. E./B.R.E., Building Research Station, Garston, England (1981).

[14] R. M. Stephen *et al.*, "Structural Dynamic Testing Facilities at the University of California, Berkeley," *Report No. EERC 69-8*, Earthquake Engineering Research Center, University of California, Berkeley (1969).

[15] D. Rea, S. Abedi-Hayati, and Y. Takahashi, "Dynamic Analyses of Electrohydraulic Shaking Tables," *Report No. UCB/EERC-77/29*, Earthquake Engineering Research Center, University of California, Berkeley (1977).

[16] H. G. Harris and V. V. Bertero, "One-Fifth Scale Model of a Seven-Story R/C Frame-Wall Building Under Earthquake Loading," in-house Report, University of California, Berkeley (1981).

[17] V. V. Bertero *et al.*, "Mechanical Characteristics of Materials Used in the 1/5 Scale Model of the 7-Story Reinforced Concrete Test Structure," *Report No. UCB/EERC-83/21*, Earthquake Engineering Research Center, University of California, Berkeley (1983).

[18] R. Sause and V. V. Bertero, "A Transducer for Measuring the Internal Forces in the Columns of a Frame-Wall Reinforced Concrete Structure," *Report No. UCB/EERC-83/05*, Earthquake Engineering Research Center, University of California, Berkeley (1983).

[19] P. D. Monkarz and H. Krawinkler, "Theory and Application of Experimental Model Analysis in Earthquake Engineering," *Report No. 50*, The John A. Blume Earthquake Engineering Center, Dept. of Civil Engineering, Stanford University, Stanford, California (1981).

[20] J. K. Wight and S. Nakata, "Construction of the Full-Scale Seven-Story Reinforced Concrete Test Structure," *Proceedings of the Second Joint Technical Coordinating Committee*, U.S.-Japan Joint Cooperative Earthquake Research Program, Tsukuba, Japan (1982).

[21] F. A. Noor and S. Wijayasri, "Modelling the Stress-Strain Relationship of Structural Concrete," *Magazine of Concrete Research*, Vol. 34, No. 116 (1983).

[22] A. E. Aktan and V. V. Bertero, "1/5 Scale Model of the 7-Story R/C Frame-Wall Test Building: Design and Construction," *Proceedings of the Third Joint Technical Coordinating Committee*, U.S.-Japan Joint Cooperative Earthquake Research Program, Tsukuba, Japan (1982).

[23] C. H. Willetts, "Investigation of the Schmidt Concrete Test Hammer," *Miscellaneous Paper No. 6-287*, U.S. Army Corps of Engineer Waterways Experiment Station, Vicksburg, Mississippi (1958).

[24] A. E. Aktan *et al.*, "Experimental and Analytical Predictions of the Mechanical Characteristics of a 7-Story 1/5 Scale Model R/C Frame-Wall Building Structure," *Report No. UCB/EERC-83/13*, Earthquake Engineering Research Center, University of California, Berkeley (1983).

[25] S. Okamoto, "Characteristics of BRI Facilities," *Proceedings of the First Joint Coordinating Committee*, U.S.-Japan Joint Cooperative Earthquake Research Program, Tsukuba, Japan (1981).

[26] M. T. Wagner and V. V. Bertero, "Mechanical Behavior of Shear Wall Vertical Boundary Members: An Experimental Investigation," *Report No. UCB/EERC-82/18*, Earthquake Engineering Research Center, University of California, Berkeley (1982).

[27] R. J. Hansen, editor, *Seismic Design for Nuclear Power Plants,* The M.I.T. Press, Cambridge, Massachusetts (1970).

[28] R. Sause and V. V. Bertero, "The Experimental Study of the Global Response and the Development and Distribution of Forces at the Base of a 7-Story 1/5 Scale R/C Frame-Wall Structure Subjected to Simulated Earthquake Shaking," Earthquake Engineering Research Center, University of California, Berkeley, in preparation.

[29] G. M. Sabnis *et al., Structural Modeling and Experimental Techniques*, Prentice Hall, Inc., New Jersey (1983).

[30] F. Filippou, E. P. Popov, and V. V. Bertero, "Effects of Bond Deterioration on Hysteretic Behavior of Reinforced Concrete Joints," *Report No. UCB/EERC-83/19*, Earthquake Engineering Research Center, University of California, Berkeley (1983).

[31] D. P. Mondkar and G. H. Powell, "ANSR-I: General Purpose Computer Program for Analysis of Non-Linear Structural Response," *Report No. UCB/EERC-76/2,* Earthquake Engineering Research Center, University of California, Berkeley (1976).

[32] A. A. Chowdhury, "Mechanical Characteristics of Members of the 1/5th-Scale Model of the U.S.-Japan Seven-Story R/C Test Building," *Master of Engineering Thesis,* Division of Structural Engineering & Structural Mechanics, Department of Civil Engineering, University of California, Berkeley (1983).

[33] V. V. Bertero, "Implications of Recent Research Results on Present Methods for Seismic Resistant Design of R/C Frame-Wall Building Structures," *Proceedings,* 51st Annual Convention of SEAOC, Sacramento, California, pp. 79-116 (1982).

[34] V. V. Bertero, "State of the Art in the Seismic Resistant Construction of Structures," *Proceedings,* Third International Earthquake Microzonation Conference, June 1982, University of Washington, Seattle, Washington, Vol. II, pp. 767-809 (1982).

TABLES

TABLE 1 COMPARISON OF EXPERIMENTAL AND ANALYTICAL FLEXIBILITY

(a) ANALYTICAL FLEXIBILITY OF FULL-SCALE STRUCTURE* (10^{-3} in./kip)							
7	6	5	4	3	2	1	
8.57	6.98	5.39	3.88	2.51	1.35	0.49	7
6.98	5.89	4.67	3.42	2.25	1.23	0.46	6
5.39	4.67	3.87	2.93	1.98	1.10	0.42	5
3.88	3.42	2.93	2.37	1.66	0.95	0.37	4
2.51	2.25	1.98	1.66	1.28	0.78	0.32	3
1.35	1.23	1.10	0.95	0.78	0.56	0.25	2
0.49	0.46	0.42	0.37	0.32	0.25	0.17	1

* Based on cracked, transformed section inertia.

(b) ANALYTICAL FLEXIBILITY OF FULL-SCALE STRUCTURE* (10^{-3} in./kip)							
7	6	5	4	3	2	1	
2.35	1.94	1.52	1.11	0.75	0.43	0.18	7
1.94	1.68	1.35	1.01	0.69	0.40	0.17	6
1.52	1.35	1.16	0.90	0.62	0.37	0.16	5
1.11	1.01	0.90	0.76	0.55	0.34	0.15	4
0.75	0.69	0.62	0.55	0.46	0.29	0.14	3
0.43	0.40	0.37	0.34	0.29	0.24	0.12	2
0.18	0.17	0.16	0.15	0.14	0.12	0.10	1

* Based on uncracked, transformed section inertia.

(c) EXPERIMENTAL FLEXIBILITY OF FULL-SCALE STRUCTURE* (10^{-3} in./kip)							
7	6	5	4	3	2	1	
2.34	1.78	1.35	0.98	0.64	0.39	0.19	7
1.78	1.46	1.19	0.86	0.60	0.33	0.15	6
1.35	1.19	1.04	0.76	0.55	0.30	0.14	5
0.98	0.86	0.76	0.64	0.48	0.16	0.12	4
0.64	0.60	0.55	0.48	0.41	0.22	0.11	3
0.39	0.33	0.30	0.26	0.22	0.15	0.08	2
0.19	0.15	0.14	0.12	0.11	0.08	0.08	1

* From tests of full-scale model in Tsukuba, Japan [3].

(d) ANALYTICAL FLEXIBILITY OF FULL-SCALE STRUCTURE AFTER INTRODUCTION OF HINGE AT WALL BASE (10^{-3} in./kip)							
7	6	5	4	3	2	1	
17.84	15.42	12.95	10.45	7.93	5.41	2.90	7
15.42	13.59	11.59	9.46	7.24	4.97	2.67	6
12.95	11.59	10.09	8.36	6.47	4.47	2.41	5
10.45	9.46	8.36	7.09	5.57	3.89	2.11	4
7.93	7.24	6.47	5.57	4.49	3.20	1.75	3
5.41	4.97	4.47	3.89	3.20	2.34	1.31	2
2.90	2.67	2.41	2.11	1.75	1.31	0.76	1

1 in./kip = 5.71 mm/kN

TABLE 2 AREA* OF FULL-SCALE AND 1/5th-SCALE MODEL REINFORCEMENT

Bars	Prototype Area	Area Required for Similitude	Obtained Model Area	% Error
Column/ Edge Member	(D22 Bar) 0.5890	0.0236	(PCA/D2.5 Bar) 0.0214	(-) 9.17
Beam	(D19 Bar) 0.4394	0.0176	(PCA/D2.0 Bar) 0.0186	(+) 5.80
Wall/Slab/ Ties/Stirrups	(D10 bar) 0.1217	0.00487	(Knurled Wire 14 Gauge) 0.00464	(-) 4.68

*All areas are given in square inches.
1 in. = 25.4 mm

TABLE 3 STRESS-STRAIN CHARACTERISTICS OF FULL-SCALE MODEL STEEL*

Bar Size Bar	Test Series Test	E ksi	f_y ksi	ϵ_{STH} in./in.	E_{STH} ksi	f_u ksi	ϵ_u in./in.
D22	1	26300	57.79	-	-	88.91	0.242
	2		50.21	0.0125	915.97	81.78	0.191
D19	1	29500	52.23	-	-	62.24	0.229
	2		51.91	0.0165	785.12	81.50	0.214
D10	1	26200	52.55	-	-	77.33	0.204
	2		55.04	0.0185	735.33	81.21	0.210

*All quantities are average of three tests except E, which is the average of six tests.
E = modulus of elasticity
f_y = yield stress
ϵ_{STH} = strain at onset of strain hardening
E_{STH} = strain hardening modulus
f_u = maximum tensile stress
ϵ_u = ultimate strain

1 ksi = 6.89 MPa
1 in. = 25.4 mm

TABLE 4 CROSS-SECTION AREAS (in.^{2}) OF MODEL REINFORCEMENT OBTAINED BY DIFFERENT TECHNIQUES

Bar	Area Based on Volume/Length	Area Based on Direct Measurement		Effective Area*
		Maximum	Minimum	
PCA D2.5	0.0255	0.0238	0.0203	0.0214
PCA D2.0	0.0193	0.0190	0.0181	0.0186
14 Gauge Wire, Knurled	0.0051	0.0047	0.0041	0.0046

*Adopted as representative of area of bar for evaluating sectional characteristics.

1 in.^{2} = 6.45 cm^2

TABLE 5 STRESS-STRAIN CHARACTERISTICS OF MODEL STEEL

Bar	Statistics	E ksi	f_y ksi	ϵ_{STH} in./in.	E_{STH} ksi	f_u ksi	ϵ_u in./in.
PCA D2.5 Columns	Upper Bound*		60.58	0.0172	388.20	81.74	0.2386
	Lower Bound*		58.16	0.0128	357.60	76.26	0.1856
	Mean	28700	59.37	0.0150	372.90	79.00	0.2121
	Standard Deviation	3900	4.23	0.0068	53.33	9.58	0.0456
PCA D2 Beams	Upper Bound*		54.80	0.0260	506.00	72.40	0.216
	Lower Bound*		54.20	0.0250	482.00	72.00	0.202
	Mean	28900	54.50	0.0255	494.00	72.20	0.209
	Standard Deviation	4000	1.06	0.0018	48.60	0.80	0.019
14 Gauge Wire Walls/ Slabs	Upper Bound*		62.72	0.0337	236.00	79.51	0.1918
	Lower Bound*		60.42	0.0283	222.20	78.84	0.1758
	Mean	28800	61.57	0.0310	229.10	79.18	0.1838
	Standard Deviation	3200	3.21	0.0073	19.11	0.94	0.0207

* 90% confidence limit
E = modulus of elasticity
f_y = yield stress
ϵ_{STH} = strain at onset of strain hardening
E_{STH} = strain hardening modulus
f_u = maximum tensile stress
ϵ_u = ultimate strain

1 ksi = 6.89 MPa

TABLE 6 FORCE AND STRAIN RESPONSE CHARACTERISTICS FOR PROTOTYPE AND MODEL REINFORCEMENT

(a)

Reinforcement	E_p (ksi)	E_m (ksi)	F_{yp}* (kips)	F_{ym} (kips)	ϵ_{STH_p} (in./in.)	ϵ_{STH_m} (in./in.)
Columns	26300	28700	1.183	1.271	0.0125	0.0150
Beams	29500	28900	0.912	1.014	0.0165	0.0255
Walls/Slabs	26200	28800	0.258	0.286	0.0185	0.0130

(b)

Reinforcement	E_{STH_p} (ksi)	E_{STH_m} (ksi)	F_{up}* (kips)	F_{um} (kips)	ϵ_{up} (in./in.)	ϵ_{um} (in./in.)
Columns	916	373	1.927	1.691	0.191	0.2121
Beams	785	495	1.432	1.343	0.214	0.2090
Walls/Slabs	735	229	0.385	0.367	0.210	0.1838

* F_{yp} and F_{up} were divided by $(L_p/L_m)^2$.
Notes: Prototype values were from test series 2.
Mean values were used for model reinforcement properties.
E_p , E_m = modulus of elasticity for prototype and model.
F_{yp} , F_{ym} = yield force of prototype and model.
ϵ_{STH_p} , ϵ_{STH_m} = strain at onset of strain hardening.
E_{STH_p} , E_{STH_m} = strain hardening modulus for prototype and model.
F_{up} , F_{um} = maximum tensile force for prototype and model.
ϵ_{up} , ϵ_{um} = ultimate strain for prototype and model.

1 in. = 25.4 mm
1 ksi = 6.89 MPa
1 kip = 453 kg = 4450 N

TABLE 7 MAIN RESPONSE PARAMETERS OF FULL-SCALE AND 1/5th-SCALE MODEL REINFORCEMENT

Reinforcement	$\frac{E_m}{E_p}$	$\frac{F_{ym}}{F_{yp}}$	$\frac{\epsilon_{STH_m}}{\epsilon_{STH_p}}$	$\frac{E_{STH_m}}{E_{STH_p}}$	$\frac{F_{um}}{F_{up}}$	$\frac{\epsilon_{um}}{\epsilon_{up}}$
Columns	1.091	1.074	1.20	0.407	0.878	1.110
Beams	0.980	1.112	1.545	0.629	0.938	0.977
Walls/ Slabs	1.099	1.067	1.676	0.311	0.953	0.875

E_m, E_p = modulus of elasticity for model and prototype
F_{ym}, F_{yp} = yield force of model and prototype
ϵ_{STH_m}, ϵ_{STH_m} = strain at onset of strain hardening of model and prototype
E_{STH_m}, E_{STH_p} = strain-hardening modulus for model and prototype
F_{um}, F_{up} = maximum tensile force for model and prototype
ϵ_{um}, ϵ_{up} = ultimate strain for model and prototype

TABLE 8 CONCRETE MIXES USED IN FULL-SCALE MODEL

Story	Design Strengths (ksi)	Materials (lbs/cu. yd.)			
		Cement	Water	Sand	Gravel*
1 to 4	3.63	551.17	281.48	1336.62	1682.16
5 to 7	3.84	559.59	266.31	1309.65	1752.95

*Maximum size = 1-in. (2.54 mm) round aggregate.
1 ksi = 6.89 MPa
1 lb/cu. yd. = 5.82 N/m^3

TABLE 9 MECHANICAL CHARACTERISTICS OF FULL-SCALE CONCRETE

Location	Age (days)	$f_{c\max}$ (ksi)	ϵ_0 (in./in.)	$E_{0.33f_{c\max}}$ (ksi)	$E_{0.45f_{c\max}}$ (ksi)	f_{sp} (ksi)
First Floor	28	3.60				
	145	4.11	0.00218	3390	3150	0.34
Second Floor	28	3.68				
	132	4.15	0.00240	3360	3110	0.35
Third Floor	28	3.37				
	119	3.90	0.00228	3140	2950	0.34
Fourth Floor	28	3.43				
	111	4.13	0.00225	3000	2930	0.33
Fifth Floor	28	3.56				
	98	4.20	0.00210	3330	3150	0.34
Sixth Floor	28					
	87	2.05	0.00185	1980		0.19
Seventh Floor	28					
	67	2.69	0.00192	2470		0.19

1 ksi = 6.89 MPa

$f_{c\max}$ = maximum compressive concrete stress
ϵ_0 = strain at maximum concrete stress
$E_{0.33f_{c\max}}$ = secant modulus of elasticity at 33% of maximum compressive concrete stress
$E_{0.45f_{c\max}}$ = secant modulus of elasticity at 45% of maximum compressive concrete stress
f_{sp} = tensile strength from split cylinder test

TABLE 10 CONCRETE MIX USED IN 1/5th-SCALE MODEL

Materials	Parts by Weight	Weight per Cubic Yard, lbs.
Water	0.67	400
Cement, Lone Star Type I-II	1.00	597
Coarse Sand*, Radum Top	3.75	1139
Coarse Gravel*, Radum (1/4 in.)	1.00	597
Admixture, Pozzolith-300R	4 oz./100 lbs.	-

*Saturated surface-dry condition.

1 in. = 25.4 mm
1 lb. = 0.453 kg = 4.45 N
1 lb/cu. yd. = 0.592 kg/m^3
1 oz = 0.278 N

TABLE 11 MECHANICAL CHARACTERISTICS OF 1/5th-SCALE MODEL MICROCONCRETE*

Location	Age, days	Sample Size	$\bar{f}_{c\max}$ ksi	$\sigma_{f_{c\max}}$ ksi	$\bar{\epsilon}_0$ in./in.	σ_{ϵ_0} in./in.	$\bar{E}_{0.45f_{c\max}}$ ksi	$\sigma_{E_{0.45f_{c\max}}}$ ksi
Footing	254	1	5.44	--	0.00340	--	2970	--
Column Stubs	254	1	6.51	--	0.00330	--	3490	--
First Floor	28	3	3.61	0.116	0.00250	0.000325	2800	123.94
	216	2	5.68	0.032	0.00350	0.000141	3160	183.85
	456	4	5.67	0.215	0.00380	0.000206	2940	61.22
Second Floor	28	3	4.18	0.141	0.00292	0.000157	2940	109.70
	208	2	5.66	--	0.00350	0.000283	3380	158.39
	446	3	5.70	0.026	0.00355	0.000132	2990	123.52
Third Floor	28	3	3.93	0.146	0.00282	0.000274	3340	63.17
	195	2	5.99	--	0.00350	--	3380	28.99
	434	4	5.59	0.465	0.00345	0.000208	3070	125.55
Fourth Floor	28	3	3.68	0.142	0.00261	0.000153	2930	85.91
	187	2	5.26	--	0.00320	--	3320	229.10
	425	4	5.54	0.156	0.00361	0.000189	2930	81.18
Fifth Floor	28	3	4.75	0.086	0.00283	0.000293	3080	61.65
	175	1	5.88	--	0.00320	--	3530	--
	413	2	5.50	0.110	0.00330	0.000141	3030	22.63
Sixth Floor	28	2	4.16	0.040	0.00288	0.000354	2880	11.31
	168	1	5.48	--	0.00350	--	3290	--
	408	3	5.45	0.263	0.00344	0.000351	2970	59.77
Seventh Floor	28	3	4.87	0.122	0.00284	0.000290	3060	93.40
	159	1	5.84	--	0.00290	--	3020	--
	399	4	5.80	0.421	0.00353	0.000340	3150	154.00

*As determined from load control tests of 3-in. x 6-in. field-cured cylinders.

$\bar{f}_{c\max}$, $\sigma_{f_{c\max}}$ = mean and standard deviation of maximum concrete compressive stress.

$\bar{\epsilon}_o$, σ_{ϵ_o} = mean and standard deviation of strain at maximum compressive concrete stress.

$\bar{E}_{0.45f_{c\max}}$, $\sigma_{E_{0.45f_{c\max}}}$ = mean and standard deviation of secant modulus at 45% of maximum compressive concrete stress.

1 in. = 25.4 mm
1 ksi = 6.89 MPa

TABLE 12 FUNDAMENTAL FREQUENCY AND DAMPING COEFFICIENTS OF 1/5th-SCALE MODEL IN LOADING DIRECTION

TECHNIQUE OF EVALUATION	FREQUENCY & DAMPING BEFORE BALLAST Column 1	FREQUENCY & DAMPING AFTER BALLAST Column 2
Ambient Vibration	9.75 Hz	4.75 Hz
Dynamic Analyzer	9.75 Hz / 2.36%	4.78 Hz / 2.20%
Forced Vibration	8.25 Hz / 2.57%	4.55 Hz / 2.03%
Free Vibration	8.70 Hz / 2.45%	4.75 Hz / 1.94%
Pure Analytical*	12.45 Hz	5.09 Hz
Semi-Analytical**	9.55 Hz	4.79 Hz

Note: The frequency of the full-scale structure, after modification by a time-scale factor of $\sqrt{S_l} = \sqrt{5}$, was determined from a free-vibration test to be 5.2 Hz with a damping coefficient of 2.1%.

* Pure analytical results are based on the analytical work discussed in Reference 24.

** Semi-analytical results are based on the measured flexibility matrices and an analytical lumped mass model of the structure.

TABLE 13 EXCITATION PROGRAM FOR 1/5th-SCALE MODEL

Initial Dynamic Characteristics			f = 4.75 Hz , $\xi^{(5)}$ = 2.0%
SERIES	TEST NO.	INPUT SIGNAL	PEAK AMPLITUDE (% g)
1 Diagnostic Tests	1-6	MO[1]	0.3-2.6
	7	MO	5.0*
	8	MO	7.6
	9	MO	9.7*
	10-13	T[2]	4.0-6.3
	14, 15	H(4 Hz)[3]	1.5-2.0
	16, 31	H(3.25-4 Hz)	6.7
	32	MO	3.6
	33	MO	9.0
	34, 35†	FV[4] (5 kips pull)	f = 3.67 Hz , ξ = 3.5%
2 Damageability and Collapse Limit State Responses	36-42	FV (5 kips pull)	f = 3.41 Hz , ξ = 3.7%
	43	MO	8.2
	44	MO	10.8
	45	MO	14.7*
	46	MO	24.7*
	47	FV (pulse)	f = 2.63 Hz , ξ = 6.87%
	48	MO	28.3*
	49	FV (pulse)	f = 2.50 Hz , ξ = 7.50%
	50	T	40.3*
	51, 52††	FV (pulse)	f = 2.33 Hz , ξ = 7.70%
3 Post-Retrofitting Responses	53-55	FV (pulse)	f = 2.33 Hz , ξ = 6.40%
	56	MO	8.6
	57	T	30.3
	58	FV (pulse)	f = 1.96 Hz , ξ = 6.20%
	59	T	48.4
	60	MO	32.9
	61	FV (pulse)	f = 1.96 Hz , ξ = 8.30%
	62	T	46.3*

1 kip = 4.45 kN

(1) Miyagi-Oki Record
(2) Taft Record
(3) Harmonic Vibration
(4) Free Vibration
(5) ξ = Damping Ratio

* The responses from these tests are evaluated in this paper.
† After this test the model was removed from the table and repaired by epoxy injection.
†† The main wall was retrofit at the base after this test, with the structure remaining on the table.

TABLE 14 DAMAGE POTENTIAL OF SOURCE AND MEASURED EXCITATIONS

Series	Test No.	Signal	Peak Acceleration (% g)		Intensity Cofficient of Output Signal I^* (in./sec)
			Measured Output	Scaled Input	
			Column 1	Column 2	Column 3
1	7	MO	5.0	5.0	1.43
	9	MO	9.7	9.0	4.58
	33	MO	9.0	8.0	3.67
2	43	MO	8.2	6.9	2.68
	44	MO	10.8	8.6	4.22
	45	MO	14.7	14.0	11.21
	46	MO	24.7	19.2	20.95
	48	MO	28.3	23.5	31.37
	50	T	40.3	37.3	73.95
3	56	MO	8.6	7.0	2.79
	57	T	30.3	27.0	38.82
	59	T	48.4	39.3	82.22
	60	MO	32.9	33.8	65.15
	62	T	46.3	38.9	80.43

* $I = \frac{\pi}{2g}\int_0^t a^2(t)\,dt$ where $a(t)$ is acceleration at time t.

TABLE 15 MAXIMUM RESPONSE OF COMPLETE MODEL STRUCTURE AND WALL

(a)

Test Signal Acceleration (% g)	Effective Frequency	Maximum Base Shear (% W)	Maximum Overturning Moment (% WH)	Maximum Top Acceleration (% g)
MO 5.0	4.2 Hz	9.9% W (3.83 sec)†	6.72% WH (3.83 sec)	15.1 (3.84 sec)
MO 9.7	3.9 Hz	17.5% W (3.86 sec)	11.5% WH (3.86 sec)	27.4 (3.84 sec)
MO 14.7	2.9 Hz	27.3% W (3.11 sec)	18.2% WH (4.67 sec)	44.5 (4.65 sec)
MO 24.7	2.7 Hz	41.7% W (7.27 sec)	27.1% WH (7.26 sec)	65.2 (7.23 sec)
MO 28.3	2.1 HZ	46.8% W (5.50 sec)	30.9% WH (5.26 sec)	81.3 (5.45 sec)
T 40.3	1.8 Hz	50.8% W (3.14 sec)	33.71% WH (3.14 sec)	88.8 (3.18 sec)
T 46.3	1.5 Hz	47.8% W (3.26 sec)	30.5% WH (3.58 sec)	78.4 (1.95 sec)

(b)

Test Signal Acc. (% g)	Roof Drift Index (% H)	1st Story Drift Index (% h)	Max. Interst. Drift Index (% h)	Max. Wall Base Shear (% W)	Max. Wall Flexure (% WH)
MO 5.0	0.05 (3.83 sec)	0.08 (12.5 sec)	0.10 (5th St.) (3.98 sec)	8.1% W (3.83 sec)	3.9% WH (3.83 sec)
MO 9.7	0.09 (3.86 sec)	0.10 (3.86 sec)	0.17 (5th St.) (3.85 sec)	14.0% W (3.86 sec)	6.4% WH (3.86 sec)
MO 14.7	0.30 (6.03 sec)	0.27 (4.69 sec)	0.38 (4th St.) (4.66 sec)	21.0% W (3.11 sec)	8.8% WH (4.67 sec)
MO 24.7	0.61 (7.50 sec)	0.62 (7.51 sec)	0.69 (4th St.) (7.50 sec)	29.6% W (7.27 sec)	11.5% WH (7.26 sec)
MO 28.3	0.93 (5.51 sec)	1.00 (5.51 sec)	1.08 (4th St.) (5.52 sec)	31.4% W (5.50 sec)	11.5% WH (5.26 sec)
T 40.3	1.47 (3.17 sec)	1.68 (3.16 sec)	1.68 (1st St.) (2.50 sec)	33.7% W (3.14 sec)	9.0% WH (3.14 sec)
T 46.3	1.83 (3.62 sec)	2.37* (3.62 sec)	2.37* (1st St.) (3.62 sec)	28.4% W 3.26 sec)	6.7% WH (3.58 sec)

W = weight of the structure above foundation, 106 kips
H = total height above foundation, 171.26 in.
h = story height, 29.53 in. first story, 23.62 in. thereafter
† ( ) time at which maximum response occurred
* After repair, h for wall became 23.03 in. at the first story.
If this is used, maximum interstory drift becomes 3.04% h.

1 kip = 4.45 kN ; 1 in. = 25.4 mm

TABLE 16 TEST PROGRAM FOR FULL-SCALE MODEL

TEST	INPUT SIGNAL	DAMPING & FREQUENCY† BEFORE TEST	AFTER TEST	MAX. BASE SHEAR (% *W*)	MAXIMUM MOMENT (% *WH*)	MAX. ROOF DRIFT (% *H*)
PSD-1	Miyagi-Oki (1.3 sec) 2.4% g	(2.1%) 2.33 Hz	(1.2%) 2.33 Hz	2.67% *W*	1.78% *WH*	0.01% *H*
PSD-2	Miyagi-Oki (1.3 sec) 10.7% g	2.33 Hz	(2.0%) 1.82 Hz	19.14% *W*	12.76% *WH*	0.15% *H*
PSD-3	Taft (10 sec) 32.7% g	1.82 Hz	(7.7%) 0.86 Hz	34.81% *W*	23.21% *WH*	1.10% *H*
PSD-4	Hachinohe (6.5 sec) 35.7% g	0.86 Hz	(11.4%) 0.68 Hz	37.18% *W*	24.79% *WH*	1.56% *H*

† The damping coefficients obtained after tests were through a simulated free-vibration test by the pseudo-dynamic method using 1.5 cycles. The roof drift amplitudes during these tests were of the same order of magnitude as the drift amplitudes during the pseudo-dynamic test itself. The reported damping values should therefore include a considerable contribution from *hysteretic damping* in addition to contributions from *structural damping, viscous damping*, and *Coulomb damping.*

TABLE 17 PARAMETERS CONSIDERED IN LIMIT ANALYSES

Analytical Model	Material Properties	Slab Contribution To Girder Capacities	Collapse Mechanisms Considered			
			Wall Hinge At Section Centroid	Wall Hinge At Neutral Axis	Wall Hinge At Edge Column Centroid	Wall Hinge At Edge Column Extreme Face
2-D	Specified	None for (-) Moment* ¼ Span for(+)Moment	A	B	-	-
		¼ Span for Both (+) and (-) Moments	C	D	-	-
	Measured	Entire Slab Width Considered Effective for (+) and (-) Moments	E	F	-	-
3-D	Measured	Entire Slab Width Considered Effective For (+) and (-) Moments	G	H	I	J

* (-) Moment is when flange is in tension.

TABLE 18 RESULTS OF LIMIT ANALYSES

Collapse Mechanism (Table 17)	Maximum Resistance of the Structure (kips) Lateral Force Distribution			Computed Axial Force at the Base of Wall(Kips)
	Triangular	Uniform	Measured*	
A	20.3	24.8	22.5	26.0
B	20.3	24.8	22.5	26.0
C	23.4	28.5	25.9	26.0
D	23.4	28.5	25.9	26.0
E	42.2	51.6	46.8	26.2
F	42.2	51.6	46.8	26.2
G	46.2	56.5	51.2	25.9
H	47.0	57.4	52.1	34.9
I	46.5	56.8	51.5	48.8
J	45.4	55.5	50.3	62.8

* At peak shear response under T 40.3 1 kip = 4.45 kN

TABLE 19 MAXIMUM NOMINAL SHEAR STRESS AT CRITICAL REGIONS OF STRUCTURAL COMPONENTS

STRUCTURAL COMPONENT	MAXIMUM NOMINAL SHEAR STRESS v_{max}		
	UBC DESIGN	MAXIMUM SHEAR DEVELOPED IN TEST	
	SPECIFIED f_c'*	SPECIFIED f_c'*	MEASURED f_c'**
BEAMS	$2.8\sqrt{f_c'}$	$4.3\sqrt{f_c'}$	$3.5\sqrt{f_{cm}'}$
COLUMNS			
1st Story	$2.8\sqrt{f_c'}$	$4.7\sqrt{f_c'}$	$3.9\sqrt{f_{cm}'}$
Other Stories	$3.7\sqrt{f_c'}$	--	--
BEAM-COLUMN JOINTS†	$6.7\sqrt{f_c'}$	$10.2\sqrt{f_c'}$	$8.4\sqrt{f_{cm}'}$
WALL			
K = 0.8	$4.6\sqrt{f_c'}$	$10.5\sqrt{f_c'}$	$8.7\sqrt{f_{cm}'}$
K = 1.0	$5.7\sqrt{f_c'}$	$10.5\sqrt{f_c'}$	$8.7\sqrt{f_{cm}'}$

* specified f_c' = 3850 psi
** measured in model, f_{cm}' = 5610 psi
† values obtained considering only the shear transferred by the beam main steel through the core of the joint.

1 psi = 6.89 kPa

FIGURES

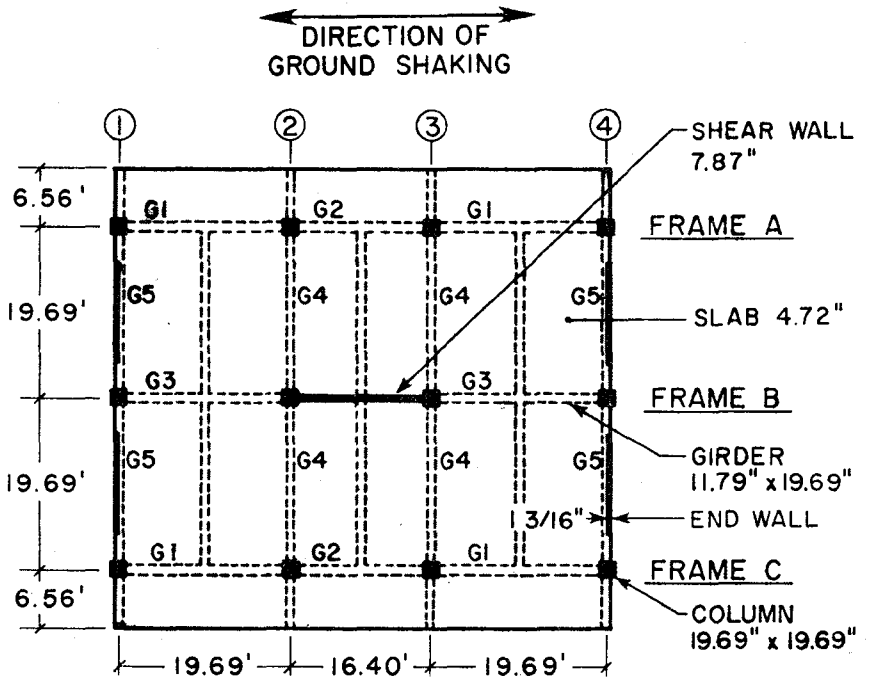

(a) PLAN WITH FRAME AND GIRDER LOCATIONS

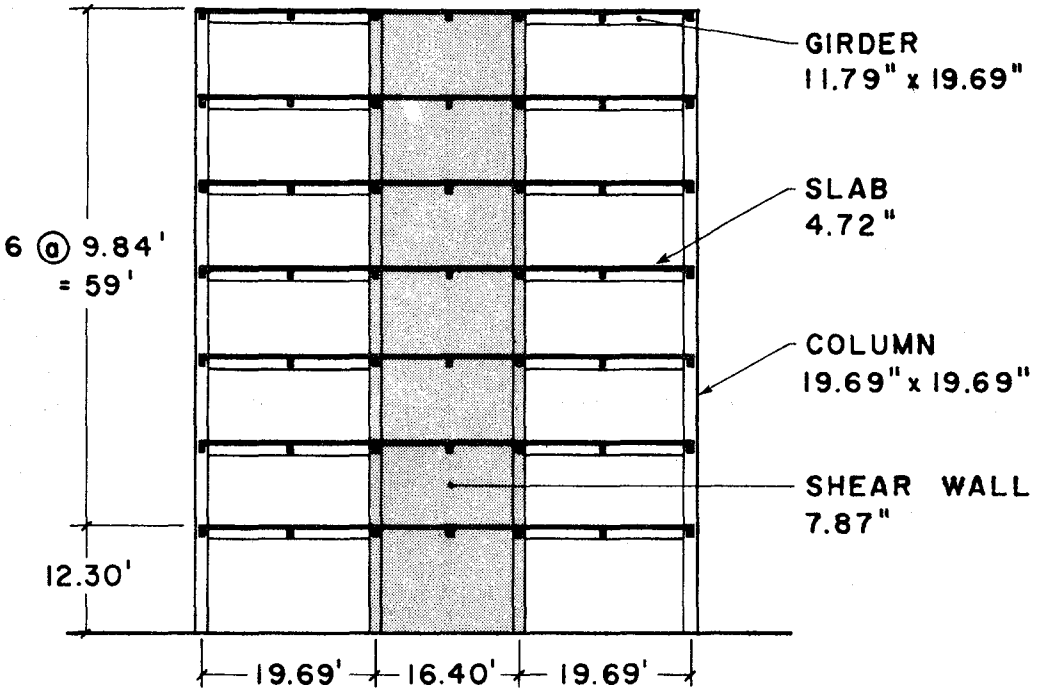

(b) SECTION SHOWING FRAME B

FIG. 1 PLAN AND SECTION OF FULL-SCALE MODEL
(1 in. = 25.4 mm ; 1 ft = 0.305 m)

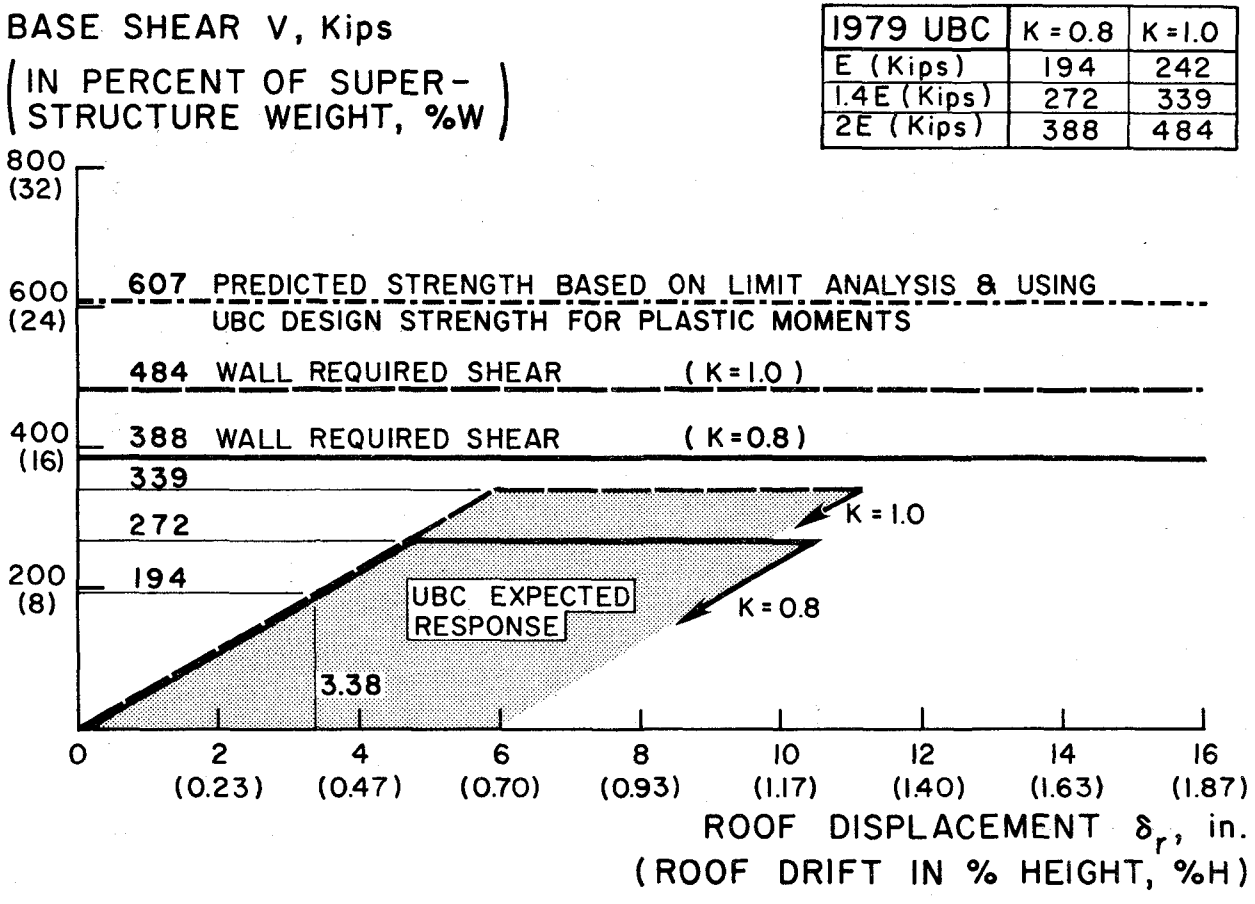

FIG. 2 1979 U.B.C. EXPECTED MIMIMUM STIFFNESS AND STRENGTH OF STRUCTURE FOR $K = 0.8$ AND $K = 1$
(1 in. = 25.4 mm ; 1 kip = 4.45 kN)

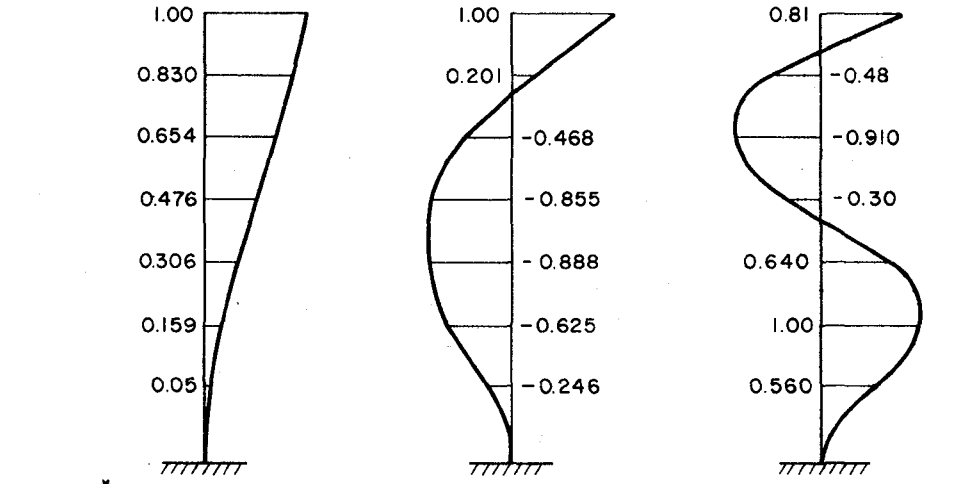

(a) ANALYTICAL RESULTS

* = MODE SHAPES ARE FOR CRACKED I

TEST	FUNDAMENTAL PERIOD (Sec)	
	BEFORE TEST	AFTER TEST
PSD1	0.43	0.43
PSD2	0.43	0.55
PSD3	0.55	1.16
PSD4	1.16	1.47

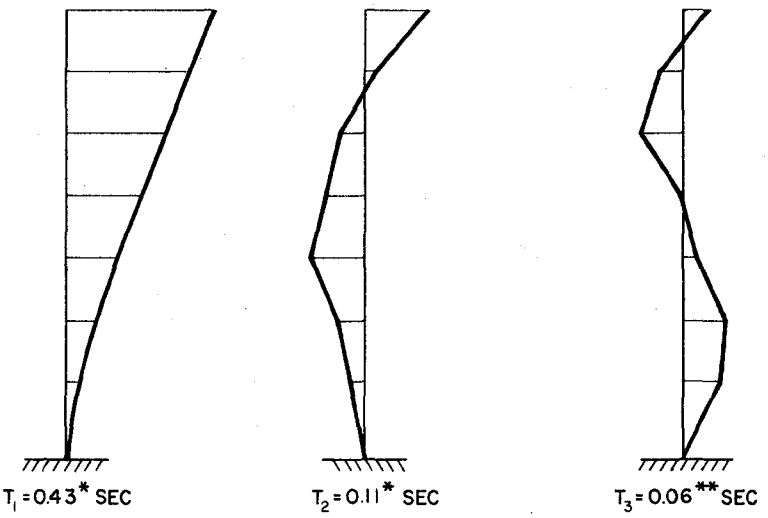

(b) EXPERIMENTAL RESULTS

FIG. 3 MODE SHAPES AND PERIODS OF VIBRATION OF FULL-SCALE MODEL

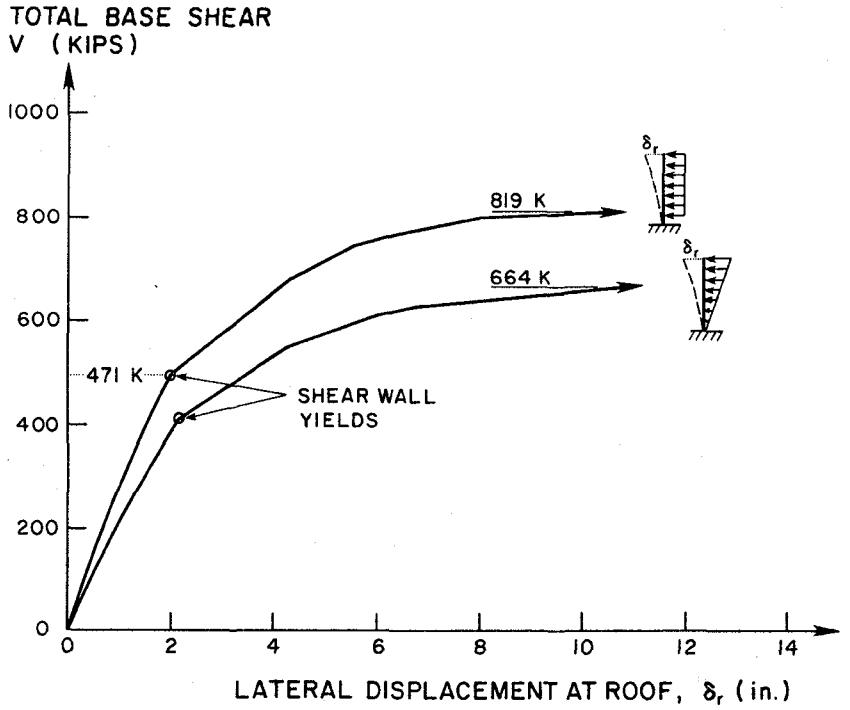

(a) EFFECT OF LATERAL LOAD DISTRIBUTION

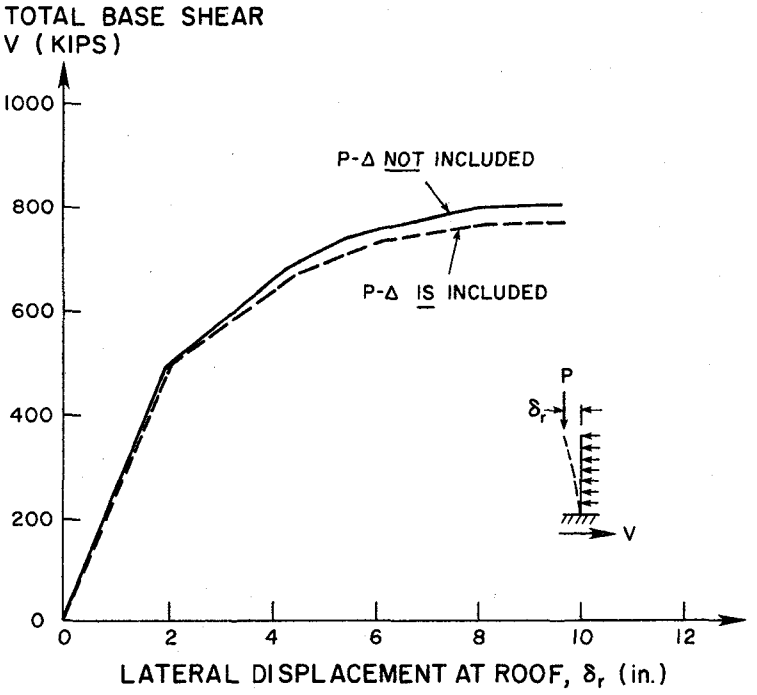

(b) EFFECT OF *P-DELTA*

FIG. 4 LATERAL FORCE vs LATERAL ROOF DISPLACEMENT RELATIONS OF FULL-SCALE MODEL SUBJECTED TO MONOTONICALLY INCREASING LATERAL LOAD (1 in. = 25.4 mm ; 1 kip = 4.45 kN)

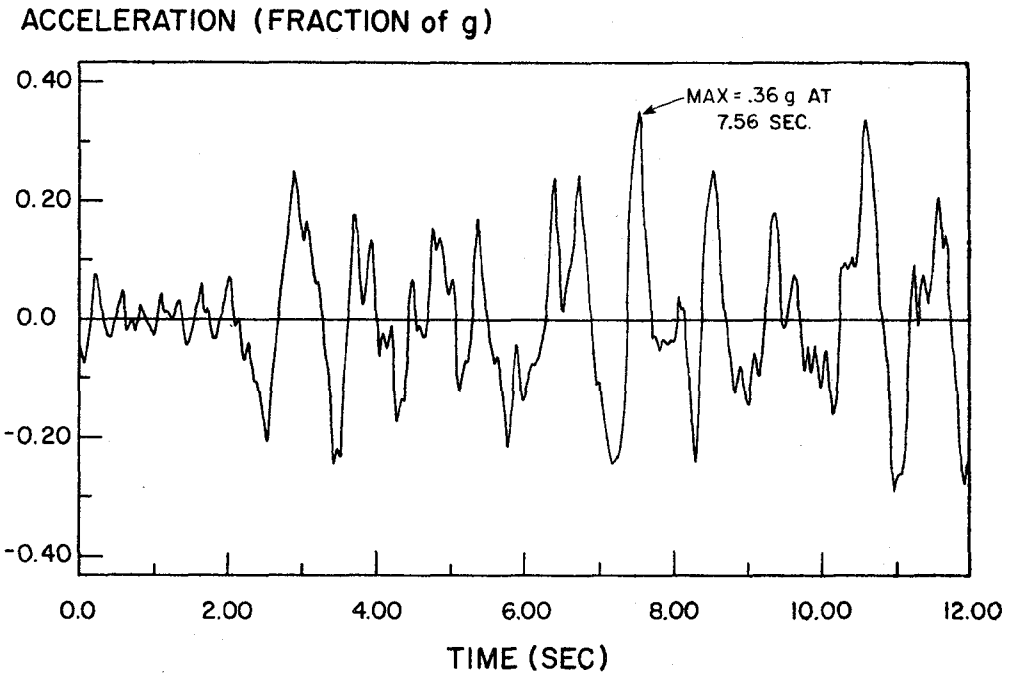

FIG. 5 FIRST 12 SECONDS OF MIYAGI-OKI HORIZONTAL GROUND ACCELERATION RECORD USED IN ANALYSIS

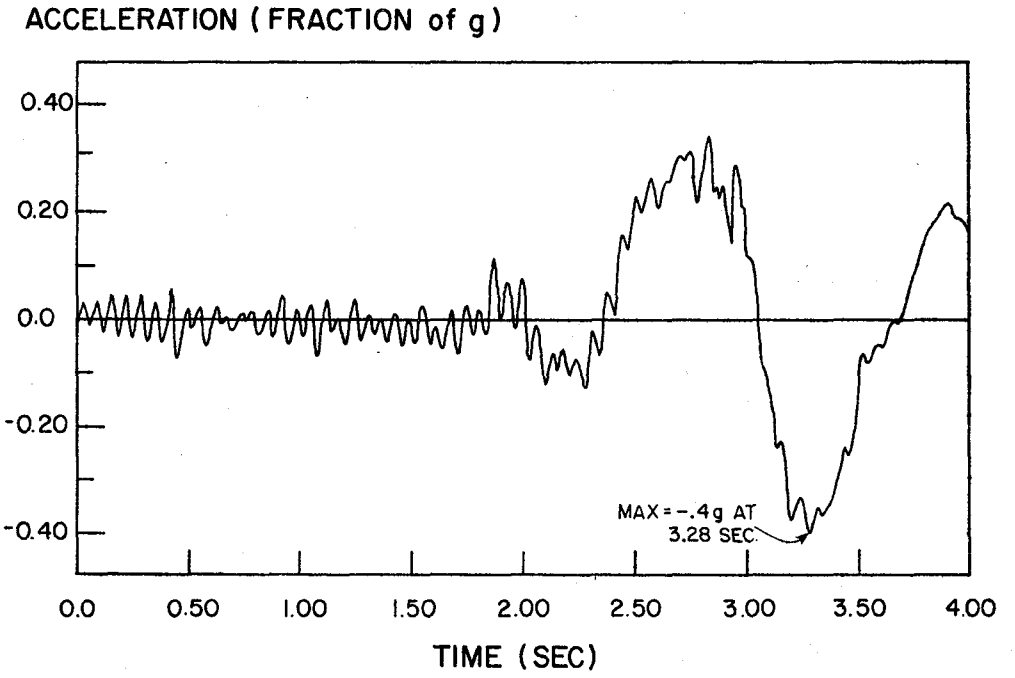

FIG. 6 FIRST 4 SECONDS OF DERIVED PACOIMA DAM HORIZONTAL GROUND ACCELERATION RECORD USED IN ANALYSES

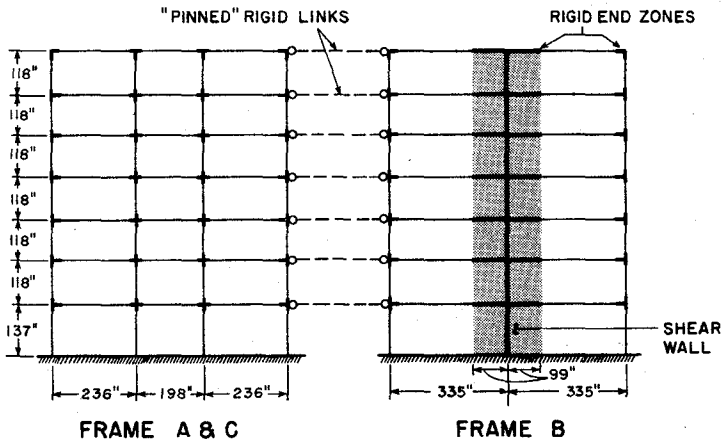

FIG. 7 ANALYTICAL MODEL USED FOR LINEAR AND NONLINEAR ANALYSES OF FULL-SCALE STRUCTURE (1 in. = 25.4 mm)

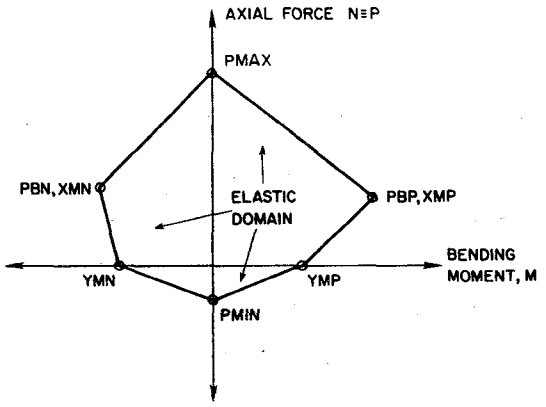

FIG. 8 YIELD SURFACE FOR BEAM-COLUMN ELEMENTS INCORPORATED IN ULARC

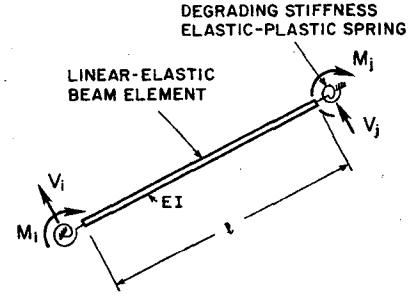

(a) SINGLE-COMPONENT BEAM MODEL WITH DEGRADING STIFFNESS

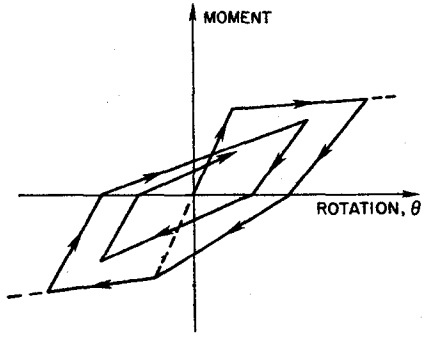

(b) MODIFIED TAKEDA BILINEAR MOMENT-ROTATION DIAGRAM

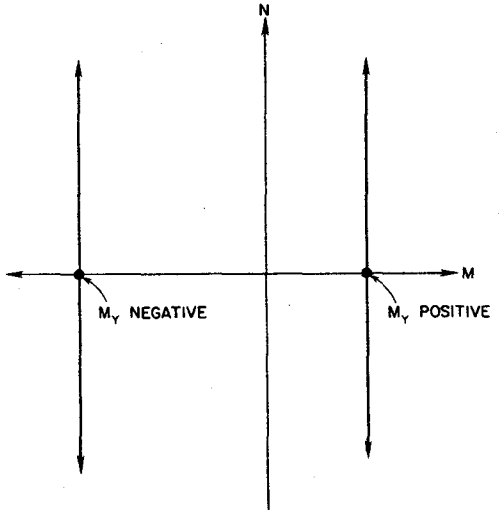

(c) YIELD SURFACE

FIG. 9 SINGLE-COMPONENT DEGRADING STIFFNESS MODEL

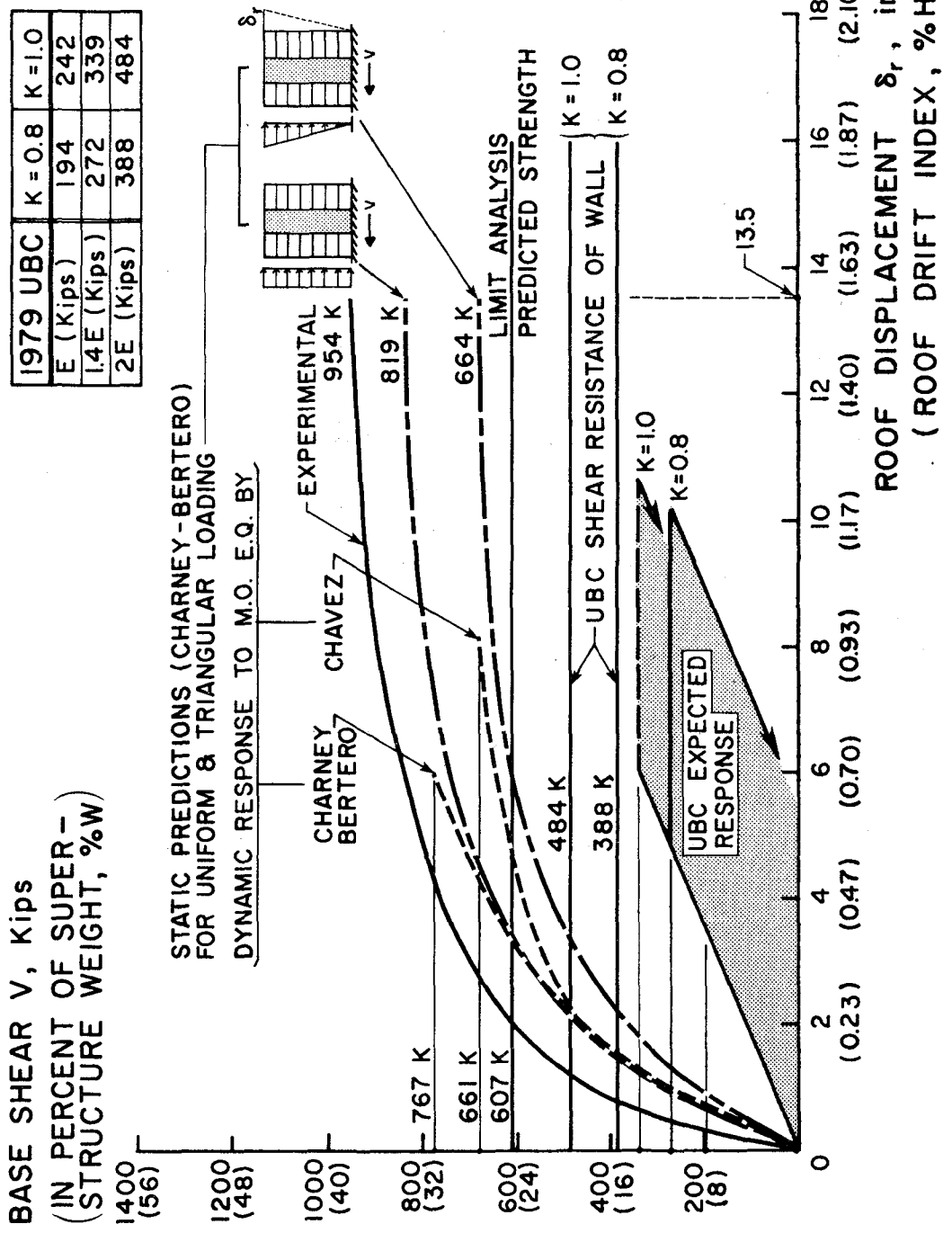

FIG. 10 ANALYTICALLY PREDICTED AND U.B.C. EXPECTED BASE SHEAR vs ROOF DISPLACEMENT RESPONSES
(1 kip = 4.45 kN; 1 in. = 25.4 mm)

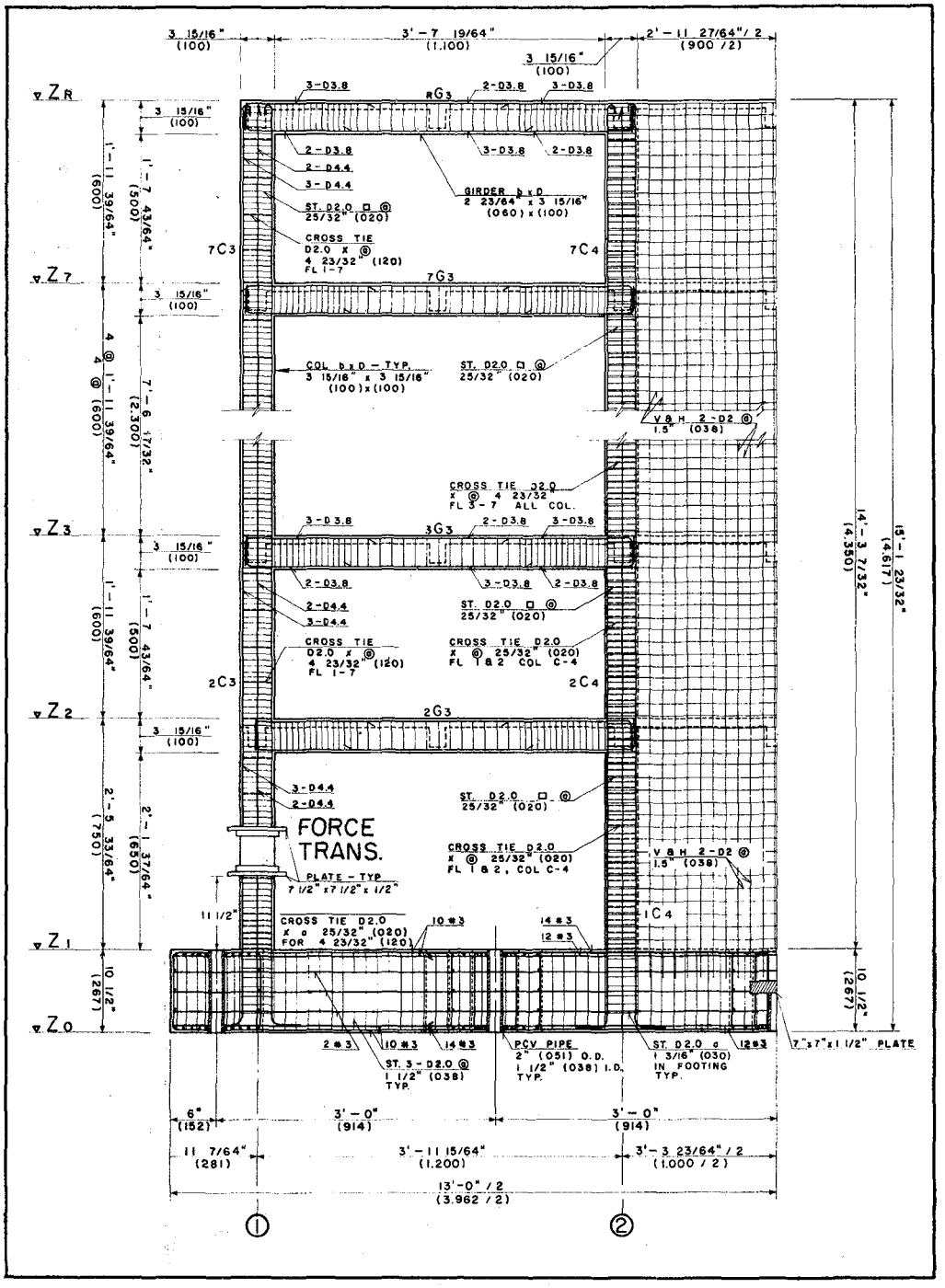

FIG. 11(a) TYPICAL DETAILING OF INTERIOR WALL-FRAME B OF 1/5th-SCALE MODEL
(1 in. = 25.4 mm ; 1 ft = 0.305 m)

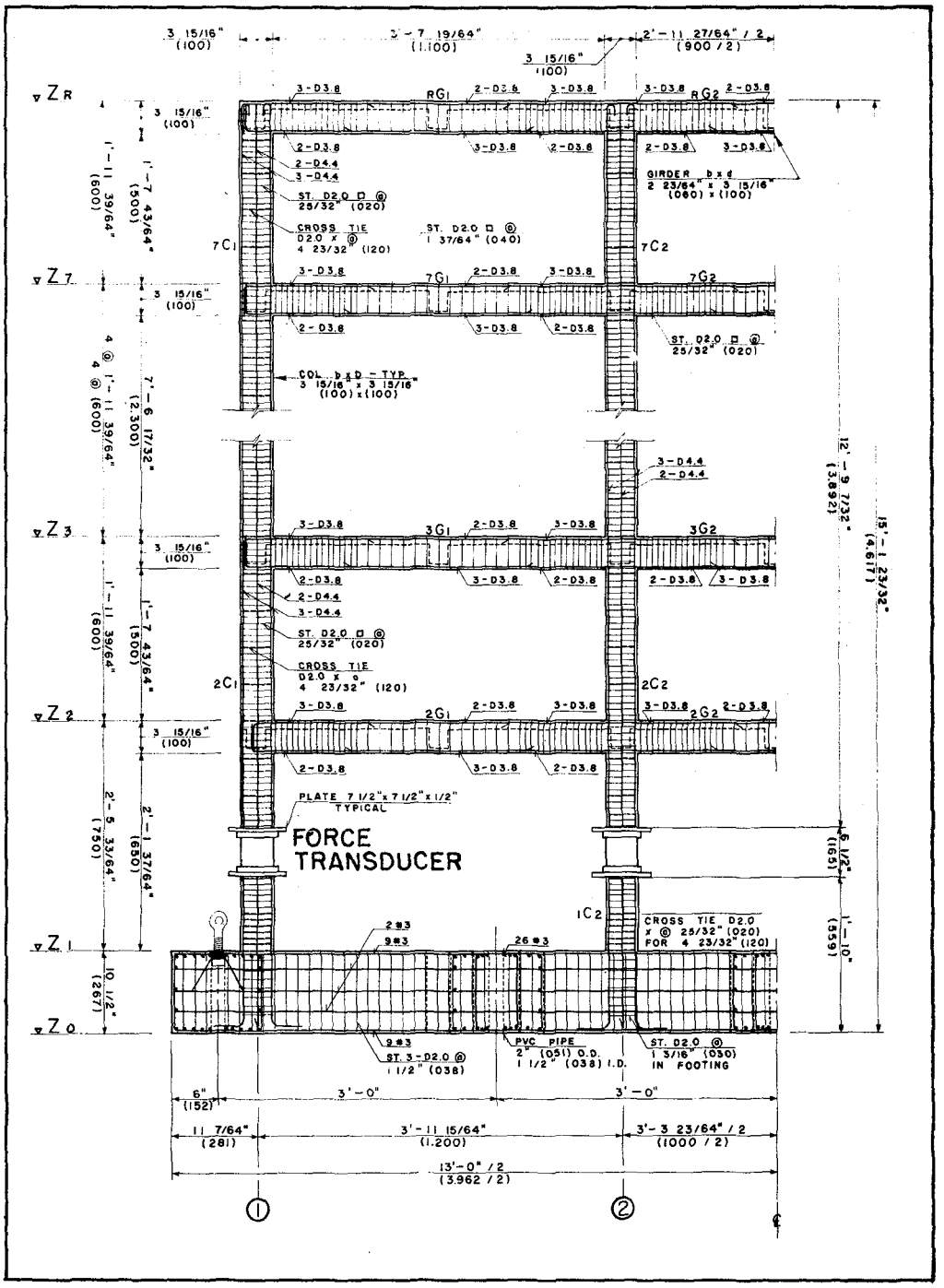

FIG. 11(b) TYPICAL DETAILING OF EXTERIOR FRAMES A AND C OF 1/5-SCALE MODEL
(1 in. = 25.4 mm ; 1 ft = 0.305 m)

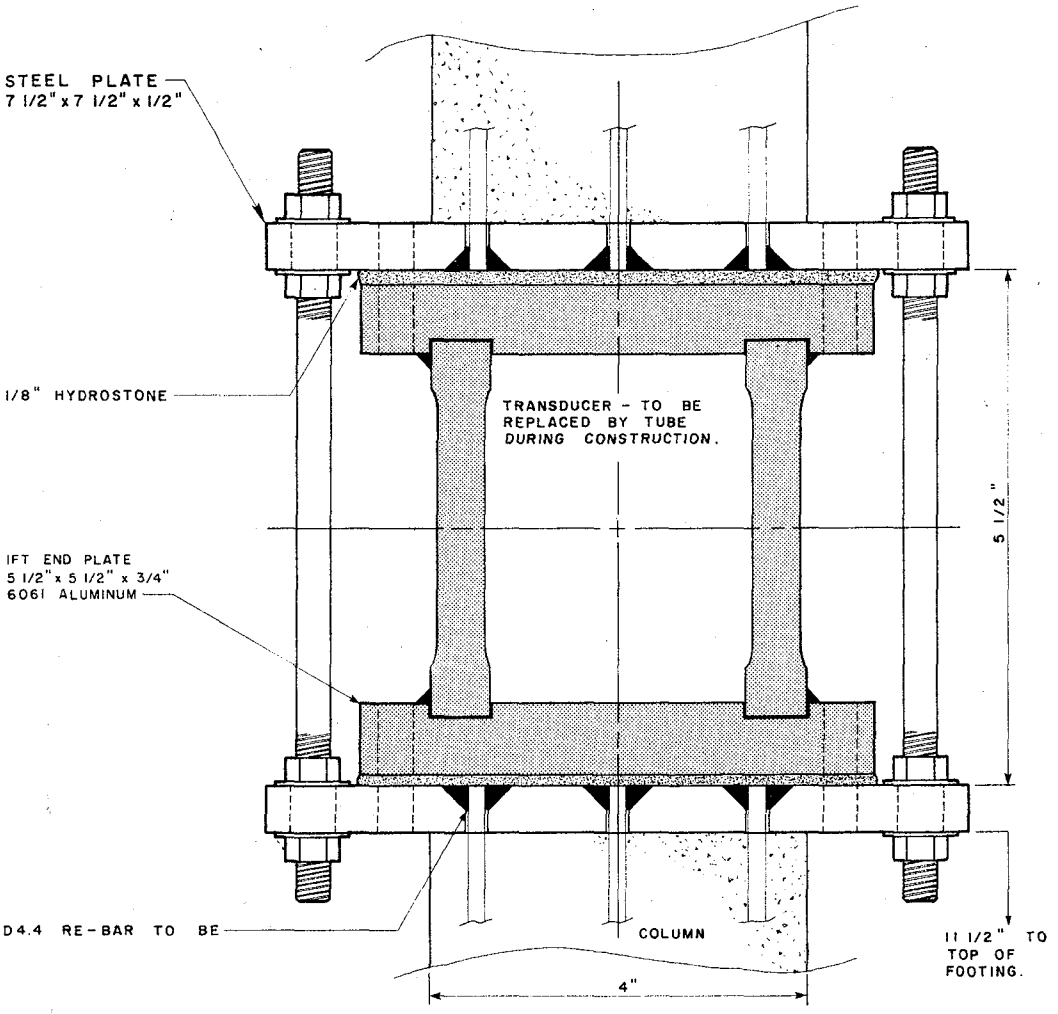

FIG. 11(c) INTERNAL FORCE TRANSDUCER INSTALLATION
(1 in. = 25.4 mm)

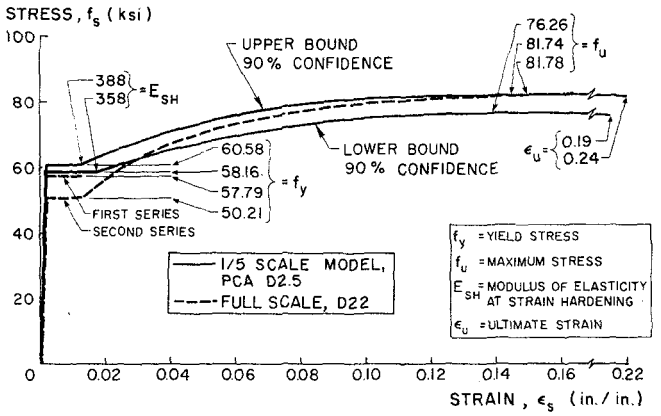

FIG. 12 STRESS-STRAIN RELATIONS FOR COLUMN REINFORCEMENT (1 ksi = 6.9 MPa; 1 in. = 25.4 mm)

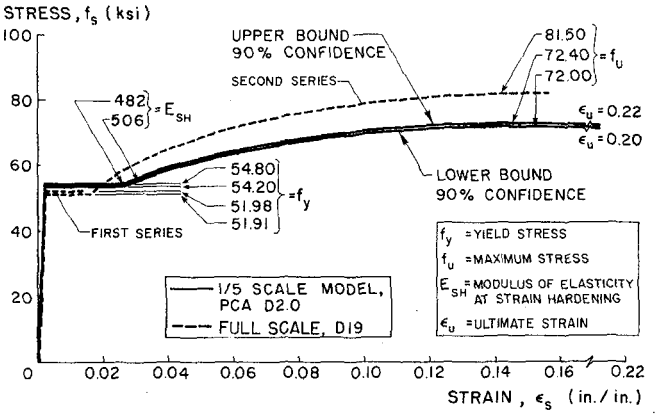

FIG. 13 STRESS-STRAIN RELATIONS FOR BEAM REINFORCEMENT (1 ksi = 6.9 MPa; 1 in. = 25.4 mm)

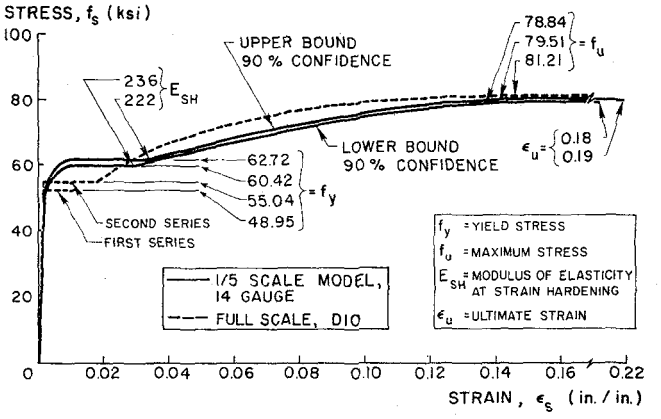

FIG. 14 STRESS-STRAIN RELATIONS FOR WALL, SLAB, TIE, AND STIRRUP REINFORCEMENT (1 ksi = 6.9 MPa; 1 in. = 25.4 mm)

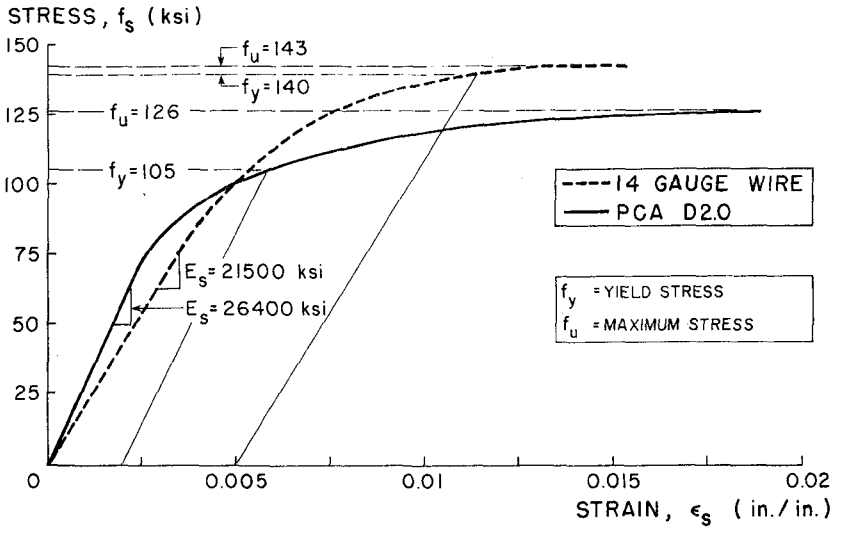

FIG. 15 STRESS-STRAIN RELATIONS FOR ORIGINAL (VIRGIN) 14 GAUGE WIRE AND PCA/D2 REINFORCING BARS (1 ksi = 6.9 MPa; 1 in. = 25.4 mm)

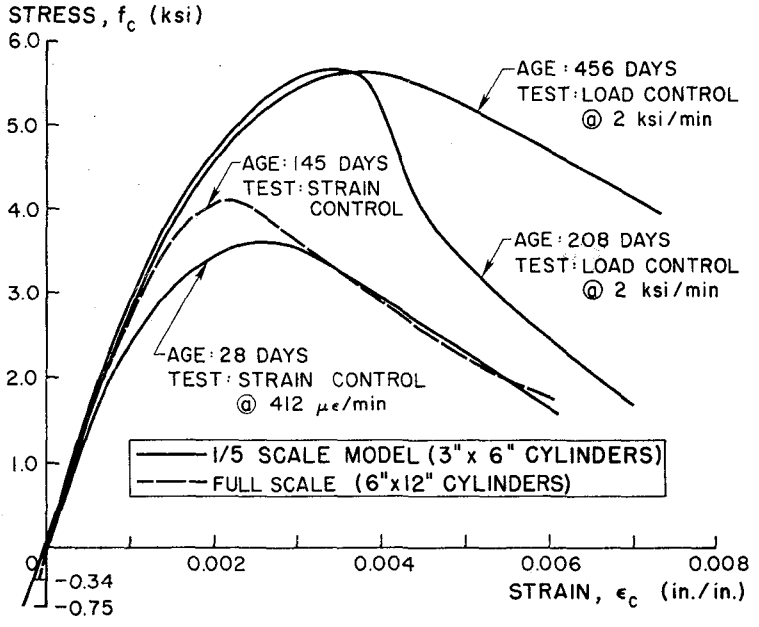

FIG. 16 STRESS-STRAIN RELATIONS FOR FIRST-STORY CONCRETE IN FULL-SCALE MODEL AND OF 1/5th-SCALE MODEL (1 ksi = 6.9 MPa; 1 in. = 25.4 mm)

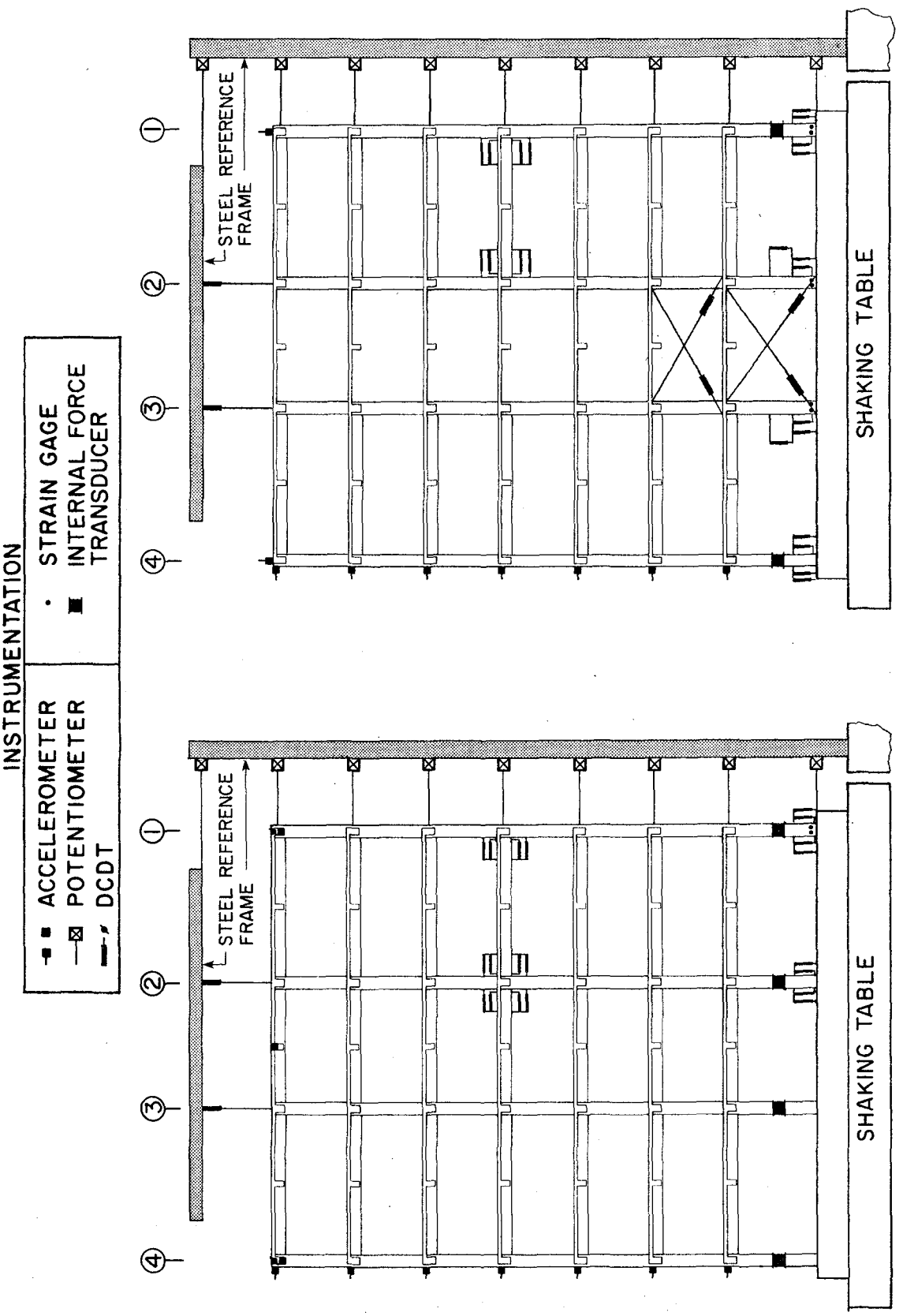

(a) INSTRUMENTATION OF FRAME A

(b) INSTRUMENTATION OF WALL-FRAME B

FIG. 17 INSTRUMENTATION DETAILS FOR 1/5th-SCALE MODEL

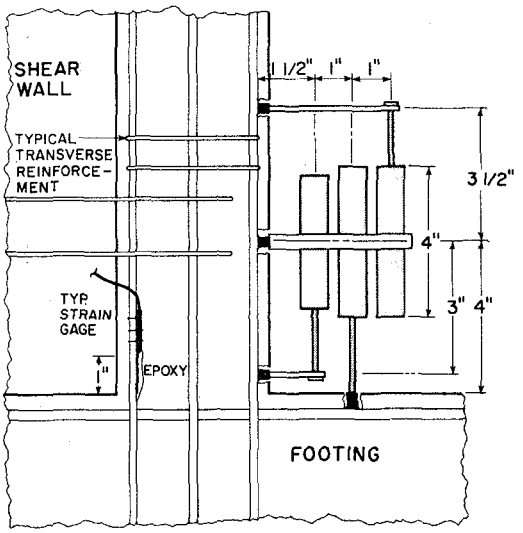

(c) TYPICAL SHEAR WALL EDGE MEMBER FOOTING INTERFACE DETAIL

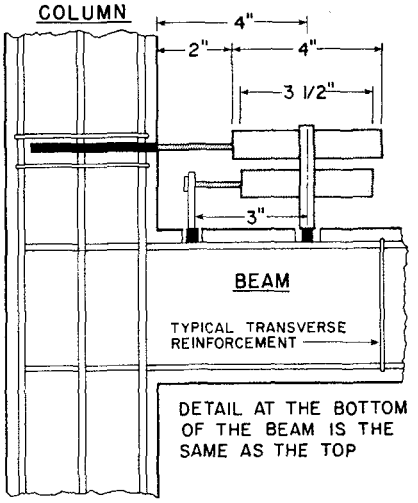

(d) TYPICAL BEAM-COLUMN DETAIL

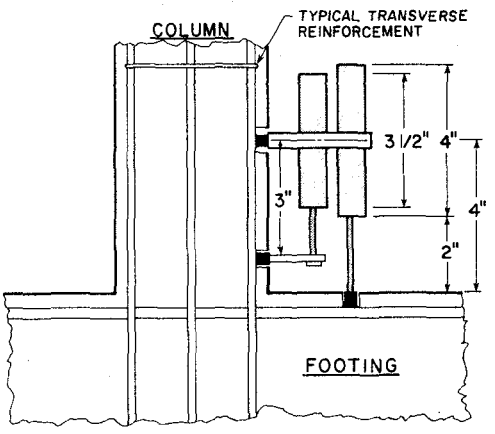

(e) TYPICAL COLUMN-FOOTING INTERFACE DETAIL

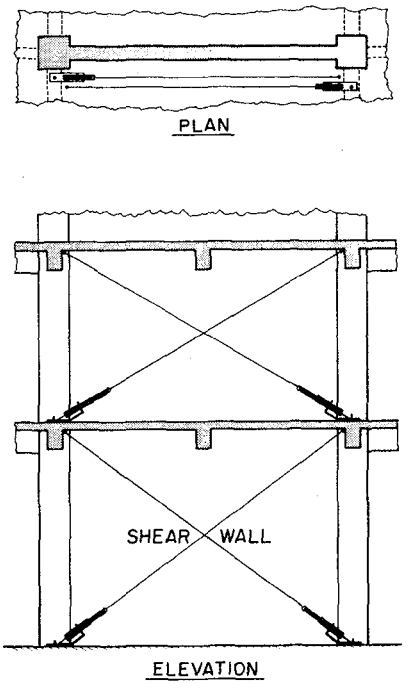

(f) SHEAR DEFORMATION INSTRUMENTATION OF WALL

FIG. 17 INSTRUMENTATION DETAILS FOR 1/5th-SCALE MODEL
(1 in. = 25.4 mm)

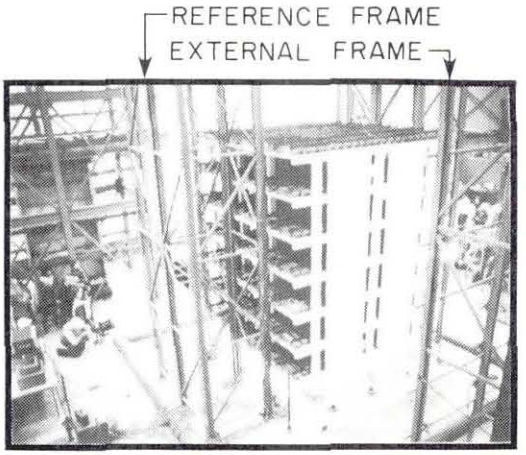

FIG. 18 TESTING OF 1/5th-SCALE MODEL ON SHAKING TABLE WITH INSTRUMENTATION FRAMES

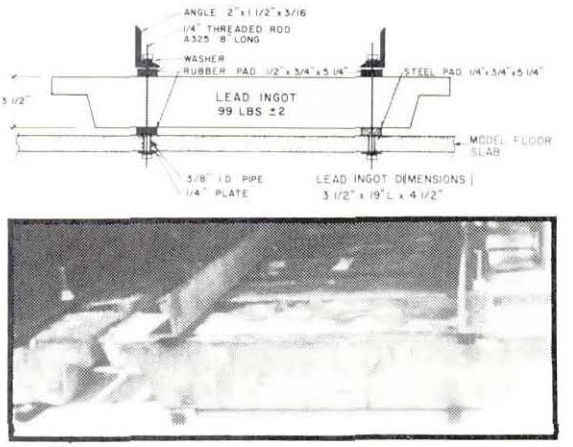

(b) ATTACHMENT OF LEAD INGOT (USED AS BALLAST) TO THE MODEL SLAB

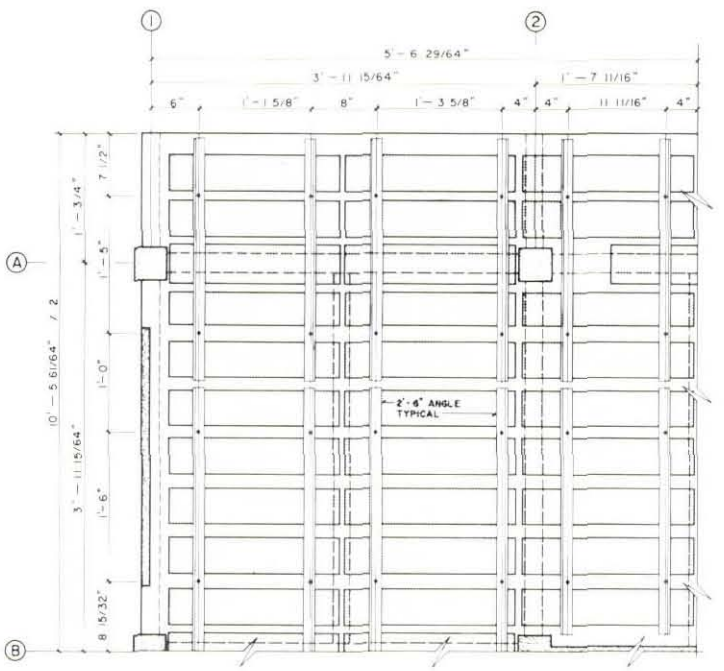

(a) DISTRIBUTION OF BALLAST ON FLOOR SLABS

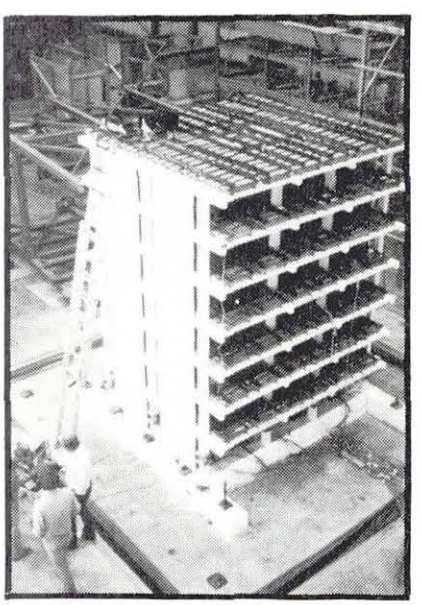

(c) 1/5th-SCALE MODEL LOADED WITH BALLAST

FIG. 19 1/5-SCALE MODEL LOADED WITH REQUIRED LEAD BALLAST
(1 in. = 25.4 mm ; 1 ft = 0.305 m)

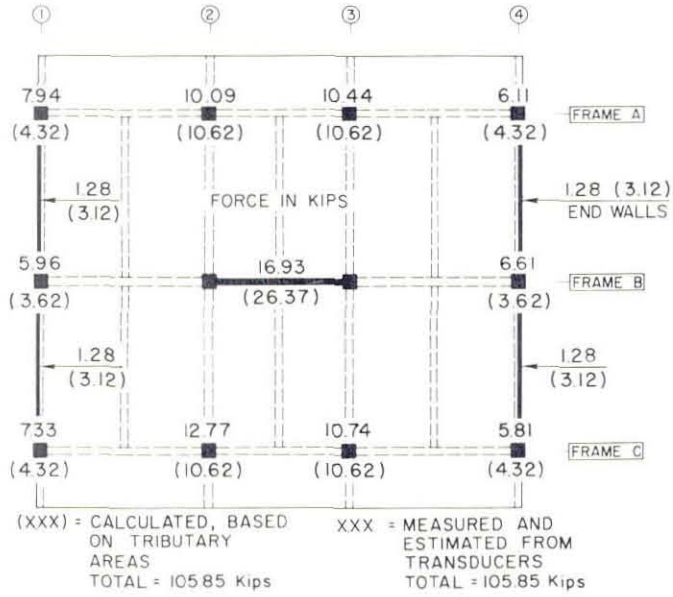

FIG. 20 COMPARISON OF EXPERIMENTAL AND CALCULATED DISTRIBUTIONS OF AXIAL FORCE AT BASE OF STRUCTURE (1 kip = 4.45 kN)

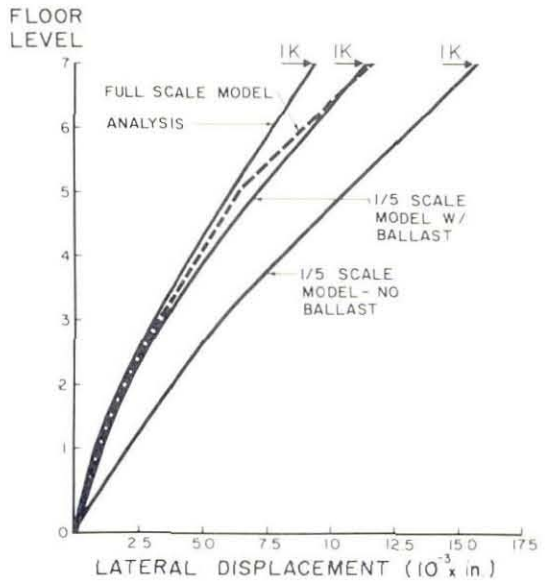

(a) LOADED AT SEVENTH FLOOR LEVEL

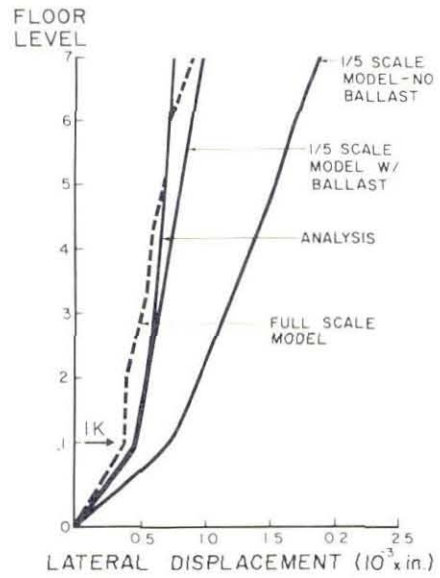

(b) LOADED AT FIRST FLOOR LEVEL

FIG. 21 DISPLACEMENT PROFILES FOR 1/5th-SCALE MODEL AND FULL-SCALE STRUCTURE (1 in. = 25.4 mm)

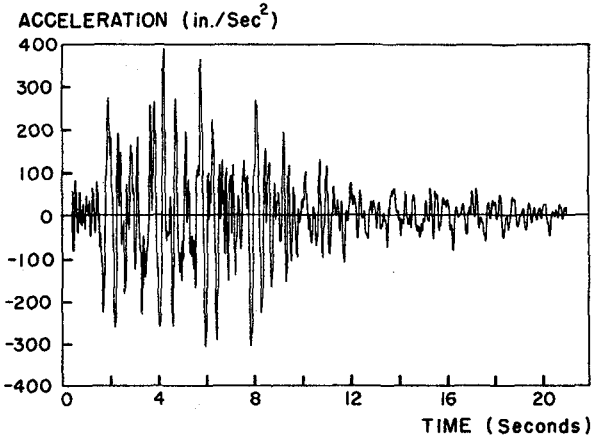

(a) MIYAGI-OKI ACCELERATION RECORD

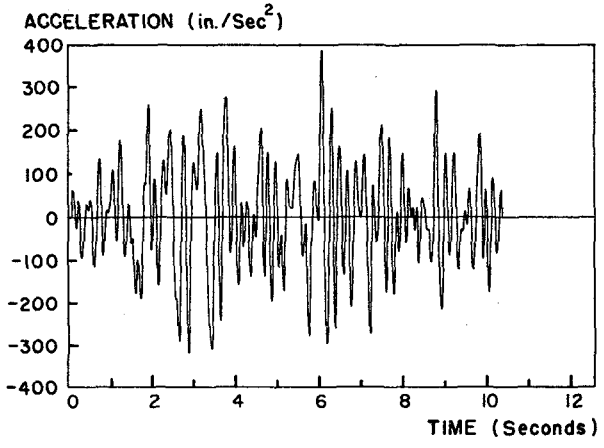

(b) TAFT ACCELERATION RECORD

FIG. 22 ACCELERATION RECORDS, NORMALIZED TO PEAK ACCELERATION OF 1.0g, USED AS SOURCE EXCITATIONS IN THE TEST PROGRAM (1 in. = 25.4 mm)

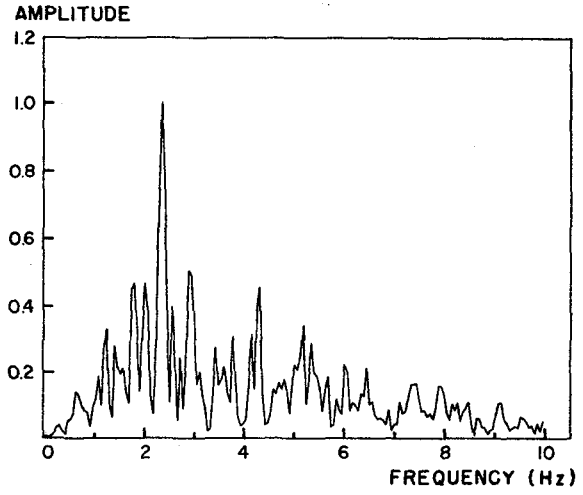

(a) MIYAGI-OKI INPUT RECORD

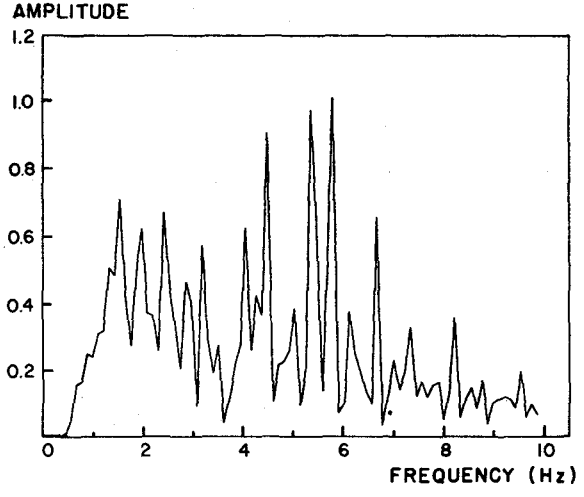

(b) TAFT INPUT RECORD

FIG. 23 FOURIER AMPLITUDE SPECTRA OF ACCELERATION RECORDS

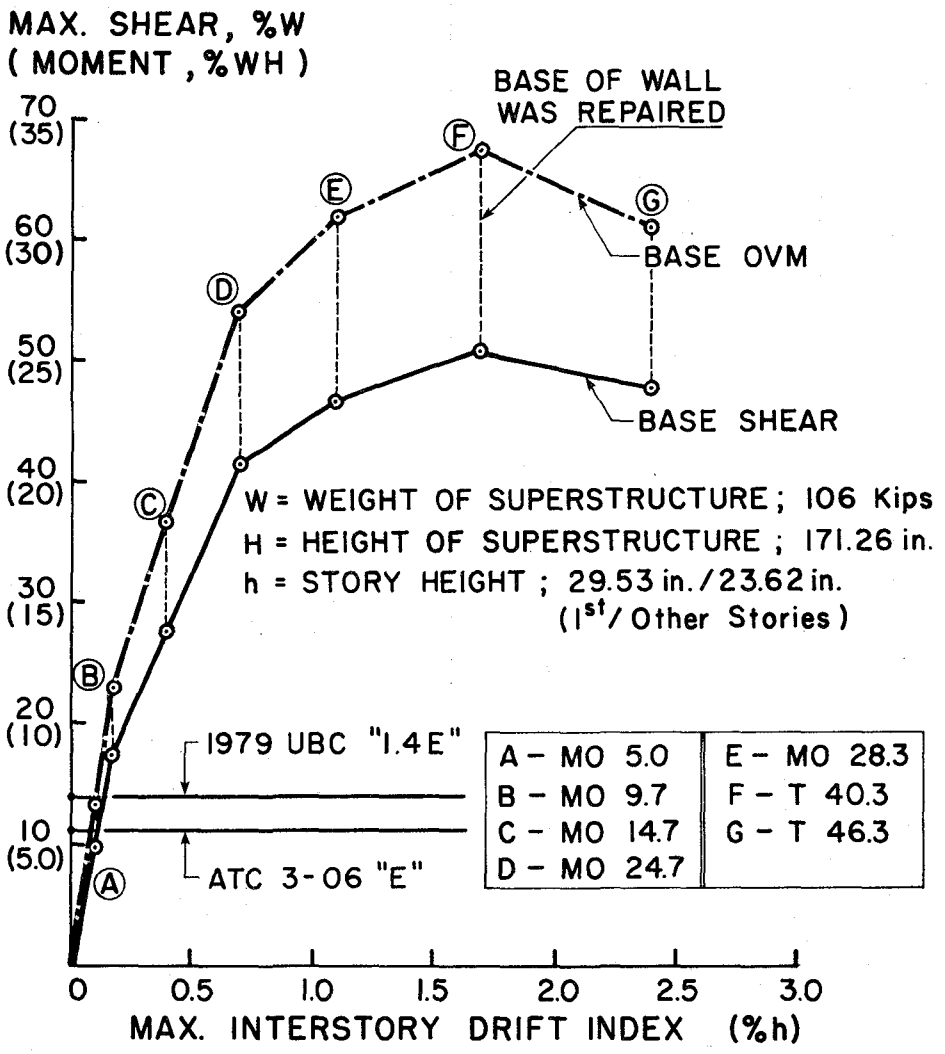

FIG. 24 MAXIMUM BASE SHEAR AND OVERTURNING MOMENT-MAXIMUM INTERSTORY DRIFT INDEX ENVELOPES FROM TESTS ON 1/5 SCALE MODEL (1 in. = 25.4 mm ; 1 kip = 4.45 kN)

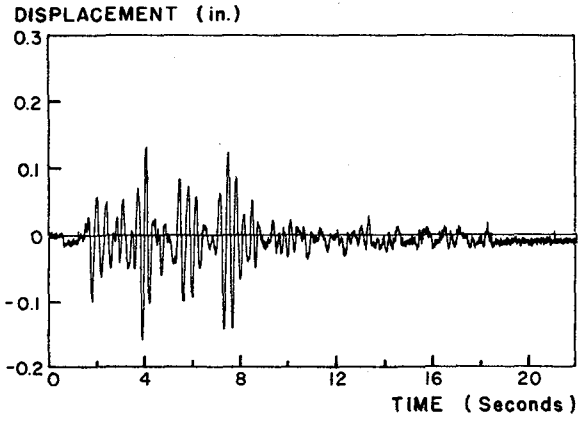

(a) MIYAGI-OKI 9.7

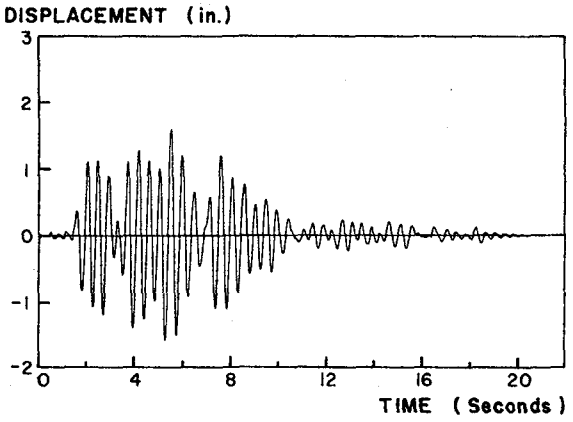

(c) MIYAGI-OKI 28.3

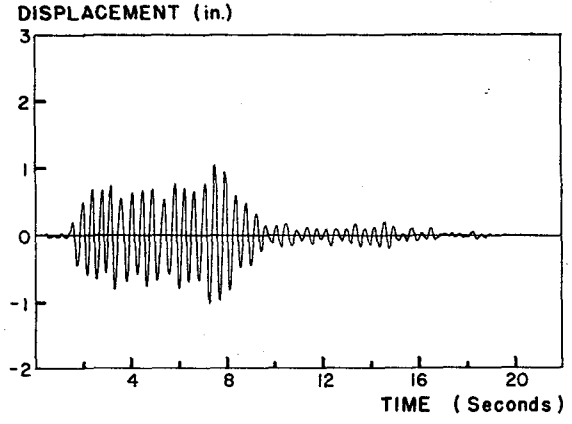

(b) MIYAGI-OKI 24.7

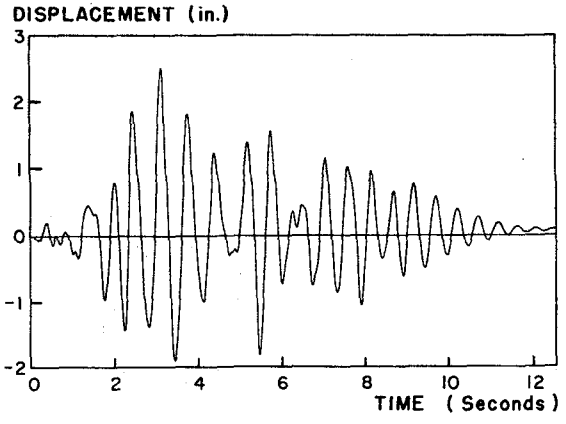

(d) TAFT 40.3

FIG. 25 RELATIVE LATERAL ROOF DISPLACEMENT TIME HISTORIES
(1 in. = 25.4 mm)

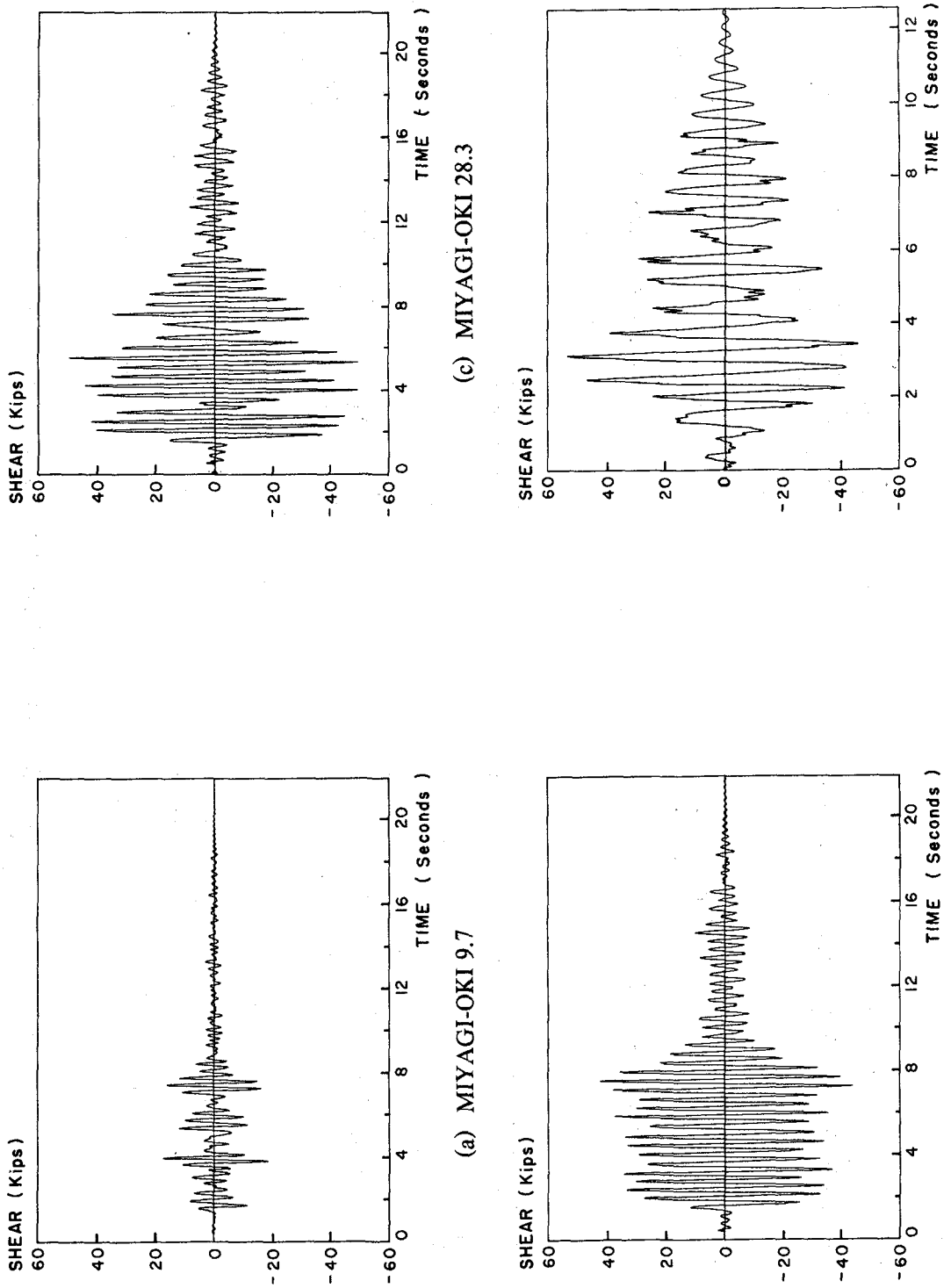

(a) MIYAGI-OKI 9.7

(b) MIYAGI-OKI 24.7

(c) MIYAGI-OKI 28.3

(d) TAFT 40.3

FIG. 26 BASE SHEAR TIME HISTORIES OF 1/5th-SCALE MODEL
(1 kip = 4.45 kN)

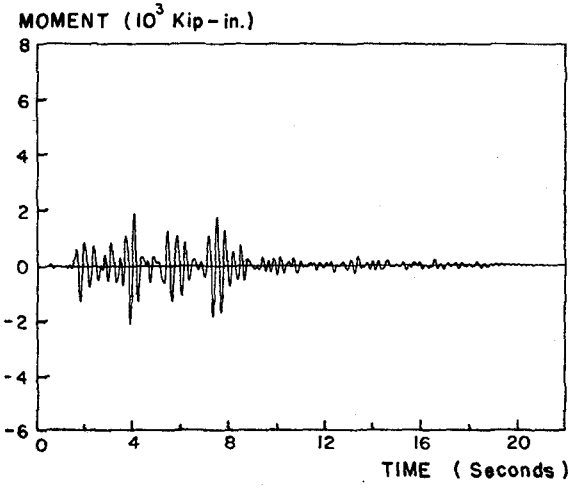

(a) MIYAGI-OKI 9.7

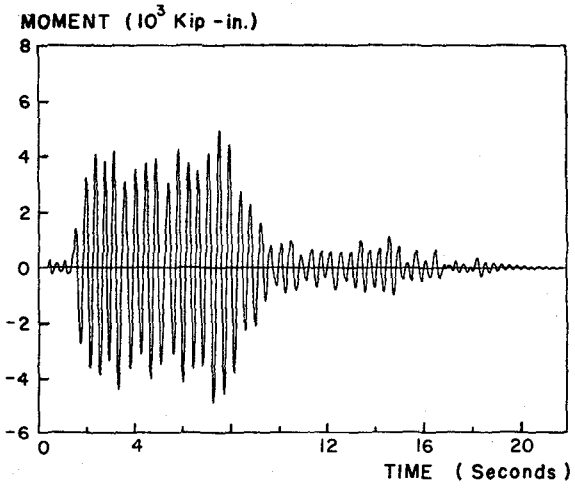

(b) MIYAGI-OKI 24.7

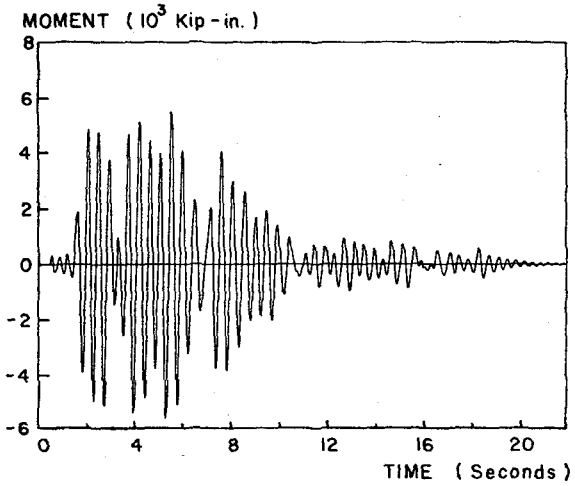

(c) MIYAGI-OKI 28.3

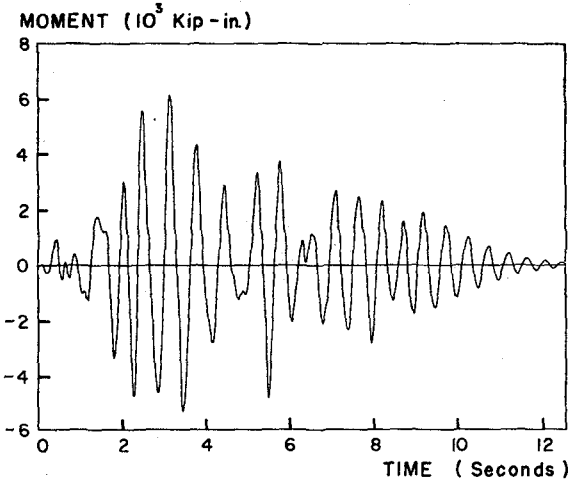

(d) TAFT 40.3

FIG. 27 BASE OVERTURNING MOMENT-TIME HISTORIES OF 1/5th-SCALE MODEL
(1 kip-in. = 0.113 kNm)

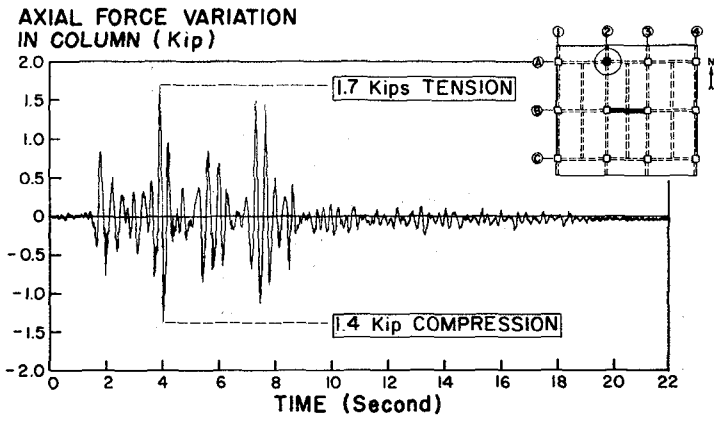

(a) COLUMN A2: MIYAGI-OKI 9.7

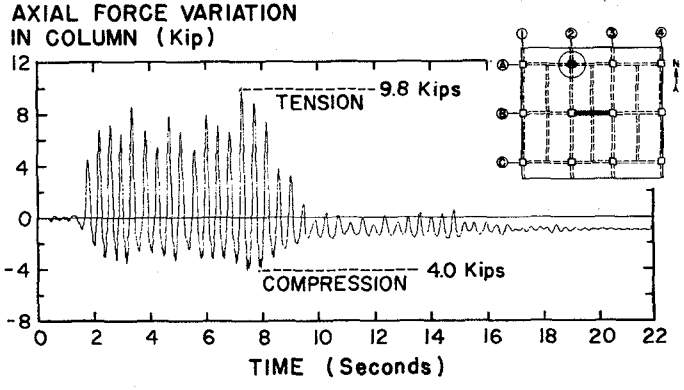

(b) COLUMN A2: MIYAGI-OKI 24.7

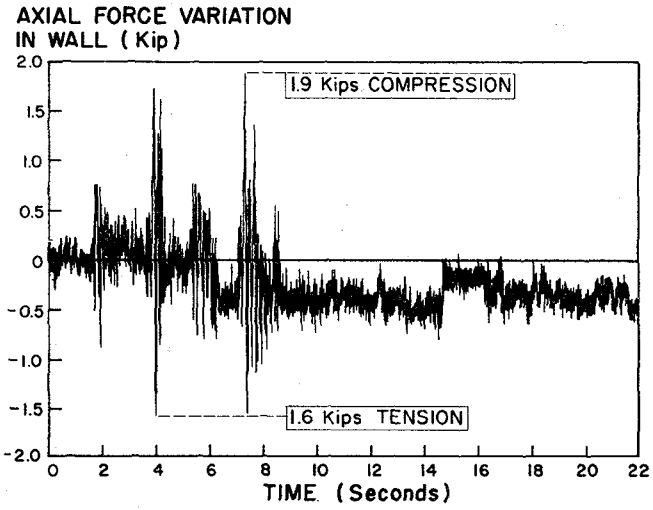

(e) SHEAR WALL: MIYAGI-OKI 9.7

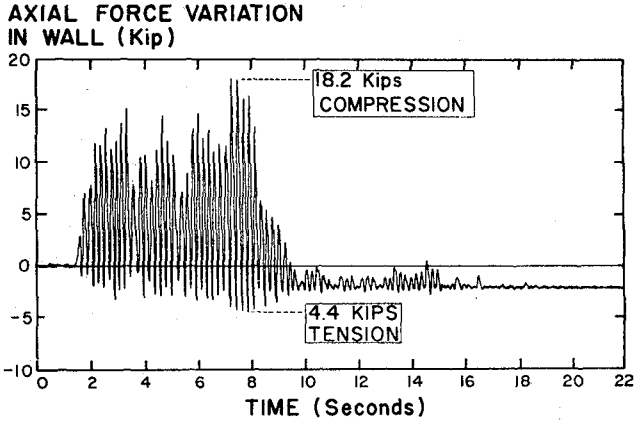

(f) SHEAR WALL: MIYAGI-OKI 24.7

FIG. 28 CONTINUES....

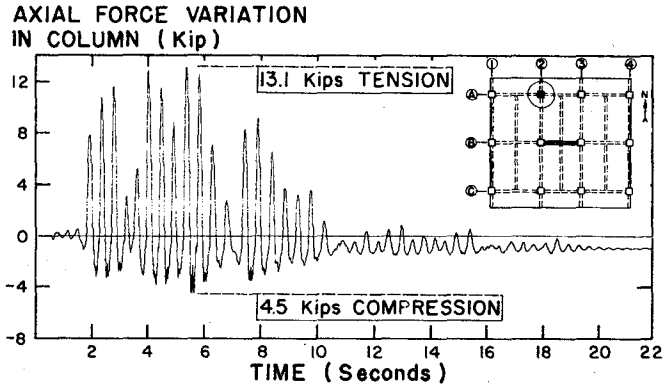

(c) COLUMN A2: MIYAGI-OKI 28.3

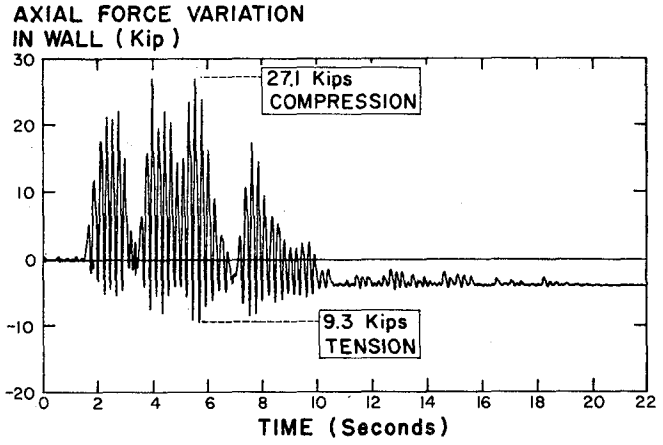

(g) SHEAR WALL: MIYAGI-OKI 28.3

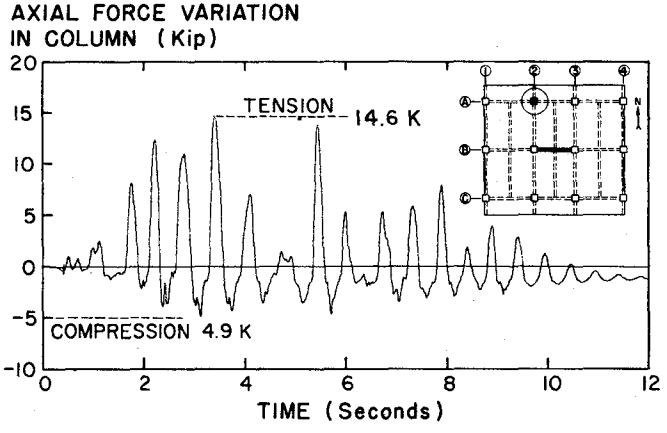

(d) COLUMN A2: TAFT 40.3

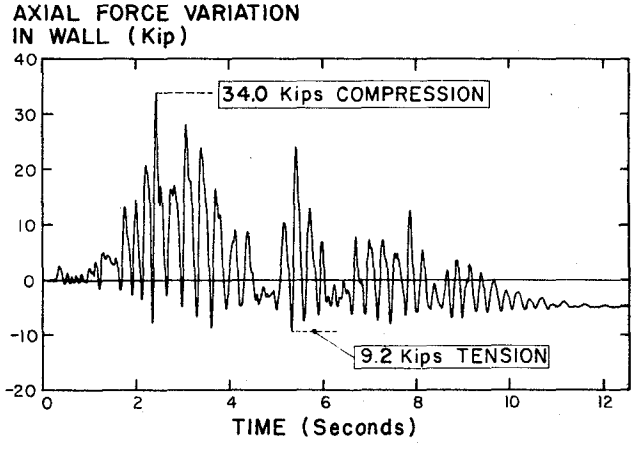

(h) SHEAR WALL: TAFT 40.3

FIG. 28 EXPERIMENTAL VARIATION IN AXIAL FORCE IN SHEAR WALL AND TYPICAL COLUMN (1 kip = 4.45 kN)

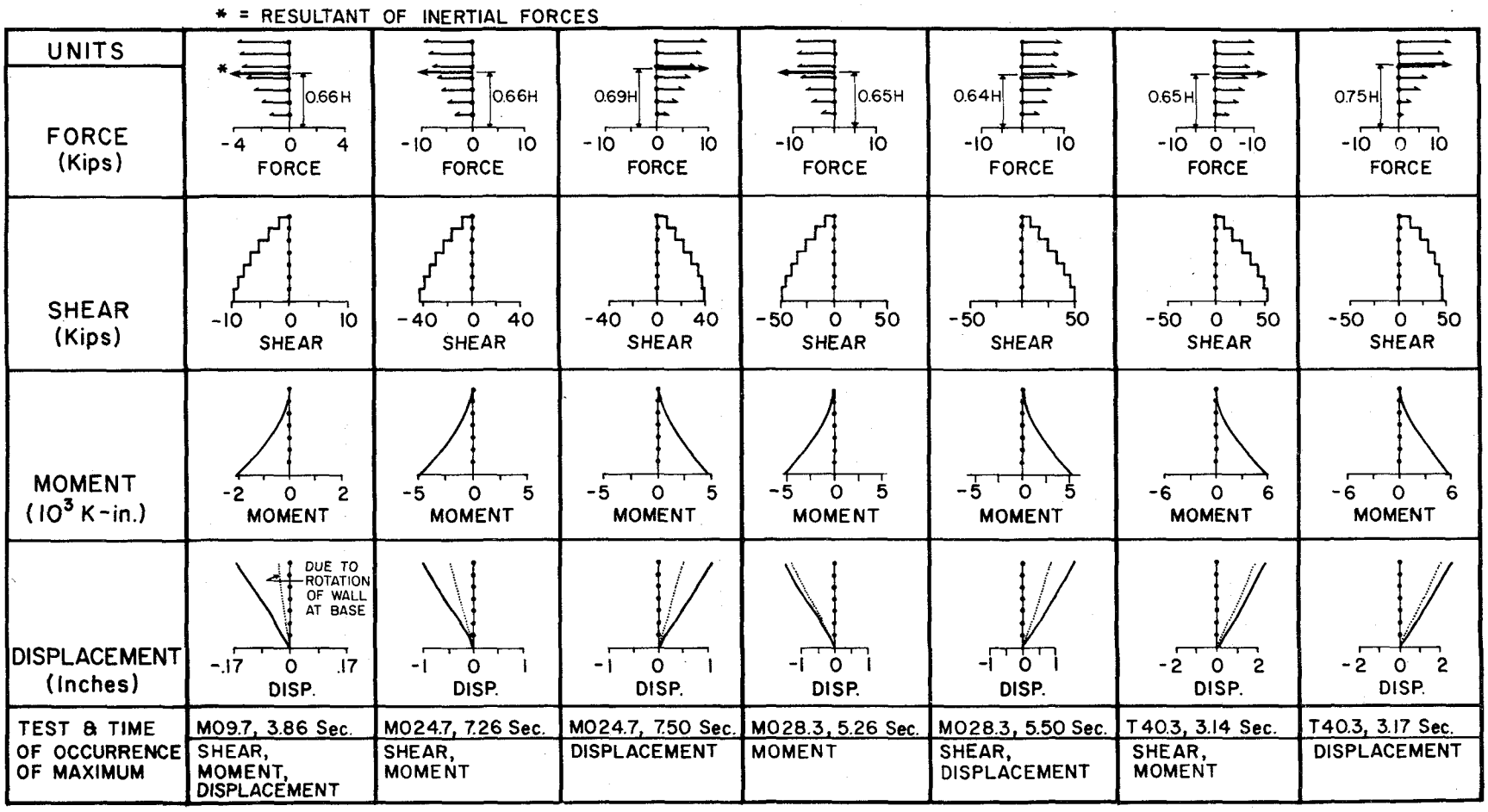

FIG. 29 LATERAL INTERNAL FORCES, STORY SHEARS, MOMENTS AND LATERAL DISPLACEMENT PROFILES OF THE STRUCTURE AT MAXIMUM RESPONSES DURING MO 9.7, MO 24.7, MO 28.3, AND T 40.3 EXCITATIONS
(1 kip = 4.45 kN; 1 kip-in. = 0.113 kNm; 1 in. = 25.4 mm)

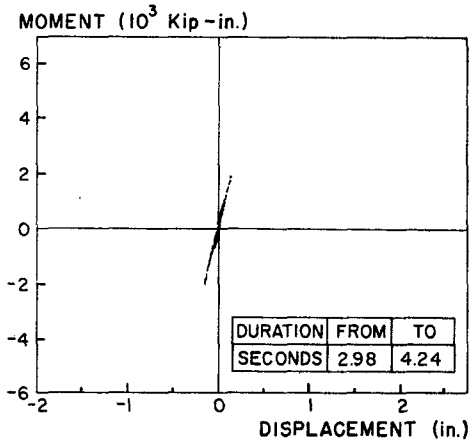

(a) MIYAGI-OKI 9.7

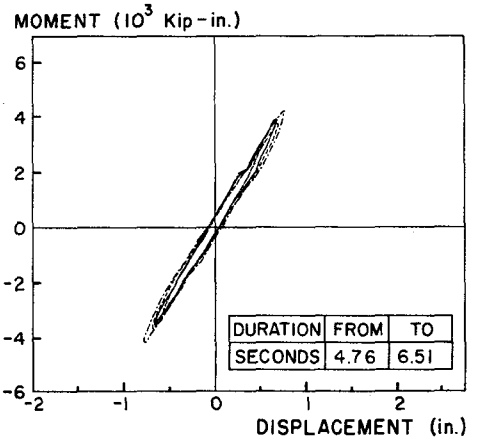

(b) MIYAGI-OKI 24.7

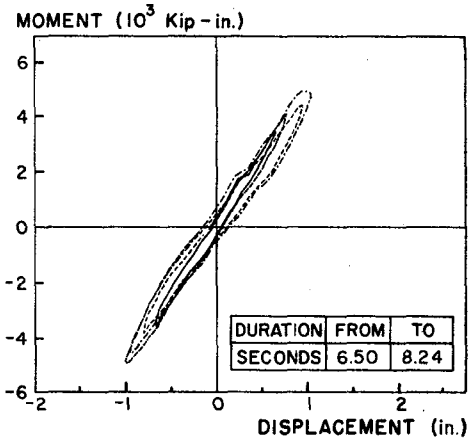

(c) MIYAGI-OKI 24.7

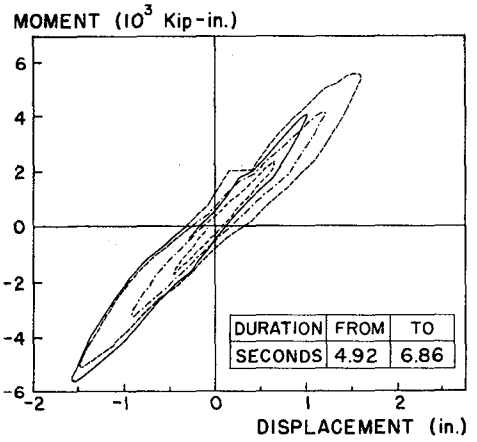

(d) MIYAGI-OKI 28.3

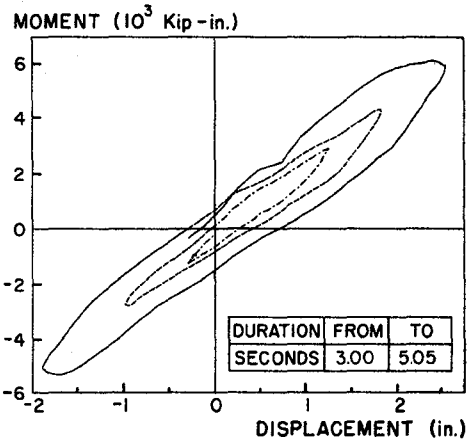

(e) TAFT 40.3

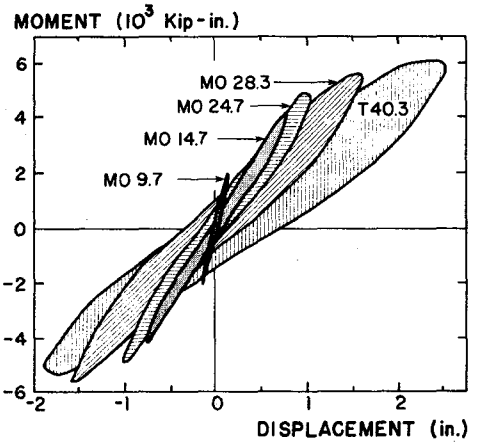

(f) COMPOSITE OF LARGEST CYCLES

FIG. 30 BASE OVERTURNING MOMENT vs TOP FLOOR RELATIVE DISPLACEMENT HYSTERESIS FOR CRITICAL DURATIONS OF MO 9.7, MO 24.7, MO 28.3, AND T 40.3 RESPONSES (1 kip-in. = 0.113 kNm; 1 in. = 25.4 mm)

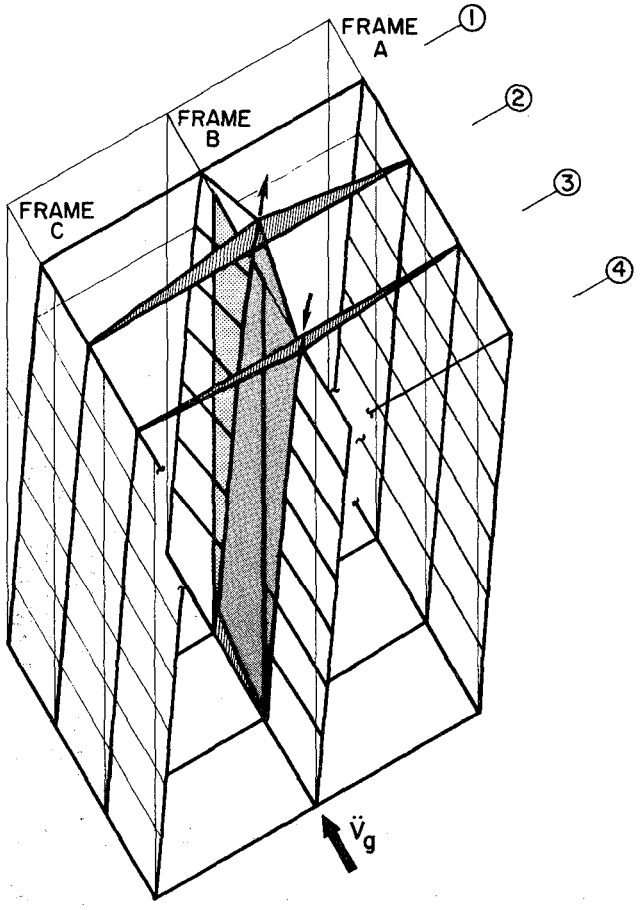

(a) ISOMETRIC VIEW OF WALL ROTATION

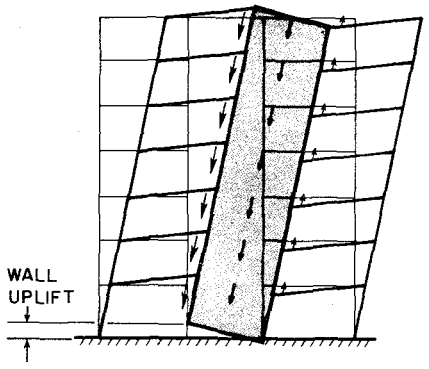

(b) EFFECT OF WALL UPLIFT ON CONNECTING GIRDERS OF FRAME

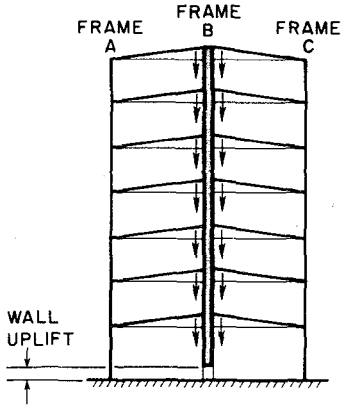

(c) EFFECT OF WALL UPLIFT ON GIRDERS FRAMING INTO WALL PERPENDICULAR TO PLANE

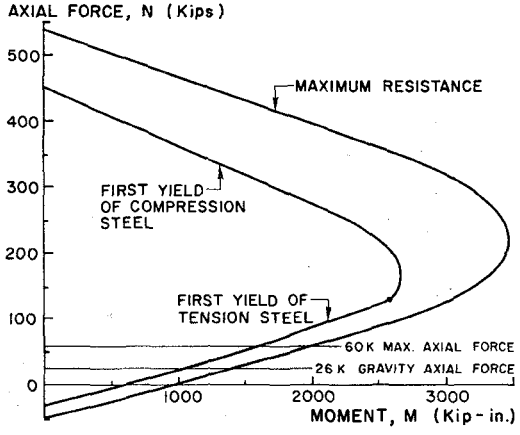

(d) MOMENT-AXIAL FORCE INTERACTION CURVES FOR SHEAR WALL SECTION BASED ON MEASURED MATERIAL PROPERTIES

FIG. 31 EFFECT OF OUTRIGGERING ACTION OF FRAMES ON WALL ON MOMENT-AXIAL FORCE INTERACTION OF THE WALL SECTION AT ITS BASE (1 kip-in. = 0.113 kNm; 1 kip = 4.45 kN)

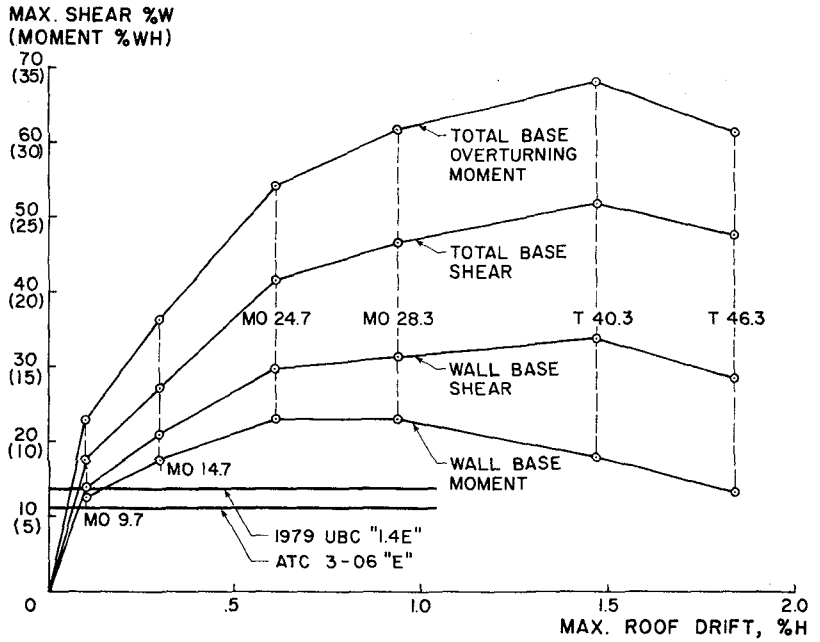

FIG. 32 MAXIMUM BASE SHEAR AND BASE OVERTURNING MOMENT vs MAX. ROOF DRIFT INDEX OF TOTAL STRUCTURE AND WALL ALONE

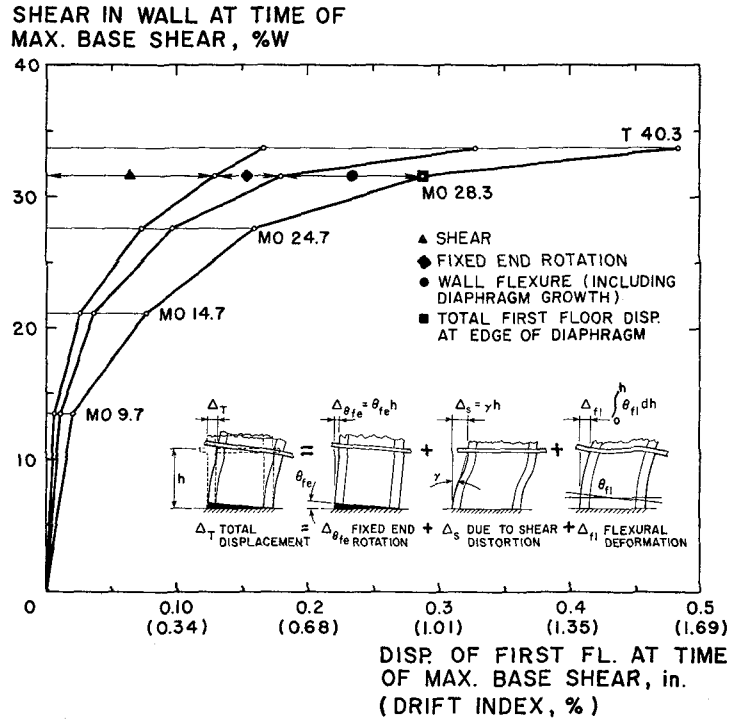

FIG. 33 CONTRIBUTION OF SHEAR, ROTATION, AND FLEXURAL DEFORMATION OF WALL TO LATERAL TOTAL DISPLACEMENT OF WALL (1 in. = 25.4 mm)

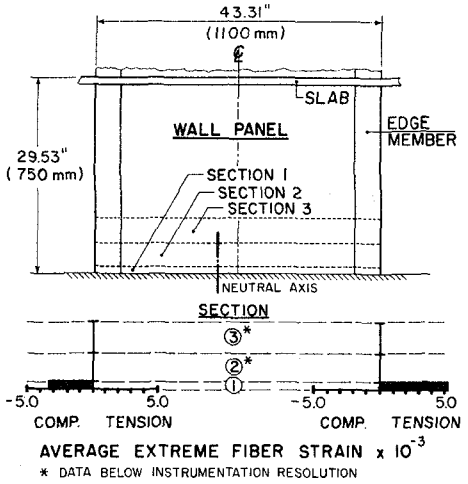

(a) MIYAGI-OKI 9.7; t = 3.86 sec.

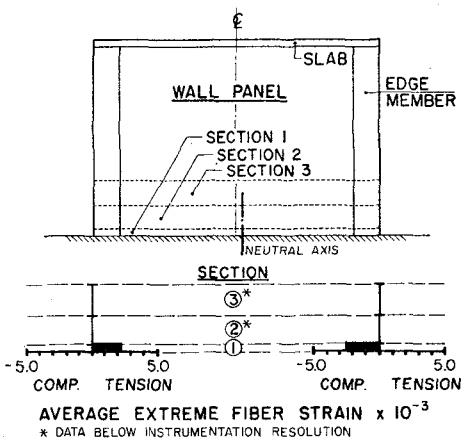

(b) MIYAGI-OKI 9.7; t = 4.05 sec.

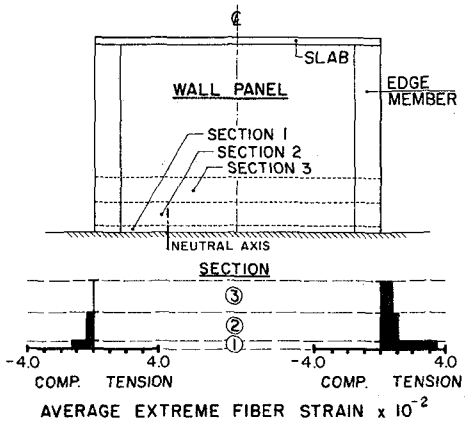

(c) MIYAGI-OKI 24.7; t = 7.29 sec.

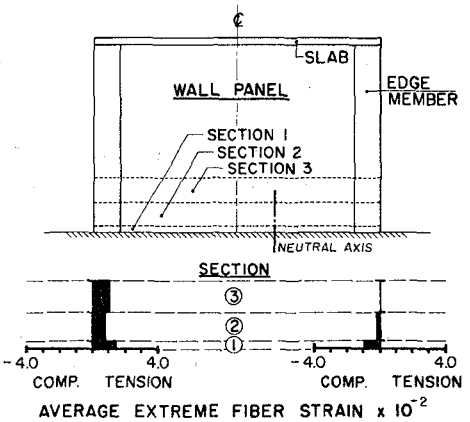

(d) MIYAGI-OKI 24.7; t = 7.51 sec.

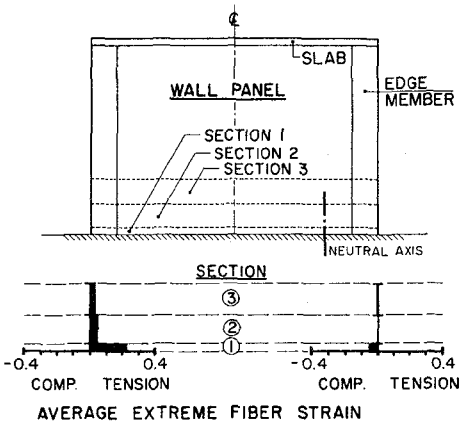

(e) TAFT 40.3; t = 3.16 sec.

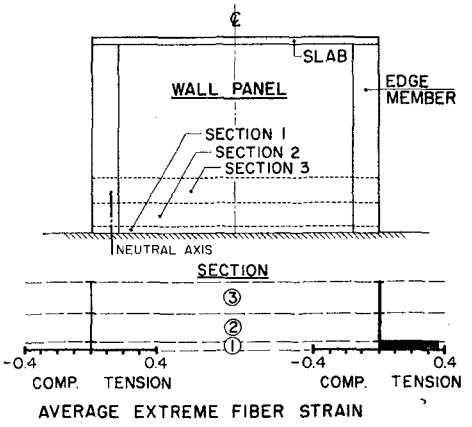

(f) TAFT 40.3; t = 3.49 sec.

FIG. 34 WALL BOUNDARY ELEMENT AXIAL DISTORTIONS AND LOCATION OF NEUTRAL AXIS AT BASE DURING MAXIMUM FIRST FLOOR DISPLACEMENT RESPONSES (1 in. = 25.4 mm)

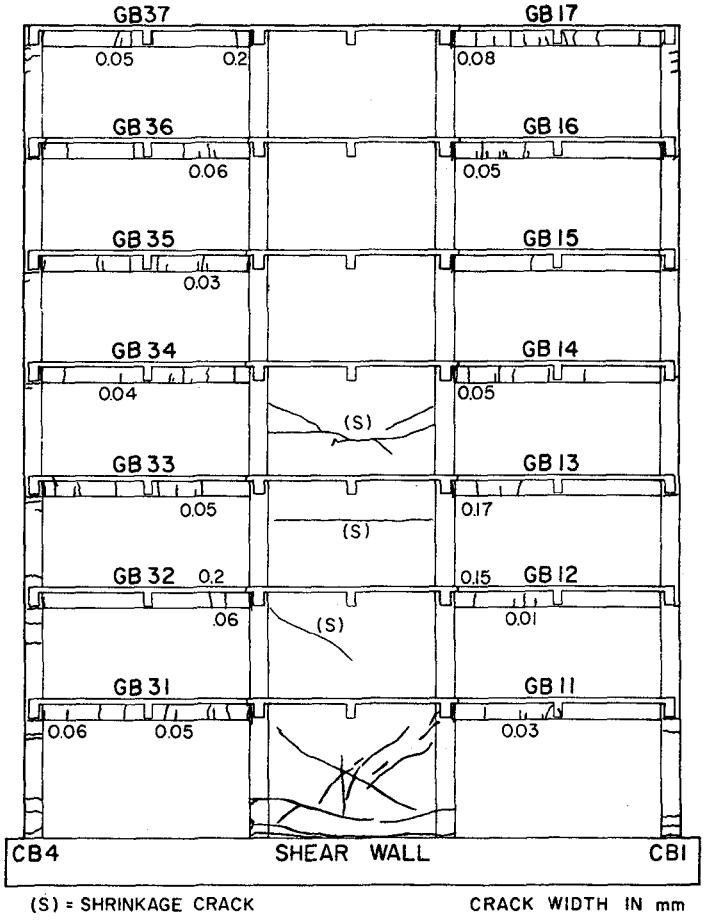

FIG. 35 CRACK PATTERN OF FRAME B
AFTER MO 24.7 TEST
(1 mm = 0.0394 in.)

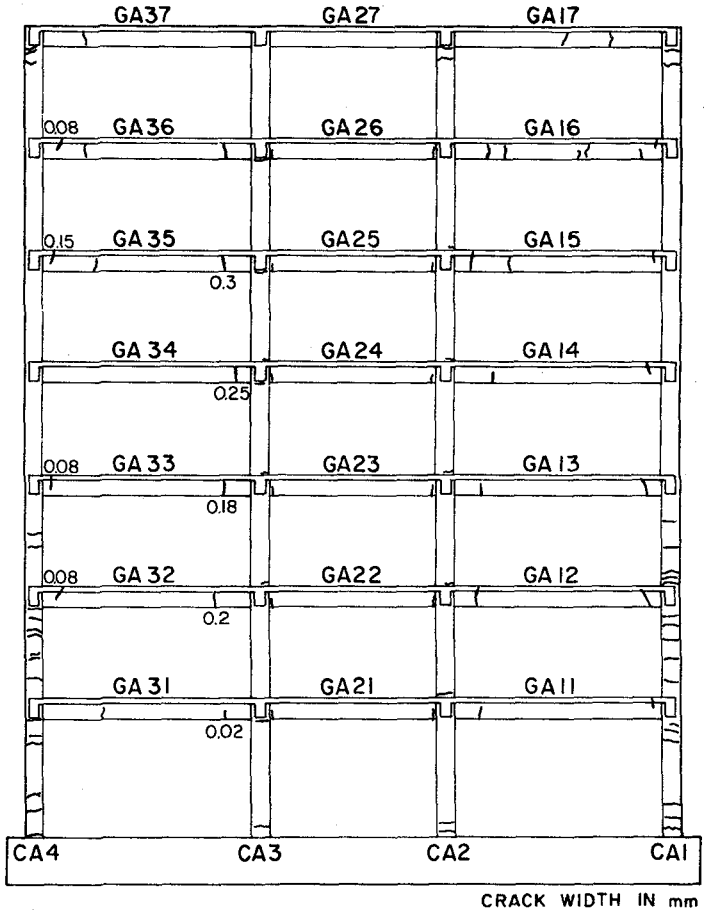

FIG. 36 CRACK PATTERN OF FRAME A
AFTER M0 24.7 TEST
(1 mm = 0.0394 in.)

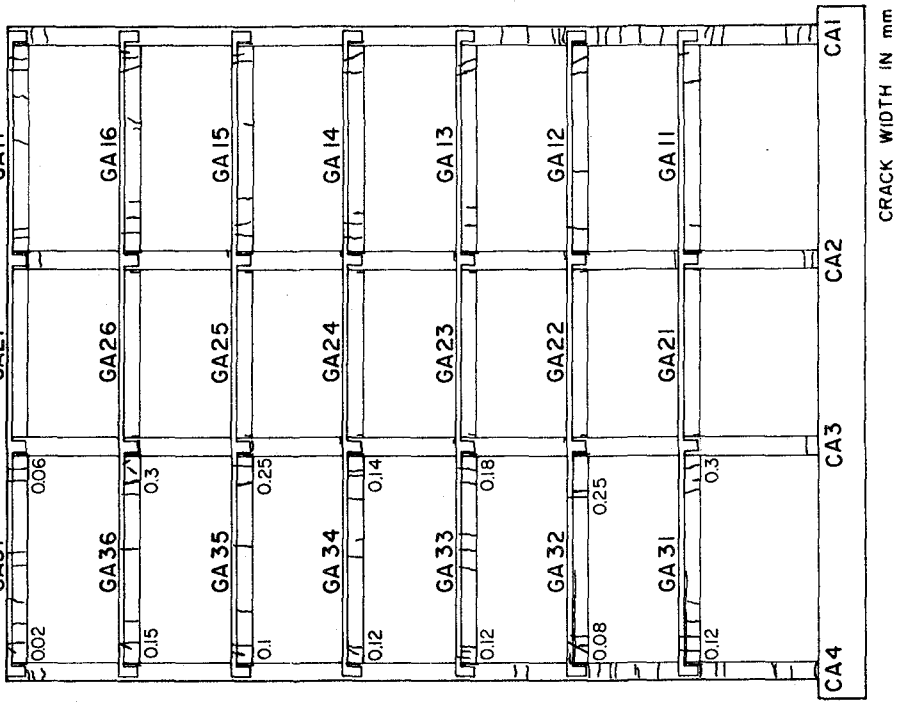

FIG. 38 CRACK PATTERN OF FRAME A
AFTER T 40.3 TEST
(1 mm = 0.0394 in.)

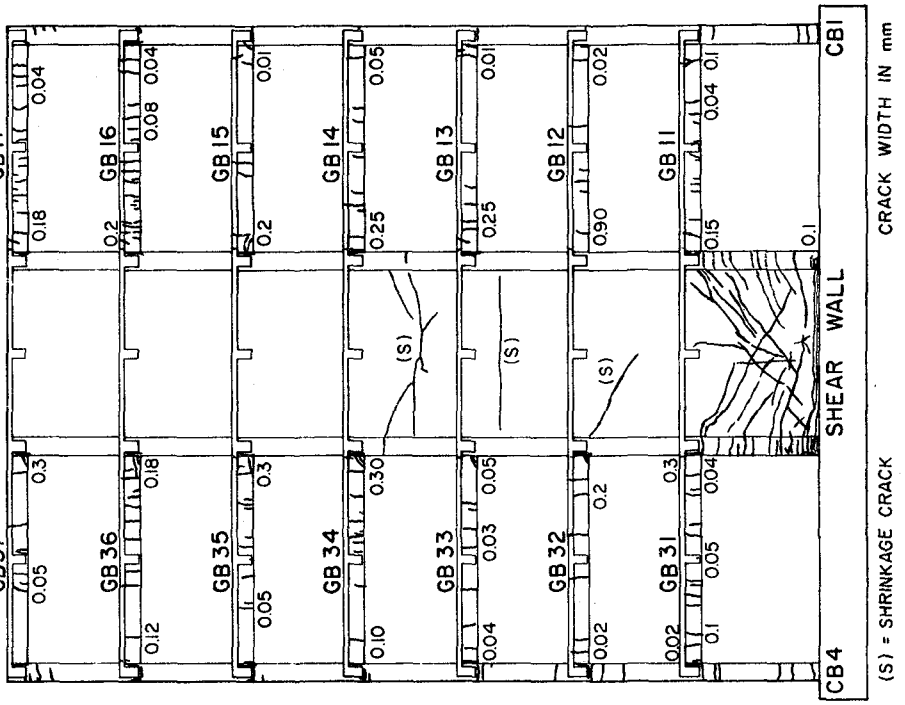

FIG. 37 CRACK PATTERN OF FRAME B
AFTER T 40.3 TEST
(1 mm = 0.0394 in.)

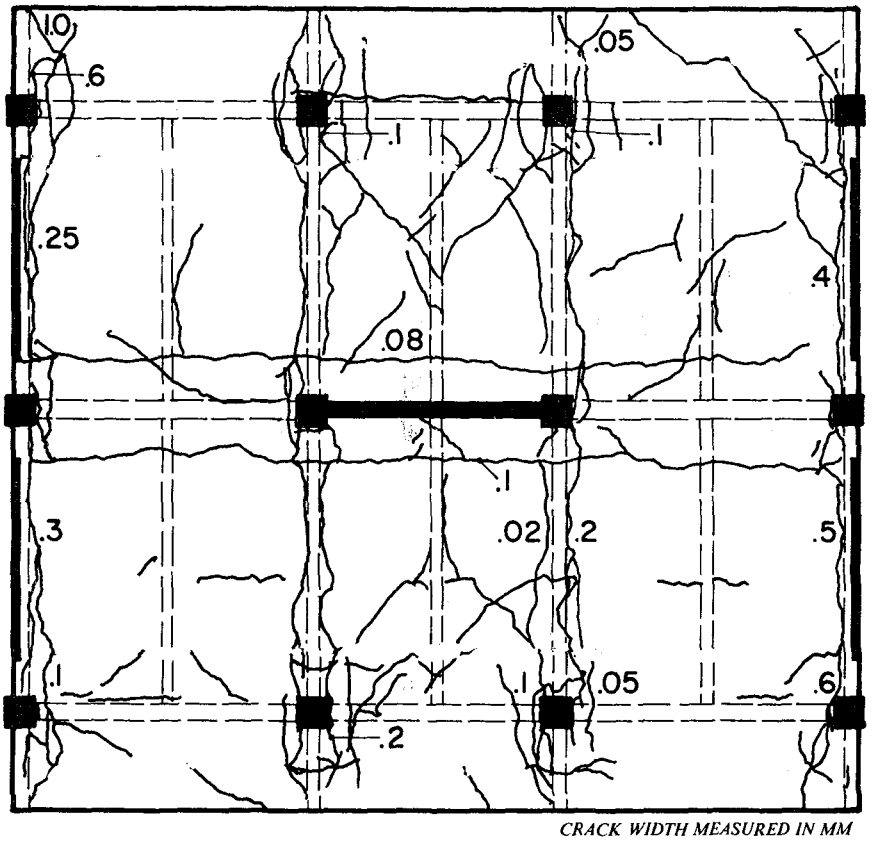

FIG. 39 CRACK PATTERN OBSERVED AT TOP OF FIRST FLOOR SLAB AFTER T 46.3 TEST (1 mm = 0.0394 in.)

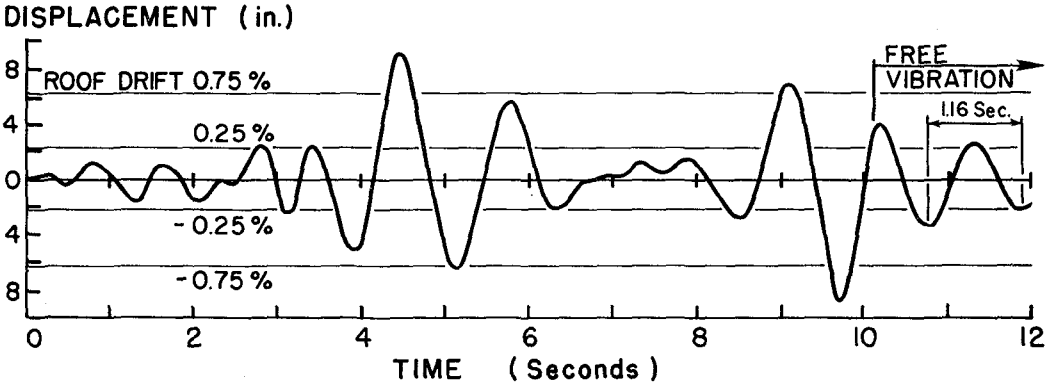

FIG. 40 TIME HISTORY OF ROOF DISPLACEMENT DURING THE PSD-3 TEST OF THE FULL-SCALE MODEL (1 in. = 25.4 mm)

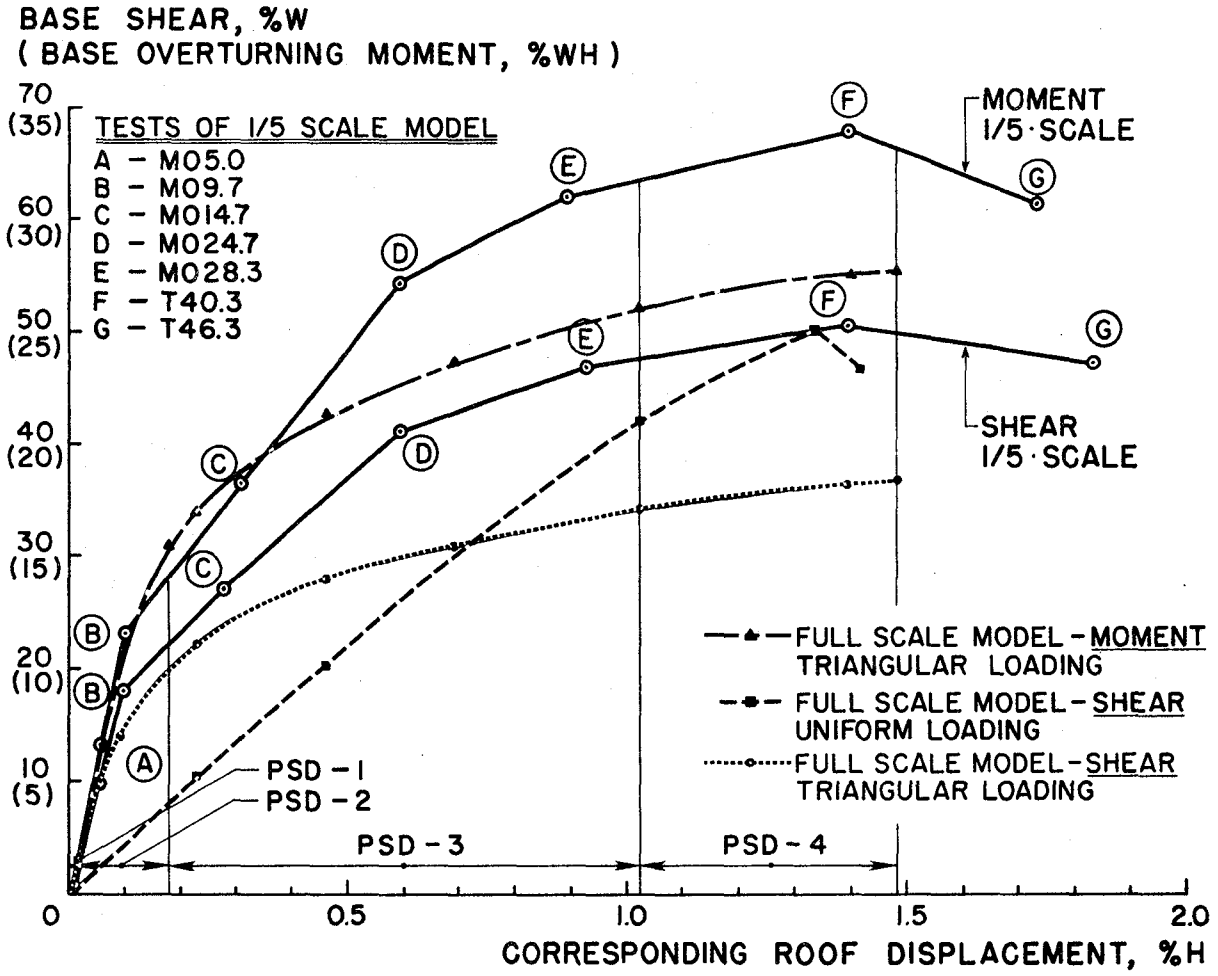

FIG. 41 COMPARISON OF ENVELOPE RESPONSES ATTAINED FOR THE 1/5-SCALE AND FULL-SCALE MODELS

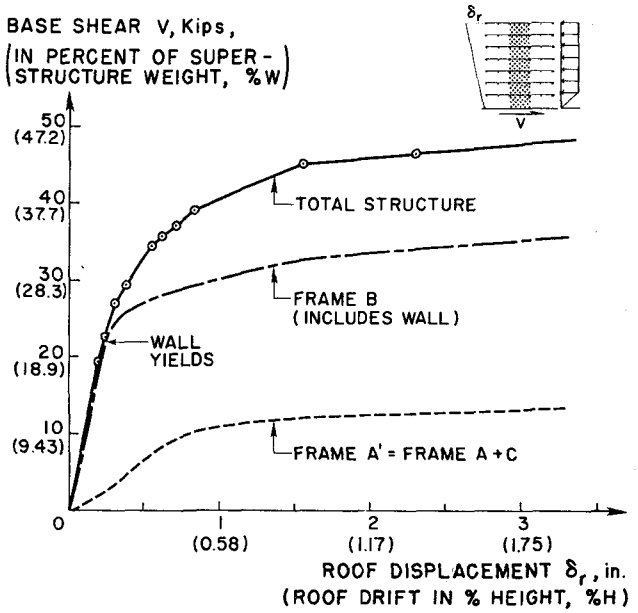

FIG. 50 ANALYTICAL LOAD vs DISPLACEMENT RESPONSE FOR 1/5th-SCALE MODEL SUBJECTED TO STATIC UNIFORM LOAD (1 in. = 25.4 mm ; 1 kip = 4.45 kN)

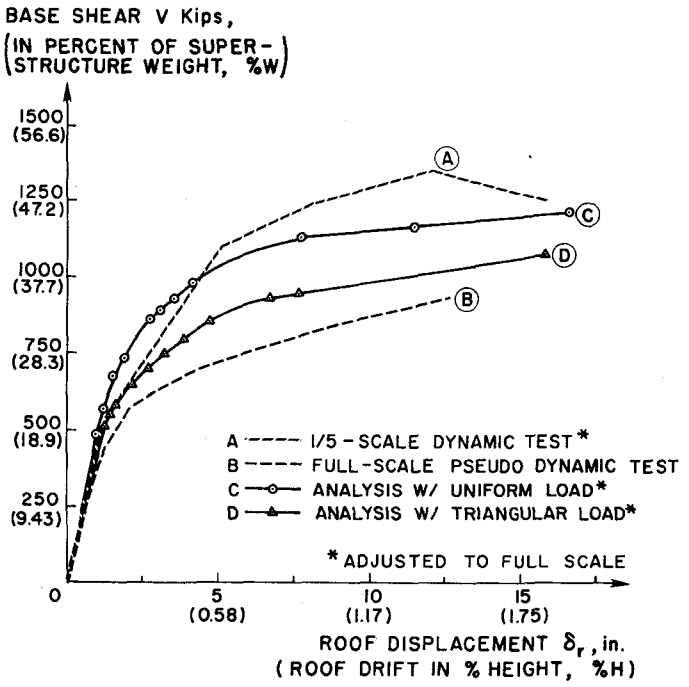

FIG. 51 COMPARISON OF ANALYTICAL AND EXPERIMENTAL RESPONSES (1 in. = 25.4 mm ; 1 kip = 4.45 kN)

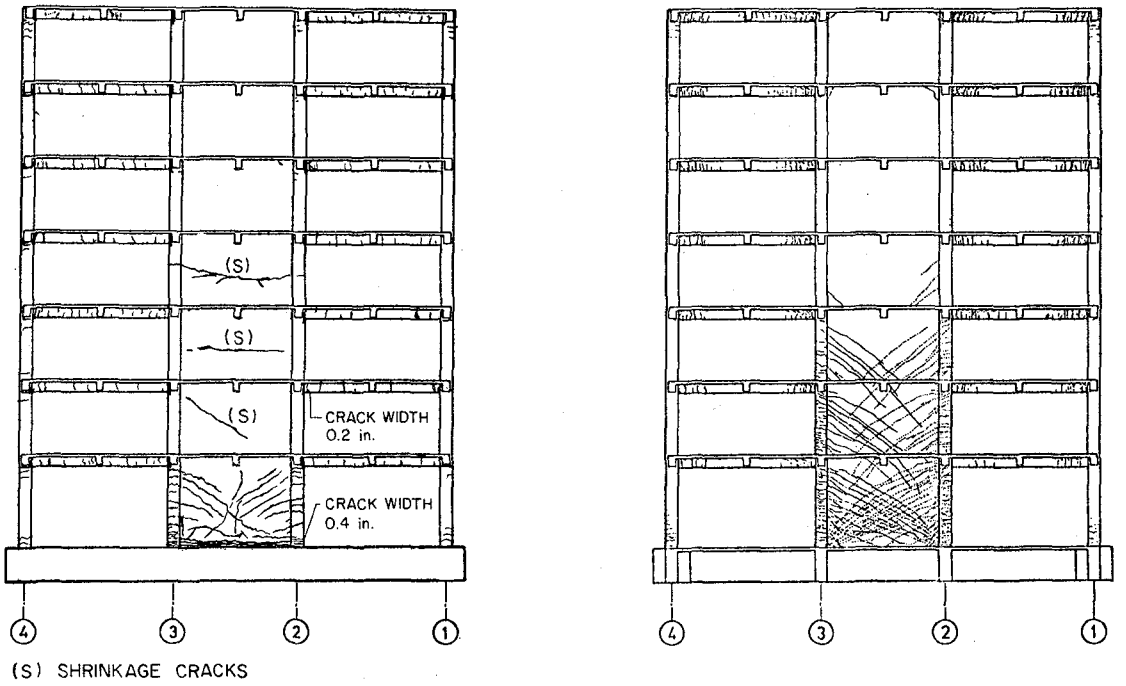

(a) 1/5-SCALE MODEL AFTER TAFT 40.3 TEST

(b) FULL-SCALE MODEL AFTER PSD-4 TEST (HACHINOHE 35.7% G.)

FIG. 42 CRACK PATTERNS IN 1/5th-SCALE AND FULL-SCALE MODELS AFTER 1.4% ROOF DRIFT (1 in. = 25.4 mm)

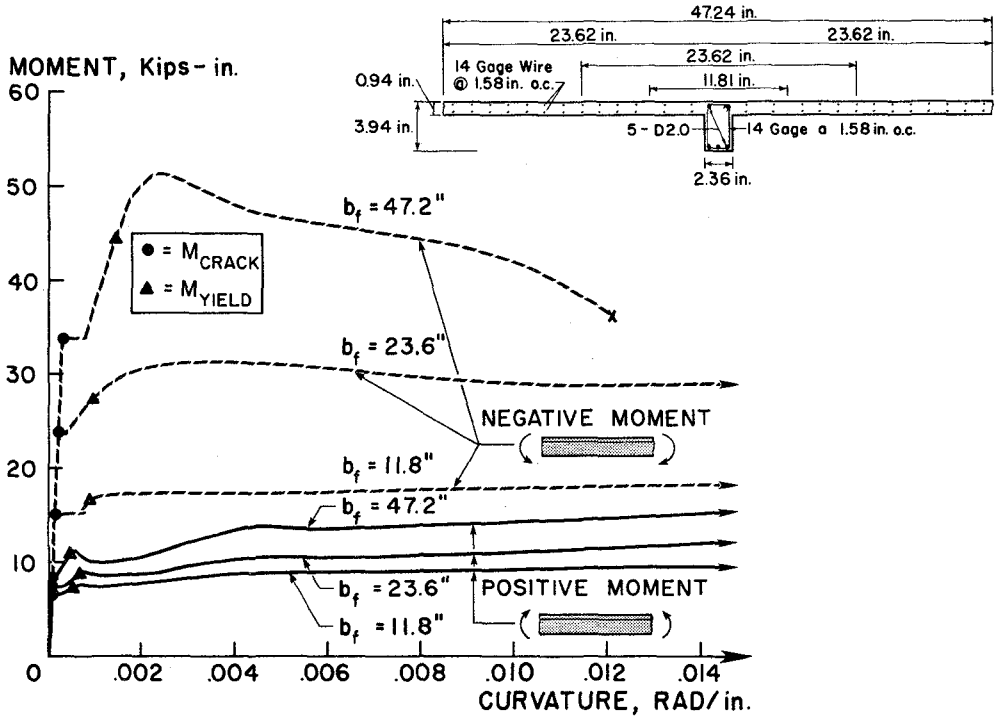

FIG. 43 MOMENT-CURVATURE RELATIONS GENERATED FOR GIRDER G3 (1 kip-in. = 0.113 kNm; 1 in. = 25.4 mm)

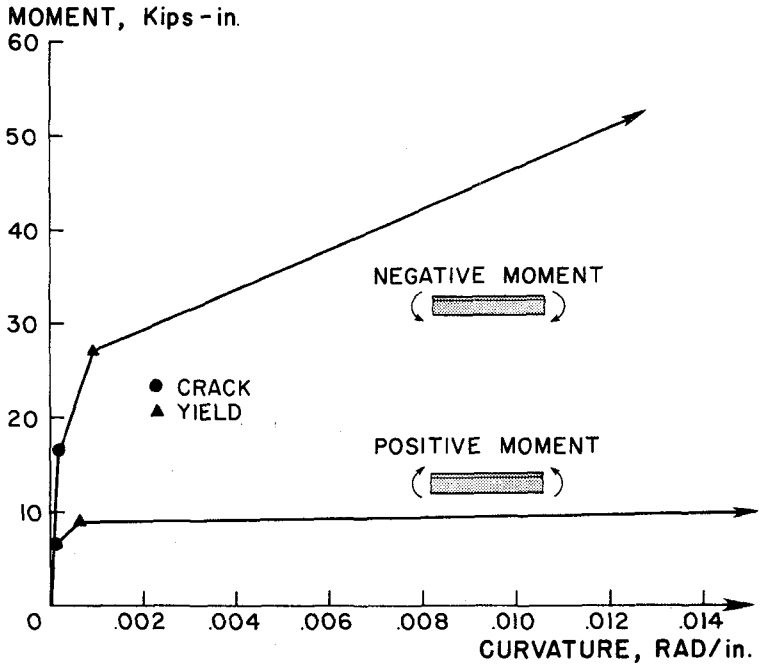

FIG. 44 IDEALIZED MOMENT-CURVATURE RELATIONS USED TO MODEL GIRDER G3
(1 kip-in. = 0.113 kNm; 1 in. = 25.4 mm)

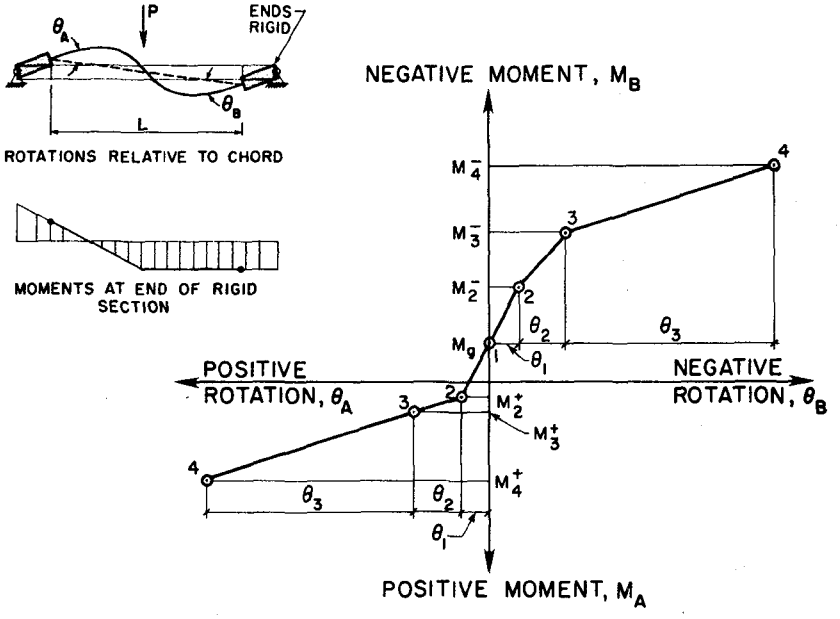

FIG. 45 IDEALIZED BEHAVIOR OF TWO-COMPONENT MODEL LOADED BY GRAVITY LOADS AND SUBJECTED TO SUBSEQUENT EQUAL END ROTATIONS

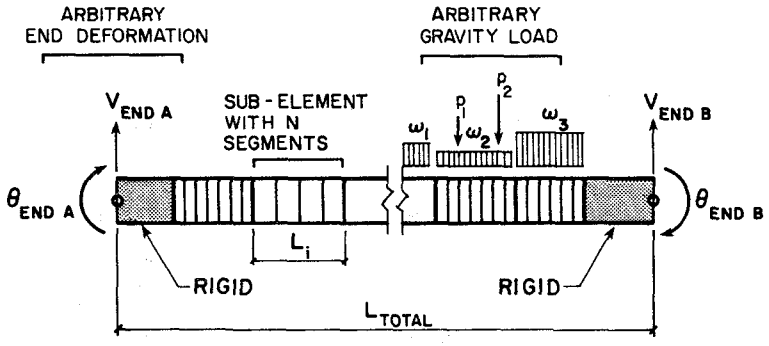

(a) ELEMENT DISCRETIZATION USING "ELMO" ELEMENT MODELING PROGRAM

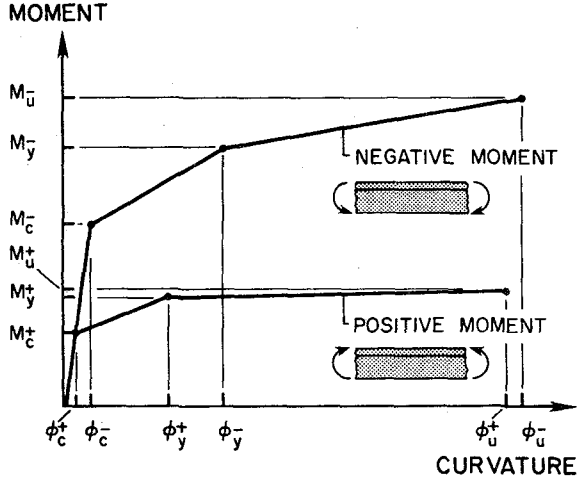

(b) ASSUMED MOMENT CURVATURE RELATIONSHIP FOR TYPICAL SUB-ELEMENT OF "ELMO" MODEL

FIG. 46 "ELMO" BEAM ELEMENTS AND SUB-ELEMENT PROPERTIES

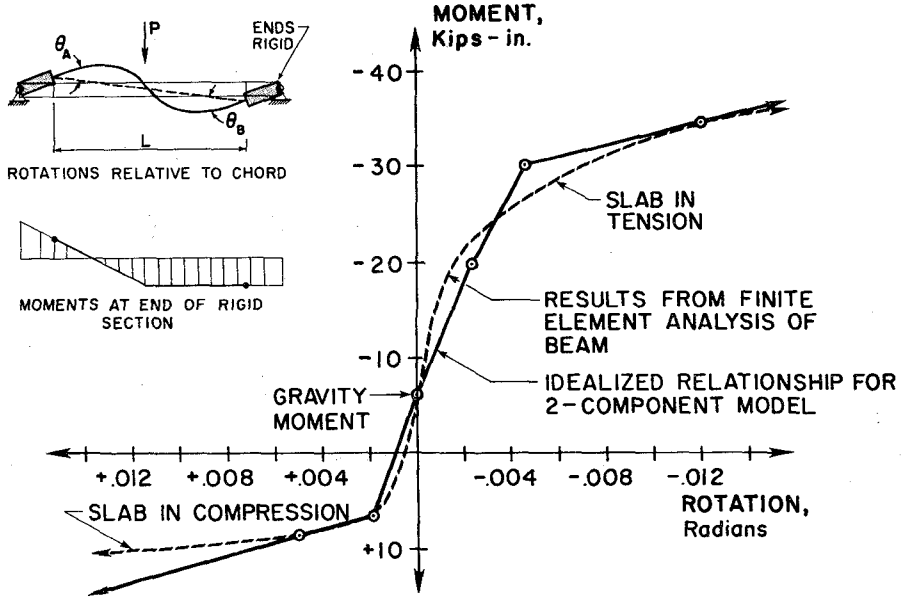

FIG. 47 RESULTS OF ELMO ANALYSIS AND IDEALIZED MOMENT-ROTATION RELATIONSHIP FOR GIRDER G3 (1 kip-in. = 0.113 kNm)

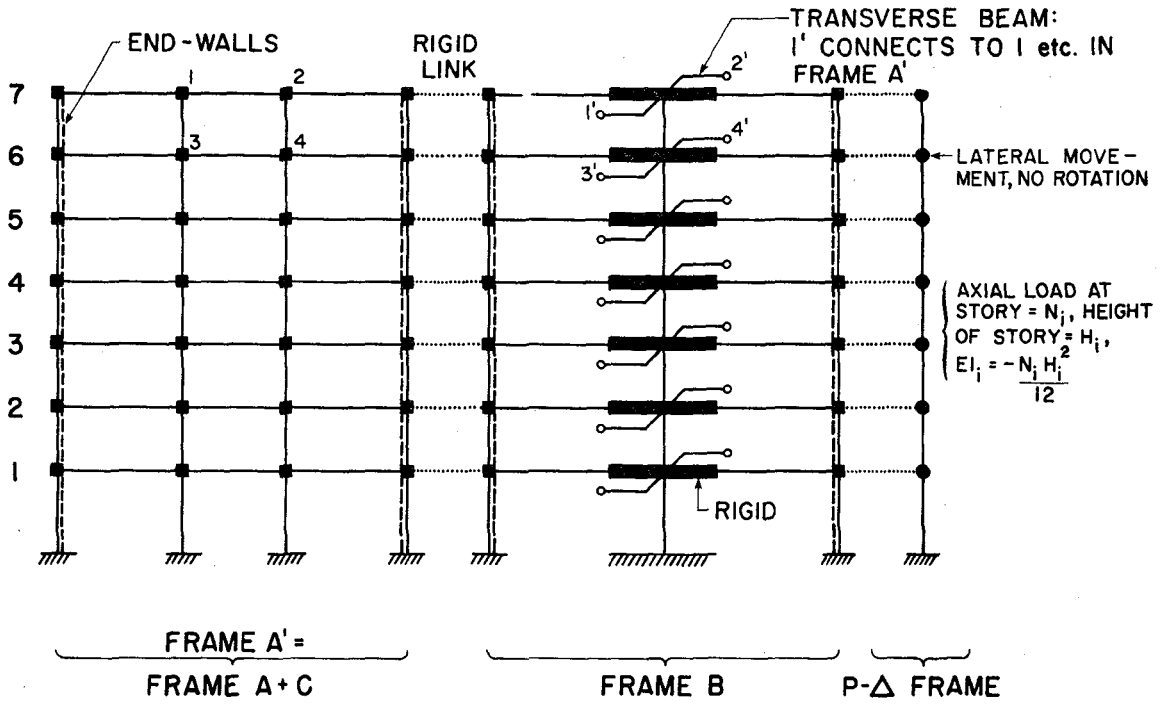

FIG. 48 GLOBAL MODELING OF STRUCTURE, INCORPORATING OUT-OF-PLANE FRAME-WALL INTERACTION

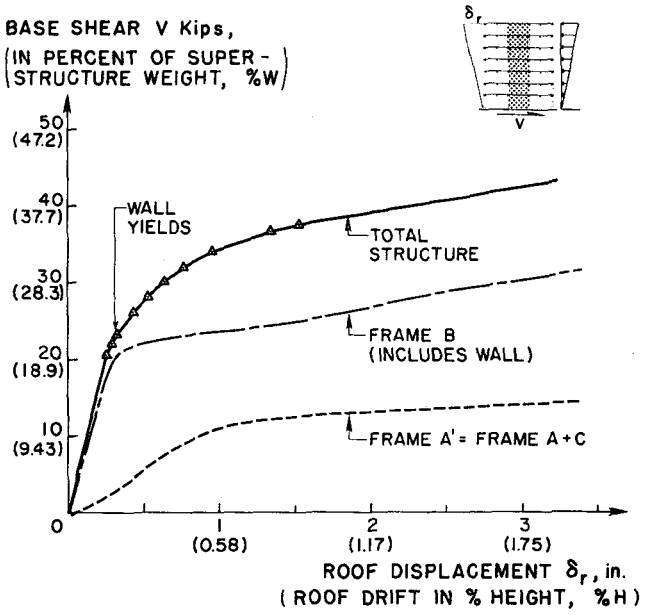

FIG. 49 ANALYTICAL LOAD vs DISPLACEMENT RESPONSE FOR 1/5th-SCALE MODEL SUBJECTED TO STATIC TRIANGULAR LOAD (1 kip = 4.45 kN; 1 in. = 25.4mm)

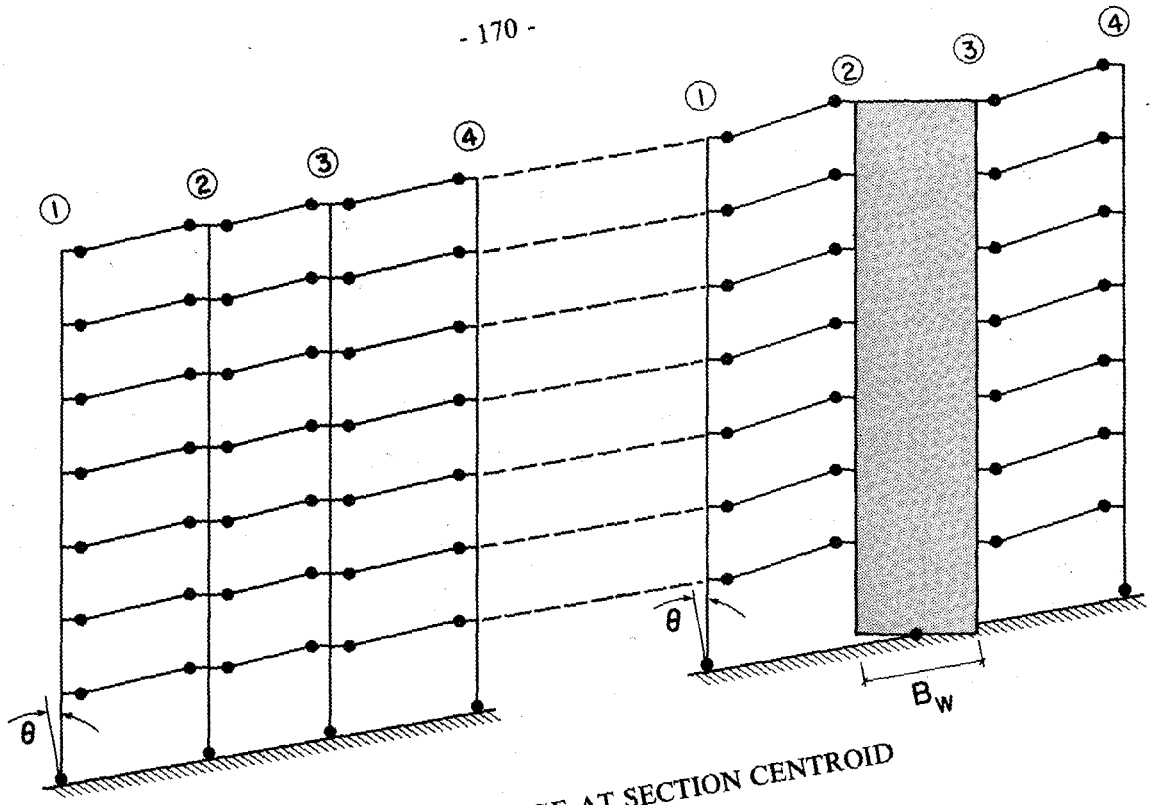

(a) PLASTIC HINGE AT SECTION CENTROID

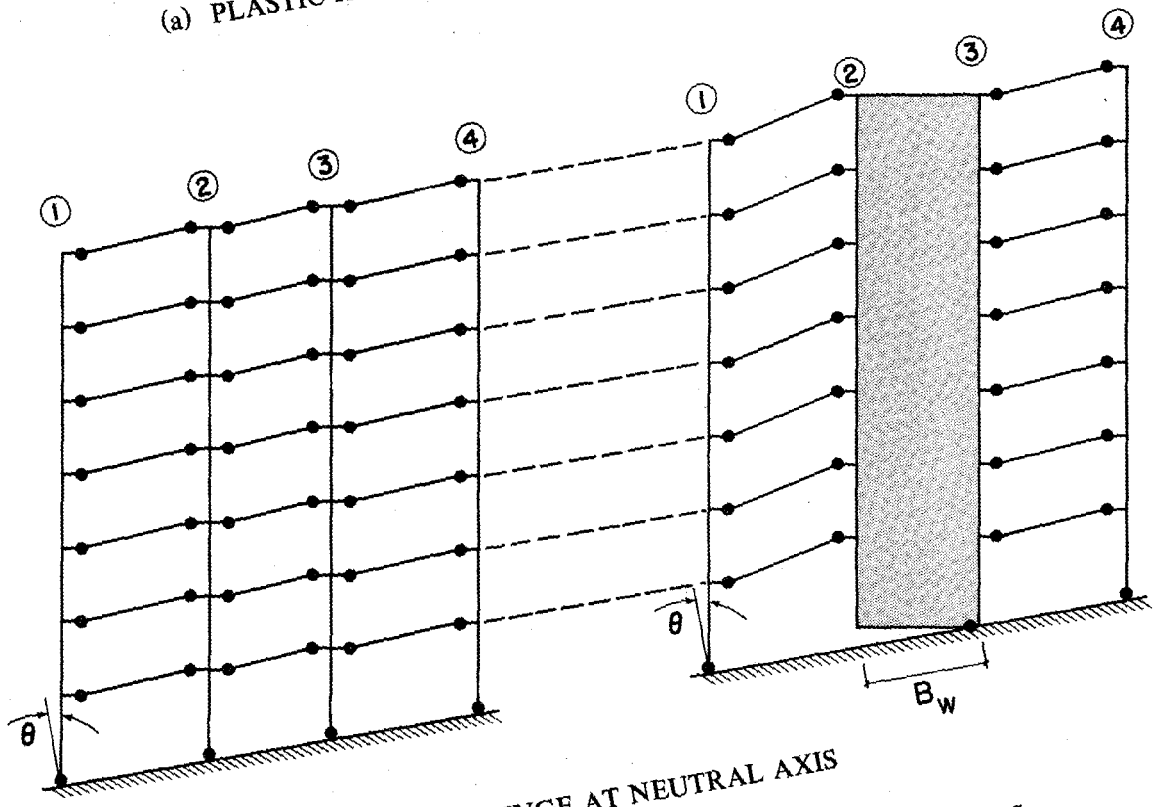

(b) PLASTIC HINGE AT NEUTRAL AXIS

FIG. 52 MECHANISMS CONSIDERED IN LIMIT ANALYSIS

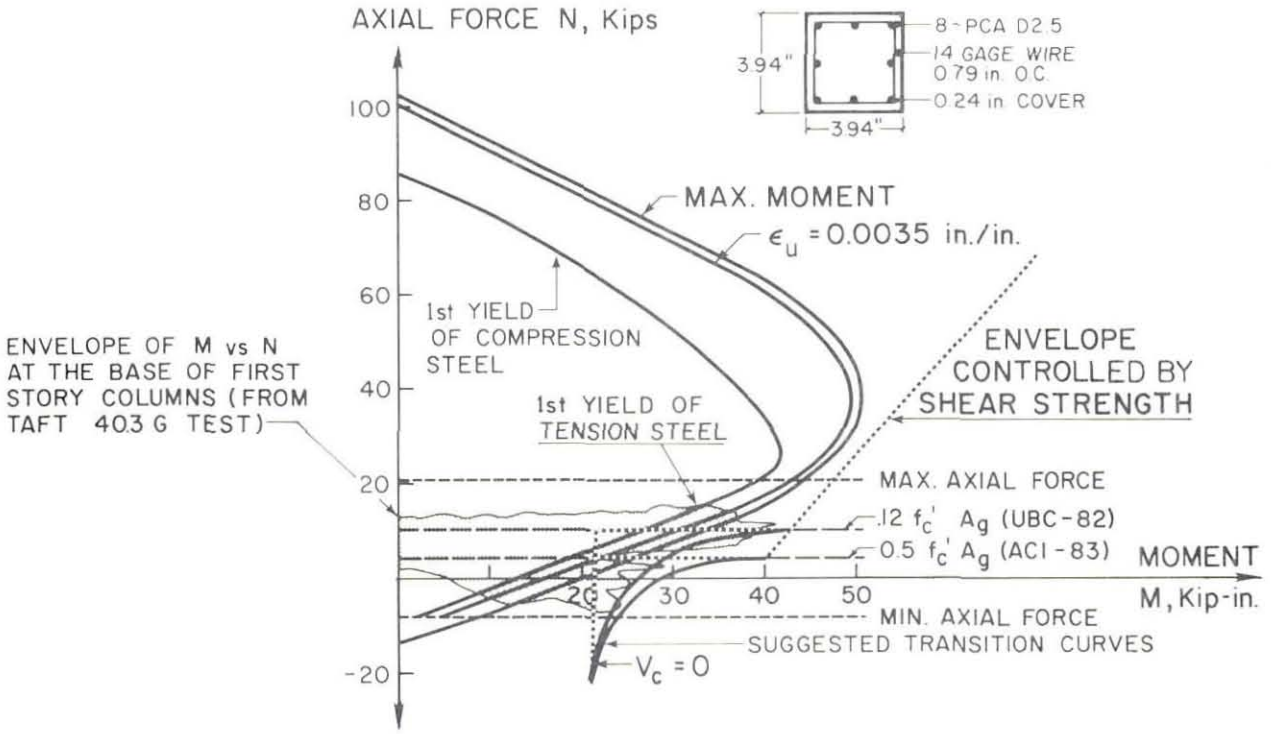

FIG. 53 ENVELOPES OF AXIAL-FLEXURAL STRENGHT CONTROLLED BY SHEAR STRENGHT FOR FIRST-STORY COLUMN OF 1/5-SCALE MODEL FOR FIRST-STORY COLUMN OF TEST BUILDING
(1 kip-in. = 0.113 kNm;1 kip = 4.45 kN)

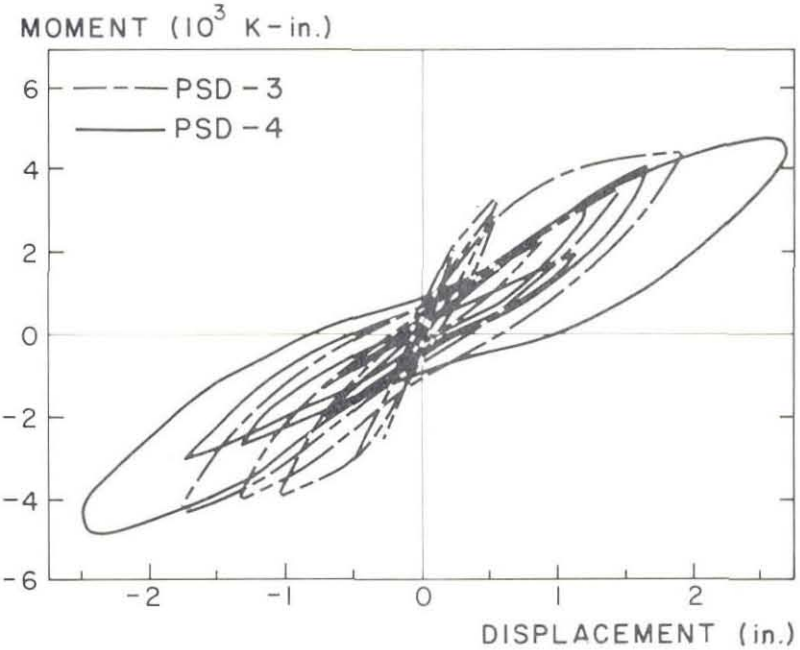

FIG. 54 BASE OVERTURNING MOMENT-ROOF DISPLACEMENT HYSTERETIC RESPONSE OF FULL-SCALE MODEL CONVERTED TO 1/5-SCALE
(1 kip-in. = 0.113 kNm; 1 in. = 25.4 mm)

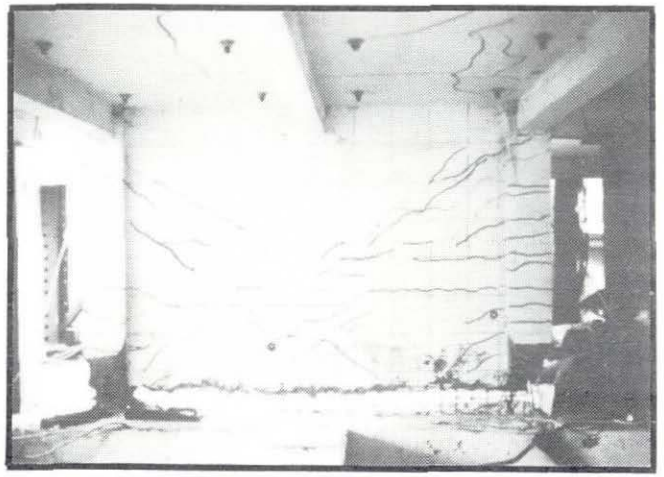

(a) CLOSE-UP OF WALL DAMAGE PATTERN AT FAILURE OF 1/5th-SCALE MODEL AFTER REMOVAL OF DAMAGED CONCRETE

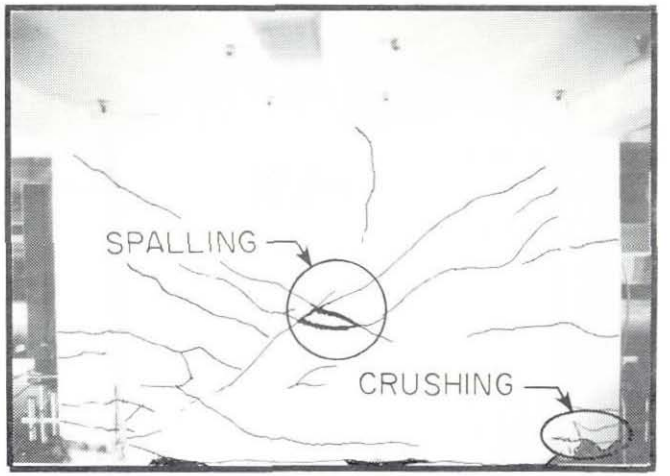

(b) CLOSE UP OF WALL DAMAGE

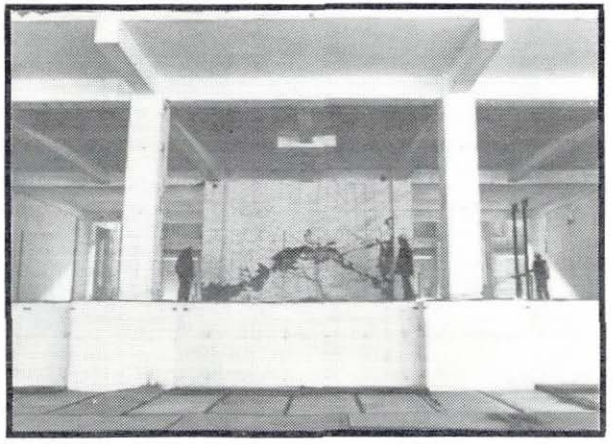

(c) FULL-SCALE MODEL

FIG. 55 PHOTOS ILLUSTRATING FAILURE MECHANISMS

EARTHQUAKE ENGINEERING RESEARCH CENTER REPORTS

NOTE: Numbers in parentheses are Accession Numbers assigned by the National Technical Information Service; these are followed by a price code. Copies of the reports may be ordered from the National Technical Information Service, 5285 Port Royal Road, Springfield, Virginia, 22161. Accession Numbers should be quoted on orders for reports (PB --- ---) and remittance must accompany each order. Reports without this information were not available at time of printing. The complete list of EERC reports (from EERC 67-1) is available upon request from the Earthquake Engineering Research Center, University of California, Berkeley, 47th Street and Hoffman Boulevard, Richmond, California 94804.

UCB/EERC-77/01 "PLUSH - A Computer Program for Probabilistic Finite Element Analysis of Seismic Soil-Structure Interaction," by M.P. Romo Organista, J. Lysmer and H.B. Seed - 1977 (PB81 177 651)A05

UCB/EERC-77/02 "Soil-Structure Interaction Effects at the Humboldt Bay Power Plant in the Ferndale Earthquake of June 7, 1975," by J.E. Valera, H.B. Seed, C.F. Tsai and J. Lysmer - 1977 (PB 265 795)A04

UCB/EERC-77/03 "Influence of Sample Disturbance on Sand Response to Cyclic Loading," by K. Mori, H.B. Seed and C.K. Chan - 1977 (PB 267 352)A04

UCB/EERC-77/04 "Seismological Studies of Strong Motion Records," by J. Shoja-Taheri - 1977 (PB 269 655)A10

UCB/EERC-77/05 Unassigned

UCB/EERC-77/06 "Developing Methodologies for Evaluating the Earthquake Safety of Existing Buildings," by No. 1 - B. Bresler; No. 2 - B. Bresler, T. Okada and D. Zisling; No. 3 - T. Okada and B. Bresler; No. 4 - V.V. Bertero and B. Bresler - 1977 (PB 267 354)A08

UCB/EERC-77/07 "A Literature Survey - Transverse Strength of Masonry Walls," by Y. Omote, R.L. Mayes, S.W. Chen and R.W. Clough - 1977 (PB 277 933)A07

UCB/EERC-77/08 "DRAIN-TABS: A Computer Program for Inelastic Earthquake Response of Three Dimensional Buildings," by R. Guendelman-Israel and G.H. Powell - 1977 (PB 270 693)A07

UCB/EERC-77/09 "SUBWALL: A Special Purpose Finite Element Computer Program for Practical Elastic Analysis and Design of Structural Walls with Substructure Option," by D.Q. Le, H. Peterson and E.P. Popov - 1977 (PB 270 567)A05

UCB/EERC-77/10 "Experimental Evaluation of Seismic Design Methods for Broad Cylindrical Tanks," by D.P. Clough (PB 272 280)A13

UCB/EERC-77/11 "Earthquake Engineering Research at Berkeley - 1976," - 1977 (PB 273 507)A09

UCB/EERC-77/12 "Automated Design of Earthquake Resistant Multistory Steel Building Frames," by N.D. Walker, Jr. - 1977 (PB 276 526)A09

UCB/EERC-77/13 "Concrete Confined by Rectangular Hoops Subjected to Axial Loads," by J. Vallenas, V.V. Bertero and E.P. Popov - 1977 (PB 275 165)A06

UCB/EERC-77/14 "Seismic Strain Induced in the Ground During Earthquakes," by Y. Sugimura - 1977 (PB 284 201)A04

UCB/EERC-77/15 Unassigned

UCB/EERC-77/16 "Computer Aided Optimum Design of Ductile Reinforced Concrete Moment Resisting Frames," by S.W. Zagajeski and V.V. Bertero - 1977 (PB 280 137)A07

UCB/EERC-77/17 "Earthquake Simulation Testing of a Stepping Frame with Energy-Absorbing Devices," by J.M. Kelly and D.F. Tsztoo - 1977 (PB 273 506)A04

UCB/EERC-77/18 "Inelastic Behavior of Eccentrically Braced Steel Frames under Cyclic Loadings," by C.W. Roeder and E.P. Popov - 1977 (PB 275 526)A15

UCB/EERC-77/19 "A Simplified Procedure for Estimating Earthquake-Induced Deformations in Dams and Embankments," by F.I. Makdisi and H.B. Seed - 1977 (PB 276 820)A04

UCB/EERC-77/20 "The Performance of Earth Dams during Earthquakes," by H.B. Seed, F.I. Makdisi and P. de Alba - 1977 (PB 276 821)A04

UCB/EERC-77/21 "Dynamic Plastic Analysis Using Stress Resultant Finite Element Formulation," by P. Lukkunapvasit and J.M. Kelly - 1977 (PB 275 453)A04

UCB/EERC-77/22 "Preliminary Experimental Study of Seismic Uplift of a Steel Frame," by R.W. Clough and A.A. Huckelbridge 1977 (PB 278 769)A08

UCB/EERC-77/23 "Earthquake Simulator Tests of a Nine-Story Steel Frame with Columns Allowed to Uplift," by A.A. Huckelbridge - 1977 (PB 277 944)A09

UCB/EERC-77/24 "Nonlinear Soil-Structure Interaction of Skew Highway Bridges," by M.-C. Chen and J. Penzien - 1977 (PB 276 176)A07

UCB/EERC-77/25 "Seismic Analysis of an Offshore Structure Supported on Pile Foundations," by D.D.-N. Liou and J. Penzien 1977 (PB 283 180)A06

UCB/EERC-77/26 "Dynamic Stiffness Matrices for Homogeneous Viscoelastic Half-Planes," by G. Dasgupta and A.K. Chopra - 1977 (PB 279 654)A06

UCB/EERC-77/27 "A Practical Soft Story Earthquake Isolation System," by J.M. Kelly, J.M. Eidinger and C.J. Derham - 1977 (PB 276 814)A07

UCB/EERC-77/28 "Seismic Safety of Existing Buildings and Incentives for Hazard Mitigation in San Francisco: An Exploratory Study," by A.J. Meltsner - 1977 (PB 281 970)A05

UCB/EERC-77/29 "Dynamic Analysis of Electrohydraulic Shaking Tables," by D. Rea, S. Abedi-Hayati and Y. Takahashi 1977 (PB 282 569)A04

UCB/EERC-77/30 "An Approach for Improving Seismic - Resistant Behavior of Reinforced Concrete Interior Joints," by B. Galunic, V.V. Bertero and E.P. Popov - 1977 (PB 290 870)A06

UCB/EERC-78/01 "The Development of Energy-Absorbing Devices for Aseismic Base Isolation Systems," by J.M. Kelly and D.F. Tsztoo - 1978 (PB 284 978)A04

UCB/EERC-78/02 "Effect of Tensile Prestrain on the Cyclic Response of Structural Steel Connections, by J.G. Bouwkamp and A. Mukhopadhyay - 1978

UCB/EERC-78/03 "Experimental Results of an Earthquake Isolation System using Natural Rubber Bearings," by J.M. Eidinger and J.M. Kelly - 1978 (PB 281 686)A04

UCB/EERC-78/04 "Seismic Behavior of Tall Liquid Storage Tanks," by A. Niwa - 1978 (PB 284 017)A14

UCB/EERC-78/05 "Hysteretic Behavior of Reinforced Concrete Columns Subjected to High Axial and Cyclic Shear Forces," by S.W. Zagajeski, V.V. Bertero and J.G. Bouwkamp - 1978 (PB 283 858)A13

UCB/EERC-78/06 "Three Dimensional Inelastic Frame Elements for the ANSR-I Program," by A. Riahi, D.G. Row and G.H. Powell - 1978 (PB 295 755)A04

UCB/EERC-78/07 "Studies of Structural Response to Earthquake Ground Motion," by O.A. Lopez and A.K. Chopra - 1978 (PB 282 790)A05

UCB/EERC-78/08 "A Laboratory Study of the Fluid-Structure Interaction of Submerged Tanks and Caissons in Earthquakes," by R.C. Byrd - 1978 (PB 284 957)A08

UCB/EERC-78/09 Unassigned

UCB/EERC-78/10 "Seismic Performance of Nonstructural and Secondary Structural Elements," by I. Sakamoto - 1978 (PB81 154 593)A05

UCB/EERC-78/11 "Mathematical Modelling of Hysteresis Loops for Reinforced Concrete Columns," by S. Nakata, T. Sproul and J. Penzien - 1978 (PB 298 274)A05

UCB/EERC-78/12 "Damageability in Existing Buildings," by T. Blejwas and B. Bresler - 1978 (PB 80 166 978)A05

UCB/EERC-78/13 "Dynamic Behavior of a Pedestal Base Multistory Building," by R.M. Stephen, E.L. Wilson, J.G. Bouwkamp and M. Button - 1978 (PB 286 650)A08

UCB/EERC-78/14 "Seismic Response of Bridges - Case Studies," by R.A. Imbsen, V. Nutt and J. Penzien - 1978 (PB 286 503)A10

UCB/EERC-78/15 "A Substructure Technique for Nonlinear Static and Dynamic Analysis," by D.G. Row and G.H. Powell - 1978 (PB 288 077)A10

UCB/EERC-78/16 "Seismic Risk Studies for San Francisco and for the Greater San Francisco Bay Area," by C.S. Oliveira - 1978 (PB 81 120 115)A07

UCB/EERC-78/17 "Strength of Timber Roof Connections Subjected to Cyclic Loads," by P. Gülkan, R.L. Mayes and R.W. Clough - 1978 (HUD-000 1491)A07

UCB/EERC-78/18 "Response of K-Braced Steel Frame Models to Lateral Loads," by J.G. Bouwkamp, R.M. Stephen and E.P. Popov - 1978

UCB/EERC-78/19 "Rational Design Methods for Light Equipment in Structures Subjected to Ground Motion," by J.L. Sackman and J.M. Kelly - 1978 (PB 292 357)A04

UCB/EERC-78/20 "Testing of a Wind Restraint for Aseismic Base Isolation," by J.M. Kelly and D.E. Chitty - 1978 (PB 292 833)A03

UCB/EERC-78/21 "APOLLO - A Computer Program for the Analysis of Pore Pressure Generation and Dissipation in Horizontal Sand Layers During Cyclic or Earthquake Loading," by P.P. Martin and H.B. Seed - 1978 (PB 292 835)A04

UCB/EERC-78/22 "Optimal Design of an Earthquake Isolation System," by M.A. Bhatti, K.S. Pister and E. Polak - 1978 (PB 294 735)A06

UCB/EERC-78/23 "MASH - A Computer Program for the Non-Linear Analysis of Vertically Propagating Shear Waves in Horizontally Layered Deposits," by P.P. Martin and H.B. Seed - 1978 (PB 293 101)A05

UCB/EERC-78/24 "Investigation of the Elastic Characteristics of a Three Story Steel Frame Using System Identification," by I. Kaya and H.D. McNiven - 1978 (PB 296 225)A06

UCB/EERC-78/25 "Investigation of the Nonlinear Characteristics of a Three-Story Steel Frame Using System Identification," by I. Kaya and H.D. McNiven - 1978 (PB 301 363)A05

UCB/EERC-78/26 "Studies of Strong Ground Motion in Taiwan," by Y.M. Hsiung, B.A. Bolt and J. Penzien - 1978 (PB 298 436)A06

UCB/EERC-78/27 "Cyclic Loading Tests of Masonry Single Piers: Volume 1 - Height to Width Ratio of 2," by P.A. Hidalgo, R.L. Mayes, H.D. McNiven and R.W. Clough - 1978 (PB 296 211)A07

UCB/EERC-78/28 "Cyclic Loading Tests of Masonry Single Piers: Volume 2 - Height to Width Ratio of 1," by S.-W.J. Chen, P.A. Hidalgo, R.L. Mayes, R.W. Clough and H.D. McNiven - 1978 (PB 296 212)A09

UCB/EERC-78/29 "Analytical Procedures in Soil Dynamics," by J. Lysmer - 1978 (PB 298 445)A06

UCB/EERC-79/01 "Hysteretic Behavior of Lightweight Reinforced Concrete Beam-Column Subassemblages," by B. Forzani, E.P. Popov and V.V. Bertero - April 1979(PB 298 267)A06

UCB/EERC-79/02 "The Development of a Mathematical Model to Predict the Flexural Response of Reinforced Concrete Beams to Cyclic Loads, Using System Identification," by J. Stanton & H. McNiven - Jan. 1979(PB 295 875)A10

UCB/EERC-79/03 "Linear and Nonlinear Earthquake Response of Simple Torsionally Coupled Systems," by C.L. Kan and A.K. Chopra - Feb. 1979(PB 298 262)A06

UCB/EERC-79/04 "A Mathematical Model of Masonry for Predicting its Linear Seismic Response Characteristics," by Y. Mengi and H.D. McNiven - Feb. 1979(PB 298 266)A06

UCB/EERC-79/05 "Mechanical Behavior of Lightweight Concrete Confined by Different Types of Lateral Reinforcement," by M.A. Manrique, V.V. Bertero and E.P. Popov - May 1979(PB 301 114)A06

UCB/EERC-79/06 "Static Tilt Tests of a Tall Cylindrical Liquid Storage Tank," by R.W. Clough and A. Niwa - Feb. 1979 (PB 301 167)A06

UCB/EERC-79/07 "The Design of Steel Energy Absorbing Restrainers and Their Incorporation into Nuclear Power Plants for Enhanced Safety: Volume 1 - Summary Report," by P.N. Spencer, V.F. Zackay, and E.R. Parker - Feb. 1979(UCB/EERC-79/07)A09

UCB/EERC-79/08 "The Design of Steel Energy Absorbing Restrainers and Their Incorporation into Nuclear Power Plants for Enhanced Safety: Volume 2 - The Development of Analyses for Reactor System Piping,""Simple Systems" by M.C. Lee, J. Penzien, A.K. Chopra and K, Suzuki "Complex Systems" by G.H. Powell, E.L. Wilson, R.W. Clough and D.G. Row - Feb. 1979(UCB/EERC-79/08)A10

UCB/EERC-79/09 "The Design of Steel Energy Absorbing Restrainers and Their Incorporation into Nuclear Power Plants for Enhanced Safety: Volume 3 - Evaluation of Commercial Steels," by W.S. Owen, R.M.N. Pelloux, R.O. Ritchie, M. Faral, T. Ohhashi, J. Toplosky, S.J. Hartman, V.F. Zackay and E.R. Parker - Feb. 1979(UCB/EERC-79/09)A04

UCB/EERC-79/10 "The Design of Steel Energy Absorbing Restrainers and Their Incorporation into Nuclear Power Plants for Enhanced Safety: Volume 4 - A Review of Energy-Absorbing Devices," by J.M. Kelly and M.S. Skinner - Feb. 1979(UCB/EERC-79/10)A04

UCB/EERC-79/11 "Conservatism In Summation Rules for Closely Spaced Modes," by J.M. Kelly and J.L. Sackman - May 1979(PB 301 328)A03

UCB/EERC-79/12 "Cyclic Loading Tests of Masonry Single Piers; Volume 3 - Height to Width Ratio of 0.5," by P.A. Hidalgo, R.L. Mayes, H.D. McNiven and R.W. Clough - May 1979(PB 301 321)A08

UCB/EERC-79/13 "Cyclic Behavior of Dense Course-Grained Materials in Relation to the Seismic Stability of Dams," by N.G. Banerjee, H.B. Seed and C.K. Chan - June 1979(PB 301 373)A13

UCB/EERC-79/14 "Seismic Behavior of Reinforced Concrete Interior Beam-Column Subassemblages," by S. Viwathanatepa, E.P. Popov and V.V. Bertero - June 1979(PB 301 326)A10

UCB/EERC-79/15 "Optimal Design of Localized Nonlinear Systems with Dual Performance Criteria Under Earthquake Excitations," by M.A. Bhatti - July 1979(PB 80 167 109)A06

UCB/EERC-79/16 "OPTDYN - A General Purpose Optimization Program for Problems with or without Dynamic Constraints," by M.A. Bhatti, E. Polak and K.S. Pister - July 1979(PB 80 167 091)A05

UCB/EERC-79/17 "ANSR-II, Analysis of Nonlinear Structural Response, Users Manual," by D.P. Mondkar and G.H. Powell July 1979(PB 80 113 301)A05

UCB/EERC-79/18 "Soil Structure Interaction in Different Seismic Environments," A. Gomez-Masso, J. Lysmer, J.-C. Chen and H.B. Seed - August 1979(PB 80 101 520)A04

UCB/EERC-79/19 "ARMA Models for Earthquake Ground Motions," by M.K. Chang, J.W. Kwiatkowski, R.F. Nau, R.M. Oliver and K.S. Pister - July 1979(PB 301 166)A05

UCB/EERC-79/20 "Hysteretic Behavior of Reinforced Concrete Structural Walls," by J.M. Vallenas, V.V. Bertero and E.P. Popov - August 1979(PB 80 165 905)A12

UCB/EERC-79/21 "Studies on High-Frequency Vibrations of Buildings - 1: The Column Effect," by J. Lubliner - August 1979 (PB 80 158 553)A03

UCB/EERC-79/22 "Effects of Generalized Loadings on Bond Reinforcing Bars Embedded in Confined Concrete Blocks," by S. Viwathanatepa, E.P. Popov and V.V. Bertero - August 1979(PB 81 124 018)A14

UCB/EERC-79/23 "Shaking Table Study of Single-Story Masonry Houses, Volume 1: Test Structures 1 and 2," by P. Gülkan, R.L. Mayes and R.W. Clough - Sept. 1979 (HUD-000 1763)A12

UCB/EERC-79/24 "Shaking Table Study of Single-Story Masonry Houses, Volume 2: Test Structures 3 and 4," by P. Gülkan, R.L. Mayes and R.W. Clough - Sept. 1979 (HUD-000 1836)A12

UCB/EERC-79/25 "Shaking Table Study of Single-Story Masonry Houses, Volume 3: Summary, Conclusions and Recommendations," by R.W. Clough, R.L. Mayes and P. Gülkan - Sept. 1979 (HUD-000 1837)A06

UCB/EERC-79/26 "Recommendations for a U.S.-Japan Cooperative Research Program Utilizing Large-Scale Testing Facilities," by U.S.-Japan Planning Group - Sept. 1979(PB 301 407)A06

UCB/EERC-79/27 "Earthquake-Induced Liquefaction Near Lake Amatitlan, Guatemala," by H.B. Seed, I. Arango, C.K. Chan, A. Gomez-Masso and R. Grant de Ascoli - Sept. 1979(NUREG-CR1341)A03

UCB/EERC-79/28 "Infill Panels: Their Influence on Seismic Response of Buildings," by J.W. Axley and V.V. Bertero Sept. 1979(PB 80 163 371)A10

UCB/EERC-79/29 "3D Truss Bar Element (Type 1) for the ANSR-II Program," by D.P. Mondkar and G.H. Powell - Nov. 1979 (PB 80 169 709)A02

UCB/EERC-79/30 "2D Beam-Column Element (Type 5 - Parallel Element Theory) for the ANSR-II Program," by D.G. Row, G.H. Powell and D.P. Mondkar - Dec. 1979(PB 80 167 224)A03

UCB/EERC-79/31 "3D Beam-Column Element (Type 2 - Parallel Element Theory) for the ANSR-II Program," by A. Riahi, G.H. Powell and D.P. Mondkar - Dec. 1979(PB 80 167 216)A03

UCB/EERC-79/32 "On Response of Structures to Stationary Excitation," by A. Der Kiureghian - Dec. 1979(PB 80166 929)A03

UCB/EERC-79/33 "Undisturbed Sampling and Cyclic Load Testing of Sands," by S. Singh, H.B. Seed and C.K. Chan Dec. 1979(ADA 087 298)A07

UCB/EERC-79/34 "Interaction Effects of Simultaneous Torsional and Compressional Cyclic Loading of Sand," by P.M. Griffin and W.N. Houston - Dec. 1979(ADA 092 352)A15

UCB/EERC-80/01 "Earthquake Response of Concrete Gravity Dams Including Hydrodynamic and Foundation Interaction Effects," by A.K. Chopra, P. Chakrabarti and S. Gupta - Jan. 1980(AD-A087297)A10

UCB/EERC-80/02 "Rocking Response of Rigid Blocks to Earthquakes," by C.S. Yim, A.K. Chopra and J. Penzien - Jan. 1980 (PB80 166 002)A04

UCB/EERC-80/03 "Optimum Inelastic Design of Seismic-Resistant Reinforced Concrete Frame Structures," by S.W. Zagajeski and V.V. Bertero - Jan. 1980(PB80 164 635)A06

UCB/EERC-80/04 "Effects of Amount and Arrangement of Wall-Panel Reinforcement on Hysteretic Behavior of Reinforced Concrete Walls," by R. Iliya and V.V. Bertero - Feb. 1980(PB81 122 525)A09

UCB/EERC-80/05 "Shaking Table Research on Concrete Dam Models," by A. Niwa and R.W. Clough - Sept. 1980(PB81 122 368)A06

UCB/EERC-80/06 "The Design of Steel Energy-Absorbing Restrainers and their Incorporation into Nuclear Power Plants for Enhanced Safety (Vol 1A): Piping with Energy Absorbing Restrainers: Parameter Study on Small Systems," by G.H. Powell, C. Oughourlian and J. Simons - June 1980

UCB/EERC-80/07 "Inelastic Torsional Response of Structures Subjected to Earthquake Ground Motions," by Y. Yamazaki April 1980(PB81 122 327)A08

UCB/EERC-80/08 "Study of X-Braced Steel Frame Structures Under Earthquake Simulation," by Y. Ghanaat - April 1980 (PB81 122 335)A11

UCB/EERC-80/09 "Hybrid Modelling of Soil-Structure Interaction," by S. Gupta, T.W. Lin, J. Penzien and C.S. Yeh May 1980(PB81 122 319)A07

UCB/EERC-80/10 "General Applicability of a Nonlinear Model of a One Story Steel Frame," by B.I. Sveinsson and H.D. McNiven - May 1980(PB81 124 877)A06

UCB/EERC-80/11 "A Green-Function Method for Wave Interaction with a Submerged Body," by W. Kioka - April 1980 (PB81 122 269)A07

UCB/EERC-80/12 "Hydrodynamic Pressure and Added Mass for Axisymmetric Bodies," by F. Nilrat - May 1980(PB81 122 343)A08

UCB/EERC-80/13 "Treatment of Non-Linear Drag Forces Acting on Offshore Platforms," by B.V. Dao and J. Penzien May 1980(PB81 153 413)A07

UCB/EERC-80/14 "2D Plane/Axisymmetric Solid Element (Type 3 - Elastic or Elastic-Perfectly Plastic) for the ANSR-II Program," by D.P. Mondkar and G.H. Powell - July 1980(PB81 122 350)A03

UCB/EERC-80/15 "A Response Spectrum Method for Random Vibrations," by A. Der Kiureghian - June 1980(PB81 122 301)A03

UCB/EERC-80/16 "Cyclic Inelastic Buckling of Tubular Steel Braces," by V.A. Zayas, E.P. Popov and S.A. Mahin June 1980(PB81 124 885)A10

UCB/EERC-80/17 "Dynamic Response of Simple Arch Dams Including Hydrodynamic Interaction," by C.S. Porter and A.K. Chopra - July 1980(PB81 124 000)A13

UCB/EERC-80/18 "Experimental Testing of a Friction Damped Aseismic Base Isolation System with Fail-Safe Characteristics," by J.M. Kelly, K.E. Beucke and M.S. Skinner - July 1980(PB81 148 595)A04

UCB/EERC-80/19 "The Design of Steel Energy-Absorbing Restrainers and their Incorporation into Nuclear Power Plants for Enhanced Safety (Vol 1B): Stochastic Seismic Analyses of Nuclear Power Plant Structures and Piping Systems Subjected to Multiple Support Excitations," by M.C. Lee and J. Penzien - June 1980

UCB/EERC-80/20 "The Design of Steel Energy-Absorbing Restrainers and their Incorporation into Nuclear Power Plants for Enhanced Safety (Vol 1C): Numerical Method for Dynamic Substructure Analysis," by J.M. Dickens and E.L. Wilson - June 1980

UCB/EERC-80/21 "The Design of Steel Energy-Absorbing Restrainers and their Incorporation into Nuclear Power Plants for Enhanced Safety (Vol 2): Development and Testing of Restraints for Nuclear Piping Systems," by J.M. Kelly and M.S. Skinner - June 1980

UCB/EERC-80/22 "3D Solid Element (Type 4-Elastic or Elastic-Perfectly-Plastic) for the ANSR-II Program," by D.P. Mondkar and G.H. Powell - July 1980(PB81 123 242)A03

UCB/EERC-80/23 "Gap-Friction Element (Type 5) for the ANSR-II Program," by D.P. Mondkar and G.H. Powell - July 1980 (PB81 122 285)A03

UCB/EERC-80/24 "U-Bar Restraint Element (Type 11) for the ANSR-II Program," by C. Oughourlian and G.H. Powell July 1980(PB81 122 293)A03

UCB/EERC-80/25 "Testing of a Natural Rubber Base Isolation System by an Explosively Simulated Earthquake," by J.M. Kelly - August 1980(PB81 201 360)A04

UCB/EERC-80/26 "Input Identification from Structural Vibrational Response," by Y. Hu - August 1980(PB81 152 308)A05

UCB/EERC-80/27 "Cyclic Inelastic Behavior of Steel Offshore Structures," by V.A. Zayas, S.A. Mahin and E.P. Popov August 1980(PB81 196 180)A15

UCB/EERC-80/28 "Shaking Table Testing of a Reinforced Concrete Frame with Biaxial Response," by M.G. Oliva October 1980(PB81 154 304)A10

UCB/EERC-80/29 "Dynamic Properties of a Twelve-Story Prefabricated Panel Building," by J.G. Bouwkamp, J.P. Kollegger and R.M. Stephen - October 1980(PB82 117 128)A06

UCB/EERC-80/30 "Dynamic Properties of an Eight-Story Prefabricated Panel Building," by J.G. Bouwkamp, J.P. Kollegger and R.M. Stephen - October 1980(PB81 200 313)A05

UCB/EERC-80/31 "Predictive Dynamic Response of Panel Type Structures Under Earthquakes," by J.P. Kollegger and J.G. Bouwkamp - October 1980(PB81 152 316)A04

UCB/EERC-80/32 "The Design of Steel Energy-Absorbing Restrainers and their Incorporation into Nuclear Power Plants for Enhanced Safety (Vol 3): Testing of Commercial Steels in Low-Cycle Torsional Fatigue," by P. Spencer, E.R. Parker, E. Jongewaard and M. Drory

UCB/EERC-80/33 "The Design of Steel Energy-Absorbing Restrainers and their Incorporation into Nuclear Power Plants for Enhanced Safety (Vol 4): Shaking Table Tests of Piping Systems with Energy-Absorbing Restrainers," by S.F. Stiemer and W.G. Godden - Sept. 1980

UCB/EERC-80/34 "The Design of Steel Energy-Absorbing Restrainers and their Incorporation into Nuclear Power Plants for Enhanced Safety (Vol 5): Summary Report," by P. Spencer

UCB/EERC-80/35 "Experimental Testing of an Energy-Absorbing Base Isolation System," by J.M. Kelly, M.S. Skinner and K.E. Beucke - October 1980(PB81 154 072)A04

UCB/EERC-80/36 "Simulating and Analyzing Artificial Non-Stationary Earthquake Ground Motions," by R.F. Nau, R.M. Oliver and K.S. Pister - October 1980(PB81 153 397)A04

UCB/EERC-80/37 "Earthquake Engineering at Berkeley - 1980," - Sept. 1980(PB81 205 874)A09

UCB/EERC-80/38 "Inelastic Seismic Analysis of Large Panel Buildings," by V. Schricker and G.H. Powell - Sept. 1980 (PB81 154 338)A13

UCB/EERC-80/39 "Dynamic Response of Embankment, Concrete-Gravity and Arch Dams Including Hydrodynamic Interaction," by J.F. Hall and A.K. Chopra - October 1980(PB81 152 324)A11

UCB/EERC-80/40 "Inelastic Buckling of Steel Struts Under Cyclic Load Reversal," by R.G. Black, W.A. Wenger and E.P. Popov - October 1980(PB81 154 312)A08

UCB/EERC-80/41 "Influence of Site Characteristics on Building Damage During the October 3, 1974 Lima Earthquake," by P. Repetto, I. Arango and H.B. Seed - Sept. 1980(PB81 161 739)A05

UCB/EERC-80/42 "Evaluation of a Shaking Table Test Program on Response Behavior of a Two Story Reinforced Concrete Frame," by J.M. Blondet, R.W. Clough and S.A. Mahin

UCB/EERC-80/43 "Modelling of Soil-Structure Interaction by Finite and Infinite Elements," by F. Medina - December 1980(PB81 229 270)A04

UCB/EERC-81/01 "Control of Seismic Response of Piping Systems and Other Structures by Base Isolation," edited by J.M. Kelly - January 1981 (PB81 200 735)A05

UCB/EERC-81/02 "OPTNSR - An Interactive Software System for Optimal Design of Statically and Dynamically Loaded Structures with Nonlinear Response," by M.A. Bhatti, V. Ciampi and K.S. Pister - January 1981 (PB81 218 851)A09

UCB/EERC-81/03 "Analysis of Local Variations in Free Field Seismic Ground Motions," by J.-C. Chen, J. Lysmer and H.B. Seed - January 1981 (AD-A099508)A13

UCB/EERC-81/04 'Inelastic Structural Modeling of Braced Offshore Platforms for Seismic Loading," by V.A. Zayas, P.-S.B. Shing, S.A. Mahin and E.P. Popov - January 1981(PB82 138 777)A07

UCB/EERC-81/05 "Dynamic Response of Light Equipment in Structures," by A. Der Kiureghian, J.L. Sackman and B. Nour-Omid - April 1981 (PB81 218 497)A04

UCB/EERC-81/06 "Preliminary Experimental Investigation of a Broad Base Liquid Storage Tank," by J.G. Bouwkamp, J.P. Kollegger and R.M. Stephen - May 1981(PB82 140 385)A03

UCB/EERC-81/07 "The Seismic Resistant Design of Reinforced Concrete Coupled Structural Walls," by A.E. Aktan and V.V. Bertero - June 1981(PB82 113 358)A11

UCB/EERC-81/08 "The Undrained Shearing Resistance of Cohesive Soils at Large Deformations," by M.R. Pyles and H.B. Seed - August 1981

UCB/EERC-81/09 "Experimental Behavior of a Spatial Piping System with Steel Energy Absorbers Subjected to a Simulated Differential Seismic Input," by S.F. Stiemer, W.G. Godden and J.M. Kelly - July 1981

UCB/EERC-81/10 "Evaluation of Seismic Design Provisions for Masonry in the United States," by B.I. Sveinsson, R.L. Mayes and H.D. McNiven - August 1981 (PB82 166 075)A08

UCB/EERC-81/11 "Two-Dimensional Hybrid Modelling of Soil-Structure Interaction," by T.-J. Tzong, S. Gupta and J. Penzien - August 1981(PB82 142 118)A04

UCB/EERC-81/12 "Studies on Effects of Infills in Seismic Resistant R/C Construction," by S. Brokken and V.V. Bertero - September 1981 (PB82 166 190)A09

UCB/EERC-81/13 "Linear Models to Predict the Nonlinear Seismic Behavior of a One-Story Steel Frame," by H. Valdimarsson, A.H. Shah and H.D. McNiven - September 1981(PB82 138 793)A07

UCB/EERC-81/14 "TLUSH: A Computer Program for the Three-Dimensional Dynamic Analysis of Earth Dams," by T. Kagawa, L.H. Mejia, H.B. Seed and J. Lysmer - September 1981(PB82 139 940)A06

UCB/EERC-81/15 "Three Dimensional Dynamic Response Analysis of Earth Dams," by L.H. Mejia and H.B. Seed - September 1981 (PB82 137 274)A12

UCB/EERC-81/16 "Experimental Study of Lead and Elastomeric Dampers for Base Isolation Systems," by J.M. Kelly and S.B. Hodder - October 1981 (PB82 166 182)A05

UCB/EERC-81/17 "The Influence of Base Isolation on the Seismic Response of Light Secondary Equipment," by J.M. Kelly - April 1981 (PB82 255 266)A04

UCB/EERC-81/18 "Studies on Evaluation of Shaking Table Response Analysis Procedures," by J. Marcial Blondet - November 1981 (PB82 197 278)A10

UCB/EERC-81/19 "DELIGHT.STRUCT: A Computer-Aided Design Environment for Structural Engineering," by R.J. Balling, K.S. Pister and E. Polak - December 1981 (PB82 218 496)A07

UCB/EERC-81/20 "Optimal Design of Seismic-Resistant Planar Steel Frames," by R.J. Balling, V. Ciampi, K.S. Pister and E. Polak - December 1981 (PB82 220 179)A07

UCB/EERC-82/01 "Dynamic Behavior of Ground for Seismic Analysis of Lifeline Systems," by T. Sato and A. Der Kiureghian - January 1982 (PB82 218 926)A05

UCB/EERC-82/02 "Shaking Table Tests of a Tubular Steel Frame Model," by Y. Ghanaat and R. W. Clough - January 1982 (PB82 220 161)A07

UCB/EERC-82/03 "Behavior of a Piping System under Seismic Excitation: Experimental Investigations of a Spatial Piping System supported by Mechanical Shock Arrestors and Steel Energy Absorbing Devices under Seismic Excitation," by S. Schneider, H.-M. Lee and W. G. Godden - May 1982 (PB83 172 544)A09

UCB/EERC-82/04 "New Approaches for the Dynamic Analysis of Large Structural Systems," by E. L. Wilson - June 1982 (PB83 148 080)A05

UCB/EERC-82/05 "Model Study of Effects of Damage on the Vibration Properties of Steel Offshore Platforms," by F. Shahrivar and J. G. Bouwkamp - June 1982 (PB83 148 742)A10

UCB/EERC-82/06 "States of the Art and Practice in the Optimum Seismic Design and Analytical Response Prediction of R/C Frame-Wall Structures," by A. E. Aktan and V. V. Bertero - July 1982 (PB83 147 736)A05

UCB/EERC-82/07 "Further Study of the Earthquake Response of a Broad Cylindrical Liquid-Storage Tank Model," by G. C. Manos and R. W. Clough - July 1982 (PB83 147 744)A11

UCB/EERC-82/08 "An Evaluation of the Design and Analytical Seismic Response of a Seven Story Reinforced Concrete Frame - Wall Structure," by F. A. Charney and V. V. Bertero - July 1982(PB83 157 628)A09

UCB/EERC-82/09 "Fluid-Structure Interactions: Added Mass Computations for Incompressible Fluid," by J. S.-H. Kuo - August 1982 (PB83 156 281)A07

UCB/EERC-82/10 "Joint-Opening Nonlinear Mechanism: Interface Smeared Crack Model," by J. S.-H. Kuo - August 1982 (PB83 149 195)A05

UCB/EERC-82/11 "Dynamic Response Analysis of Techi Dam," by R. W. Clough, R. M. Stephen and J. S.-H. Kuo - August 1982 (PB83 147 496)A06

UCB/EERC-82/12 "Prediction of the Seismic Responses of R/C Frame-Coupled Wall Structures," by A. E. Aktan, V. V. Bertero and M. Piazza - August 1982 (PB83 149 203)A09

UCB/EERC-82/13 "Preliminary Report on the SMART 1 Strong Motion Array in Taiwan," by B. A. Bolt, C. H. Loh, J. Penzien, Y. B. Tsai and Y. T. Yeh - August 1982 (PB83 159 400)A10

UCB/EERC-82/14 "Shaking-Table Studies of an Eccentrically X-Braced Steel Structure," by M. S. Yang - September 1982

UCB/EERC-82/15 "The Performance of Stairways in Earthquakes," by C. Roha, J. W. Axley and V. V. Bertero - September 1982 (PB83 157 693)A07

UCB/EERC-82/16 "The Behavior of Submerged Multiple Bodies in Earthquakes," by W.-G. Liao - Sept. 1982 (PB83 158 709)A07

UCB/EERC-82/17 "Effects of Concrete Types and Loading Conditions on Local Bond-Slip Relationships," by A. D. Cowell, E. P. Popov and V. V. Bertero - September 1982 (PB83 153 577)A04

UCB/EERC-82/18 "M chanical Behavior of Shear Wall Vertical Boundary Members: An Experimental Investigation," by M. T. Wagner and V. V. Bertero - October 1982 (PB83 159 764)A05

UCB/EERC-82/19 "Experimental Studies of Multi-support Seismic Loading on Piping Systems," by J. M. Kelly and A. D. Cowell - November 1982

UCB/EERC-82/20 "Generalized Plastic Hinge Concepts for 3D Beam-Column Elements," by P. F.-S. Chen and G. H. Powell - November 1982

UCB/EERC-82/21 "ANSR-III: General Purpose Computer Program for Nonlinear Structural Analysis," by C. V. Oughourlian and G. H. Powell - November 1982

UCB/EERC-82/22 "Solution Strategies for Statically Loaded Nonlinear Structures," by J. W. Simons and G. H. Powell - November 1982

UCB/EERC-82/23 "Analytical Model of Deformed Bar Anchorages under Generalized Excitations," by V. Ciampi, R. Eligehausen, V. V. Bertero and E. P. Popov - November 1982 (PB83 169 532)A06

UCB/EERC-82/24 "A Mathematical Model for the Response of Masonry Walls to Dynamic Excitations," by H. Sucuoğlu, Y. Mengi and H. D. McNiven - November 1982 (PB83 169 011)A07

UCB/EERC-82/25 "Earthquake Response Considerations of Broad Liquid Storage Tanks," by F. J. Cambra - November 1982

UCB/EERC-82/26 "Computational Models for Cyclic Plasticity, Rate Dependence and Creep," by B. Mosaddad and G. H. Powell - November 1982

UCB/EERC-82/27 "Inelastic Analysis of Piping and Tubular Structures," by M. Mahasuverachai and G. H. Powell - November 1982

UCB/EERC-83/01 "The Economic Feasibility of Seismic Rehabilitation of Buildings by Base Isolation," by J. M. Kelly - January 1983

UCB/EERC-83/02 "Seismic Moment Connections for Moment-Resisting Steel Frames," by E. P. Popov - January 1983

UCB/EERC-83/03 "Design of Links and Beam-to-Column Connections for Eccentrically Braced Steel Frames," by E. P. Popov and J. O. Malley - January 1983

UCB/EERC-83/04 "Numerical Techniques for the Evaluation of Soil-Structure Interaction Effects in the Time Domain," by E. Bayo and E. L. Wilson - February 1983

UCB/EERC-83/05 "A Transducer for Measuring the Internal Forces in the Columns of a Frame-Wall Reinforced Concrete Structure," by R. Sause and V. V. Bertero - May 1983

UCB/EERC-83/06 "Dynamic Interactions between Floating Ice and Offshore Structures," by P. Croteau - May 1983

UCB/EERC-83/07 "Dynamic Analysis of Multiply Tuned and Arbitrarily Supported Secondary Systems," by T. Igusa and A. Der Kiureghian - June 1983

UCB/EERC-83/08 "A Laboratory Study of Submerged Multi-body Systems in Earthquakes," by G. R. Ansari - June 1983

UCB/EERC-83/09 "Effects of Transient Foundation Uplift on Earthquake Response of Structures," by C.-S. Yim and A. K. Chopra - June 1983

UCB/EERC-83/10 "Optimal Design of Friction-Braced Frames under Seismic Loading," by M. A. Austin and K. S. Pister - June 1983

UCB/EERC-83/11 "Shaking Table Study of Single-Story Masonry Houses: Dynamic Performance under Three Component Seismic Input and Recommendations," by G. C. Manos, R. W. Clough and R. L. Mayes - June 1983

UCB/EERC-83/12 "Experimental Error Propagation in Pseudodynamic Testing," by P. B. Shing and S. A. Mahin - June 1983

UCB/EERC-83/13 "Experimental and Analytical Predictions of the Mechanical Characteristics of a 1/5-scale Model of a 7-story R/C Frame-Wall Building Structure," by A. E. Aktan, V. V. Bertero, A. A. Chowdhury and T. Nagashima - August 1983

UCB/EERC-83/14 "Shaking Table Tests of Large-Panel Precast Concrete Building System Assemblages," by M. G. Oliva and R. W. Clough - August 1983

UCB/EERC-83/15 "Seismic Behavior of Active Beam Links in Eccentrically Braced Frames," by K. D. Hjelmstad and E. P. Popov - July 1983

UCB/EERC-83/16 "System Identification of Structures with Joint Rotation," by J. S. Dimsdale and H. D. McNiven - July 1983

UCB/EERC-83/17 "Construction of Inelastic Response Spectra for Single-Degree-of-Freedom Systems," by S. Mahin and J. Lin - July 1983

UCB/EERC-83/18 "Interactive Computer Analysis Methods for Predicting the Inelastic Cyclic Behavior of Sections," by S. Kaba and S. Mahin - July 1983 (PB84 192 012) A06

UCB/EERC-83/19 "Effects of Bond Deterioration on Hysteretic Behavior of Reinforced Concrete Joints," by F. C. Filippou, E. P. Popov and V. V. Bertero - August 1983 (PB84 192 020) A10

UCB/EERC-83/20 "Analytical and Experimental Correlation of Large-Panel Precast Building System Performance," M. G. Oliva, R. W. Clough, M. Velkov, P. Gavrilovic and J. Petrovski - November 1983

UCB/EERC-83/21 "Mechanical Characteristics of the Materials Used in the 1/5 Scale and Full Scale Models of the 7-Story Reinforced Concrete Test Structure," by V. V. Bertero, A. E. Aktan and A. A. Chowdhury - September 1983 (PB84 193 697) A05

UCB/EERC-83/22 "Hybrid Modelling of Soil-Structure Interaction in Layered Media," by T.-J. Tzong and J. Penzien - October 1983 (PB84 192 178) A08

UCB/EERC-83/23 "Local Bond Stress-Slip Relationships of Deformed Bars Under Generalized Excitations," by R. Eligehausen, E. P. Popov and V. V. Bertero - October 1983 (PB84 192 848) A09

UCB/EERC-83/24 "Design Considerations for Shear Links in Eccentrically Braced Frames," by J. O. Malley and E. P. Popov - November 1983 (PB84 192 186) A07

UCB/EERC-84/01 "Pseudodynamic Test Method for Seismic Performance Evaluation: Theory and Implementation," by P.-S. B. Shing and S. A. Mahin - January 1984 (PB84 190 644) A08

UCB/EERC-84/02 "Dynamic Response Behavior of Xiang Hong Dian Dam," by R. W. Clough, K.-T. Chang, H.-Q. Chen, R. M. Stephen, G.-L. Wang, and Y. Ghanaat - April 1984

UCB/EERC-84/03 "Refined Modelling of Reinforced Concrete Columns for Seismic Analysis," by S.A. Kaba and S.A. Mahin - April 1984

UCB/EERC-84/04 "A New Floor Response Spectrum Method for Seismic Analysis of Multiply Supported Secondary Systems," by A. Asfura and A. Der Kiureghian - June 1984

UBC/EERC-84/05 "U.S.-Japan Cooperative Earthquake Research Program: Earthquake Simulation Test And Associated Studies of a 1/5th Scale Model of a 7-Story R/C Frame-Wall Test Structure," by V.V. Bertero, A.E. Aktan, F.A. Charney and R. Sause - June 1984